UNIVERSITY OF SOUTHAMPTON

FACULTY OF ENGINEERING, SCIENCE & MATHEMATICS

SCHOOL OF OCEAN & EARTH SCIENCES

Carbon Export from Natural Iron Fertilisation in the Southern Ocean

by

Paul James Morris

Thesis for the degree of Doctor of Philosophy

August 2008

UNIVERSITY OF SOUTHAMPTON

Abstract

FACULTY OF ENGINEERING, SCIENCE & MATHEMATICS

SCHOOL OF OCEAN & EARTH SCIENCES

Doctor of Philosophy

Carbon Export from Natural Iron Fertilisation in the Southern Ocean

by Paul James Morris

It has long been recognised that some oceanic regions have persistently low chlorophyll levels, even though inorganic nutrients are plentiful. Studies have shown that these high-nutrient, low-chlorophyll (HNLC) areas are depleted in iron, which is an essential micronutrient for phytoplankton growth. In HNLC regions biological production can be enhanced with artificial mesoscale iron fertilisation. However, the ability of artificially induced phytoplankton blooms to efficiently sequester carbon to mesopelagic depths is still an open question. SubAntarctic islands in the HNLC Southern Ocean are a natural source of iron and thus fuel the annual phytoplankton blooms observed in their proximity. One such bloom, tied to the Crozet Islands (52ºE, 46ºS), provided the opportunity to examine particulate organic carbon (POC) export during the austral summer of 2004/5. This work was imbedded into the multi-disciplinary CROZEX project thus providing a rich context for data interpretation.

Based on satellite imagery, a high chlorophyll region (max = 4 μg l^{-1}) north and downstream of the Crozet Islands was distinguished from a low chlorophyll region (typically 0.3 μg l^{-1}) south and upstream of the islands. POC export estimates, obtained with the naturally occurring particle reactive radionuclide tracer, ^{234}Th, were initially ≈15 mmol C m^{-2} d^{-1} in the high chlorophyll region, compared with ≈5 mmol C m^{-2} d^{-1} in the low chlorophyll region. After a moderately small increase in chlorophyll in the south (max = 0.7 μg l^{-1}) the spatial variability in POC export was lost, resulting in equally high levels of POC export (*ca.* 20 mmol C m^{-2} d^{-1}) throughout the study area. After comparing the daily rates of POC export with temporally integrated new production calculated from nitrate budgets, a different spatial pattern emerged. New production (NP) presented consistently higher values in the north, when compared to the south. Two hypotheses were formulated to explain this, 1) dissolved organic matter (DOM) and suspended particulate organic matter (sPOM) produced from NP was stored in the mixed layer with this effect relatively greater in the north, 2) the export event in the north was longer resulting in greater seasonal POC export. Investigation of the DOM pool revealed that DOM accounted for 46±7% of NP and was consistent across the whole study area. In contrast, sPOM accumulated at differential rates of 18±7% in the north and 0±7% in the south. This suggested that differential storage of sPOM was responsible for the lack of a latitudinal gradient in POC export after the relatively small increase in chlorophyll in the south. After investigating the second hypothesis, the daily rates of POC export were scaled to seasonal integrals using a silicon budget, which allowed the formulation of a seasonal carbon budget. This revealed that over the time-scale of the study the magnitude of NP and POC export were not the same with this difference greatest within the northern high chlorophyll region. This was the result of relatively greater storage of sPOM in the north and had the effect of reducing the amount of easily exportable POC to mesopelagic depths. Thus both hypotheses contributed to better understanding carbon export in the Crozet region.

Table of contents

Table of figures

Table of tables

DECLARATION OF AUTHORSHIP

I, Paul James Morris, declare that the thesis entitled:

Carbon Export from Natural Iron Fertilisation in the Southern Ocean

and the work presented in the thesis are both my own, and have been generated by me as the result of my own original research. I confirm that:

- this work was done wholly or mainly while in candidature for a research degree at this University;
- where any part of this thesis has previously been submitted for a degree or any other qualification at this University or any other institution, this has been clearly stated;
- where I have consulted the published work of others, this is always clearly attributed;
- where I have quoted from the work of others, the source is always given. With the exception of such quotations, this thesis is entirely my own work;
- I have acknowledged all main sources of help;
- where the thesis is based on work done by myself jointly with others, I have made clear exactly what was done by others and what I have contributed myself;
- parts of this work have been published as:

Morris, P.J., Sanders, R., Turnewitsch, R., Thomalla, S., (2007) ^{234}Th-derived particulate organic carbon export from an island-induced phytoplankton bloom in the Southern Ocean. *Deep-Sea Research II*, 54(18-20), 2208-2232.

Sanders, R., Morris, P.J., Stinchcombe, M., Seeyave, S., Venables, H., Lucas, M., (2007) New production and the f ratio around the Crozet Plateau in austral summer 2004-2005 diagnosed from seasonal changes in inorganic nutrient levels. *Deep-Sea Research II*, 54(18-20), 2191-2207.

Signed:.....

Date:.....

Acknowledgments

To complete a PhD, it takes a whole group of people working together and this is where I pay thanks to all those who have helped me over the past four years. Firstly there is one person that stands above the rest, without whom this thesis would never have been possible. My lead supervisor Richard Sanders has tirelessly tolerated my need for supervision, guidance and direction. Richard's inspiration and drive for oceanography has kept me on track when I needed it the most and his stimulating discussion and endless patience is more than any student could wish for.

Two additional supervisors have also provided support. At the start of my PhD Robert Turnewitsch played an invaluable role in teaching me the intricacies of the thorium technique. Robert is a fantastic source of technical detail and he taught me much about radiochemistry. In the background Rachel Mills has provided me with a friendly ear and honest advice whenever I needed it.

The CROZEX team led by Raymond Pollard and Richard Sanders are too numerous to list here but there are some fellow students and staff that I have worked with closely. Sandy Thomalla taught me the thorium technique, how to do origami with tweezers and did the thorium analysis on leg 2. Ian Salter has been an endless source of information about particle flux and biogenic silica. Ian also processed all my SAPS bSi samples. Mark Stinchcombe (aka "The Stinch") has dealt with my every request for assistance in the lab. There are many others in the CROZEX team that I have had discussions with about carbon export, bloom ecology, satellite imagery and the little whizzy things in plankton hauls, all of which contribute to the bigger understanding needed for a PhD. Conducting work at sea would not be possible without the ship's officers, crew and logistical and scientific support staff. All of whom contributed to a safe, comfortable and practical environment for cruises D285 and D286.

Additional thanks goes to Bob Head at PML for processing POC samples, Sinhue Torres-Valdes for teaching me how to process DON samples, Becky Bell for help with GMT script, Phil Wallhead for guiding me through the minefield of statistics and Hugh Venables for help and discussion on the physics.

In the year 2000, my oceanography career started on a damp autumnal day in Menai Bridge. My oceanographic mentor, Peter J. le B. Williams, asked if I would like to go to Hawaii to learn how to surf, drink mai tais and do some oceanography in my spare time. After three years of working on the Hawaii Ocean Time-series led by Dave Karl my future in oceanography was set. Both Peter and Dave, I thank you for giving me this opportunity and for teaching me much about biogeochemistry.

This leaves me with only a few more people to thank. Firstly I would like to thank my partner, Sarah, who has been an outstanding help, with her true appreciation for what oceanography entails. She has been the balance in my life that has helped me to successfully survive my PhD. Sarah's lead in finishing her PhD and love of hydrothermal vents has been an inspiration to me.

Thanos, my house mate of two years has given me much friendship and entertainment. I look forward to visiting Athens in the future.

Finally, my family. Without their continued love, encouragement and support I would not be where I am today. For this I am greatly indebted and can never thank you enough.

I would like to dedicate this thesis
to my Auntie Sarah
who I love and miss very much.

Definitions and abbreviations

^{14}C	Carbon-14
^{15}N	Nitrogen-15
^{234}Th	Thorium-234
^{238}U	Uranium-238
^{234}Th-Cex	^{234}Th-derived Carbon Export
^{234}Th-Nex	^{234}Th-derived Nitrogen Export
^{234}Th-bSiex	^{234}Th-derived Biogenic Silica Export
$\Sigma^{15}N$ uptake	Total ^{15}N uptake
ΔNO_3^-	Nitrate draw-down
ACC	Antarctic Circumpolar Current
ASW	Artificial Seawater
bSi	Biogenic Silica
$bSiex_t$	Seasonal Biogenic Silica Export
chl-*a*	Chlorophyll-*a*
Cex_t	Seasonal Carbon Export
CTD	Conductivity, Temperature and Depth
DIC	Dissolved Inorganic Carbon
DOC	Dissolved Organic Carbon
DOM	Dissolved Organic Matter
DON	Dissolved Organic Nitrogen
HNLC	High-Nutrient, Low-Chlorophyll
K_z	Vertical Turbulent Diffusion Coefficient
LADCP	Lowered Acoustic Doppler Current Profiler
MLD	Mixed Layer Depth
NP	New Production
PF	Polar Front
PFZ	Polar Frontal Zone
POC	Particulate Organic Carbon
POM	Particulate Organic Matter
PON	Particulate Organic Nitrogen
PP	Primary Production
$t_{½}$	Half-life
ThE	Thorium Export Efficiency
ThE_C	Thorium Export Efficiency of Carbon
ThE_N	Thorium Export Efficiency of Nitrogen
TON	Total Organic Nitrogen
RSD	Residual Standard Deviation
SAPS	Stand Alone Pump System
SAZ	SubAntarctic Zone
SD or σ	Standard Deviation
sPOM	Suspended Particulate Organic Matter
V_z	Vertical Turbulent Diffusive Flux
$\overline{x}$	Mean
z	Depth

Graduate School of the National Oceanography Centre, Southampton

This PhD dissertation by

Paul James Morris

has been produced under the supervision of the following persons

Supervisors

Dr. Richard Sanders

Dr. Rachel Mills

Dr. Robert Turnewitsch

Chair of Advisory Panel

Dr. Richard Lampitt

1 Introduction

1.1 Carbon - An Opening Statement

Given the importance of carbon as a primary and essential element for all life on Earth, it is surprising that it is only the 15th most abundant element in continental crust (Taylor, 1964). Carbon can form four stable covalent bonds, allowing it to make a dazzling array of both simple and hugely complex compounds. This sets it apart from other elements and consequently forms the backbone of organic molecules and life as we know it. The role of carbon in the Earth system is becoming ever more prominent because humanity's reliance on burning fixed forms of this element for fuel is growing at an ever increasing rate. Only through ensuring we understand the implications and acknowledge the potential outcomes of our reliance on carbon, will humanity fully appreciate their impact on planet Earth. Carbon, the essence of life, is also humanity's greatest challenge.

1.1.1 The Global Carbon Cycle

The global carbon cycle is the combination of processes that moves carbon from one reservoir to another. The storage of carbon in the four reservoirs (oceans, atmosphere, geological and terrestrial) is different in both size and residence time, and the fluxes between them vary by more than three orders of magnitude. The largest of these reservoirs is contained within the lithosphere as geological deposits, predominantly as inorganic biogenic limestone ($CaCO_3$), and organic sediments and fossil fuels. Limestone is formed from the lithified deposits of calcium bearing marine organisms, predominantly marine phytoplankton, and fossil fuels and are formed through the diagenesis and lithification of organic material (Libes, 1992).

The geological reservoir cycles on a time-scale of millions of years and therefore plays a minor role in the shorter time-scales of natural carbon cycling within the oceanic, atmospheric and terrestrial spheres. Human interferences are currently shifting the balance of the global carbon cycle, as will be introduced in Section 1.1.3. The terrestrial, atmospheric and marine components of the carbon cycle operate on much shorter time-scales, *ca.* less than one to a few thousand years, and with the marine environment constituting the second largest reservoir of carbon its importance in the

global carbon cycle is clear. Figure 1.1 shows a model of the global carbon cycle with estimates of reservoir sizes and fluxes between them (taken from Prentice *et al.*, 2001).

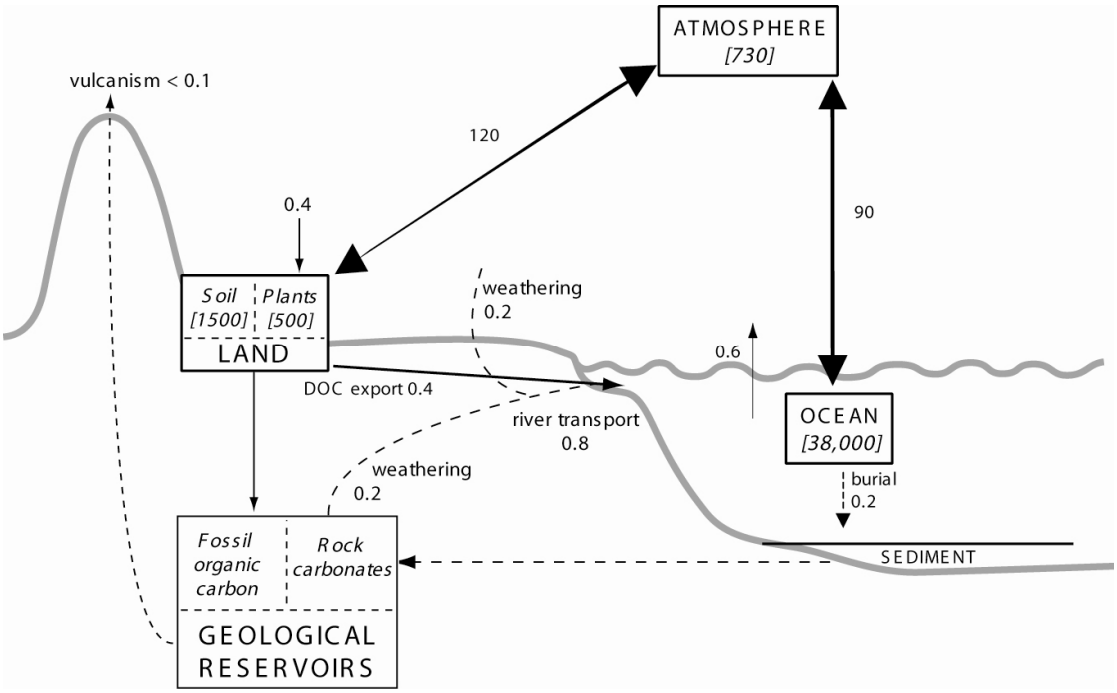

Figure 1.1 The global carbon cycle with magnitude of (Gt C), and fluxes (Gt C y^{-1}) between reservoirs. Taken from Prentice *et al.* (2001).

1.1.2 The Marine Carbon Cycle

The marine carbon cycle is shown in Figure 1.2. CO_2 that enters the dissolved inorganic carbon (DIC) pool of the surface ocean becomes available to autotrophic phytoplankton that can fix CO_2 into organic material. This process is known as photosynthesis, and supplies all higher trophic levels with organic material. Photosynthesis is the process of fixing CO_2 and H_2O with energy from the sun to produce a simple sugar. This reaction can be simply represented by Eq 1.1.

$$6CO_2 + 6H_2O + Light\ Energy \rightarrow C_6H_{12}O_6 + 6O_2 \qquad \text{Eq. 1.1}$$

Eq. 1.1 is still a very simple representation of photosynthesis but the details of the complex anabolic processes involved are not required here. Once photoautotrophs have produced their own sugars these can then be metabolised and allow phytoplankton to respire, grow and reproduce. However, for these life processes to occur a host of

additional elements are required, the main ones of which are the macro-nutrients nitrogen, phosphorus and silicon and are present as the free negatively charged ions: nitrate, phosphate and silicate respectively. For a phytoplankton community to remain healthy and productive all the necessary factors required for growth need to be in abundant supply. Should only one of these essential nutrients become depleted through a lack of supply then growth will stop. This is an example of Liebig's law of the minimum (Liebig, 1847).

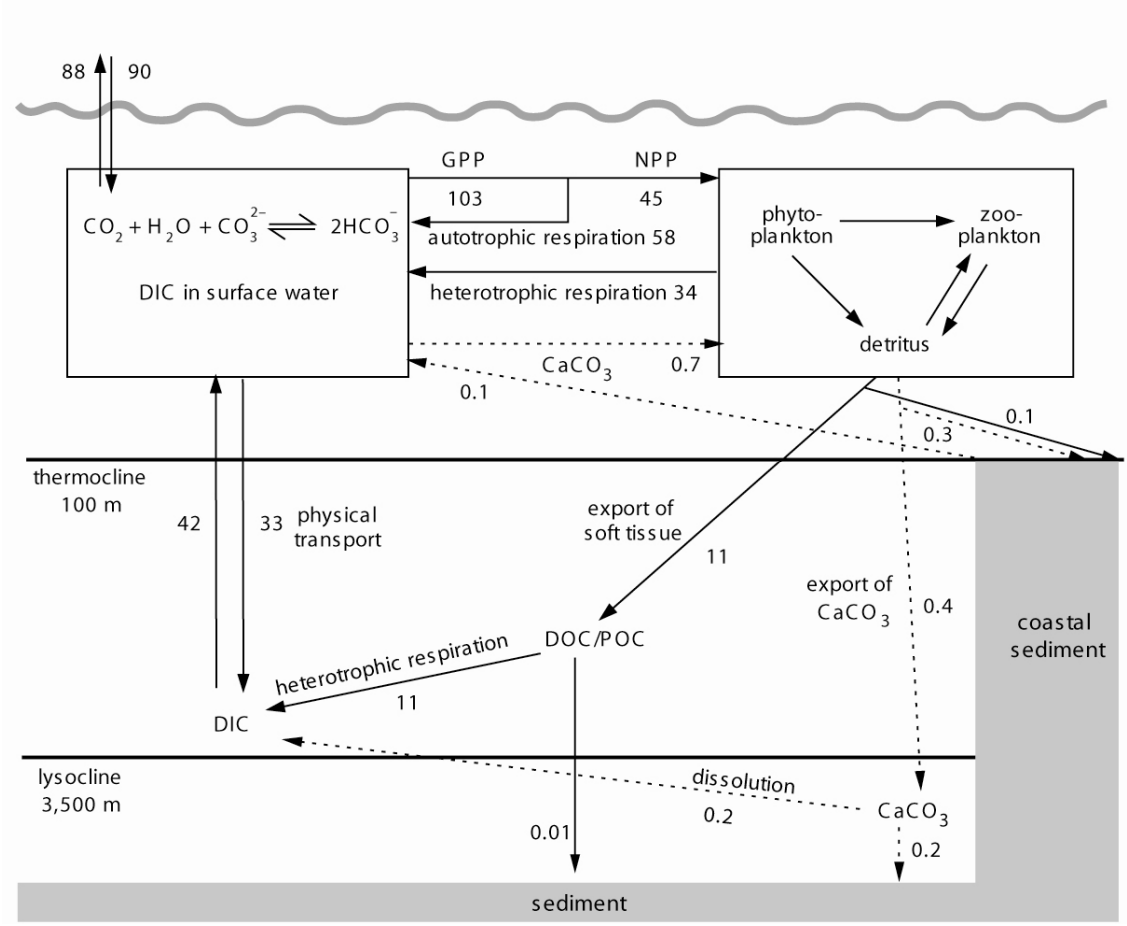

Figure 1.2 The marine carbon cycle showing the pathways and size of fluxes (Gt C y^{-1}). Taken from Prentice *et al.* (2001).

Fixed organic material in the surface ocean has several pathways it may follow. The majority of organic carbon is respired back to DIC within the surface ocean. A fraction is exported downwards out of the surface ocean and an even smaller fraction is ultimately buried in the deep-sea sediments. At all stages, heterotrophs are respiring organic material back into the DIC pool thus making it available once again for photosynthesis. However, the length of time it takes for DIC to return to the surface

ocean is a function of depth, with deep waters not ventilated with the atmosphere for >1000 years (Treguer *et al.*, 2003). Carbon only finally leaves the marine carbon cycle once it is buried in deep ocean sediments where it then remains for geological periods of time. The biologically mediated process of moving carbon from the surface ocean and into the deep ocean is know as the biological pump and will be discussed in more detail in Section 1.2.1.

1.1.3 The Human Perturbation to the Global Carbon Cycle

Since the advent of the industrial revolution in the late 18th century atmospheric levels of CO_2 have steadily increased as a result of burning fossil fuels, changes in land use and production of cement. Preindustrial levels of atmospheric CO_2 are estimated to have been 280 ppm, determined through the analysis of ancient air trapped within ice (Neftel *et al.*, 1985). In 2005 CO_2 levels were at 380 ppm (Denman *et al.*, 2007) and will continue to increase for as long as fossil fuels continue to be burnt; because the sinks of anthropogenically released CO_2, terrestrial storage through photosynthesis and oceanic dissolution, do not balance the rate of CO_2 release to the atmosphere (Figure 1.3). The atmospheric increase in CO_2 has been well documented and the steady rise in atmospheric CO_2 levels is now referred to as the "Keeling Curve" (Keeling *et al.*, 1995).

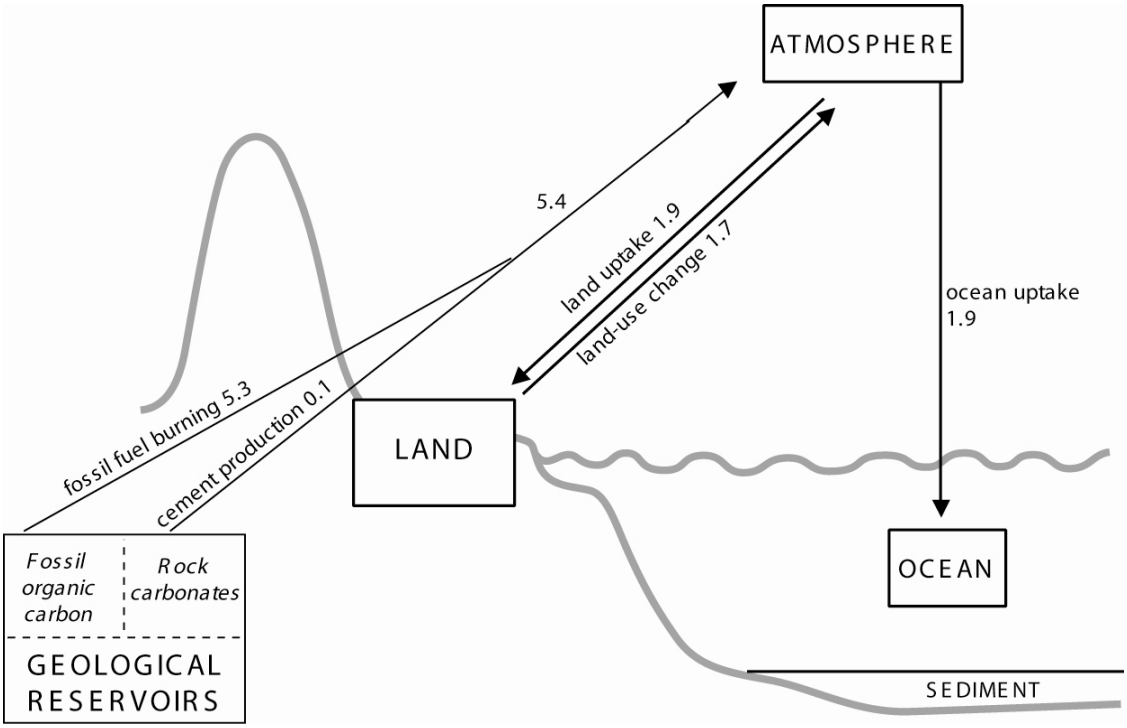

Figure 1.3 The human perturbation in the carbon cycle. Fluxes of anthropogenic CO_2 (Gt C y^{-1}). Taken from Prentice *et al.* (2001).

The rapid anthropogenic release of carbon from geological reservoirs into the atmosphere is now propagating into other parts of the carbon cycle, in particular the marine environment where it is estimated that about 30% of anthropogenic CO_2 is stored (Raven and Falkowski, 1999). CO_2 readily dissolves into seawater and dissociates into carbonic acid, bicarbonate and carbonate known collectively as DIC (Eq. 1.2).

$$CO_2 + H_2O \leftrightarrow H_2CO_3 \leftrightarrow HCO_3^- + H^+ \leftrightarrow CO_3^{2-} + 2H^+ \qquad \text{Eq. 1.2}$$

The increasing levels of oceanic DIC have been shown to track the trend of the Keeling curve (Dore *et al.*, 2003), resulting in a reduction of seawater pH through the release of free hydrogen ions, thus resulting in more acidic conditions as shown by Eq. 1.2 (Jacobson, 2005).

Ocean acidification has major implications for the health of calcareous marine plankton such as coccolithophores, foraminiferans and pteropods (Iglesias-Rodriguez *et al.*, 2008; Orr *et al.*, 2005; Riebesell *et al.*, 2000). Marine plankton play an essential

role in the carbon cycle because they are responsible for maintaining the biological pump - an efficient mechanism for moving particulate carbon from the surface ocean to the deep ocean (Section 1.2.1). Given the current changes in atmospheric CO_2 and marine DIC, and the potential consequences these may have on the health of the ocean and the carbon cycle, it is imperative that this area of research is given our full attention. Only through consistent and routine monitoring of the marine carbon cycle and research on how the flow of carbon may be affected by changing environmental conditions will a thorough understanding of the carbon cycle be attained. Thus part of this thesis will be to assess the strength of the biological pump under different environmental regimes.

1.2 Concepts of Carbon Export

1.2.1 The Biological Pump

Biological activity uses dissolved CO_2 during photosynthesis, as discussed in Section 1.1.2, to form organic material. The reverse of this reaction is the catabolic process of respiration and the photosynthetic reaction expressed in Eq. 1.1 can be shown as reversible to include both photosynthesis and respiration (Eq. 1.3).

$$6CO_2 + 6H_2O \underset{\text{Respiration}}{\overset{\text{Photosynthesis}}{\leftrightarrow}} C_6H_{12}O_6 + 6O_2 \qquad \text{Eq. 1.3}$$

When CO_2 is fixed during photosynthesis, carbon enters the particulate organic carbon (POC) pool. Particulate forms of carbon, such as dead organisms and faecal pellets, readily sink through the water column with sinking rates of up to several hundred metres per day (Peterson *et al.*, 2005). This therefore promotes the downward transport of carbon (Behrenfeld and Falkowski, 1997) through the water column. This sinking of particulate carbon to the deep ocean is a key step in the carbon cycle because without it the downward movement of carbon through the water column would be left only to physical process such as downwelling and turbulent mixing that would result in a much slower movement of carbon to the deep ocean. Of the CO_2 that enters the surface ocean about 5-20% is transported to the deep ocean by means of the biological pump (Broecker, 1974; Buesseler, 1998; Buesseler *et al.*, 2007; Prentice *et al.*, 2001). This

biologically mediated process in the movement of carbon in the marine environment is chronically understudied (Buesseler *et al.*, 2007). Reviews on this subject can be found in (Boyd *et al.*, 1999; Boyd and Trull, 2007). The majority of organic carbon that enters the ocean interior (mesopelagic zone) is respired by heterotrophs back into the deep ocean DIC pool.

1.2.2 Carbon Export

Particles settling through the water column constitute a complex mix of biogeochemical material, the makeup of which can vary considerably from one type of ocean setting to another (Gross and Gross, 1996). Major constituents of settling particles include organic carbon, calcite and silica and can be directly representative of the dominant planktonic groups in the overlying waters (DiTullio *et al.*, 2000; Haidar *et al.*, 2000; Sarthou *et al.*, 2005). Below the euphotic surface ocean, organic carbon is of particular importance because it fuels all biological respiration. To put the biological pump in perspective, the flux of carbon to the deep ocean is an order of magnitude greater than the current dissolution of anthropogenic CO_2 into the surface ocean (Prentice *et al.*, 2001).

There are several approaches to measuring carbon export; direct techniques that use bottom moored, surface tethered or neutrally buoyant sediment traps (Honjo and Doherty, 1988; Knauer *et al.*, 1979; Salter *et al.*, 2007; Sanders *et al.*, 2003; Stanley *et al.*, 2004; Valdes and Price, 2000), indirect proxy style measurements such as the thorium-234 particle tracer technique (Bhat *et al.*, 1969) or with estimates of new production using techniques such as nutrient draw-down budgets and ^{15}N assimilation estimates (Dugdale and Goering, 1967; Jennings *et al.*, 1984; Sanders *et al.*, 2005). Each of these techniques offers an insight into carbon export at varying depths in the water column and over varying temporal and spatial scales.

1.2.3 New Production, the *f*-ratio and Export Production

Dugdale and Goering (1967) recognised that primary production can be supported by two sources of nutrients: 1) new nutrients and 2) regenerated nutrients. Sources of new nutrients include nutrients that have been diffused or upwelled from deep nutrient rich waters, deposited from atmospheric sources such as dust and rain water, riverine inputs and the more recently recognised diazotrophic input of nitrogen

fixation (Carpenter and Romans, 1991; Dugdale *et al.*, 1961; Simpson, 1966). Regenerated nutrients are nutrients that are released above the nutricline during the process of remineralisation. Therefore it follows that production which results from new nutrients is called new production, and production that results from regenerated nutrients is called regenerated production. The ratio of new production to total production (new + regenerated) is known as the *f*-ratio (Eq. 1.4) (Eppley and Peterson, 1979).

$$f-ratio = \frac{new\ production}{new + regenerated\ production} \qquad \text{Eq. 1.4}$$

The *f*-ratio shows how much of total primary production is fuelled by new nutrients entering the euphotic zone. *f*-ratios can be determined by tracing any major element contained within phytoplankton but is typically measured using nitrogen as this is a major constituent of cells and has a reasonably constant ratio with carbon and phosphorus (Dugdale and Goering, 1967). The forms of new (nitrate) and regenerated (ammonium and urea) nitrogen are also chemically distinct allowing for easy distinction.

However, this clear-cut idea of new nitrate only originating from deep waters and external sources has become more complex with the knowledge that nitrate can also originate from within surface waters through nitrification (Dore and Karl, 1996; Dore *et al.*, 1998; Yool *et al.*, 2007). This study will use the classical definition of new production because nitrogen fixation is constrained to low latitudes (Hood *et al.*, 2004); and nitrification global distributions are not well constrained (Yool *et al.*, 2007) but may possibly be lower in high latitudes that are characterised by higher *f*-ratios (Yool *et al.*, 2007) and lower concentrations of N_2O, which is a by-product of nitrification (Nevison *et al.*, 2003).

To sustain a balance of organic material in the surface ocean, the amount of production that results from new sources of nitrogen must be equal to the amount of organic material exported, otherwise concentrations of organic material would continually increase or decrease. Consequentially the amount of material exported (export production) must equal that of new production so as to maintain a balance over appropriate temporal and spatial scales (Eppley and Peterson, 1979). By combining the

f-ratio with production estimates from satellite-derived chlorophyll distributions it then becomes possible to estimate the global export of photosynthetic carbon at between 11-16 Gt C y^{-1} (Figure 1.4) (Behrenfeld and Falkowski, 1997; Falkowski *et al.*, 1998; Falkowski *et al.*, 2003).

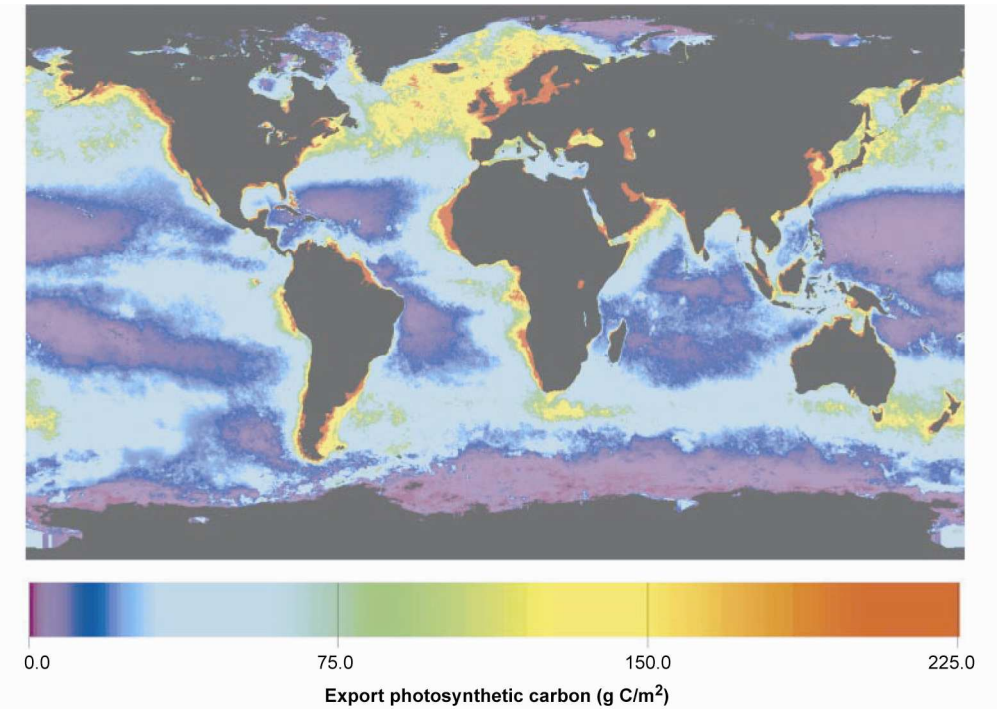

Figure 1.4 Map of export production taken from Falkowski *et al.* (1998). Note the large area of low export in the Southern Ocean.

1.3 The Iron Hypothesis

The high latitude Southern Ocean is typically regarded as a high-nutrient, low-chlorophyll (HNLC) environment. Despite an abundance of inorganic nutrients (nitrate, silicate and phosphate) the Southern Ocean fails to support extensive phytoplankton blooms. This phenomenon was reported in the scientific literature as far back as the 1930's by investigators such as Ruud (1930) and Gran (1931), and the idea that iron was a limiting nutrient for phytoplankton growth was reported in papers by Harvey (1933; 1937). Other early works on the relationships of iron and phytoplankton growth were also published by Cooper (1935), Braarud (1935) and Braarud and Klem (1931). The hypothesis of iron limitation in the Southern Ocean was also clearly stated twice in the Discovery Reports by Hart (1934) and again by Hart (1942). This early work in forming the idea of iron limitation suggested that neritic sources were

introducing iron through rivers discharging humic acids, thus explaining the reason why coastal and open Southern Ocean areas displayed such different characteristics in phytoplankton abundance. Although the influence of river runoff on phytoplankton is often seen it did not explain the large-scale patterns of open ocean HNLC areas simply because of analytical limitations of the day. Consequently the idea of this early iron hypothesis remained unchanged for half a century and it was only with the advent of trace-metal clean techniques in the 1970's did the extent of vanishingly low iron concentrations in the open ocean become apparent (review by Martin, 1991). This sparked a revolution in trace-metal analysis and resulted in the understanding that new production in HNLC areas is potentially mediated by multiple sources: upwelling of deep iron-rich waters, atmospheric dust deposition and potentially hydrothermal inputs (Bennett *et al.*, 2008; Charette *et al.*, 2007; Donaghay *et al.*, 1991; Duce and Tindale, 1991; Jenkins *et al.*, 2007; Planquette *et al.*, 2007; Winckler *et al.*, 2007). Additionally, aeolian sources of iron are mainly in the northern hemisphere resulting in approximately eight times more iron deposited in the northern hemisphere when compared to the southern hemisphere (Duce and Tindale, 1991). Therefore the remoteness of the Southern Ocean from the major terrestrial sources results in very low (pM) dissolved iron concentrations (Martin *et al.*, 1990b). For a more detailed discussion on iron in the oceans see reviews by Johnson *et al.* (1997) and Ussher *et al.* (2004).

This new understanding of iron's limiting role was successfully tested in Antarctic waters by Martin *et al.* (1990b). This was published in parallel to the modern day iron hypothesis that tackled the idea of the inter-relation between glacial/interglacial atmospheric CO_2 concentrations and the iron limited productivity of Southern Ocean phytoplankton (Martin, 1990). Other early iron limitation experiments also lead to similar but less convincing results as to the sole role of iron in limiting phytoplankton growth (Buma *et al.*, 1991; de Baar *et al.*, 1990). Consequently these studies provided the motivation, along with ever increasing atmospheric CO_2, for a host of meso-scale, *in situ* iron fertilisation experiments to determine the effects that iron fertilisation may have on carbon sequestration to the deep ocean (Boyd *et al.*, 2004; Boyd *et al.*, 2000; Coale *et al.*, 2004; Coale *et al.*, 1996; Gervais *et al.*, 2002; Hoffmann *et al.*, 2006; Martin *et al.*, 1994; Tsuda *et al.*, 2003) (Figure 1.5).

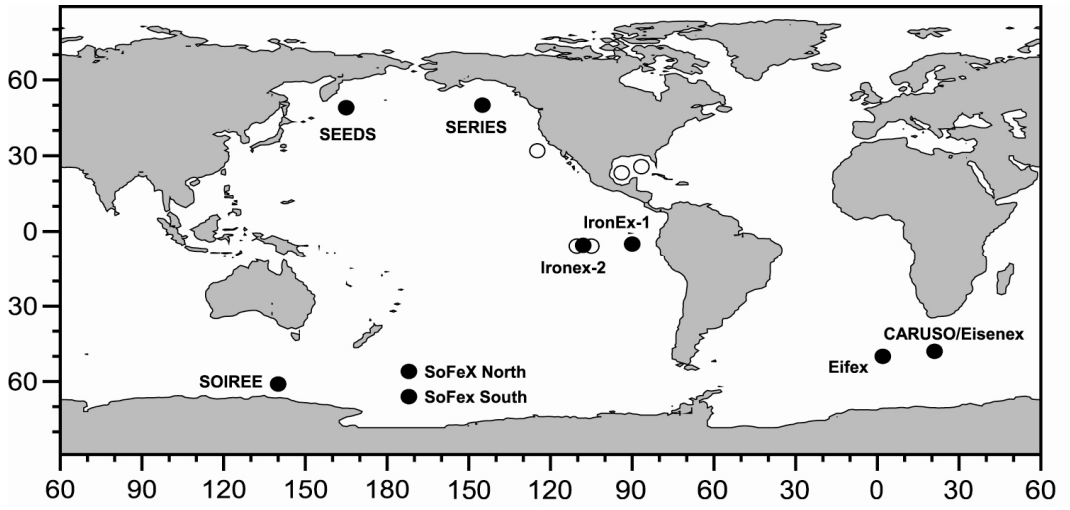

Figure 1.5 Map showing locations of all the artificial fertilisation experiments to date. Map taken from de Baar *et al.* (2005).

During this period of scientific endeavour the Southern Ocean received most attention, not only because it covers such a large area *ca.* 20 x 10^6 km^2, but also because it is the largest HNLC area (Watson, 2001) and it has the potential to play a significant role in the global carbon cycle by acting as a sink of atmospheric CO_2. Current estimates suggest that the Southern Ocean is responsible for the uptake of about 1 Gt C y^{-1} (Metzl *et al.*, 1999), approximately 1% of the 90 Gt C y^{-1} taken up by the world's oceans annually (Prentice *et al.*, 2001). However, models indicate that this figure has the potential to rise to 6-30 Gt C y^{-1} given a scenario of complete nutrient utilisation supported by iron replete conditions (Sarmiento and Orr, 1991). The ability to induce phytoplankton blooms with the addition of iron raised hopes that it may be actually possible to sequester anthropogenic CO_2 in the deep ocean (Martin, 1990). However, the implications, uncertainties and ethics of large-scale geoengineering was hotly debated in the scientific literature (Joos *et al.*, 1991a; Joos *et al.*, 1991b; Martin *et al.*, 1990a; Peng and Broecker, 1991a; b; Sarmiento, 1991a; b; Sarmiento and Orr, 1991; Watson *et al.*, 1991) and still is today (Buesseler *et al.*, 2008a).

1.3.1 Artificial Iron Fertilisation Experiments

To date, four iron fertilization experiments have been carried out in the Southern Ocean (Figure 1.5) and have successfully produced phytoplankton blooms: SOIREE (Boyd *et al.*, 2000), EISENEX (Gervais *et al.*, 2002), SOFEX (Coale *et al.*, 2004) and EIFEX (Hoffmann *et al.*, 2006), but the extent to which iron induced blooms can

sequester carbon to the deep ocean is still poorly constrained (Bishop *et al.*, 2004; Buesseler *et al.*, 2005; Charette and Buesseler, 2000; Nodder *et al.*, 2001; Rutgers van der Loeff and Vöge, 2001). This is probably because carbon export may mainly occur significantly after the initial iron fertilisation (Buesseler *et al.*, 2005; Buesseler and Boyd, 2003), a time period that has been poorly sampled. Today there is generally no doubt in the scientific community that iron can be used to promote phytoplankton growth in the Southern Ocean. However, determining whether iron fertilisation could be used to reduce atmospheric CO_2 has been an elusive question to answer (Chisholm *et al.*, 2001; Johnson and Karl, 2002; Zeebe and Archer, 2005; Zeebe and Archer, 2006). Even though there remains continued discussion in the scientific literature as to whether iron fertilization is a feasible strategy to sequester anthropogenic CO_2 (Buesseler and Boyd, 2003; Buesseler *et al.*, 2008a), the impetus and need to understand the effects of iron on phytoplankton productivity and the biological pump should be no less great.

Artificial iron fertilisation experiments have focussed on just the alleviation of iron limitation by adding iron in the form of $FeSO_4$. Although these elegant experiments have successfully shown the *in situ* link between iron enrichment and enhanced productivity they are nonetheless simple perturbations of complex natural systems. Investigations over the past ten years have also revealed the extent to which other growth factors such as light, silicic acid and cell size also play a co-limiting role with iron (Franck *et al.*, 2000; Northcote and Neil, 2005; Sedwick *et al.*, 2002; Sunda and Huntsman, 1997; Timmermans *et al.*, 2001). Therefore, in addition to artificial iron fertilization experiments, recent years have seen efforts to try and understand the effects of natural iron fertilization in HNLC regions. In naturally fertilised systems the marine environment is influenced by a host of environmental factors, more than could ever be manipulated in artificial experiments, such as upwelling, mixed layer depth and the supply of other limiting micronutrients like vitamin B_{12} (Bertrand *et al.*, 2007). This contrasts with artificial iron fertilization experiments in which the concentration of only one micronutrient is changed. Thus the challenge with natural fertilization experiments will be to establish links between specific limiting factors and environmental responses.

1.3.2 Natural Iron Fertilisation Experiments

The existence of large-scale blooms in the Southern Ocean tied to topographic features is clearly observable with satellite imagery and it is hypothesised that these

blooms are sustained by a release of iron into the surrounding waters (Figure 1.6). The most notable of these are austral summer blooms associated with South Georgia, Crozet and Kerguelen (Bucciarelli *et al.*, 2001; Korb and Whitehouse, 2004; Pollard *et al.*, 2002). Evidence supporting this hypothesis for the Kerguelen Islands, South Georgia and the Crozet Islands has been reported by Blain *et al.* (2007; 2001), Holeton *et al.* (2005) and Planquette *et al.* (2007) respectively. In studying these areas it may be possible to better understand the implications of iron fertilisation and thereby improve our ability to assess the response and efficiency of the biological pump to inputs of iron. This type of approach to investigating iron limitation holds the advantage over artificial fertilisation experiments in that iron is supplied naturally all year round. This allows the timing of the cruise to coincide with the processes of interest, in this case, the resultant carbon export.

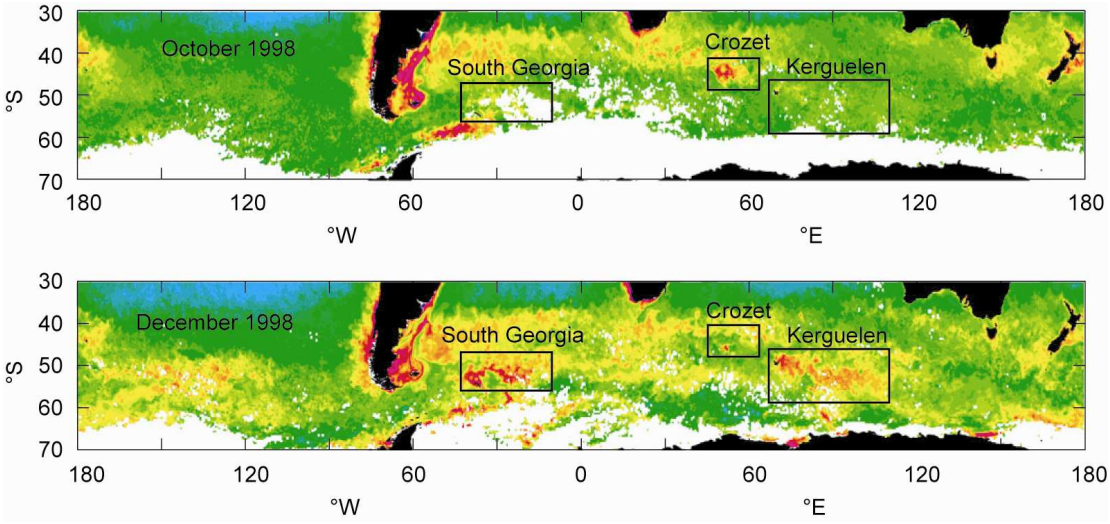

Figure 1.6 Southern Ocean satellite chlorophyll map. SeaWIFS image taken from Pollard *et al.* (2007a) showing phytoplankton blooms associated with topographic features.

1.4 Importance of the Southern Ocean

Much of this introduction has focused on the Southern Ocean as the region of interest but has not attempted to define the Southern Ocean or highlight the physical and chemical reasons why it is so important. This section aims to explain the biogeochemical importance of the Southern Ocean as a carbon sink after a brief introduction to the physical characteristics of the region.

The body of water that encircles the Antarctic continent is not always routinely regarded as a distinct ocean, but this oceanic region is often referred to as the Southern Ocean implying it is an ocean in its own right, and there are good reasons for this. Apart from being a meteorologically unique area with year round strong prevailing westerlies that drive the transport of the eastward flowing Antarctic Circumpolar Current (ACC) (Nowlin and Klinck, 1986), there are also strong and definite water structures that separate it from the oceans farther north. Strong latitudinal boundaries in physical parameters such as salinity and temperature exist as one progresses north from the cold waters that surround Antarctica, across the ACC and into the warm waters of the subtropical gyres (Belkin and Gordon, 1996; Orsi *et al.*, 1995; Whitworth and Nowlin, 1987). If a boundary had to be placed on where one leaves the Southern Ocean and enters either the Atlantic, Pacific or Indian Ocean it would have to be the SubAntarctic Zone (SAZ) (Pollard *et al.*, 2002). The SAZ is characterised by surface temperatures that are high enough to allow stratification to be controlled by temperature rather than by salinity, and thus allows the possibility for salinity to decrease with depth. Therefore the SAZ is also characterised with a distinct subsurface salinity minimum (Pollard *et al.*, 2002). Henceforth the Southern Ocean will be regarded as a discrete ocean with the SAZ as a boundary between the other oceans further north.

The Southern Ocean is also crucially important for allowing the completion of the global thermohaline circulation. Simply, the Oceanic Conveyor Belt starts with the formation of cold dense water in the North Atlantic that sinks and travels south and into the eastward flowing circumpolar Southern Ocean. Branches from the Southern Ocean reach into the Indian and Pacific Oceans before finally completing the circuit by returning to the North Atlantic (Broecker, 1987; 1991). The oldest waters of the deep circulation take about 1600 years before they are ventilated by the atmosphere (Primeau, 2005). This is an over simplification of a hugely complex ocean circulation system but highlights the importance of the Southern Ocean in linking the oceanic basins together. The Southern Ocean allows all the major oceans to be mixed resulting in the transport of heat, nutrients and gases around the world, thus creating a global ocean system.

The Southern Ocean also has characteristic biogeochemcial features. As discussed in Section 1.3 the Southern Ocean is an HNLC area - despite abundant inorganic nutrients (nitrate, silicate and phosphate), chlorophyll levels remain low. Reasons for this paradox were discussed in Section 1.3 with limited iron shown to be

the main mediating element of phytoplankton growth. Surface nutrient concentrations are high when compared to the subtropical oligotrophic gyres further north (Sarmiento *et al.* 2004). Nutrient rich deep water is upwelled close to the Antarctic continent and is then moved northwards by Ekman transport where biological use of nutrients is seen during the austral summer. Although nitrate and phosphate never become limiting south of the SAZ evidence of silicate limitation during diatom blooms has been recorded (Franck *et al.* 2000, Read *et al.* 2000, Sedwick *et al.* 2002, Smetacek 1998). Finally, it will be reiterated here that because the Southern Ocean has an abundant supply of nitrate and phosphate it has the potential to act as a major sink of carbon, which is the reason why its function as part of the Earth system needs to be investigated (see discussion in Section 1.3).

1.5 Rationale for the CROZEX Project

The focus of the CROZEX (CROZet natural iron bloom and EXport experiment) project is the annual bloom observed to the north of the Crozet Islands situated in the Indian sector of the Southern Ocean (Pollard *et al.*, 2007a; Pollard and Sanders, 2006). Pollard *et al.* (2002) hypothesised that this area is likely to be fertilised with iron from the plateau, giving rise to iron replete conditions that induce a phytoplankton bloom in this otherwise HNLC region. The multi-disciplinary CROZEX project aimed to survey the pervasive phytoplankton bloom to the north of the Crozet Islands and test the hypothesis that the islands and surrounding plateau are a source of bioavailable iron. In addition to an extensive physical hydrographic survey to better constrain the circulation and flow of the ACC in this region, a comprehensive set of biogeochemical observations was also made to categorise water column chemistry, bloom ecology and resultant carbon export.

Further to artificial iron fertilisation experiments, which have demonstrated that blooms can be induced with the purposeful addition of iron (Section 1.3.1), the CROZEX project can be viewed as a natural iron fertilisation experiment. The bloom observed around the Crozet Plateau offers itself nicely to study iron fertilisation because the bloom occurs consistently every year in the same region (Figure 1.7). Therefore this allows a good opportunity to plan for and execute a detailed study of what is now known to be a naturally iron-fertilised bloom (Planquette *et al.*, 2007). The bloom also allows the opportunity for observation during latter stages; without the need for artificial

fertilisation, sampling can be biased towards the exporting phases of the bloom therefore overcoming the time-scale issue of artificial fertilisation experiments discussed in Section 1.3.1.

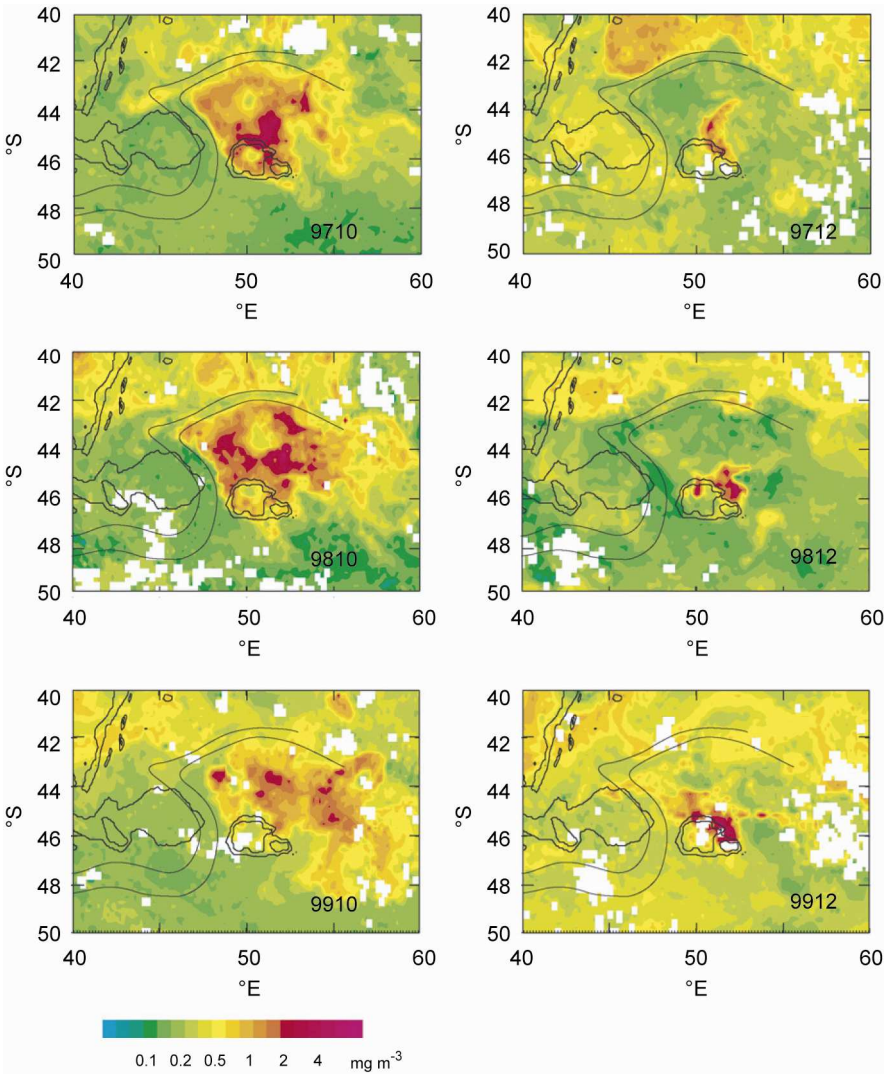

Figure 1.7 Monthly SeaWIFS chlorophyll composites (October and December) for 1997 - 1999 of the Crozet region (taken from Pollard *et al.*, 2007a). Note the consistency and regularity of the bloom each year. The two smooth curving lines show the major northern permanent branch of the ACC that forms the SAF.

1.5.1 Physical Setting

The Crozet Islands lie within the ACC that has a generally eastwards flow. As the ACC encounters the Del Caño Rise and the Crozet Plateau it is forced to fragment with one filament pushed northwards and another filament skirting south of the topographic features (Figure 1.8). The northern filament flows north between the

Del Caño Rise and the Crozet Plateau, turns west following constant depth topography, resulting in an anticyclonic flow, before finally turning east as part of the Crozet Front (Pollard and Read, 2001) (Figure 1.8). It is believed that the northern branch of the ACC is a physical constraint on the spatial distribution of the Crozet bloom (Pollard *et al.*, 2002). For a complete overview of the circulation around the Crozet archipelago see Pollard *et al.* (2007b).

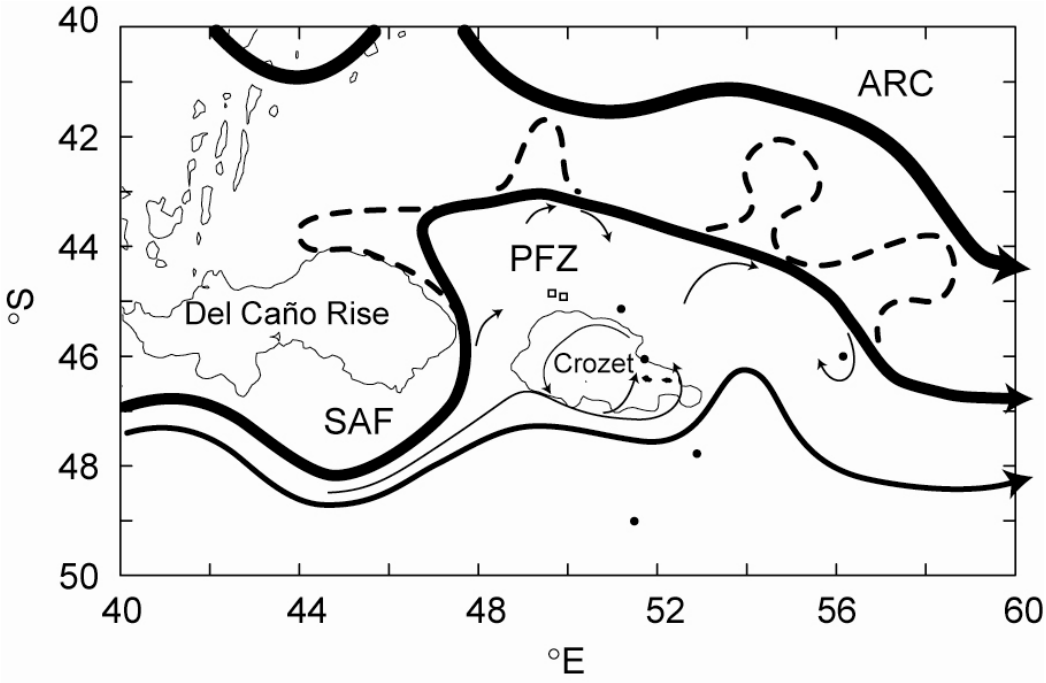

Figure 1.8 Water transport around the Del Caño Rise and the Crozet Plateau. Agulhas Return Current (ARC), SubAntarctic Front (SAF) and Polar Frontal Zone (PFZ). Also shown is the eastward flow south of Crozet and 2000 m bathymetry contours (taken from Pollard *et al.*, 2007b).

The Crozet archipelago consists of 5 islands, with a plateau that covers an area of approximately 1200 × 600 km. The plateau rises from a surrounding abyssal depth of ≈3800 m to form a subsurface plateau 0-1000 m deep. The two major islands, *Île de l'Est* and *Île de la Possession*, are centred around 52°E and 46.4°S, approximately 2500 km southeast of Durban, South Africa (Figure 1.9). *Île de l'Est* and *Île de la Possession* reach maximum heights of 1090 m and 934 m and cover areas of 130 km^2 and 150 km^2 respectively. Their remoteness from continental landmasses means they are ideally located for studying island effects in this HNLC region.

1.5.2 Cruise Overview

Sampling for the CROZEX project took place from November 2004 to January 2005 on two cruises onboard the RRS *Discovery*, cruises D285 and D286, which will be referred to as leg 1 and leg 2 respectively from hereon (Pollard *et al.*, 2007a; Pollard and Sanders, 2006). Figure 1.9 shows the location of the working area and Table 1.1 gives the timing of major cruise waypoints.

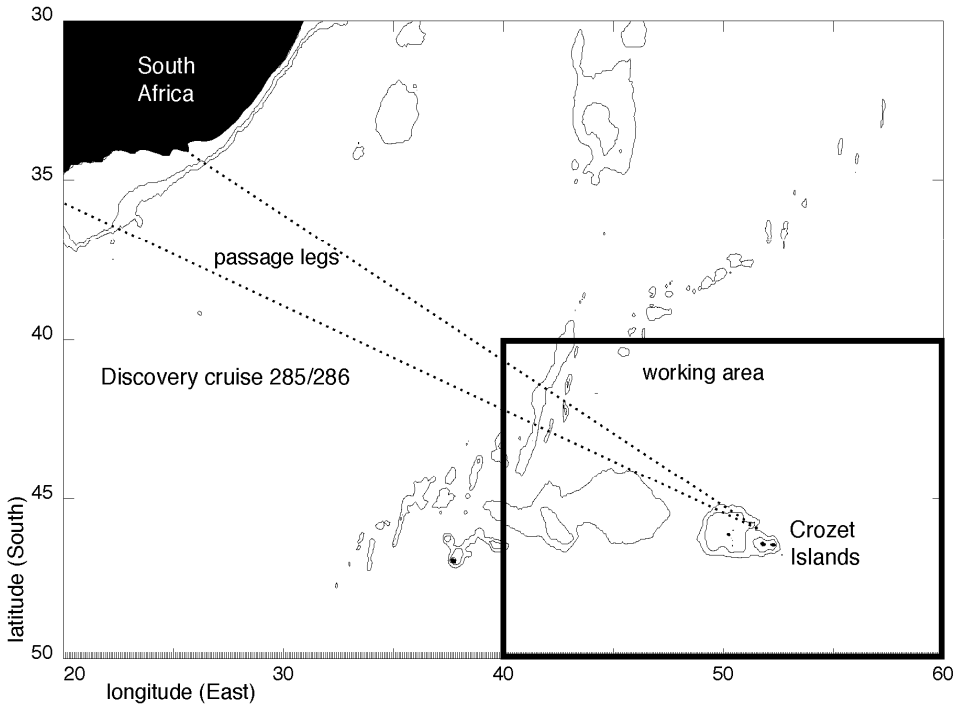

Figure 1.9 Location map of the Crozet Islands, Indian sector of the Southern Ocean (courtesy of Raymond Pollard).

Table 1.1 Dates of arrival and departure from South Africa and the study site.

Cruise	Departure from South Africa	Arrival at study site	Departure from study site	Arrival at South Africa
D285	03/11/04	09/11/04	05/12/04	10/12/04
Leg 1	Cape Town	Station J	Station K	Port Elizabeth
D286	13/12/04	18/12/04	15/01/05	21/01/05
Leg 2	Port Elizabeth	Station K	Station M3	Durban

1.6 Thesis Objectives

The key research goals of the CROZEX project as a whole were to better constrain the circulation and mixing regime around the Crozet Islands, to test the hypothesis that bioavailable iron is sourced from the plateau and to examine the

biological response to iron release (Pollard *et al.*, 2007a). A key aspect of how this *Ph.D.* thesis contributes to the CROZEX project will be to assess and quantify the magnitude and activity of the bloom's biological pump. Several techniques will be used to achieve this with the proxy particle tracer thorium-234 (^{234}Th) forming the central tool to quantify carbon export. Finally, by combining information on primary, new and export production a carbon budget will be formulated. The overarching hypothesis to be tested is: does a topographically associated bloom in the HNLC Southern Ocean export more POC to mesopelagic depths, than a low productivity non-bloom control site?

1.6.1 Thesis Structure

Chapter 2 presents a detailed account of all the methods used with focused discussion on the complex ^{234}Th proxy particle tracer technique. Other methods include accounts of inorganic nutrient analysis and dissolved organic nitrogen analysis. Additionally, brief descriptions of several ancillary parameters made by other CROZEX participants are also presented. Chapter 3 presents the results of ^{234}Th-derived carbon export (^{234}Th-Cex) and makes a preliminary comparison between daily rates of ^{234}Th-Cex and estimates of temporally integrated primary and new production. Chapter 3 concludes that daily rates of export do not show the same pattern as new production and presents four possible explanations of why this might be. Chapters 4 and 5 then explore the inventories and variations in the dissolved and particulate organic phases respectively, in an attempt to explain the observed patterns in new and export production. Finally, Chapter 6 reconciles the differences in new and export production by reassessing the ^{234}Th data in the context of the silicon cycle to formulate a complete carbon budget for the Crozet region. Chapter 7 thus presents the major findings of the thesis and suggests ideas for future work.

1.6.2 Terminology

Although some of these terms have already been used in the introduction this is a good point at which to define some key terms that will be used from hereon. In doing so it is hoped that the reader will have a clear (definitive) understanding of the definition of each term.

Primary production

Primary production, if not defined for the context in which it is to be used, is a term that can mean two different things: total primary production and net primary production (or alternatively, total community production and net community production respectively). Total primary production is the total amount of organic matter production. Net primary production is total primary production minus respiration, see below. Primary production consumes CO_2 and releases O_2.

Respiration

The metabolic degradation of organic material into inorganic forms. Respiration consumes O_2 and releases CO_2, and is the major contributor to the process of remineralisation (See below).

Remineralisation

The breakdown of biogenic minerals or organic material into soluble mineral forms.

New production

The amount of nitrogen (or carbon) production that is sustained by new forms of nitrogen, classically nitrate that has been brought up to the surface from deep nitrate rich waters (Dugdale and Goering, 1967; Eppley and Peterson, 1979) (Section 1.2.3).

Regenerated production

Also referred to as recycled production, is the amount of nitrogen (or carbon) production that is sustained by regenerated forms of nitrogen (ammonium and urea) that originate from within the surface ocean (Eppley and Peterson, 1979) (Section 1.2.3).

Export production

This is the amount of production that is exported out of the surface ocean. To maintain a steady-state (over seasonal time-scales) of organic material in the surface ocean, any production that is the result of new nutrient sources must be exported out of the surface ocean (Eppley and Peterson, 1979). Otherwise, stocks of organic material would continually increase. Consequently, export production and new production are often considered as equivalent (Section 1.2.3).

Carbon export

This is the active downward pathway that removes organic carbon and inorganic calcite from the surface ocean. Carbon export is mediated by biology, a process known as the biological pump (See below and Section 1.2.2).

Biological pump

This is the biologically mediated process that aids in the transport of carbon from the surface ocean to the ocean interior (Section 1.2.1).

HNLC

High-nutrient, low-chlorophyll. Some areas of the world ocean have low chlorophyll levels despite high levels of macro-nutrients (Section 1.3).

2 Methods

2.1 Introduction

Of the methods used for this work, some are well established and some are used less frequently. There are many reasons why one method is chosen over another when measuring one particular parameter. These reasons include the level of accuracy and precision required, ease of carrying out the assay while at sea or on land, volume of sampling device, sample volume required, time restrictions for sampling (wire-time) and for sample processing, equipment availability, compatibility with other assays, data comparison with other studies and of course, cost.

The methods for the various parameters measured will be presented here. The main methods include total thorium-234 (^{234}Th), use of *in situ* pumps, determination of inorganic nutrients and dissolved organic nitrogen and sample preparation of POC/N samples. In addition to these a brief outline of several ancillary measurements will also be given. Of the methods used, the determination of ^{234}Th is the most involved, both conceptually, analytically and mathematically. The ^{234}Th technique is a very powerful method for quantifying particle export, however it carries with it an array of technicalities and limitations which are only now becoming better understood by the wider oceanographic community (Rutgers van der Loeff *et al.*, 2006). Therefore more in depth discussion of the ^{234}Th method will be presented.

2.2 Determination of ^{234}Th

In this study the radioactive particle tracer ^{234}Th (Bhat *et al.*, 1969) was used to estimate how much photosynthetically fixed CO_2 was exported to mesopelagic depths as particulate organic carbon (POC) (Buesseler *et al.*, 1992). ^{234}Th is the daughter isotope of naturally occurring uranium-238 (^{238}U), which is conservative in seawater and proportional to salinity (Chen *et al.*, 1986; Ku *et al.*, 1977). Unlike ^{238}U, ^{234}Th is insoluble in seawater and adheres to particles in the water column. As particles sink through the water column a radioactive disequilibrium is formed between ^{238}U and ^{234}Th which can be used to quantify the rate of particle export from the surface ocean when combined with data on the ratio of POC to particulate ^{234}Th activity (Tsunogai and Minagawa, 1976). The remainder of this section will be dedicated to a detailed explanation of this novel particle tracer technique.

2.2.1 The Crux of the ^{234}Th Technique

To understand how the ^{234}Th technique works there are several basic principles that must be understood and these are discussed in the following sections. The first concept to be introduced is that ^{238}U is conservative and ^{234}Th is non-conservative. ^{234}Th ($t_{½}$ = 24.1 d) is a naturally occurring radioactive isotope and only exists through the radioactive decay of its parent isotope ^{238}U ($t_{½} = 4.47 \times 10^9$ y). This pair of isotopes makes up the first part of the ^{238}U decay-series that only finishes once the stable isotope of lead-206 (^{206}Pb) is reached (Figure 2.1). ^{238}U, which is a long-lived primordial nuclide, behaves as a conservative dissolved element in oxygenated seawater. In contrast, its daughter ^{234}Th is not conservative. ^{234}Th is particle reactive and readily "sticks" to particles it encounters in the water column, hence this property can be used to trace the movement of particles. This switch in properties from conservative to particle reactive, as ^{238}U decays to ^{234}Th is the key concept behind the ^{234}Th technique when used to trace particle movement. For introductory texts see Bourdon *et al.* (2003), Cochran and Masqué (2003), Krishnaswami (2001) and Rutgers van der Loeff (2001).

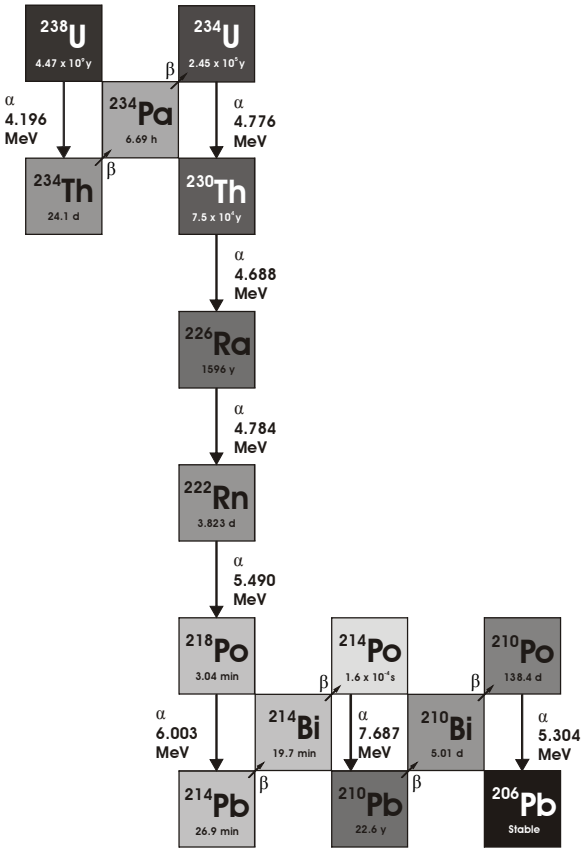

Figure 2.1 ^{238}U decay-series redrawn from Bourdon *et al.* (2003). Half-lives and decay energies are given for each isotope. The gray scale reflects the half-life with darker grays for longer half-lives.

2.2.2 Radioactive Equilibrium

The property that makes it possible to use the ^{238}U series decay-series (and other decay-series) for time-scale studies are the rates of decay of daughter radionuclides. ^{238}U has a longer half-life ($t_{½}$) than any of its daughter products in the decay-series chain with, of course, the exception of ^{206}Pb which is stable (Figure 2.1). If this decay-series is left unperturbed in a closed system, with no form of fractionation for *ca.* 1.5×10^6 y ($6 \times t_{½}$ of longest lived daughter, ^{234}U), then the decay-series will reach a state of equilibrium, commonly referred to as secular equilibrium or radioactive equilibrium. Simply, this means that the activities of all the isotopes are the same.

Taking $^{238}U/^{234}Th$, the nuclide pair of interest, secular equilibrium will be reached in *ca.* 150 d ($6 \times t_{½}$ of ^{234}Th), providing the isotope pair is in a closed system. This results in an activity of ^{234}Th that is equal to the activity of ^{238}U - when an atom of ^{238}U decays to ^{234}Th, this atom of ^{234}Th can then decay to ^{234}Pa, but an additional atom of ^{234}Th can only decay when another one is produced from the decay of ^{238}U. The mathematical derivations that surround the idea of secular equilibrium within a decay-series were originally solved by Bateman (1910). These equations will not be presented here, however a clear account of these formulae can be found in Faure (1986) and Bourdon *et al.* (2003).

It must be made clear that activity (A) with units of disintegrations per minute (dpm), should not be confused with the rate of decay (λ) with units of time^{-1}. However, the activity is linked to the rate of decay by Eq. 2.1 where N is the number of parent atoms. λ is calculated by Eq. 2.2 and is linked to the half-life by a natural log 2 ($\ln 2 = 0.693$) function that explains the exponential nature of radioactive decay. The values of λ and $t_{½}$ are specific to individual radionuclides.

$$A = \lambda N \qquad \text{Eq. 2.1}$$

$$\lambda = \frac{\ln 2}{t_{1/2}} \qquad \text{Eq. 2.2}$$

2.2.3 Radioactive Disequilibrium

Section 2.2.2 discussed the principles of secular equilibrium, provided the only process that is acting on these isotopes is radioactive decay. The concept of radioactive disequilibrium will now be introduced and how this is brought about by the "sticky" property of ^{234}Th. Radioactive disequilibrium is when the activity of a parent-daughter pair is not the same.

Whenever a parent-daughter pair is out of secular equilibrium it is said to be in disequilibrium. Disequilibrium can either be positive or negative and both of these are observed in ^{238}U/^{234}Th studies, although the predominant type of disequilibrium observed when looking at surface particle fluxes is a negative disequilibrium: one in which the activity of ^{234}Th is less than ^{238}U. A negative disequilibrium is set up in the following way: conservative ^{238}U decays to particle reactive ^{234}Th. The ^{234}Th sticks to particles in the water column. These particles sink through the water column taking ^{234}Th with them which leaves behind lower levels of ^{234}Th than would be expected based on ^{238}U concentrations. Therefore a negative disequilibrium is set up in the surface water. See overviews by Krishnaswami (2001) and Cochran and Masqué (2003). Figure 2.2 is a schematic of a disequilibrium profile. The dashed line is the activity of ^{238}U and the solid line is the activity of ^{234}Th. The hashed area is the disequilibrium between ^{238}U and ^{234}Th and is representative of the removal of ^{234}Th through the downward movement of particles. Ultimately the measured disequilibrium will be converted into an estimate of particulate flux.

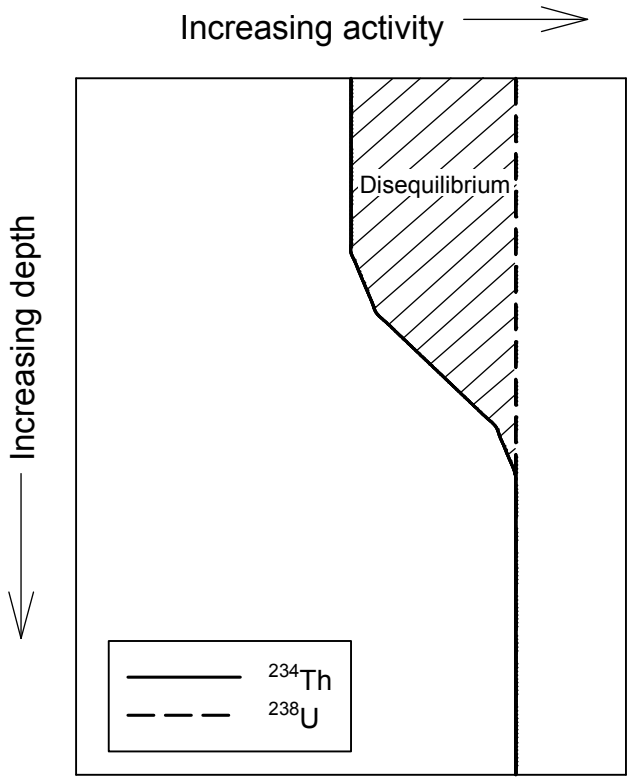

Figure 2.2 Schematic of the disequilibrium observed in the upper water column between ^{238}U and ^{234}Th. The hashed area is representative of ^{234}Th removal.

2.2.4 ^{238}U-Salinity Relationship

^{238}U is conservative in oxygenated seawater and can therefore be calculated from salinity (Chen *et al.*, 1986; Delanghe *et al.*, 2002; Ku *et al.*, 1977; Rutgers van der Loeff *et al.*, 2006). ^{238}U activities (A_U, dpm l^{-1}) were calculated from the relationship published by Chen *et al.* (1986) where $A_U = 0.0686 \times$ salinity, based on the average uranium concentration in seawater of 3.238 ng g^{-1} normalised to a salinity of 35. The uncertainty in the ^{238}U-salinity relationship was estimated to be ≈3.3%, an average of linear regression errors at the 68.3% (1σ) and 95.4% (2σ) confidence levels in the data by Chen *et al.* (1986). Traditionally the 1σ uncertainty of the Chen *et al.* (1986) data-set has been used as a representative uncertainty of ^{238}U activities. However, since the work of Chen *et al.* (1986) more data have been added to the ^{238}U-salinity relationship (eg. see compilations in Rutgers van der Loeff *et al.*, 2006; Speicher *et al.*, 2006) (Figure 2.3). Given the evolving shape of the ^{238}U-salinity data-set, an uncertainty of 3.3% is probably more representative than the 1σ uncertainty in the Chen *et al.* (1986) data-set usually used.

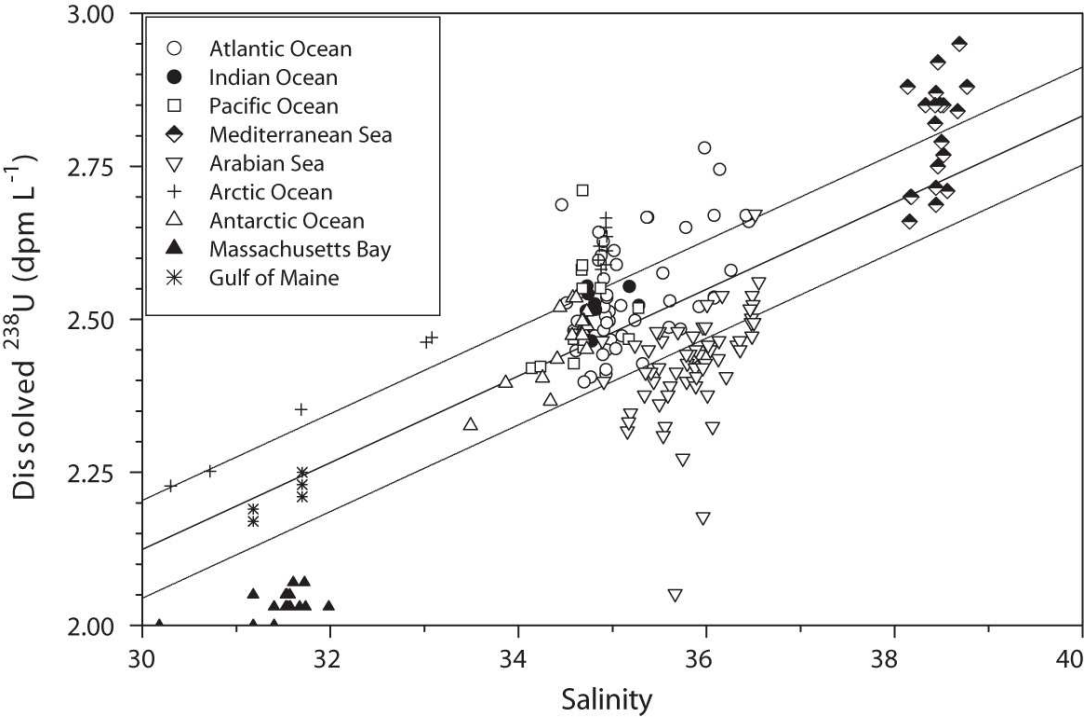

Figure 2.3 Taken from Rutgers van der Loeff *et al.* (2006) this figures shows a compilation of ^{238}U-salinity data (Chen *et al.*, 1986; Delanghe *et al.*, 2002; Gustafsson *et al.*, 1998; Ku *et al.*, 1977; Rengarajan *et al.*, 2003; Schmidt and Reyss, 1991, Charette, unpubl. results) from multiple ocean basins. The solid line is the Chen *et al.* (1986) relationship with ±2 σ spread in the data.

2.2.5 Laboratory Protocol

Two people were responsible for ^{234}Th analysis: Paul Morris (NOC) on leg 1 and Sandy Thomalla (UCT) on leg 2. The measurement of total (dissolved + particulate) ^{234}Th activity in seawater samples was based on the MnO_2 precipitation method described by Rutgers van der Loeff and Moore (1999), similar to the procedures used by Turnewitsch and Springer (2001) and Thomalla *et al.* (2006). The procedure was scaled to use 10 l samples and all apparatus were washed with a solution of 10 ml of 30% H_2O_2 in 1 litre of 1 M HCl followed by rinsing with Milli-Q water.

To 10 l (±0.002 l) aliquots of each sample, 3 drops of 25% NH_3 and 125 µl of 60 g l^{-1} $KMnO_4$ were added and mixed, followed by 50 µl of 400 g l^{-1} $MnCl_2 \cdot 4H_2O$. After thoroughly mixing again, which produces a MnO_2 precipitate, the samples were allowed to stand for 8 h. The precipitate was re-suspended and then filtered by positive pressure filtration onto a 142 mm diameter (0.8 µm pore size), polycarbonate, Isopore filter, (Millipore product ATTP 142 50), ensuring all the solution passed through the filtration apparatus. Before departure for fieldwork the filters were checked for

background activity in accordance with Rutgers van der Loeff and Moore (1999), and showed a combined filter and detector blank of 0.12 ± 0.02 cpm ($\bar{x}$ ± 1σ, n = 8) (cpm = counts per minute). Following filtration, the filters were rinsed with 50 ml of Milli-Q water to remove any salt and drained of excess water under vacuum. While filters were still damp they were folded exactly in half and allowed to air dry. Once dry, filters were folded with repeatable geometry into 18 × 18 mm squares, wrapped in mylar film, and counted onboard ship on a low-level beta GM multicounter system (Model Risø GM-25-5) using a 1% isobutene-99% argon carrier gas. Samples were counted to give a counting standard error of better than ±3% (*ca.* ≥1000 counts) and the final activity of ^{234}Th had a propagated error ranging from ±5-10%. Counting was conducted as soon as possible after sampling with repeated counting over a 6 month period (>6 $t_{½}$). This was to check that the activity decrease followed the decay of ^{234}Th and also allowed a background correction for activity intrinsic to the detector and from other long lived natural β-emitters. Counting of samples immediately after the cruise was done at the UCT by Sandy Thomolla, then counting was continued at NOC by Paul Morris after the samples and counter had returned to the UK. A regression analysis was carried out on the repeated counts to back calculate the ^{234}Th activity to the time of sampling. All ^{234}Th data are reported in units of disintegrations per minute per litre of seawater (dpm l^{-1}).

2.2.6 Calibration of the ^{234}Th Method

To calibrate the total ^{234}Th technique mid-water (1000 m) samples were used. These samples were collected well away from the surface ocean, coastal areas and seafloor nepheloid layers where rates of processes other than radioactive production and decay of ^{234}Th are negligible. Therefore ^{234}Th and ^{238}U are assumed to be in secular equilibrium with equal activities (Bacon and Anderson, 1982; Bacon *et al.*, 1996; Bacon and Rutgers van der Loeff, 1989; Bhat *et al.*, 1969; Buesseler *et al.*, 2005; Charette and Moran, 1999; Rutgers van der Loeff *et al.*, 2006; Rutgers van der Loeff *et al.*, 2002; Rutgers van der Loeff *et al.*, 1997). Based on these known ^{234}Th activities counting efficiencies of 0.26 ± 0.01 cpm dpm^{-1} and 0.28 ± 0.01 cpm dpm^{-1} (x ± 1σ) were determined for legs 1 and 2 respectively. The likeliest explanation for this slight difference between these two sets of samples is that a different operator performed the total ^{234}Th extractions and filter folding on each leg. Using the counting efficiencies for each leg and individual ^{238}U and ^{234}Th values for each sample, ^{234}Th:^{238}U activity ratios

at 1000 m were 1.00 ± 0.02 and 1.00 ± 0.02 ($\bar{x}$ ± 1σ, n = 10, n = 9) for legs 1 and 2 respectively. The corresponding reproducibility for total ^{234}Th activities was 2.44 ± 0.12 dpm l^{-1} (4.9%) and 2.46 ± 0.08 dpm l^{-1} (3.3%) ($\bar{x}$ ± 1σ, n = 10, n = 9) for legs 1 and 2 respectively. The extraction efficiency of ^{234}Th from seawater samples was estimated by re-precipitating a number of samples for a second time that were then processed in the same way as for a routine sample. The difference of ^{234}Th measured on the first and second precipitations was used to estimate the extraction efficiency. Extraction efficiencies were 98 ± 3% and 99 ± 3% ($\bar{x}$ ± 1σ, n = 10, n = 8) for legs 1 and 2 respectively and were therefore not considered to be significantly different from 100%. These extraction efficiencies compare well with the efficiencies reported by Rutgers van der Loeff and Moore (1999) and Turnewitsch and Springer (2001). The *in situ* activity per unit volume of water was calculated based on the *in situ* density.

2.3 High Volume Collection of Particulate Matter

To estimate POC export, the ratio of POC to particulate ^{234}Th activity (C:Th μmol dpm^{-1}) has to be applied to the measured ^{234}Th disequilibria. Although the majority of particles fall into the smaller (<10 μm) size classes (Simpson, 1982), it is thought that the larger particles dominate particle export (Fowler and Knauer, 1986). Therefore the >53 μm size class is considered to represent the bulk of particulates rapidly settling through the water column (Bishop *et al.*, 1977). To adequately sample the rarer large particles, large sample volumes must be filtered to allow enough material to be collected for analysis, with *in situ* filter pumps typically the method of choice (Buesseler *et al.*, 2006). Therefore, every time a profile for total ^{234}Th was taken, particles were collected by filtering large volumes of seawater through a 293 mm diameter, 53 μm nylon mesh. High volume filtration was carried out with an *in situ* stand-alone pump system (SAPS; Challenger Oceanic) deployed approximately 20 m below the mixed layer. The depth of the mixed layer was deduced from a combination of temperature, fluorescence and transmittance data collected in real time from the CTD package. Once on board, the particles were rinsed off the mesh and re-suspended with 1 l of thorium-free-seawater (the filtrate remaining after particulate and MnO_2 extraction). The suspension was split using a Folsom sample splitter so that ^{234}Th, POC, PON (POC/N) and biogenic silica (bSi) could be quantitatively measured on the same sample. Splits for POC/N and bSi were filtered onto a pre-combusted, pre-weighed, 25 mm GF/F filter and a 25 mm, 0.2 μm pore size, polycarbonate filter

respectively and stored at -20 °C. See Section 2.6.1 for POC/N and bSi analysis. The split for ^{234}Th analysis was filtered onto a 142 mm diameter, 0.8 μm pore size, polycarbonate, Isopore filter, (Millipore product ATTP 142 50), ensuring all the particles passed through the filtration apparatus. These filters were prepared for beta counting in the same way as that described for total ^{234}Th and using the same counting efficiency as that used for the total ^{234}Th samples.

2.4 Determination of Inorganic Nutrients

Four people were responsible for nutrient analysis: Mark Stinchcombe (NOC) and Richard Sanders (NOC) on leg 1, and Paul Morris and Megan French (UEA) on leg 2. Samples for inorganic nutrients: nitrate + nitrite (nitrate from hereon), silicate and phosphate were taken directly from Niskin bottles into 35 ml polystyrene coulter counter cups, pre-washed with sample, capped, and stored at 4 °C until analysis, typically within 24 h of sampling. Samples were measured on a three channel, segmented flow, Skalar SansPlus nutrient analyser based on the method by Kirkwood (1996). Nutrients are measured using colorimetry, whereby in general terms the chemical reaction between nutrients with certain compounds forms coloured complexes. The intensity of this colour can then be measured through the absorbance of light at the wavelength corresponding to the colour. The reagents used are shown in Table 2.1

Table 2.1 Summary of reagents and extinction wavelength for the analysis of each nutrient.

Assay & extinction	Reagent name	Reagents[a]	Quantity[b]
Nitrate	Buffer	Ammonium chloride	6.0 g
543 nm	Mixed reagent	Sulfanilamide	1.0 g
		4 M HCl	30 ml
		NEDD[c]	0.1 g
		10% BRIJ-35	1.0 ml
Silicate	Molybdate mix	5 M H_2SO_4	40 ml
810 nm		Ammonium molybdate	14 g
		Sodium dodecyl sulphate	2 g
	Oxalic acid	Oxalic acid	12 g
	Ascorbic acid	Ascorbic acid	32 g
Phosphate	Molybdate mix	5 M H_2SO_4	800 ml
880 nm		Ammonium molybdate	20 g
		Potassium antimonyl tartrate	0.4 g
	Ascorbic acid	Ascorbic acid	16 g
		Sodium dodecyl sulphate	2 g

[a]Analytical reagent grade.
[b]Quantities given are for making up a 2 l solution.
[c]Full name: n-(1-napthyl)-ethylenediamine dihydrochloride.

The 40 place autosampler was set to deliver a sample separated with a wash, each of 90 s duration, thus allowing one sample to be analysed every 3 minutes. The wash solution was an artificial seawater (ASW) solution (Section 2.4.1). The nutrient analyser was controlled by a computer running the FlowAccess software that automatically integrated sample peak heights and calculated the nutrient concentration based on a predefined calibration regime. A first order forced through zero calibration was used for phosphate and a second order forced through zero calibration was used for nitrate and silicate.

2.4.1 Calibration and Quality Control

One of the major challenges with running large batches of samples, such as nutrients, is that of ensuring consistency both within and between sample runs. Additionally, sample analysis was also carried out by four different users. Consequently, a series of procedures were implemented for quality control and to ensure consistent calibrations.

Artificial seawater (ASW)

ASW was the underlying matrix used in the nutrient analyser and was made up of a solution of 40 g l^{-1} of NaCl (Fisher Certified AR) in Milli-Q water. This gives a salinity approximately equal to seawater and therefore serves to reduce changes in the refractive index between inter-sample washes, standards and samples. ASW was used to make up standards and as an inter-sample wash that also generates the baseline. The ASW was checked for purity and that it was free of contaminants with an independent low nutrient seawater (see LNS below).

Standards

Working standards were made up from primary standards, which in turn were made up from stock standards purchased from Seawater Solutions. Primary standards were made up to have a concentration of 5 mM and working standards had concentration ranges detailed in Table 2.2. All standards were made up in ASW and measured out using pipettes and volumetric flasks. Working standards were made up containing nitrate, silicate and phosphate thus making a combined working standard. All standards were stored at 4 °C in the dark, however, before making up standards all solutions were allowed to warm to room temperature to minimise thermal biases in volume. Working standards were incorporated at the start of every batch of nutrient samples, and were run from high to low, then low to high. Running the standards from high to low checked that there was no carry-over between samples. Placing the working standards at the start of a run allowed the user to check that the instrument was working well. Through visual inspection of the absorbance peaks, displayed in real time on the computer, any problems could usually be caught before any samples were taken up by the autosampler. If problems did occur during the calibration phase the run was either stopped and restarted once the problem was diagnosed and fixed, or fixed during the run provided it did not have a detrimental effect on the calibration or samples. If a problem occurred during the middle of a run a similar approach was taken, however this was a rare occurrence and the majority of problems were caught during the calibration phase.

Table 2.2 An example of mixing ratios for making up 1 l working standards.

Standard	Volume of primary standard (ml)[a]			Final Concentration (μM)		
	Nitrate	Silicate	Phosphate	Nitrate	Silicate	Phosphate
1 - high	8	32	0.8	40	160	4
2	6	24	0.6	30	120	3
3	4	16	0.4	20	80	2
4 - low	2	8	0.2	10	40	1

[a]Primary standards are 5 mM

Low nutrient seawater (LNS)

LNS, which was bought commercially from Seawater Solutions, was used as a quality control monitor for the ASW. ASW, which was used for inter-sample washes and for making up standards, should be free of all contaminants as it was made up from NaCl and Milli-Q water, however, checking the purity of ASW against an independent, low nutrient source is an important quality check. When a LNS sample is analysed, a very small peak or no peak at all indicates that the ASW is free of nutrient contaminants. If, on the other had, the LNS shows a negative peak it means that the ASW is contaminated and happens because the LNS has a lower concentration than the baseline, which is set by ASW.

Nitrite standard

The determination of nitrate is only possible after it has been reduced to nitrite, with which the colour forming reagents react. This reduction step occurs in a reduction column packed with cadmium (Cd) granules and fine copper wires and ensuring this step remains at a sufficiently high level (≈100%) is critical to the overall procedure. Therefore, during every run one of the nitrate standards was compared to a nitrite standard of equal concentration, thus allowing the efficiency (E) of the reduction step to be calculated with Eq. 2.3 as follows, where [nitrate] and [nitrite] are standards of equal concentration.

$$E = \left(\frac{[\text{nitrate}]}{[\text{nitrite}]} \right) * 100 \qquad \text{Eq. 2.3}$$

A reduction column should have an efficiency approaching 100%, and if this drops to <90% the Cd should be renewed or reactivated using a $CuSO_4$ solution (Hansen and

Koroleff, 1999). The condition of the reduction column can also be inspected visually because as the Cd becomes "used" it changes in colour from dull grey to silver. Therefore, a column that has a moderate amount of silver coloured Cd should be reactivated or replaced. Typically the reduction column was operating at 100% efficiency.

Performance of the method

The limit of detection, estimated as three times the noise in the baseline was 0.8, 0.3 and 0.1 μmol l^{-1} for nitrate, silicate and phosphate respectively. The precision of the method was determined using groups of replicate seawater samples taken from the CTD, which were mostly duplicates. The relative standard deviation (RSD) was estimated to be 1.7, 4.5 and 2.5% for nitrate, silicate and phosphate respectively. See Section 2.7 for details on how error propagation was handled.

As a check to ensure consistency between runs a sample known as *bulk nuts* was placed at the end of every run. The bulk nuts sample was taken from a large carboy of archived seawater, preserved with $HgCl_2$. This sample served to act as an identical sample between runs which did not have to be renewed, refreshed or remade, therefore acting as the single sample of consistency between runs. The concentration of nutrients in the *bulk nuts* over both legs was 35.0 ± 2.2, 141.0 ± 6.4 and 2.5 ± 0.5 μmol l^{-1} ($\bar{x}$ ± 1σ, n = 38) for nitrate, silicate and phosphate respectively.

2.5 Determination of Dissolved Organic Nitrogen

Samples for dissolved organic nitrogen (DON) were taken directly from the CTD into sterile 60 ml Sterilin® pots pre-washed with sample and then stored at -20 °C until analysis. DON samples were analysed at NOC using the UV-photo-oxidation method described by Sanders and Jickells (2000). The methods works on the principle that the UV-oxidation process oxidises DON to nitrate that can be then analysed as an inorganic nutrient.

When the samples were ready to be analysed they were thawed overnight at room temperature and thoroughly shaken to ensure homogeneity. Duplicate 10 ml subsamples were pipetted in to 12 ml quartz tubes, capped with graphite stoppers and photo-oxidised at 85 °C using two identical Metrohm 705 UV digester systems for 2 h. After UV-oxidation samples were then analysed for nitrate using the same instrument

and method described in Section 2.4. Additionally a subsample of non-UV-oxidised sample was run in parallel to measure the nitrate present in the sample prior to UV-oxidation. This allows the calculation of DON by difference. A detailed discussion of the method, its limitations and quality control procedures will be presented in Chapter 4.

2.6 Ancillary Parameters

CROZEX was a multi-disciplinary project with a wide variety of parameters all being measured in parallel. This provided a large data-set in which to embed results thus providing a rich context for data interpretation. A brief outline of other parameters measured will now be presented along with acknowledgement to whoever was involved.

2.6.1 Particulate Phases

Particulate organic carbon and nitrogen

POC/N samples were taken from the SAPS (Section 2.3) and the CTD. CTD samples were collected and filtered by Mike Lucas (UCT) and Robert Williamson (UCT), prepared by Sophie Seeyave (NOC) and Paul Morris and analysed by Robert Head (PML). The collection of SAPS POC/N samples is detailed in Section 2.3. For CTD POC/N samples about 1-2 l of water was collected from the Niskin bottles, filtered through pre-combusted 25 mm GF/F filters and stored at -20 °C. Filters for both SAPS and CTD samples were then prepared using the same technique.

Filters were thawed at room temperature and then fumed to remove any inorganic carbonate. Fuming was carried out using sulphurous acid (6% w/v) ($SO_{2(aq)}$) (Verardo *et al.*, 1990; Windholz *et al.*, 1976), by placing ≈100 ml in the bottom of a plastic desiccator that was evacuated and left for 48 h. The filters were then dried at 60 °C for at least 24 h, before having the central filter area punched out and wrapped in 30 mm pre-combusted aluminium foil discs and compressed into a pill, similar to the technique described by Hilton *et al.* (1986). POC/N samples collected with the SAPS typically had a much higher particle loading on the filters. Therefore, some of these filters had to be divided up into smaller segments simply by cutting the filter into smaller pieces with a clean pair of scissors. Pelleted samples were then analysed with the high temperature combustion technique using a Finnegan Flash EA1112 Elemental Analyser, with acetanilide as a standard. A good account of POC/N analysis is given by Ehrhardt and Koeve (1999).

Biogenic Silica

Biogenic silica (bSi) is the biologically produced silica mineral, opal, has the general formula of $SiO_2 \cdot nH_2O$ and is the structural compound that siliceous phytoplankton use to make their frustules. bSi was measured on SAPS samples by Ian Salter (NOC) using the Mortlock and Froelich (1989) method. bSi was dissolved in NaOH at 100 °C for 3 h, then mixed with molybdate before finally being reduced to form a blue compound which was measured on a spectrophotometer (Hitachi U-2000) at 810 nm. Details of the method used can be found in Salter *et al.* (2007) and detailed method discussion in Salter (2007).

Water column bSi was measured by Megan French on water samples collected from Niskin bottles using the method of Ragueneau and Treguer (1994). 500 ml water samples were filtered through 0.4 µm polycarbonate filters, which were then dried, mixed with NaOH at 60 °C for 2 h to dissolve the bSi and then neutralised with HCl. The resultant aqueous sample was then run on the silicate channel of the nutrient analyser using the method described in Section 2.4.

Chlorophyll-a

The photosynthetic pigment chlorophyll-*a* (chl-*a*) was measured by a team consisting of Mark Moore (NOC), Robert Williamson and Mike Lucas. Size fractionated chl-*a*: >0.2 µm (total), >2 µm and >20 µm, were filtered onto 25 mm GF/F and polycarbonate filters respectively. Chl-*a* was extracted from the filters by placing them in 10 ml of 90% HPLC grade acetone for 24 h and then measured on a Turner Designs TD-700 fluorometer. The fluorometer was calibrated with a chl-*a* standard from Sigma. The method is outlined in Moore *et al.* (2007b) and is based on that of Welschmeyer (1994).

2.6.2 Biological Productivity Rate Measurements

^{14}C Primary Production

^{14}C primary production (^{14}C PP) was measured by Sophie Seeyave. Samples were taken from six light depths using a trace-metal clean CTD rosette, spiked with ^{14}C labelled $NaH^{14}CO_3$ and incubated for 24 h at sea surface temperature in deck incubators that mimicked the light attenuation at the sampled light depths. Samples were then filtered for >0.2 µm (total), >2 µm and >20 µm size fractions with 25 mm

polycarbonate filters and the filters were then acid fumed to drive off any unfixed inorganic ^{14}C. After fuming the filters were then placed in 5 ml of scintillation cocktail (Optiphase Hi-Safe 3, Packard) and counted in a Tri-Carb 3100 TR liquid scintillation counter. The method is outlined in Seeyave *et al.* (2007) and is based on that of Joint and Pomroy (1986) further based on Steemann Nielsen (1952).

^{15}N Nitrogen Uptake

Nitrogen uptake, used to calculate the *f*-ratio (Eppley and Peterson, 1979), was measured by Mike Lucas using the ^{15}N labelling technique of Dugdale and Goering (1967). ^{15}N uptake measurements of nitrate, ammonium and urea were measured using ^{15}N labelled $K^{15}NO_3$, $^{15}NH_4Cl$ and $CO(^{15}NH_2)_2$ respectively. Water was sampled from six light depths using a trace-metal clean CTD rosette, spiked with the ^{15}N labelled substrates and incubated for 24 h at sea surface temperature in deck incubators that mimicked the light attenuation at the sampled light depths. Samples were then filtered through pre-combusted GF/F filters, stored at -20 °C and later analysed by stable isotope mass spectrometry. Additionally, $^{15}NH_4^+$ uptake rates were corrected for $^{14}NH_4^+$ recycling using the isotopic dilution technique of Glibert *et al.* (Glibert *et al.*, 1982). For full details of ^{15}N uptake measurements see Lucas *et al.* (2007).

2.6.3 Dissolved Gasses

CO_2 and DIC

Inorganic carbon uptake, measured through CO_2 and DIC was measured by Dorothee Bakker (UEA) and Maria Nielsdóttir (NOC). fCO_2 in surface water and marine air was measured using a fast response equilibrator (Bakker *et al.*, 2001) attached to the underway system and a LI-COR LI-6262 infrared CO_2 detection system (Schuster and Watson, 2007). DIC samples were sampled from the CTD and measured by coulometric analysis (Johnson *et al.*, 1987). Carbon uptake was corrected for atmospheric invasion. For full details see Bakker *et al.* (2007).

2.6.4 CTD Parameters and Remote Sensing

CTD parameters

Additional information from the CTD package and from remote sensing was also required. Information from the CTD (Sea-Bird SBE 911*plus*) included salinity,

temperature and depth. Salinity was calibrated with bottle salt samples collected from the CTD and processed with a Guildline Autosal Salinometer (model 8400B) by John Allen (NOC), Paul Duncan (NOC), Alan Hughes (NOC), Dougal Mountifield (NOC) and Hugh Venables (NOC). The final CTD salinity calibrations were calculated by Raymond Pollard (Pollard and Sanders, 2006; Read *et al.*, 2007).

Remote Sensing

Merged SeaWiFs/MODIS satellite images of chl-*a* were processed by Hugh Venables and Katya Popova (NOC) to give near real time images of surface chl-*a*. The images were calibrated with *in situ* chl-*a* samples processed with the method in Section 2.6.1 (Pollard and Sanders, 2006; Venables *et al.*, 2007)

2.7 Raw Data Manipulation, Rules and Assumptions

Integration depth

For cross comparison purposes within this thesis the integration depth for all the parameters was set at 100 m. This depth was chosen for biogeochemical and physical reasons. During the summer in the study region the mixed layer depth (MLD) was generally ≤100 m (Venables *et al.*, 2007), and the 1% light depth and ensuing max primary production depth was always <100 m (Lucas *et al.*, 2007; Seeyave *et al.*, 2007). Thus all the biological productivity rate measurements were contained within the top 100 m of the water column. In addition to this, it was reported by Sanders *et al.* (2007) that the nitrate field was laterally homogenous at 100 m and below; whereas above 100 m, clear latitudinal variations were observed highlighting the effect of biological activity from 0-100 m. Similar trends in DIC were also observed by Bakker *et al.* (2007) who reports no significant change in DIC profiles below 100 m. 100 m has also been used for cross comparison of export fluxes in other Southern Ocean studies (Bishop *et al.*, 2004; Buesseler *et al.*, 2004; Morris *et al.*, 2007; Savoye *et al.*, 2008).

Extrapolating and interpolating 100 m data points for integrations

As described in the previous paragraph, 100 m was chosen as the integration depth. For most of the core parameters a water sample was always collected at *ca.* 100 m, as this was one of the predetermined core sampling depths. When this data point was slightly away from 100 m it was directly extrapolated to exactly 100 m. When a

100 ± 10 m data point was not present, a 100 m data point was linearly interpolated from data points either side of 100 m thus allowing a 100 m integration to still be performed.

Integrations

Integrations of dissolved and particulate parameters (x) were made using a trapezoidal type integration with an average concentration for each depth layer. The form of the integration is shown in Eq. 2.4.

$$x = \int_0^z dz \times \bar{x} \qquad \text{Eq. 2.4}$$

Where dz is the layer thickness and $\bar{x}$ is the averaged concentration within this layer, expressed by Eq. 2.5.

$$\bar{x} = \frac{(x_1 + x_2)}{2} \qquad \text{Eq. 2.5}$$

Error propagation

The propagation of random errors was carried out using standard propagation techniques (Miller and Miller, 2000). For calculation of errors resulting from addition and subtraction functions Eq. 2.6 was used, where σ^2 is the standard deviation (SD) squared (variance).

$$\sigma_x = \sqrt{\sigma_a^2 + \sigma_b^2 + \sigma_c^2 + \ldots} \qquad \text{Eq. 2.6}$$

For calculation of errors resulting from multiplicative expressions the relative standard deviation (RSD) was used in the form of Eq. 2.7, where $\left(\frac{\sigma_a}{a}\right)^2$ is the RSD.

$$\frac{\sigma_x}{x} = \sqrt{\left(\frac{\sigma_a}{a}\right)^2 + \left(\frac{\sigma_b}{b}\right)^2 + \left(\frac{\sigma_c}{c}\right)^2 + \ \ldots} \qquad \text{Eq. 2.7}$$

The majority of samples collected from the CTD were single replicates with a decreasing minority of duplicates and triplicates. This leads into a problem with calculating the SD of single replicate samples. It is also not possible to calculate a SD on duplicate samples using the conventional SD formula; *per contra* the SD is still required for error propagation. However, it is possible to calculate the SD on a set of duplicate measurements using a technique highlighted by Dickson *et al* (2007) using Eq. 2.8, where *d* is the difference between duplicate measurements and *k* is the number of duplicate pairs.

$$\sigma = \sqrt{\frac{\sum_{i=1} d_i^2}{2k}} \qquad \text{Eq. 2.8}$$

Eq. 2.8 can be modified as Eq. 2.9 to take into account situations where varying numbers of replicates (eg. combinations of duplicates and triplicates) are present in one data-set.

$$\sigma = \sqrt{\frac{\sum_{i=1} \left(x_i - \bar{x}\right)^2}{n-k}} \qquad \text{Eq. 2.9}$$

Where $\left(x_i - \bar{x}\right)$ is the difference between the sample value and the mean of the replicates and n is the total number samples. After a SD has been calculated for the group of duplicates the RSD can then be calculated on each of the duplicate means using Eq. 2.10.

$$RSD = \left(\frac{\sigma}{\bar{x}}\right) \times 100 \qquad \text{Eq. 2.10}$$

After calculating the mean of all the RSD an overall average RSD can then be applied to all the single replicate numbers and through the rearrangement of Eq. 2.10 a SD for each data point can then be calculated which can then be used for error propagation. This procedure was used for data-sets that had replicate samples. For the data-sets that did not have any replicate samples, namely POC/N and bSi, a value for the RSD was taken from Hawaii Ocean Time-series, the details of which are published online at http://hahana.soest.hawaii.edu/hot/methods/results.html.

Multiple CTD profiles of the same station

The format of the CROZEX cruises, with the large array of CTD sampling requirements, usually required multiple CTD casts to accommodate everyone's sampling needs. A consequence of this was the regular replication of parameters with, for example, up to three nutrient profiles when a station was occupied. Multiple observations of a single parameter were dealt with by averaging multiple integrations and propagating the associated errors using Eq. 2.6. Averaging repeat observations of single parameters has the advantage of generating only one value for a parameter thus making it easier for cross comparisons with other parameters. Additionally, replicate profiles help to reduce uncertainty that may arise from single profiles.

2.8 Sampling Strategy

It was decided before the cruise that sampling must be representative of bloom and non-bloom regions that were north and south of the Crozet Plateau respectively. Sampling the bloom area would allow a thorough characterisation of the bloom conditions; however these observations needed a non-bloom control site for comparison. Therefore the majority of the sampling effort was concentrated in the bloom region but once during each leg an excursion to the south allowed an opportunity to sample non-bloom conditions (Figure 2.4).

Stations were numbered using the sequential Discovery station number. This is now a five digit number and is the unique and sequential numbering of all the stations that RRS *Discovery* has occupied since 1925 in Clarence Bay, Ascension Island (Discovery-Reports, 1929). In addition to the Discovery station number all the major stations were designated with an M number. Repeated occupations of the same M

station was denoted by decimals, e.g., M3.1 and M3.2 are the first and second occupations of M3, respectively (Figure 2.4 Table 2.3).

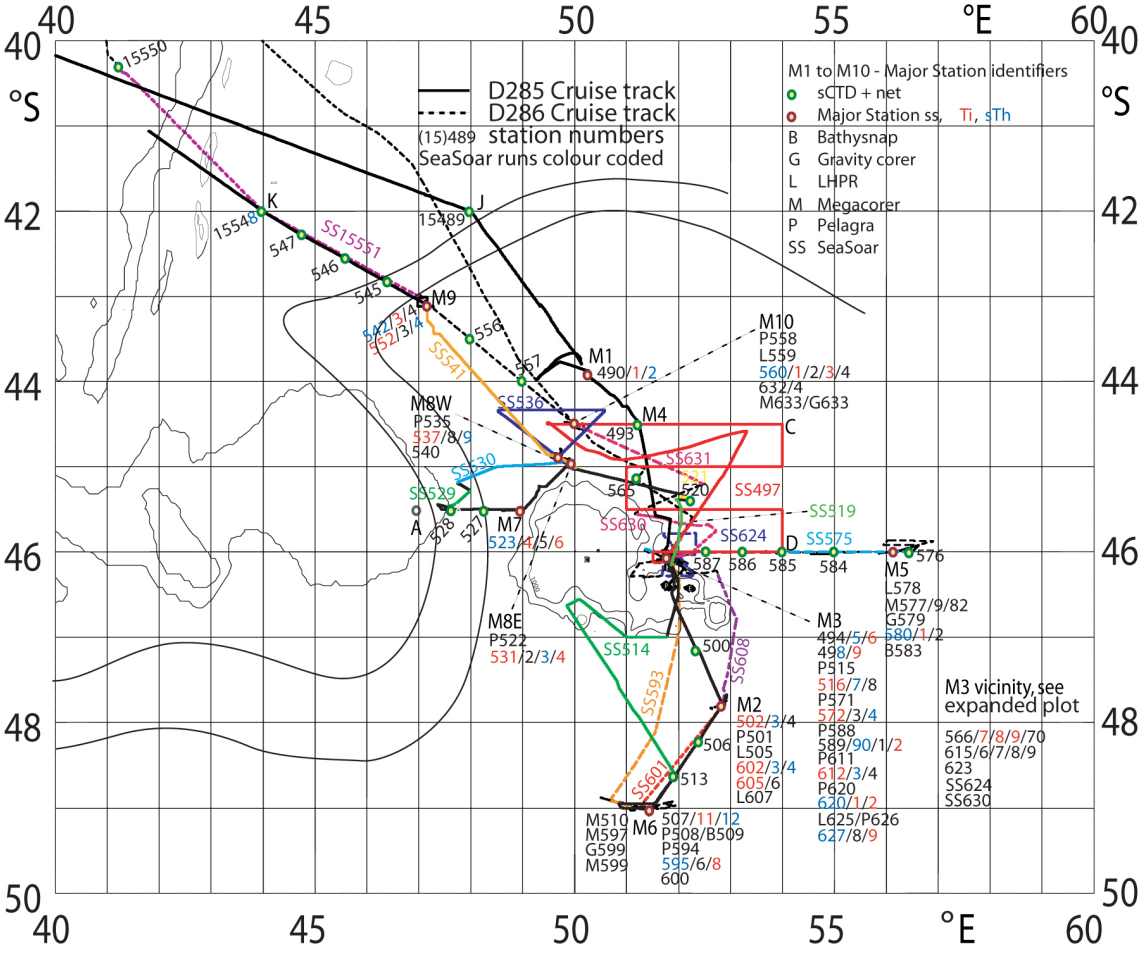

Figure 2.4 Cruise track and station locations (Pollard and Sanders, 2006). 1000 m bathymetry contours and the 'S' bend of the main branch of the Antarctic Circumpolar Current are shown for reference.

The bulk of samples taken for biogeochemical characterisation of the water column were collected using a 24 place sampling rosette with 20 l Niskin bottles and a CTD package. Full depth profiles were made at every major station but biogeochemical samples were primarily taken in the top 500 m with the highest resolution in the top 200 m of the water column. Detailed information on the samples collected will be given as each data-set is introduced in the thesis.

2.8.1 Survey Area Characteristics

As with previous years, an intense bloom lasting about 120 days was observed to the north of the islands with chl-*a* levels peaking at 4 μg l^{-1} at the start of November. To the south of the islands, no such bloom was observed, again consistent with previous years, although at the start of November for about 60 days a small increase in surface chl-*a* of up to 0.7 μg l^{-1} was observed (Figure 2.5d and e). Typical chl-*a* levels prior to the bloom development were ≈0.3 μg l^{-1} throughout the study area. For details of the bloom progression see Figure 2.5 taken from Venables *et al.* (2007). An interesting feature near M3 was the appearance of a small, secondary, eddy bloom (Allen *et al.*, 2006) that persisted after the main widespread bloom had declined. The eddy had chl-*a* levels of 6 μg l^{-1}, the highest observed during both legs, but the resolution in Figure 2.5 is too low to show this feature. Throughout the thesis the different regions of the study area will be referred to in different ways. The area to the north of the Crozet Plateau where the main bloom event occurs will be referred to as either: *northern*, *high productivity* or *bloom* region. The area to the south of the Crozet Plateau will be referred to as either: *southern*, *low productivity*, *non-bloom* or *control* region. For general information of stations used in this thesis see Table 2.3.

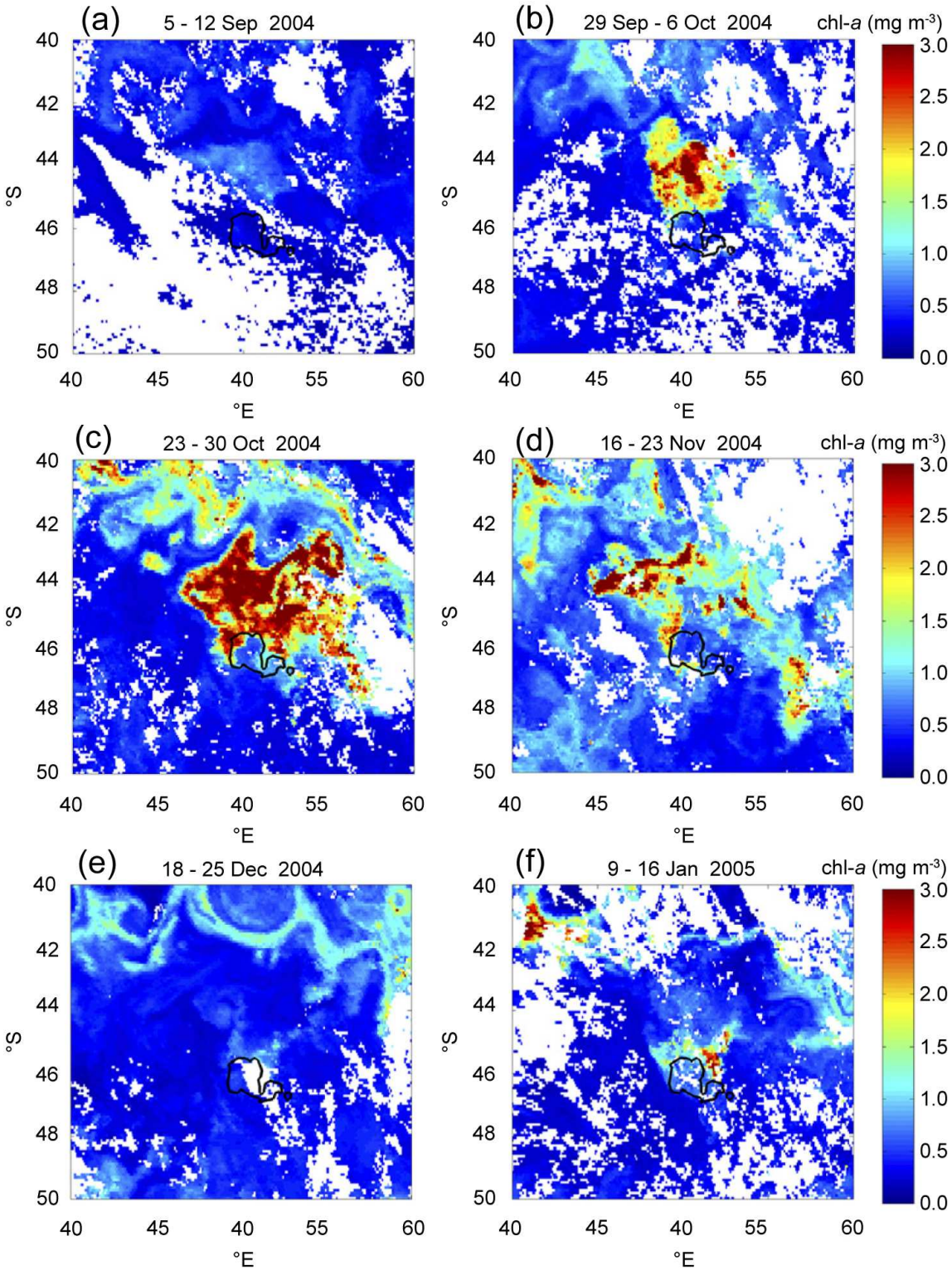

Figure 2.5 Six 8-day merged SeaWiFS/MODIS images of chl-*a* showing the bloom development. The bloom is north of the plateau with contrasting low chl-*a* levels in the south, except for a small bloom in images d and e. The black line is the 1000 m contour. Taken from Venables *et al.* (2007).

Table 2.3 List of cruise stations. Discovery station number, station name if designated, dates of sampling and location. A station name of 'T' means that the stations was part of a transect. The water depth (Pollard and Sanders, 2006) and MLD (Venables pers. comm.) are given for reference and calculated using the method described by (Venables *et al.*, 2007).

Station number	Station name	Date (dd/mm/yy)	Latitude (°S)	Longitude (°E)	Water depth (m)	MLD (m)
15490	M1	11/11/04	43.8837	50.2465	3109	85
15491	M1	11/11/04	43.9205	50.2674	3106	78
15493	M4	12/11/04	44.4969	51.2569	3106	73
15494	M3.1	13/11/04	46.0577	51.7806	3222	144
15495	M3.1	13/11/04	46.0570	51.7921	2398	138
15496	M3.1	13/11/04	46.0681	51.7853	2353	117
15498	M3.2	18/11/04	46.0424	51.8003	2304	95
15499	M3.2	18/11/04	46.0256	51.8105	2437	71
15500		19/11/04	47.1385	52.3540	2563	105
15502	M2.1	19/11/04	47.7954	52.8622	3422	124
15503	M2.1	20/11/04	47.7955	52.8554	3857	113
15504	M2.1	20/11/04	47.7729	52.8837	3859	140
15506		20/11/04	48.1915	52.4131	3869	108
15507	M6.1	21/11/04	49.0033	51.4909	4206	138
15511	M6.1	22/11/04	49.0056	51.5005	4224	131
15512	M6.1	23/11/04	49.0155	51.4731	4222	167
15513		23/11/04	48.5961	51.9478	3962	113
15516	M3.3	25/11/04	46.0596	51.7909	2353	51
15517	M3.3	25/11/04	46.0701	51.7715	2331	51
15518	M3.3	25/11/04	46.0789	51.7616	2278	50
15520		26/11/04	45.3955	52.2404	3117	69
15523	M7	27/11/04	45.5049	48.9866	2749	79
15524	M7	27/11/04	45.4989	49.0017	2747	53
15525	M7	27/11/04	45.4865	48.9976	2752	44
15527	T	28/11/04	45.4985	48.3342	2898	62
15528	T	29/11/04	45.4896	47.6336	2410	108
15532	M8E	30/11/04	44.9166	49.9069	2752	67
15533	M8E	30/11/04	44.9535	49.9410	2715	66
15534	M8E	30/11/04	44.9471	49.9669	2724	41
15537	M8W	01/12/04	44.8658	49.6633	2808	44
15538	M8W	02/12/04	44.8566	49.6522	2816	46
15539	M8W	02/12/04	44.8724	49.6471	2805	44
15540	M8W	02/12/04	44.9114	49.6293	2778	51
15542	M9.1	03/12/04	43.1176	47.1849	2911	26
15543	M9.1	03/12/04	43.1174	47.1841	2912	40
15544	M9.1	04/12/04	43.1159	47.1861	2918	49
15552	M9.2	18/12/04	42.9985	47.0039	3242	27
15553	M9.2	19/12/04	43.0029	47.0028	3228	25
15554	M9.2	19/12/04	42.9951	47.0238	3204	26
15556		19/12/04	43.4991	47.9990	2451	35
15557		20/12/04	43.9992	49.0010	2892	55
15560	M10.1	20/12/04	44.5183	49.9925	2956	43
15562	M10.1	20/12/04	44.5279	49.9603	2944	22
15563	M10.1	21/12/04	44.5253	49.9606	2946	52

15565		21/12/04	45.1387	51.1963	3060	30
15568		22/12/04	46.3233	51.8946	395	72
15569		22/12/04	46.2700	51.9708	1565	38
15570		22/12/04	46.2647	51.9577	1354	64
15572	M3.4	22/12/04	46.0622	51.7817	2375	65
15573	M3.4	22/12/04	46.0683	51.7782	2363	71
15574	M3.4	23/12/04	46.0814	51.7824	2256	77
15576		24/12/04	45.9968	56.4389	4250	76
15580	M5	27/12/04	45.9974	56.1521	4271	104
15581	M5	27/12/04	46.0006	56.1512	4268	92
15582	M5	28/12/04	46.0000	56.1516	4269	92
15584	T	29/12/04	45.9977	55.0105	3957	77
15585	T	30/12/04	46.0046	54.0037	3433	77
15586	T	30/12/04	45.9991	53.2665	3456	60
15587	T	30/12/04	45.9911	52.5228	3163	60
15589	M3.5	31/12/04	46.0644	51.7807	2358	81
15590	M3.5	31/12/04	46.0626	51.7772	2359	75
15592	M3.5	31/12/04	46.0513	51.7759	2411	46
15595	M6.2	03/01/05	48.9990	51.5380	2404	56
15596	M6.2	03/01/05	48.9996	51.5334	4214	94
15598	M6.2	04/01/05	49.0016	51.5347	4214	104
15604	M2.2	06/01/05	47.8003	52.8484	3858	73
15605	M2.2	06/01/05	47.8011	52.8495	3857	64
15606	M2.2	07/01/05	47.8038	52.8498	3852	61
15612	M3.6	08/01/05	46.1465	51.8598	2039	42
15613	M3.6	09/01/05	46.1430	51.8578	2031	30
15614	M3.6	09/01/05	46.1548	51.8521	1969	28
15615	T	09/01/05	46.2832	51.0844	1264	63
15616	T	10/01/05	46.2918	51.3336	1092	44
15617	T	10/01/05	46.2863	51.5803	718	40
15618	T	10/01/05	46.2851	51.8401	1102	35
15619	T	10/01/05	46.2842	52.2563	1524	36
15620	M3.7	10/01/05	46.0323	51.8704	2320	39
15622	M3.7	10/01/05	46.0341	51.8666	2300	39
15623	M3.75	11/01/05	45.9901	51.6787	2506	15
15627	M3.8	12/01/05	46.0422	51.9624	2529	21
15628	M3.8	12/01/05	46.0409	51.9606	2514	33
15629	M3.8	13/01/05	46.0457	51.9592	2382	34
15632	M10.2	15/01/05	44.5015	49.9856	2965	26

3 ^{234}Th-Derived Carbon Export

3.1 Introduction

The aim of this chapter is to present the ^{234}Th data and, after an explanation of the export models used, to then present the ^{234}Th-derived particle export around the Crozet Plateau. Particulates flux of carbon and nitrogen are presented. However, the focus of the chapter and ultimately the discussion is on the particulate fluxes of carbon, which has already been published in Morris *et al.* (2007).

3.1.1 Synopsis of ^{234}Th Samples Collected

During the sampling period, a total of twenty process stations were occupied (Pollard and Sanders, 2006) and sampled for ^{234}Th, blue labels of 'sTh' in Figure 2.4. Ten stations were sampled on each of legs 1 and 2. Sampling and analysis was carried out by Paul Morris on leg 1 and Sandy Thomalla on leg 2. Of the twenty stations sampled for ^{234}Th, six were duplicate occupation of three locations (M2, M6, and M9), eight were repeat occupations of M3, and six were single profile stations. Station M3 was located 38 km north of *Île de la Possession* and was deemed a time-series station at which repeated observations were made in an area that usually sustains a bloom throughout the growth season. Stations M2 and M6 were picked for their HNLC non-bloom characteristics to act as control stations, and the remainder were distributed across the northern bloom area. Profiles were taken only in the top few hundred metres of the water column, deep enough for ^{234}Th to reach equilibrium with ^{238}U, whilst shallow enough to get a high resolution profile of any observed ^{234}Th disequilibrium. Profiles were made up of ten data points. Every time a CTD profile of ^{234}Th was taken a SAPS deployment was also made to sample particulate material.

3.1.2 Profiles of ^{234}Th

The complete data-set of total ^{234}Th (dpm l^{-1}), ^{238}U (dpm l^{-1}) and associated ^{234}Th:^{238}U ratios for all stations and all depths is given in Appendix 1. The data in this table are plotted in Figures 3.1 and 3.2. A ^{234}Th:^{238}U ratio of <1 in a given parcel of water indicates particle export from this parcel (Bacon and Anderson, 1982; Kaufman *et al.*, 1981; Santschi *et al.*, 1979; Tsunogai *et al.*, 1986). A ^{234}Th:^{238}U ratio of >1 indicates particle accumulation and perhaps remineralisation (Waples *et al.*, 2006), and

a ratio of 1 indicates a situation where ^{234}Th ingrowth from ^{238}U is balanced by ^{234}Th removal by decay. In general the ^{234}Th:^{238}U activity ratios in surface waters were <1, ranging from 0.39-0.86, and reached a ratio of 1 at depths between 100-200 m. In a few instances (Stations M1, M3.1, M7 and M9.1) a ratio of ≈1.1 was observed immediately below the surface disequilibrium suggesting that remineralisation was taking place in the mesopelagic zone (Figure 3.1a,b,g). During leg 1 there was a clear difference between the disequilibria observed north and south of the Crozet Islands: large disequilibria of <<1 were observed to the north (Figure 3.1a,b,e-j) and small disequilibria of just <1 were observed to the south and in the north at M3.2 (Figure 3.1c-e). This trend was not observed during leg 2: large disequilibria were observed throughout the study region (Figure 3.2a-j).

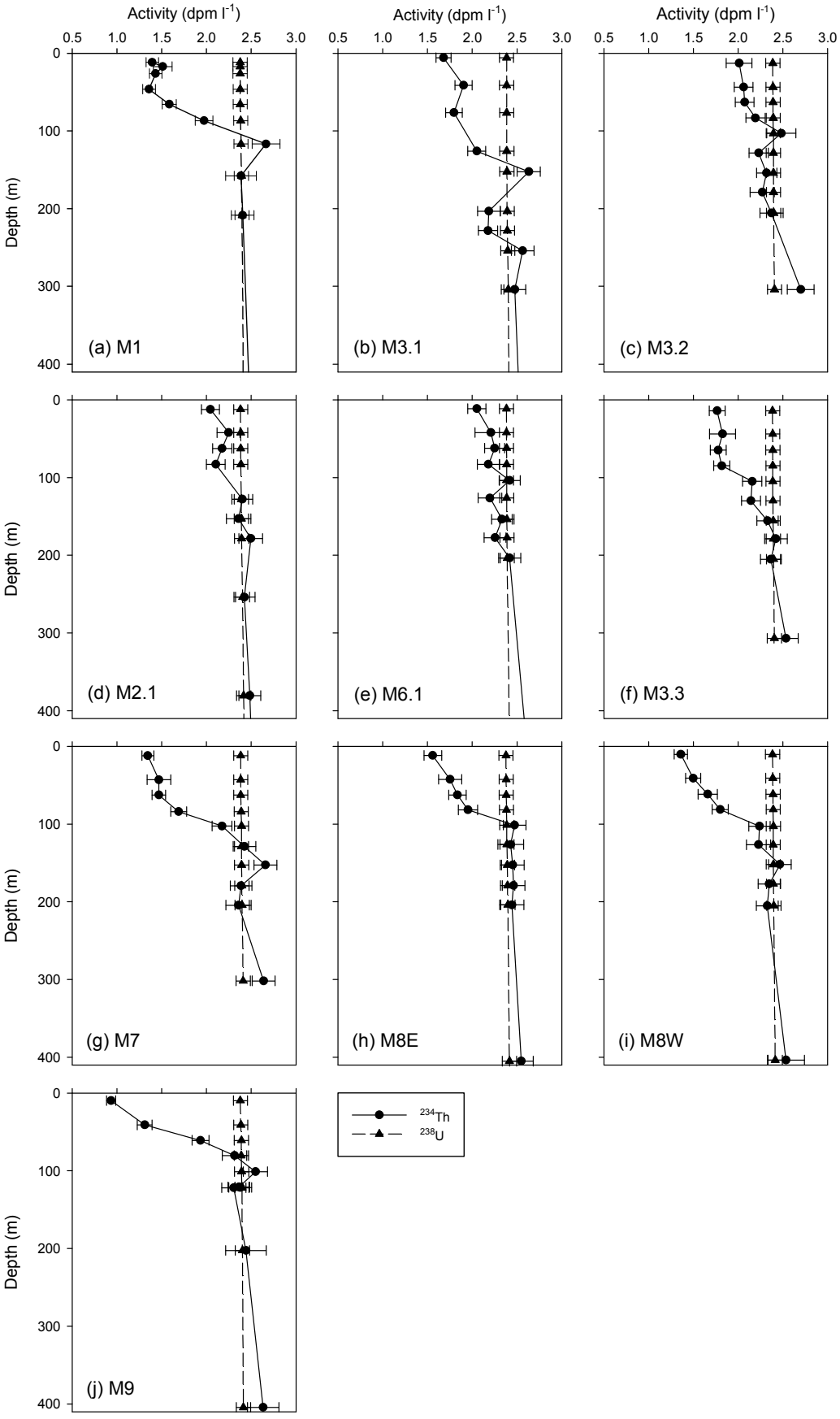

Figure 3.1(a-j) Profiles of the ^{234}Th disequilibria observed during leg 1. Circles and solid lines are total ^{234}Th activities, and triangles and dashed lines are ^{238}U activities. Error bars are 1σ for ^{234}Th and 3.3% of the calculated ^{238}U activities.

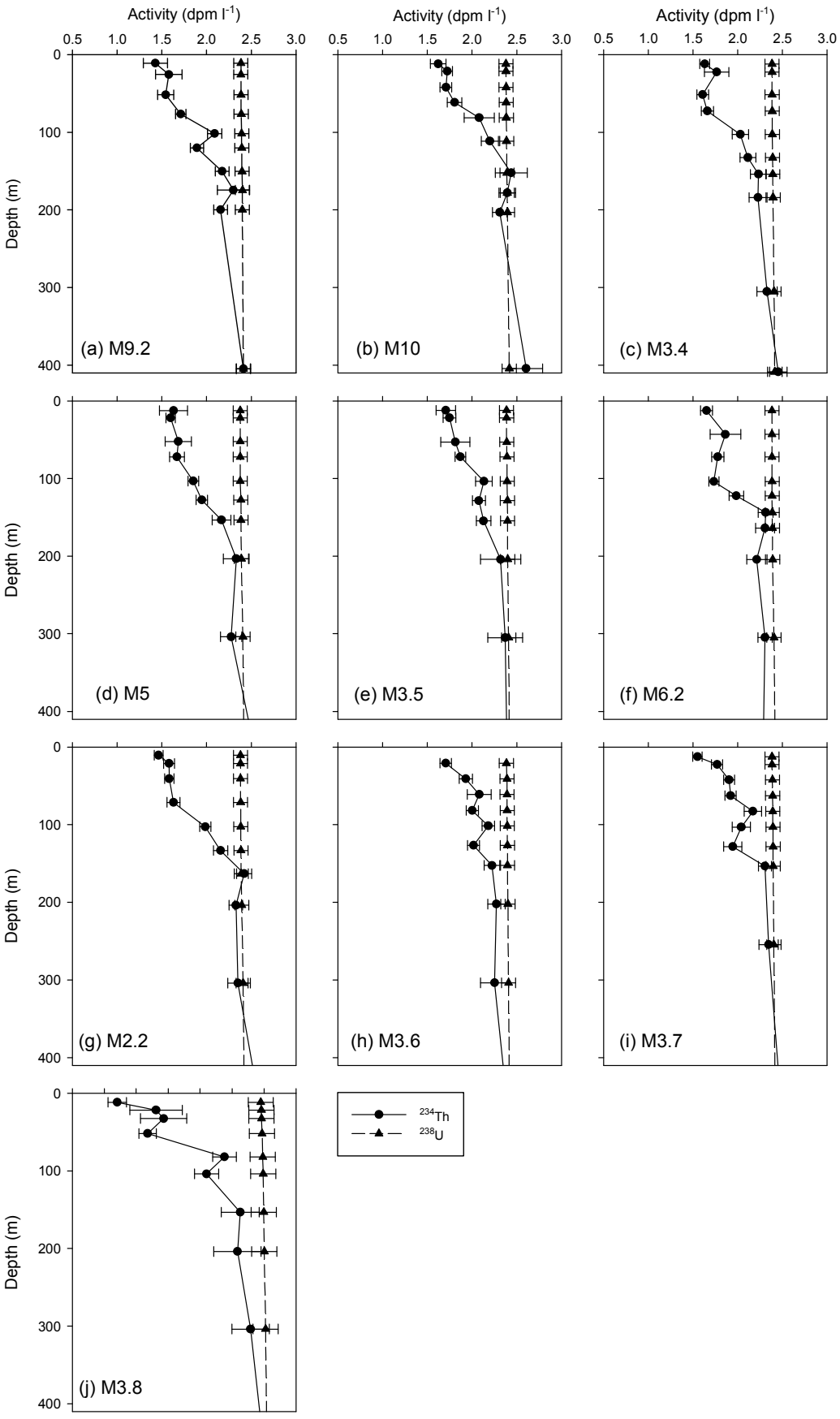

Figure 3.2(a-j) Profiles of the ^{234}Th disequilibria observed during leg 2. Circles and solid lines are total ^{234}Th activities, and triangles and dashed lines are ^{238}U activities. Error bars are 1σ for ^{234}Th and 3.3% of the calculated ^{238}U activities.

3.2 Modelling ^{234}Th Export

3.2.1 Model Description

The rate of ^{234}Th export out of the surface ocean was calculated using a steady-state scavenging model (Buesseler *et al.*, 1992; Coale and Bruland, 1985; 1987; Cochran *et al.*, 1995; Cochran *et al.*, 2000). In a given parcel of water the total (dissolved + particulate) activity of ^{234}Th is controlled by several processes: ingrowth from ^{238}U, radioactive decay, loss on settling particles, and advection and turbulent diffusion. These processes can be expressed as Eq. 3.1:

$$\frac{\partial A_t}{\partial t} = \left(A_U - \left(A_p + A_d\right)\right)\lambda - P + V \qquad \text{Eq. 3.1}$$

where $\partial A_t / \partial t$ (dpm m^{-3} d^{-1}) is the rate of change in total ^{234}Th activity (dpm m^{-3}), A_U is the ^{238}U activity (dpm m^{-3}), A_p and A_d are the particulate and dissolved ^{234}Th activities respectively (dpm m^{-3}) (the sum of which is A_t the total ^{234}Th activity (dpm m^{-3})), λ is the decay constant of ^{234}Th (d^{-1}), P is the loss of ^{234}Th activity on sinking particles (dpm m^{-3} d^{-1}), and V is the sum of advective and turbulent diffusive ^{234}Th activity fluxes into and out of the parcel of water (dpm m^{-3} d^{-1}). P is the term of interest when calculating particle flux so Eq. 3.1 can be rearranged to give Eq. 3.2:

$$P = \left(A_U - A_t\right)\lambda - \frac{\partial A_t}{\partial t} + V \qquad \text{Eq. 3.2}$$

By integrating Eq. 3.2 by depth intervals through the water column it is then possible to calculate the flux of ^{234}Th through any depth horizon that has been sampled. By treating every ^{234}Th profile separately, thus assuming steady-state conditions ($\partial A_t / \partial t = 0$) and assuming V = 0, Eq. 3.2 can be simplified to give Eq. 3.3:

$$P = \int_0^z \lambda\left(A_U - A_t\right) dz \qquad \text{Eq. 3.3}$$

The term V comprises of processes such as horizontal and vertical advection and horizontal and vertical turbulent diffusion. These processes are associated with gradients in the ^{234}Th distribution and have an impact on ^{234}Th budget calculations. It has been shown that horizontal advection, upwelling (vertical advection) and horizontal turbulent diffusion can be significant in upwelling regions such as the equatorial Pacific at 140ºW and the northwestern Arabian Sea (Bacon *et al.*, 1996; Buesseler *et al.*, 1995; Buesseler *et al.*, 1998; Dunne and Murray, 1999), and in coastal areas where enhanced particle scavenging in shallower water columns is often seen (e.g. (Gustafsson *et al.*, 1998). How valid is the assumption that V = 0 in this study?

Most sampling sites of the CROZEX process study (M1, M2, M5, M6, M7, M8, M10, 15632 (Figure 2.4)) were located away from regions that could be associated with major vertical advective current velocities. The Polar Frontal Zone (PFZ), at which cold Antarctic water is subducted beneath warm subtropical water (Deacon, 1984), is typically located >100 km from our sampling sites based on the flow on the northern branch of the Antarctic Circumpolar Current (ACC) (Figure 2.5). Thus, even if some water from the sampling sites should be entrained by the downwelling typical of the PFZ it would probably still be a rather horizontal water movement at the sampling sites. Deeper water has to flow around the Crozet Plateau and this movement may involve vertical advective flow. However, this vertical flow component is likely to occur mainly in the vicinity of the plateau. Only the topmost few hundred metres of the water column was sampled while total water depths were ≥2000 m, and horizontal distances to the slope and shallow parts of the plateau were at least several tens of kilometres. Therefore, it seems to be relatively safe to assume that large-scale topographically related vertical advective flow did not play an important role in controlling the ^{234}Th distribution at our sampling sites.

At M3, the assumption that vertical turbulent diffusive fluxes were negligible could be directly scrutinised with measured vertical turbulent diffusion coefficients (K_z). K_z at M3 was estimated by two methods: with Lowered Acoustic Doppler Current Profiler (LADCP) data (Garabato *et al.*, 2004) and with radium-228 (^{228}Ra) data (Moore, 2000). LADCP results gave a K_z in the upper 50-300 m of the water column of 0.34-0.41 cm^2 s^{-1}, whereas ^{228}Ra data gave much higher rates of 11-100 cm^2 s^{-1} (Charette *et al.*, 2007), thus presenting a very large range. Charette *et al.* (2007) suggest that the reasons for the much higher ^{228}Ra derived values for K_z may include 1) the highly dynamic nature of the surface ocean over seasonal time-scales, 2) that the ^{228}Ra

method integrates over a much longer time period, 3) the ^{228}Ra 1-D model approach for estimating K_z may be influenced by horizontal advection. Therefore the LADCP derived K_z values were considered to be more representative of vertical diffusion across the base of the mixed layer. The LADCP derived K_z at M3 agrees well with estimates of K_z measured in the Southern Ocean during SOIREE of 0.3 cm^2 s^{-1} (Law *et al.*, 2003). Therefore, to put a reasonable upper limit on the flux of ^{234}Th being brought into the surface ocean through vertical turbulent diffusion a value of 1 cm^2 s^{-1} was applied to the ^{234}Th gradient across the bottom depth horizon of ^{234}Th/^{238}U disequilibrium. The turbulent diffusive flux of ^{234}Th, V_z (dpm m^{-2} d^{-1}), across this layer was calculated using Eq. 3.4:

$$V_z = K_z\left(\frac{\partial^{234}Th}{\partial z}\right) \qquad \text{Eq. 3.4}$$

where K_z is the vertical diffusion coefficient (cm^2 s^{-1}) and ∂^{234}Th/∂z is the ^{234}Th activity gradient across the bottom depth horizon of ^{234}Th/^{238}U disequilibrium. At M3, the upward vertical turbulent diffusive flux of ^{234}Th was estimated to be in the range of 2-52 dpm m^{-2} d^{-1}, less than 3% of particle-associated downward fluxes in all cases, which is within the overall uncertainty of ^{234}Th export estimates. Based on a combination of this information it was assumed that vertical turbulent diffusion was negligible throughout the study region.

Horizontal advection and diffusion were also considered to be minimal because the residence time of water in the region is about 62 days (Pollard *et al.*, 2007b), which is greater than four times the half-life of ^{234}Th. In addition to this the profiles of ^{234}Th were reasonably consistent between stations therefore limiting horizontal gradients in ^{234}Th and resultant lateral net fluxes. Based on these results it seems reasonably safe to assume that no significant horizontal and vertical advection and horizontal and vertical turbulent diffusion was having an impact on the ^{234}Th distribution at our sampling sites. Therefore, a model without advection and turbulent diffusion term V was applied to individual total ^{234}Th profiles to give ^{234}Th flux estimates out of the surface ocean and into the deep ocean (*cf.* Moran and Buesseler, 1993; Tanaka *et al.*, 1983; Wei and Murray, 1991).

The steady-state model is a useful approach because it requires only one profile of ^{234}Th activity to calculate a ^{234}Th flux. However, if multiple profiles of ^{234}Th activities are collected from the same site over a period of time then a non steady-state model can be applied. It has been shown that a non steady-state model is more suitable during high particle export events, for example during the onset and termination of a plankton bloom (Buesseler, 1998; Buesseler *et al.*, 1992; Cochran *et al.*, 1995; Cochran *et al.*, 1997; Savoye *et al.*, 2006). However a non steady-state approach requires multiple observations of the same parcel of water. An initial analysis using the steady-state model was applied to all the stations individually and then a non steady-state model was applied to selected stations. During the cruise, four locations were sampled more than once: M2 and M6 to the south of the Crozet plateau, M9 in the NW of the study region and M3 the time-series station (Figure 2.5). The non steady-state model factors in the term $\partial A_t / \partial t$ which was originally made to equal zero in the steady-state model. The advective and turbulent diffusive term V was still made to equal zero for the reasons previously discussed. Therefore the non steady-state model for the calculation of ^{234}Th export across a depth horizon z can be represented by Eq. 3.5.

$$P = \int_0^z \lambda\left(A_U - A_t\right) - \frac{\partial A_t}{\partial t}\, dz \qquad \text{Eq. 3.5}$$

By calculating $\partial A_t / \partial t$ a non steady-state ^{234}Th flux was calculated for M2, M6 and M9. M3 will be discussed separately because of its unique situation.

3.2.2 ^{234}Th Flux

^{234}Th/^{238}U disequilibria were integrated to a depth where the ^{234}Th:^{238}U ratio reached 1. If a remineralisation peak was evident above this equilibrium depth, such as the profiles in Figure 3.1a,b,g, the integral of this peak was subtracted from the integrated ^{234}Th deficit. Integrated ^{234}Th fluxes (dpm m^{-2} d^{-1}) calculated using the steady-state model (Eq. 3.3) for each station are shown in Table 3.1. For leg 1 ^{234}Th disequilibria fall into 2 distinct groups: 573-813 dpm m^{-2} d^{-1} ($\bar{x}$ = 709 dpm m^{-2} d^{-1}) and 1619-2352 dpm m^{-2} d^{-1} ($\bar{x}$ = 2026 dpm m^{-2} d^{-1}). The first group are Stations M2, M6 and M3.2, and the second group are the other 7 stations. The ^{234}Th flux for M3.2 appeared to be anomalously low compared to the other leg 1 occupations of M3, but

very similar to the fluxes measured for M2 and M6. This was the result of water advected from south of the islands (Pollard *et al.*, 2007b). For leg 2 ^{234}Th disequilibria do not fall into any distinct groups but formed one group with fluxes ranging from 1744-2846 dpm m^{-2} d^{-1} ($\bar{x}$ = 2306 dpm m^{-2} d^{-1}). The general trend was for higher ^{234}Th disequilibria during leg 2.

Table 3.1 The integrated ^{234}Th flux down to the ^{234}Th:^{238}U equilibrium depth and to 100 m calculated using the steady-state model. All errors are 1σ.

Station	Integration depth (m)	^{234}Th flux (dpm m^{-2} d^{-1})	^{234}Th flux at 100 m (dpm m^{-2} d^{-1})
M1	158	2043 ± 483	2247 ± 342
M3.1	182	1845 ± 485	1624 ± 336
M3.2	103	813 ± 380	821 ± 376
M2.1	128	740 ± 409	677 ± 361
M6.1	104	573 ± 387	576 ± 383
M3.3	156	1965 ± 424	1641 ± 338
M7	179	2352 ± 457	2467 ± 317
M8E	101	1619 ± 349	1621 ± 347
M8W	103	2232 ± 327	2216 ± 324
M9.1	122	2125 ± 277	2107 ± 327
M9.2	175	2831 ± 434	2187 ± 330
M10	152	1744 ± 449	1603 ± 351
M3.4	184	2524 ± 443	1957 ± 319
M5	203	2846 ± 485	2029 ± 333
M3.5	204	2295 ± 503	1606 ± 346
M6.2	144	2284 ± 382	1798 ± 326
M2.2	163	2546 ± 397	2170 ± 310
M3.6	202	1978 ± 466	1340 ± 325
M3.7	154	1960 ± 416	1448 ± 335
M3.8	153	2051 ± 416	1665 ± 340

M2, M6 and M9 were each occupied twice during the sampling period with 47, 41 and 16 days respectively between subsequent occupations of the same station. Savoye *et al.* (2006) recommends that the non steady-state model is most appropriate when reoccupations of the same station are 1-4 weeks apart. This gap applied at M9 but not at M2 and M6. However, despite the long time interval between the two profiles at M2 and M6, the non steady-state model (Eq. 3.5) was nonetheless applied. To apply the non steady-state model it has to be assumed that the same water mass was sampled on both occasions. To examine this assumption, the salinity profiles were compared between subsequent occupations of the same station. Salinity varied with an average of 0.042 ± 0.01, 0.003 ± 0.004 and 0.028 ± 0.03 ($\bar{x}$ ± 1σ) for M2, M6 and M9 respectively

between subsequent profiles at the same station down to the ^{234}Th integration depth. M6 showed least variation in salinity and M2 and M9 showed more variation. This is not surprising because M6 is far enough south to be clear of circulation fronts: the SAF and a newly described southern branch of the SAF that skirts to the south of the Crozet Plateau, whereas M9 and M2 are much closer to these circulation fronts (Pollard *et al.*, 2007b). Salinity is one way of assessing whether the same water mass was sampled during subsequent profiles and only reveals if the same type of water is entering the station location. Ideally a surface drifter or conservative tracer such as SF_6 would have been released while first sampling a location so that the ship may return to that same parcel of water to sample it again, but the nature of the cruise and project did not allow for such an approach. Consequently, this limitation is recognised and for the purpose of the non steady-state calculation it was assumed that the same water mass was sampled on subsequent occupations of the same station. In addition to this, the term V comprising the advective and turbulent diffusive transport was assumed to be negligible as discussed in Section 3.2.1. Integrated ^{234}Th fluxes using the non steady-state model (Eq. 3.5) were calculated by Robert Turnewitsch and are shown in Table 3.2. The fluxes are high both to the north and to the south of the region with ^{234}Th fluxes ranging from 2326-2949 dpm m^{-2} d^{-1}. The non steady-state fluxes compare well with the leg 2 steady-state fluxes.

Table 3.2 The integrated ^{234}Th flux (dpm m^{-2} d^{-1}) down to the ^{234}Th:^{238}U equilibrium depth and to 100 m calculated using the non steady-state model. All errors are 1σ.

Station	Integration depth (m)	^{234}Th flux at equilibrium depth	^{234}Th flux at 100 m
M2	120	2931 ± 477	2673 ± 429
M6	100	2326 ± 468	2326 ± 468
M9	120	2949 ± 956	2288 ± 823

Station M3 was visited 8 times over the course of 2 cruises therefore providing a series of opportunities to take repeated profiles of ^{234}Th to be used in a non steady-state analysis. As previously described, in order for a non steady-state analysis to be applied, the same parcel of water should be sampled, otherwise the analysis runs into complications from the advective and turbulent diffusive term V, which is assumed to be zero in Eqs. 3.3 and 3.5. During various occupations of M3 it was clear that the same parcel of water was not encountered at M3 based on hydrographic observations. In particular, M3.2 was shown to be HNLC water that had been advected from south of

the Crozet Plateau (Pollard *et al.*, 2007b). In addition to this, the last three occupations of M3 were centred in a blooming eddy close to the M3 location (Allen *et al.*, 2006). It was hypothesised by Allen *et al.* (2006) that the bloom was fuelled by entraining nutrient rich coastal waters from the local *Île de la Possession* that were then vertically mixed with water in the centre of the eddy. Although the general residence time for water entering the bloom area to the north of the islands is typically 62 days (Pollard *et al.*, 2007b) the area immediately north of the islands (M3) is probably experiencing more hydrodynamic variability thus complicating the use of a non steady-state model at this site. For the interpretation of M3 fluxes it needs to be kept in mind that there is an unknown uncertainty resulting from the probable impact of lateral advection and/or a non steady-state. Therefore, only the steady-state model was applied to the data from M3 due to the uncertainties and highly complex nature of the circulation seen there.

3.3 Elemental Ratios – Carbon and Nitrogen to ^{234}Th

To estimate POC export, the ratio of POC to particulate ^{234}Th activity (C:Th ratio, μmol dpm^{-1}) has to be applied to the measured ^{234}Th export fluxes (Eq. 3.6); where POC flux is the quantity of POC (mmol m^{-2} d^{-1}) falling out the surface ocean, C:Th is the ratio of POC to ^{234}Th (μmol dpm^{-1}) on the large size class of particles (>53 μm), and P is the integrated ^{234}Th flux derived from Eqs. 3.3 and 3.5.

$$POC\ export = C{:}Th \times P \qquad \text{Eq. 3.6}$$

This procedure was first demonstrated by Tsunogai and Minagawa (1976), but was not routinely used until the concept was again highlighted by Buesseler *et al.* (1992). This same approach can be used to calculate fluxes of other elements such as nitrogen and silica by calculating ratios between ^{234}Th and particulate organic nitrogen (N:Th) and biogenic silica (bSi:Th), respectively.

The C:Th ratios from SAPS are shown in Table 3.3. Ratios ranged from 5-10 and 6-11 μmol dpm^{-1} on leg 1 and leg 2, respectively. There are no temporal or spatial large-scale patterns of C:Th ratios ($\bar{x}$ = 8.0 and 8.5 μmol dpm^{-1}, north and south respectively), suggesting that small-scale variation is controlling the small range of values that were observed. The small variation in the C:Th ratios is the most striking

aspect of the data considering the wide range of bloom conditions that were sampled. The importance of the C:Th ratio is clear when Eq. 3.6 is expressed graphically as shown in Figure 3.3 taken from Buesseler *et al.* (2006). For example, given the same ^{234}Th disequilibrium a doubling of the C:Th ratio will also result in a doubling of the calculated POC export.

Table 3.3 Elemental ratios of POC and PON with ^{234}Th in >53 μm particulate matter collected with SAPS. All errors are 1σ.

Station	Sampling depth (m)	C:Th ratio (μmol dpm^{-1})	N:Th ratio (μmol dpm^{-1})
M1	200	8.4 ± 0.9	1.3 ± 0.1
M3.1	225	8.3 ± 0.9	1.3 ± 0.1
M3.2	200	6.0 ± 0.7	1.1 ± 0.1
M2.1	150	7.2 ± 0.8	1.3 ± 0.1
M6.1	175	10.1 ± 1.1	1.9 ± 0.2
M3.3	200	7.1 ± 0.8	1.2 ± 0.1
M7	150	5.5 ± 0.7	1.1 ± 0.1
M8E	150	9.4 ± 1.1	1.6 ± 0.2
M8W	150	6.1 ± 0.7	0.9 ± 0.1
M9.1	120	7.9 ± 0.9	1.1 ± 0.1
M9.2	120	10.6 ± 1.2	1.5 ± 0.2
M10	110	7.1 ± 0.8	1.3 ± 0.1
M3.4	180	10.2 ± 1.1	1.7 ± 0.2
M5	125	6.3 ± 0.7	1.0 ± 0.1
M3.5	100	9.7 ± 1.1	1.4 ± 0.2
M6.2	120	8.0 ± 0.9	1.2 ± 0.1
M2.2	160	8.7 ± 1.0	1.4 ± 0.2
M3.6	80	10.3 ± 1.1	1.7 ± 0.2
M3.7	80	7.0 ± 0.8	1.1 ± 0.1
M3.8	80	7.3 ± 0.8	1.2 ± 0.1

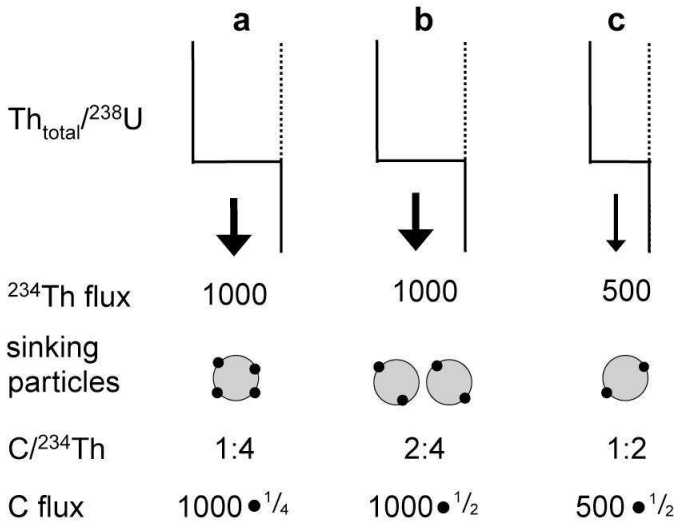

Figure 3.3 Carbon-to-thorium ratios. The carbon flux varies proportionally with differing levels of disequilibrium and differing C:Th ratios. Taken from Buesseler *et al.* (2006).

Given the proportional relationship that the C:Th ratio has over the calculated estimate of export (Figure 3.3), the conclusion that it is not driving POC export is one that should be accepted carefully. However, during CROZEX the variation of the C:Th ratio on leg 1 is less than the variation observed in the POC export estimates, varying by factors of 2 and 3, respectively. In addition to this, the highest C:Th ratio was observed at M6.1, one of the sites of lowest POC export. During leg 2, this distinction was not present but the generally homogenous nature of both the C:Th ratios and POC exports suggests that the C:Th ratio is again not the primary driving parameter of levels of POC export. The C:Th ratios measured on CROZEX generally agree well with other studies of natural systems in the Polar Front (PF) (Table 3.4).

Table 3.4 C:Th ratios measured in the PF in differing sectors of the Southern Ocean

Region[a]	Date	Size fraction (µm)	Depth (m)	C:Th ratio (µmol dpm^{-1})	Reference
Atlantic	Oct-Nov 1992	>1	20-200	20.9 (6-12)[b]	Rutgers van der Loeff *et al.* (1997)
Atlantic	Dec 1995-Jan 1996	>1	>80	10.2	Rutgers van der Loeff *et al.* (2002)
Pacific (AESOPS)	Oct 1997-Mar 1998	>70	80-150	3.0-6.2	Buesseler *et al.* (2001)
Indian	Jan-Feb 1999	>60	100	0.8-1.4	Coppola et al (2005)
Indian (KEOPS)	Jan-Feb 2005	55-210	18-129	5.9-53.4	Savoye *et al.* (2008)
Indian (CROZEX)	Nov 2004 Feb 2005	>53	80-225	5.5-10.8	Morris *et al.* (2007) This study

[a]Sector of the Southern Ocean.
[b] POC concentrations were calculate from suspended particulate matter which were then combined with particulate ^{234}Th data. The ratio of 20.9 µmol dpm^{-1} was then scaled down to 30-60% based on literature data on organic carbon and ^{234}Th in suspended matter and trap material to give ratios in parenthesis.

3.4 Export Fluxes

3.4.1 Export of Carbon and Nitrogen

The primary biogeochemical idea to be tested in this thesis is whether enhanced POC export was observed in a topographically iron-fertilised bloom in an HNLC region, when compared with a control region. By using calculated ^{234}Th fluxes, it is possible to estimate the ^{234}Th-derived POC export (^{234}Th-Cex) by multiplying it by the C:Th ratio using Eq. 3.6. These results are shown in Table 3.5. ^{234}Th-Cex for leg 1 fall into the same two distinct groups as those described for the ^{234}Th disequilibria with Stations M2, M6, and M3.2 showing low ^{234}Th-Cex (*ca.* 5 mmol C m^{-2} d^{-1}) and with high ^{234}Th-Cex (*ca.* 15 mmol C m^{-2} d^{-1}) across the rest of the study site (Figure 3.4a). Leg 2 showed high ^{234}Th-Cex across the whole region ranging from 12-30 mmol C m^{-2} d^{-1} (Figure 3.4b). The same procedure is used for calculating ^{234}Th-derived PON export (^{234}Th-Nex) using ^{234}Th fluxes and PON to ^{234}Th ratios (N:Th). ^{234}Th-Nex follow the same pattern as ^{234}Th-Cex: for leg 1 M2, M6, and M3.2 had low ^{234}Th-Nex (*ca.* 1.0 mmol N m^{-2} d^{-1}) whereas high ^{234}Th-Nex (*ca.* 2.4 mmol N m^{-2} d^{-1}) were encountered across the rest of the study site. Leg 2 showed high ^{234}Th-Nex across the whole region ranging from 2.2-4.3 mmol N m^{-2} d^{-1}.

Table 3.5 ^{234}Th-Cex and ^{234}Th-Nex calculated with the steady-state model. Values in parentheses are the fluxes at 100 m. All errors are 1σ.

Station	POC export (mmol m^{-2} d^{-1})	PON export (mmol m^{-2} d^{-1})
M1	17.1 ± 4.5 (18.8 ± 3.5)	2.7 ± 0.7 (2.9 ± 0.6)
M3.1	15.3 ± 4.4 (13.5 ± 3.2)	2.4 ± 0.7 (2.1 ± 0.5)
M3.2	4.9 ± 2.3 (4.9 ± 2.3)	0.9 ± 0.4 (0.9 ± 0.4)
M2.1	5.3 ± 3.0 (4.9 ± 2.7)	0.9 ± 0.5 (0.9 ± 0.5)
M6.1	5.8 ± 4.0 (5.8 ± 3.9)	1.1 ± 0.8 (1.1 ± 0.7)
M3.3	13.9 ± 3.4 (11.6 ± 2.7)	2.4 ± 0.6 (2.0 ± 0.5)
M7	13.0 ± 3.0 (13.6 ± 2.5)	2.6 ± 0.6 (2.7 ± 0.5)
M8E	15.3 ± 3.8 (15.3 ± 3.8)	2.5 ± 0.6 (2.6 ± 0.6)
M8W	13.7 ± 2.5 (13.6 ± 2.5)	2.1 ± 0.4 (2.0 ± 0.4)
M9.1	16.8 ± 2.9 (16.7 ± 3.2)	2.3 ± 0.4 (2.3 ± 0.4)
M9.2	30.0 ± 5.6 (23.2 ± 4.3)	4.3 ± 0.8 (3.3 ± 0.6)
M10	12.3 ± 3.4 (11.3 ± 2.8)	2.3 ± 0.6 (2.1 ± 0.5)
M3.4	25.8 ± 5.3 (20.0 ± 3.9)	4.2 ± 0.9 (3.3 ± 0.6)
M5	17.9 ± 3.6 (12.8 ± 2.5)	2.9 ± 0.6 (2.1 ± 0.4)
M3.5	22.2 ± 5.4 (15.6 ± 3.8)	3.2 ± 0.8 (2.2 ± 0.5)
M6.2	18.3 ± 3.6 (14.4 ± 3.0)	2.8 ± 0.6 (2.2 ± 0.5)
M2.2	22.0 ± 4.2 (18.8 ± 3.4)	3.5 ± 0.7 (3.0 ± 0.5)
M3.6	20.4 ± 5.3 (13.8 ± 3.7)	3.3 ± 0.9 (2.2 ± 0.6)
M3.7	13.7 ± 3.3 (10.1 ± 2.6)	2.2 ± 0.5 (1.7 ± 0.4)
M3.8	15.0 ± 3.5 (12.2 ± 2.8)	2.5 ± 0.6 (2.1 ± 0.5)

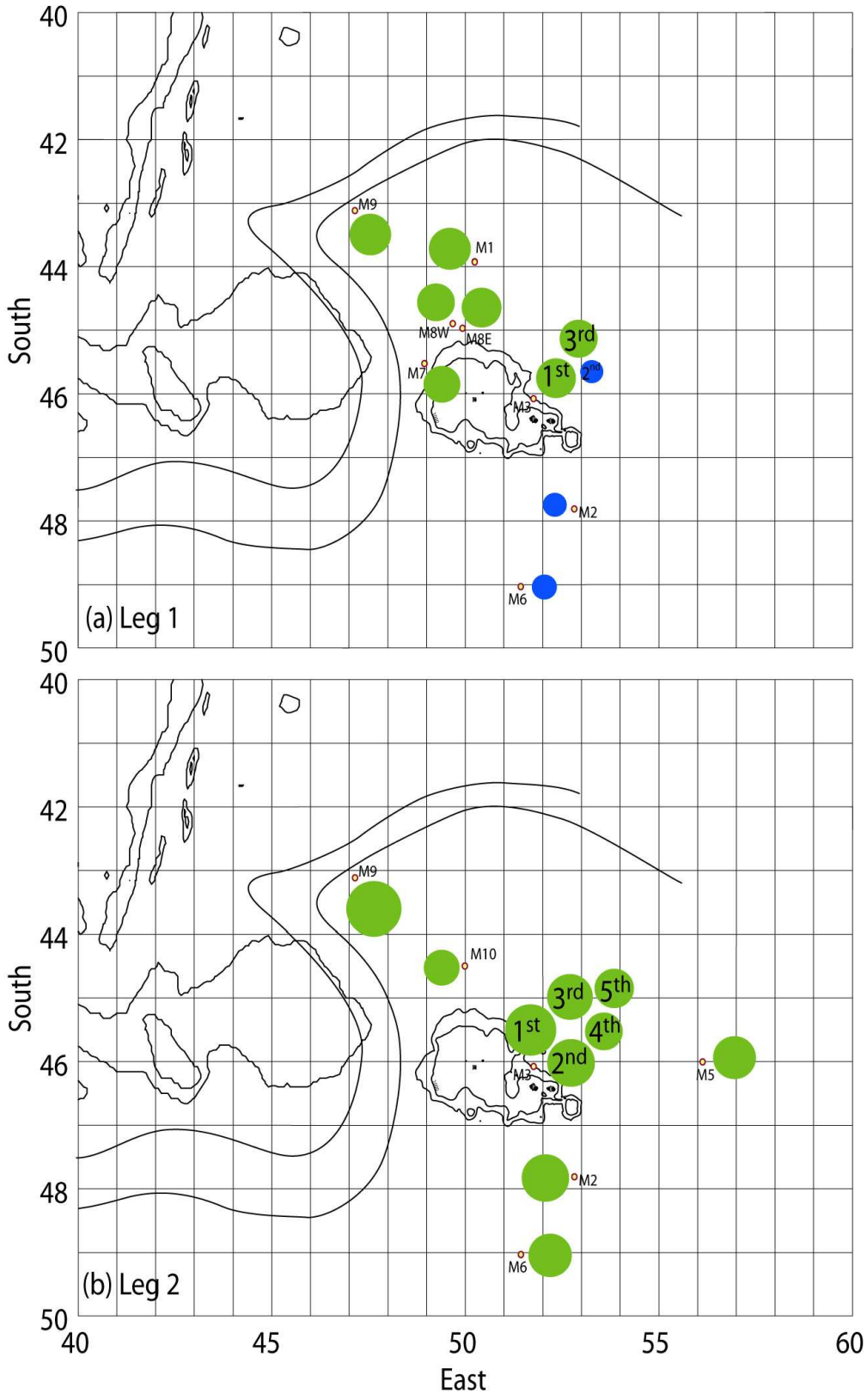

Figure 3.4 Spatial variation of ^{234}Th-Cex (mmol C m^{-2} d^{-1}) during leg 1 (a) and leg 2 (b). The area of the bubbles are proportional to carbon export. Leg 1 shows two distinct groups of export with low export to the south and high export to the north. Leg 2 does not show any spatial variation in ^{234}Th-Cex. Repeat occupations of M3 are shown with numbered bubbles. The two smooth curving lines show the major permanent branch of the ACC (Pollard *et al.*, 2007b).

To calculate the non steady-state ^{234}Th-Cex and ^{234}Th-Nex, the non steady-state ^{234}Th fluxes in Table 3.2 were multiplied by the mean of the two C:Th and N:Th ratios measured at subsequent occupations of the same station (Table 3.6). Generally, non steady-state ^{234}Th-Cex rates (Table 3.7) were comparable to the steady-state ^{234}Th-Cex rates measured during leg 2 (Table 3.5). In the north at M9 the non steady-state ^{234}Th-Cex of 27.3 mmol C m^{-2} d^{-1} agrees best with the leg 2 steady-state ^{234}Th-Cex of 30.0 mmol C m^{-2} d^{-1}. To the south at M2 and M6 the non steady-state ^{234}Th-Cex of ≈22 mmol C m^{-2} d^{-1} agrees well with the leg 2 steady-state ^{234}Th-Cex of ≈20 mmol C m^{-2} d^{-1} but is about four times higher than the leg 1 steady-state ^{234}Th-Cex of ≈5 mmol C m^{-2} d^{-1}. The confirmation of high ^{234}Th-Cex in the southern region during leg 2 suggests that the small bloom observed there resulted in ^{234}Th-Cex equivalent to the north. Again, non steady-state ^{234}Th-Nex rates (Table 3.7) followed a similar pattern as the leg 2 steady-state ^{234}Th-Nex (Table 3.5). Non steady-state ^{234}Th-Nex ranged from 3.7-3.9 mmol N m^{-2} d^{-1}.

Table 3.6 Averaged elemental ratios of POC and PON with ^{234}Th for the three non steady-state stations. All errors are 1σ.

Station name	C:Th ratio (μmol dpm^{-1})	N:Th ratio (μmol dpm^{-1})
M2	7.9 ± 0.6	1.3 ± 0.1
M6	9.0 ± 0.7	1.6 ± 0.1
M9	9.3 ± 0.7	1.3 ± 0.1

Table 3.7 ^{234}Th-Cex and ^{234}Th-Nex calculated with the non steady-state model. Values in parentheses are the fluxes at 100 m, except for M6 at which the integration depth was 100 m (Table 3.2). All errors are 1σ.

Station name	^{234}Th-Cex (mmol m^{-2} d^{-1})	^{234}Th-Nex (mmol m^{-2} d^{-1})
M2	23.3 ± 4.2 (21.2 ± 3.8)	3.9 ± 0.7 (3.6 ± 0.6)
M6	21.0 ± 4.5	3.7 ± 0.8
M9	27.3 ± 9.1 (21.2 ± 7.8)	3.8 ± 1.3 (3.0 ± 1.1)

3.4.2 Export Efficiency

To put some perspective on the proportion of primary production that is exported out of the surface ocean the *ThE* ratio can be calculated (Buesseler, 1998). The *ThE* ratio is the ratio of ^{234}Th-Cex to ^{14}C primary production (^{14}C PP) and is therefore similar in concept to the *f*-ratio which is the ratio of new production to total production as explained in Section 1.2.3 (Eppley and Peterson, 1979). Table 3.8 shows

the ^{14}C PP (mmol m^{-2} d^{-1}) measured by Seeyave *et al.* (2007) and associated *ThE* ratios at each station. Figure 3.5 shows how ^{234}ThCex varies with ^{14}C PP. In general *ThE* ratios are lower during leg 1 than leg 2. Leg 1 *ThE* ratios range from 15-35% with the exception of M8E which peaks at 133%. Leg 2 shows much higher variability in *ThE* ratios with low values in the M3 eddy bloom of 7-11%, high values of 35-81% and two values in excess of 100%. *ThE* ratios during CROZEX were almost always >10%, which is typical of the Southern Ocean (Buesseler, 1998). Higher *ThE* ratios of 12-24% have been reported by Rutgers van der Loeff *et al.* (1997) in a PF bloom, and Buesseler *et al.* (2003) reported a wide range of *ThE* ratios from 15-65% during a project to assess the effect of an ice margin on production and particle export. Therefore the majority of CROZEX *ThE* ratios agree with values reported in the literature. *ThE* ratios calculated from the non steady-state ^{234}Th-Cex at M2, M6, and M9 were 86%, 91%, and 80%, respectively (Table 3.8).

Table 3.8 ^{234}Th-Cex, ^{14}C PP (Seeyave *et al.*, 2007) and resultant *ThE* ratios for steady-state and non steady-state models. Values in parentheses are ^{234}Th-Cex and *ThE* ratios at 100 m. Errors are 1σ.

Station	^{234}Th-Cex (mmol m^{-2} d^{-1})	^{14}C PP (mmol m^{-2} d^{-1})	*ThE* ratio (%)
Steady-state			
M1	17.1 ± 4.5 (18.8 ± 3.5)	90	19 (21)
M3.1	15.3 ± 4.4 (13.5 ± 3.2)	44	35 (31)
M3.2	4.9 ± 2.3 (4.9 ± 2.3)	31	16 (16)
M2.1	5.3 ± 3.0 (4.9 ± 2.7)	36	15 (14)
M6.1	5.8 ± 4.0 (5.8 ± 3.9)	20	30 (30)
M3.3	13.9 ± 3.4 (11.6 ± 2.7)	40	35 (29)
M7	13.0 ± 3.0 (13.6 ± 2.5)	64	20 (21)
M8E	15.3 ± 3.8 (15.3 ± 3.8)	11	133 (133)
M8W	13.7 ± 2.5 (13.6 ± 2.5)	41	34 (33)
M9.1	16.8 ± 2.9 (16.7 ± 3.2)	57	29 (29)
M9.2	30.0 ± 5.6 (23.2 ± 4.3)	10	305 (235)
M10	12.3 ± 3.4 (11.3 ± 2.8)	36	35 (32)
M3.4	25.8 ± 5.3 (20.0 ± 3.9)	60	43 (34)
M5	17.9 ± 3.6 (12.8 ± 2.5)	34	52 (37)
M3.5	22.2 ± 5.4 (15.6 ± 3.8)	27	81 (57)
M6.2	18.3 ± 3.6 (14.4 ± 3.0)	25	73 (57)
M2.2	22.0 ± 4.2 (18.8 ± 3.4)	17	128 (109)
M3.6	20.4 ± 5.3 (13.8 ± 3.7)	250	8 (6)
M3.7	13.7 ± 3.3 (10.1 ± 2.6)	184	7 (5)
M3.8	15.0 ± 3.5 (12.2 ± 2.8)	138	11 (9)
Non steady-state			
M2	23.3 ± 4.2 (21.2 ± 3.8)	27	86 (79)
M6	21.0 ± 4.5	23	91
M9	27.3 ± 9.1 (21.2 ± 7.8)	34	80 (62)

Although the *ThE* ratio can be used to assess the ^{234}Th-Cex efficiency of a bloom, some caution should be exercised when interpreting the results. In particular, the two properties used to generate the *ThE* parameter operate on different time-scales. ^{14}C PP is a rate measurement typically measured with 12-24 h bottle incubations, whereas ^{234}Th export estimates integrate over the mean life-time of the tracer, which is 34.8 days (Buesseler, 1998). Given this large difference in time-scales it is easy to see how one might arrive at a *ThE* ratio of >100%. For example, should a ^{14}C PP measurement be made on a particularly cloudy day the measured rates of PP are likely to be depressed and the consequent *ThE* ratio enhanced. This could result in two different conclusions of the export efficiency: a low *ThE* ratio in the case of the sunny day (with high PP) or a high *ThE* ratio in the case of the cloudy day (with low PP). This issue is of relevance in an area of dynamic meteorological activity, such as the Southern

Ocean, and worthy of future investigation. In addition to the scenario just described, a variety of other factors can contribute to difficulties in interpreting *ThE* ratios such as the onset or decline of a bloom (Buesseler, 1998).

Given the many factors that are involved in potentially driving the *ThE* ratio of the Crozet bloom, the *ThE* ratios calculated in Table 3.8 have to be treated with some caution. However, keeping this caveat in mind, some conclusions can be drawn from the CROZEX *ThE* ratios, in particular, the general trend to higher *ThE* ratios observed during leg 2. The most likely cause of these are the decline and termination of the bloom resulting in an instantaneously efficient biological pump. However, a stable bloom supporting a continuously efficient biological pump can not be ruled out except in the cases of where *ThE* ratios exceed 100%, which clearly have to result from an offset of the characteristic time-scales of the measured parameters.

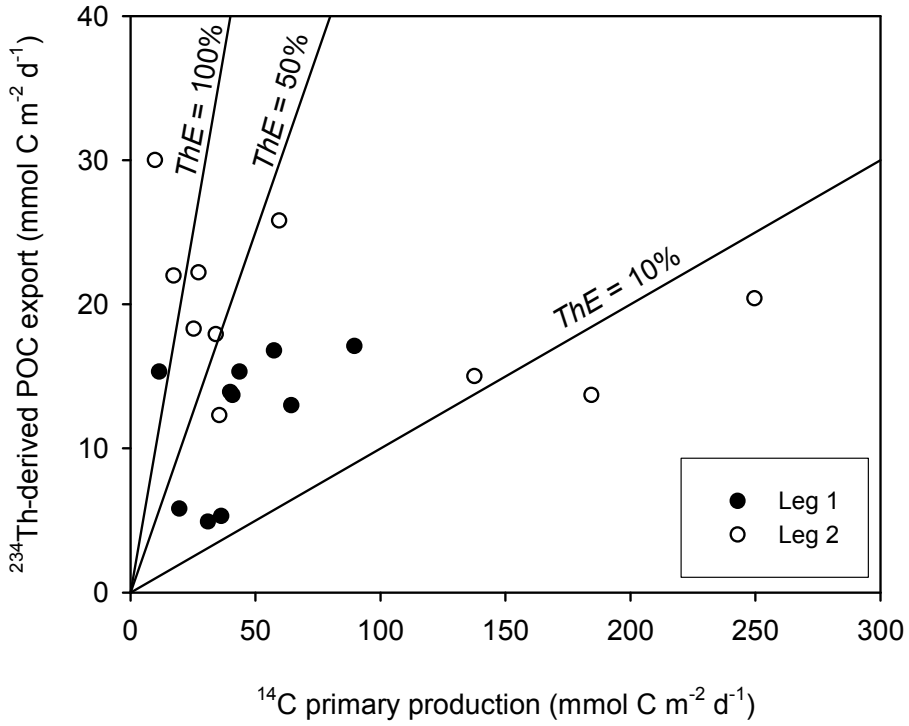

Figure 3.5 *ThE* ratios for stations sampled for ^{234}Th-derived POC export and ^{14}C-derived primary production, the latter measured by Seeyave *et al*. (2007). For reference the 10%, 50%, and 100% *ThE* ratio lines have been plotted.

3.4.3 Comparison with Literature

Since SOIREE, the first iron fertilisation experiment in the Southern Ocean in February 1999, there have been three other such experiments: EisenEx in November 2000, SOFeX in January-February 2002, and EIFEX in January-March 2004 (Boyd *et al.*, 2000; Coale *et al.*, 2004; Gervais *et al.*, 2002; Hoffmann *et al.*, 2006). All these experiments followed the same general pattern whereby an area of the ocean was artificially fertilised with iron and then the ensuing biological response was monitored in the patch of fertilisation, with a control site outside of the iron-fertilised area. All these experiments noted an increase in biomass in the fertilised patch, but have yielded varying results in the amount of POC export to mesopelagic depths when compared to their respective control sites and/or to observations made in the same oceanic region during a different time period. The SOIREE and EisenEx blooms, which were monitored for 13 and 22 days respectively, showed no significant enhancement of POC export in the iron-fertilised area (Charette and Buesseler, 2000; Nodder *et al.*, 2001; Rutgers van der Loeff and Vöge, 2001). In contrast the SOFeX bloom, which was monitored for 27 days, showed 2.5 times more POC export within the iron-fertilised patch when compared to outside the patch (Buesseler *et al.*, 2004; Buesseler *et al.*, 2005). However, the SOFeX POC export was still smaller than a natural bloom at the same site in 1998 (Buesseler *et al.*, 2001a). EIFEX, which was monitored for 36 days, recorded the highest POC export ever measured in the Southern Ocean in addition to generally higher POC export within the iron-fertilised patch (Vöge *et al.*, 2006). After SOFeX, Bishop *et al.* (2004) concluded that POC export only showed a significant increase several weeks after the first iron addition, with fluxes peaking at day 41. Unfortunately these experiments were restricted in time; therefore allowing the ship to be present in the study site for the release of iron and initial bloom development, but not for the bloom termination when particle export is likely to be highest (Buesseler *et al.*, 2005; Buesseler and Boyd, 2003). This may explain why the shorter iron-fertilisation experiments showed less POC export than the longer experiments.

CROZEX did not suffer from the issue of restricted time because the bloom area was fertilised naturally with iron from the Crozet Plateau (Charette *et al.*, 2007; Planquette *et al.*, 2007), thus allowing the study to focus its sampling on the later half of the bloom period. The first observation of ^{234}Th-Cex on CROZEX was made about 15 days after the chlorophyll peak of the main bloom in the north of the study site (Venables *et al.*, 2007) with observations then made across the study site for 2 months,

hence during the decline of the bloom. This time frame should give the opportunity to resolve the lack of data from the declining phase of a phytoplankton bloom, but before this is done the CROZEX ^{234}Th-Cex should be compared to other ^{234}Th-Cex made in the Southern Ocean under natural conditions.

There have been several studies into ^{234}Th-Cex in the PFZ in the Southern Ocean (Buesseler *et al.*, 2001a; Coppola *et al.*, 2005; Rutgers van der Loeff *et al.*, 2002; Rutgers van der Loeff *et al.*, 1997). Within the PFZ of the Indian sector of the Southern Ocean, the area in which the Crozet Plateau lies (Pollard *et al.*, 2002), Coppola *et al.* (2005) obtained ^{234}Th-Cex estimates in January-February 1999 on the ANTARES 4 cruise, approximately 10°E of the Crozet Islands in an area known as the Crozet Basin. This area is northwest of the Kerguelen Plateau in a deep basin (≈5000 m) and away from any significant bottom topography. During this study, very low ^{234}Th-Cex was measured, ranging from 0.1-2.5 mmol C m^{-2} d^{-1} at 100 m, which are less than half the lowest fluxes measured to the south of the CROZEX study site through the same depth horizon (Table 3.5). Coppola *et al.* (2005) hypothesised that these resulted from either a very efficient remineralisation process and/or a high bacterial activity, or a decoupling of PP and ^{234}Th-Cex. Diatoms are typical of PF blooms and their low abundance during the study of Coppola *et al.* (2005) was also hypothesised to contribute to the low fluxes. In other regions of the Southern Ocean, ^{234}Th-Cex at 100 m in the PF were estimated to be 19.5-39.1 and 8.8 mmol C m^{-2} d^{-1} (Atlantic PF blooms: Rutgers van der Loeff *et al.*, 2002; Rutgers van der Loeff *et al.*, 1997), and 5.5-14.5 mmol C m^{-2} d^{-1} (Pacific PF blooms Buesseler *et al.*, 2001a). The CROZEX data fit well within the range of these PF observations.

The most relevant study for comparison with the CROZEX project is the KErguelen Ocean and Plateau compared Study (KEOPS), which sampled the annual bloom observed over the Kerguelen Plateau during January-February 2005 (Blain *et al.*, 2007), and partly overlapped CROZEX. On KEOPS, ^{234}Th-Cex measured within the iron-replete bloom reference station on KEOPS gave ^{234}Th-Cex at 100 m of 10.5-38.4 mmol C m^{-2} d^{-1} (Savoye *et al.*, 2008), which is generally in good agreement with bloom export measured at 100 m, ranging from 10.1 to 23.2 mmol C m^{-2} d^{-1} on CROZEX (Table 3.5), if slightly greater in range. This compares to a 100 m ^{234}Th-Cex of 12.2 mmol C m^{-2} d^{-1} in the control, non-bloom reference station on KEOPS, which is greater than the 100 m flux observed on CROZEX during leg 1 of ≈5 mmol C m^{-2} d^{-1}, but less than the export of 14.4-18.8 mmol C m^{-2} d^{-1} during leg 2. However, the average

100 m ^{234}Th-Cex of all the CROZEX non-bloom stations was ≈10 mmol C m^{-2} d^{-1} (Table 3.5), in very close agreement with KEOPS. The *ThE* ratio during KEOPS showed a trend of increasing export efficiency at the low productivity site when compared to the high-productivity sites. 58% of PP was exported below 100 m at the non-bloom reference station, compared with 13-48% being exported below 100 m at the Fe-replete bloom station. A similar, but less clear-cut trend was evident during CROZEX. For CROZEX on leg 1 the *ThE* ratio at 100 m was 16-30% and 21-133% for non-bloom and bloom stations, respectively (Table 3.8). If the value of 133% for bloom stations is removed, as this is clearly due to a decoupling of PP and export, then the range narrows to 21-33% and is almost the same as the non-bloom observations and in close agreement with the KEOPS range of 13-48%. However, on leg 2 of CROZEX after a small bloom had occurred in the south (Venables *et al.*, 2007), the *ThE* ratio at 100 m had changed to 57-109%, 32-235%, and 5-9% for non-bloom, bloom and M3 eddy bloom stations, respectively (Table 3.8). Once again if the *ThE* ratios of >100% are removed, the export efficiencies change to 57%, 32-57%, and 5-9% for non-bloom, bloom and M3 eddy bloom stations respectively. Therefore, a trend of decreasing *ThE* ratio with increasing productivity can be seen. These results not only support the KEOPS results but are also in agreement with recent work published by Lam and Bishop (2007) on high-biomass, low-export regimes who noted a trend of persistently low export even after the addition of iron.

3.5 Comparison with CROZEX Primary and New Production

The CROZEX project benefits from its multidisciplinary nature and wide range of parameters measured. In addition to the ^{234}Th approach several other methods were used during CROZEX to estimate new and export production. These were neutrally buoyant sediment traps (Salter *et al.*, 2007), ^{15}N uptake rates (Lucas *et al.*, 2007), and nutrient draw-down budgets (Sanders *et al.*, 2007). Each of these is an alternative method of constraining export estimates, assuming that new and export production are equivalent when integrated over at least one annual cycle (Eppley and Peterson, 1979). To clarify terminology for this section: PP will refer to total carbon assimilation, new production (which relates to the export from the euphotic zone of both particulate and dissolved material (Bronk *et al.*, 1994)) will refer to production resulting from sources of nutrients from outside the euphotic zone, and export production will refer to POC that has settled out of the surface ocean.

Of the other methods used to constrain export during CROZEX the nutrient draw-down budgets of Sanders *et al.* (2007) provide the best comparison with the ^{234}Th-Cex. This is because the nutrient draw-down approach operates on a similar time-scale as the ^{234}Th approach. Sanders *et al.* (2007) calculated levels of temporally integrated primary and new production. Temporally integrated PP was calculated by coupling the relationship of chl-*a* and PP, derived by Seeyave *et al.* (2007), to satellite chl-*a* imagery. Temporally integrated new production was calculated by determining nitrate removal. Both these parameters, primary and new production, show a clear north-south gradient with high levels in the north and low levels in the south (Figure 3.6a and b).

Estimates of ^{234}Th-Cex from the study region during leg 1 show a clear north-south gradient with values of ≈15 mmol C m^{-2} d^{-1} in the north during the period immediately following the phytoplankton bloom, and ≈5 mmol C m^{-2} d^{-1} in the south prior to the small southern plankton bloom (Figure 3.6c). During leg 2 no gradient in ^{234}Th-Cex was seen once the modest bloom had occurred in the south but ranged by approximately a factor of two across the study region from about 10-23 mmol C m^{-2} d^{-1}. Both steady-state and non steady-state analyses of the ^{234}Th data suggest no significant north-south gradient of ^{234}Th-Cex existed during this leg, thus the results presented here do not fully support a higher level of POC export in the large bloom to the north when compared to the small bloom in the south (Figure 3.6c).

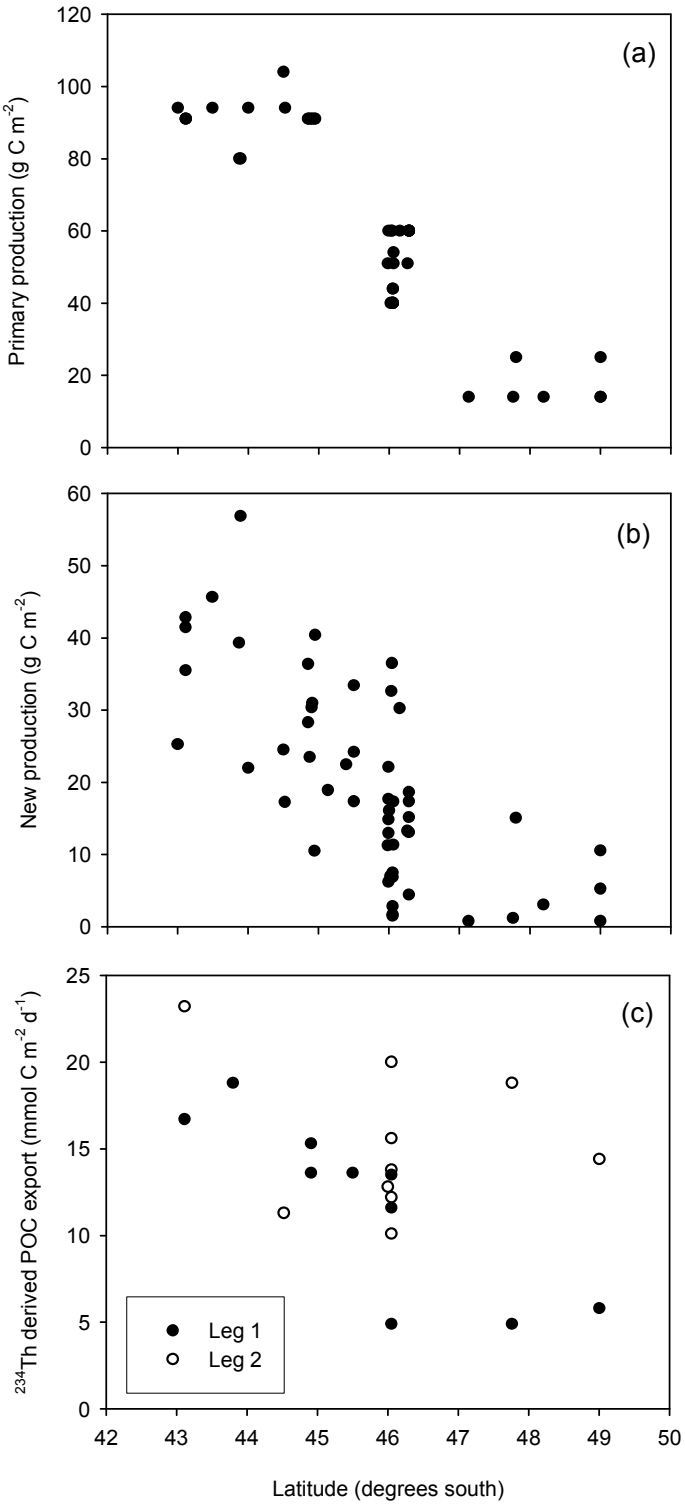

Figure 3.6 The latitudinal variation in primary production (a), new production (b), and ^{234}Th-Cex (c). Satellite-derived primary production and new production are integrated from the start of the bloom period until the date of sampling (Sanders *et al.*, 2007). Not all the units on the y-axis are the same: primary and new production are displayed in g C m^{-2} (integrating over the sampling period) and export production is displayed in mmol C m^{-2} d^{-1} thus not allowing a direct comparison. Although there is a time-scale difference between the ^{234}Th-Cex and both primary and new production, this should be somewhat dampened by the integrating properties of the ^{234}Th method that quasi-integrates over the mean life-time of the tracer (34.8 days).

Sanders *et al.* (2007) and Seeyave *et al.* (2007) concluded that primary and new production varied by approximately a factor of four between the most northern and southern sites (Figure 3.6a and b). While, during leg 1 ^{234}Th-Cex also showed a north-south gradient, it failed to show the same clear north-south gradient during leg 2 (Figure 3.6c). It is worth mentioning at this point that not all the units used in Figure 3.6 are the same. Primary and new production are displayed in g C m^{-2} and export production is displayed in mmol C m^{-2} d^{-1}, thus not allowing a direct comparison. However, this does not invalidate the comparison of the north-south trends observed, which have three possible explanations:

(1) a bulk export event from the northern bloom may not have been sampled because the cruise arrived in the region two weeks after the peak of the bloom,
(2) the estimates of new production and/or export production are inaccurate,
(3) new and export production are not equivalent, with this lack of equivalence being particularly pronounced in the north, or
(4) the rates of export may be accurate but the export even was longer in the north, hence generating more export in the northern bloom region.

These four possibilities will now be examined.

Explanation 1. The bulk export event from the northern bloom may not have been sampled because the cruise arrived in the region two weeks after the peak of the bloom.

^{234}Th-derived export measurements are representative of the export conditions over the mean life-time of the tracer, which is 34.8 days (Buesseler, 1998). Therefore ^{234}Th-derived export has a natural temporal integrating power built into the tracer. The CROZEX cruise arrived in the study region two weeks after the peak of the bloom, which is a shorter time period than the half-life of ^{234}Th, thus weakening the strength of this explanation.

Explanation 2. The estimates of new production and/or export production are inaccurate.

The possibility that the methods used generated inaccurate results is an issue that frequently arises and likewise neither the nutrient draw-down nor the ^{234}Th method are free of flaws or caveats. For example, issues may have arisen in the ΔNO_3^- new production estimates resulting from mesoscale spatial variability in nitrate concentrations (Sanders *et al.*, 2007), or with the ^{234}Th method when incorporating uncertainties such as the C:Th ratio and the issues related to advection and turbulent diffusion. Given that these issues have been already addressed with the caveats already spoken to, other explanations and hypotheses should be explored to explain the observed trends and discrepancies seen in the new and export production estimates, based on the assumption that the new and export production estimates are correct.

Explanation 3. New and export production are not equivalent, with this lack of equivalence most pronounced in the north.

The paradox to be tackled is: why do the spatial patterns of integrated new production and daily rates of export not agree? When new production takes place it generates organic carbon, essentially the organic carbon that makes up the primary producers. This organic matter then has several possible fates:

(1) it "dies" and sinks out,
(2) it enters a suspended or very slowly settling particulate organic phase,
(3) it enters the dissolved organic pool, or
(4) it is grazed and moves to a higher trophic level, which will ultimately enter routes 1, 2, or 3 nonetheless.

The first pathway is the exported production and can be regarded as the particle export measured with the ^{234}Th technique, with a 100 m flux of approximately 12-23 mmol C m^{-2} d^{-1} and 2.0-3.3 mmol N m^{-2} d^{-1} (Table 3.5). Investigating the second and third pathways (standing stocks of particulate and dissolved organic material

respectively) is of major importance if a carbon budget for CROZEX is to be constructed. A build-up of suspended POM (sPOM) and DOM is not an unreasonable suggestion and evidence of a buildup of particulate and dissolved pools of organic material has been observed before. For example increases in POC stocks have been observed in both the Ross Sea and during the SOIREE fertilisation experiment (Bakker *et al.*, 2006; Bakker *et al.*, 1997; Sweeney *et al.*, 2000). Increases in DOM stocks is not so clear with studies reporting both no DOM buildup (Kähler *et al.*, 1997) and significant DOM buildup (Bakker *et al.*, 2006; Carlson *et al.*, 2000; Sanders *et al.*, 2005). If it was observed that the buildup of sPOM and DOM was proportionally higher in the bloom region when compared to the non-bloom region then this may open the question of differential export efficiencies in the two regions. Expressed differently, this means that the high production region may have low fractional levels of export, and the low production region may have high fractional levels of export. This type of system would be akin to a high-biomass, low-export regime in the productive north, and a low-biomass, high-export regime in the south (Lam and Bishop, 2007). Sets of POC/N and DON samples were collected thus allowing an opportunity to test this explanation and will be presented in Chapters 4 and 5 for the dissolved and particulate pools respectively.

Explanation 4. The rates of export may be accurate but the export event was longer in the north, hence generating more export in the northern bloom region.

This final explanation is relatively simple in context. It makes the assumption that the rates of export measured north and south are accurate but then suggests that the duration of the export events in the two regions are different lengths. The total length of the main bloom in the north lasted for about 100 days compared to about 60 days for the relatively small bloom observed in the south. Therefore, there is the potential for a longer period of export in the north compared to the south. Even if the daily rates of ^{234}Th-Cex were the same in the two regions, a longer duration of export in the north would result in a greater seasonal export. This explanation will be explored in detail in Chapter 6.

3.6 Conclusions

It has been demonstrated here that ^{234}Th-Cex during the Crozet bloom showed high levels in the bloom area and low levels at the southern control stations during leg 1. After a relatively small bloom at the southern control stations this spatial variability was not observed during leg 2, which showed equally high levels of ^{234}Th-Cex throughout the study site. Therefore, maybe the question that should be asked is not: ‘‘Why are the POC fluxes so high at the southern control stations during leg 2?’’, but instead: ‘‘Why are the POC fluxes not even higher at the northern bloom stations?’’ It is hypothesised that this lack of latitudinal variability in ^{234}Th-Cex may the result of two different scenarios: 1) there was a storage of particulate and dissolved organic material in the northern bloom region that would have the effect of reducing the amount of POC that is available for export to mesopelagic depths, or 2) the length of the export event in the north was greater than the south, thus resulting in greater total seasonal export in the north compared to the south. These scenarios will now be investigated in Chapters 4, 5 and 6.

4 Dissolved Organic Nitrogen

4.1 Introduction

4.1.1 The Problem to be Tackled

It was shown in Chapter 3 that the latitudinal gradient of daily ^{234}Th-derived carbon export (^{234}Th-Cex) was different on legs 1 and 2. Leg 1 had about three times more ^{234}Th-Cex in the north compared to the south, whereas on leg 2 the ^{234}Th-Cex was equally high across the study region after a relatively small bloom in the south (Figure 3.6c). In comparison the integrated estimates of primary and new production had about a four-fold gradient of high to low from north to south respectively when combining data from both cruises (Figure 3.6a & b). This therefore poses the question of: why is there no observable latitudinal gradient of ^{234}Th-Cex on leg 2? In an attempt to explain this, one hypothesis presented at the end of Chapter 3 suggested that the different latitudinal patterns between ^{234}Th-Cex and ΔNO_3^- new production (ΔNO_3^- NP) may be the result of relatively more organic matter storage in the surface waters in the northern region. This would have the effect of reducing the amount of POM available for export, with this effect most pronounced in the high productivity northern region.

Chapters 4 and 5 will now consider this hypothesis in more detail, focusing on dissolved organic matter (DOM) in this chapter and suspended particulate organic matter (sPOM) in Chapter 5. This chapter will examine the quantity of DOM found in the upper water column and place this information in a spatial and temporal context. This will be done in the context of dissolved organic nitrogen (DON) on archive seawater samples because samples for dissolved organic carbon (DOC) where not collected during the CROZEX cruises. Using DON data, the flow of nitrogen from the dissolved inorganic nitrogen (DIN) pool into the DON pool will be investigated, to establish whether this pathway is significant enough to have the effect of reducing the amount of organic material available for export to deeper depths. A final discussion will then place this information in the context of the latitudinal gradients of ^{234}Th-Cex.

4.1.2 Synopsis of DON Samples Collected

DON analyses were made on archived seawater samples collected throughout the CROZEX cruise. These samples were taken routinely along with the other standard parameters from the stainless steel CTD. The samples were taken from the top twelve

depths sampled by the CTD rosette, Niskins 13-24, which typically covered 10-300 m. The samples were collected in 60 ml Sterilin® screw cap sample pots, then stored at -20 °C and returned to NOC for analysis using the analytical method described in Section 2.5. For analysis the samples were prioritised to target samples from across the study region and in the surface of the water column, with the intention of completing deeper parts of the profiles at a later date. Prioritising samples ultimately proved to be a fortuitous decision because when the time came to process deeper samples it turned out that the remaining samples had been compromised because the storage freezer had been switched off for an unknown period of time, probably >1 week, thus allowing the samples to thaw out. As no preservatives had been used to kill the samples when collected there was no way of ensuring that the samples had not been subjected to biological degradation or some other chemical alteration whilst sat in a warm freezer. Therefore it was decided that no additional samples would be analysed and what data had been collected would be sufficient. In most cases profiles had been analysed down to at least 60 m and in some down to 100 m. As the 100 m depth horizon was the depth of interest for integration purposes no further attempt at processing compromised samples was made. The locations of stations sampled are plotted in Figure 4.1. The three dashed boxes, north, centre and south, are areas defined by Venables *et al.* (2007) to assess the satellite observed time progression of chl-*a* in different regions. These boxes were used as a guide to regionalise the stations sampled for DON, solid boxes north, centre, south, with the addition of an east and west region.

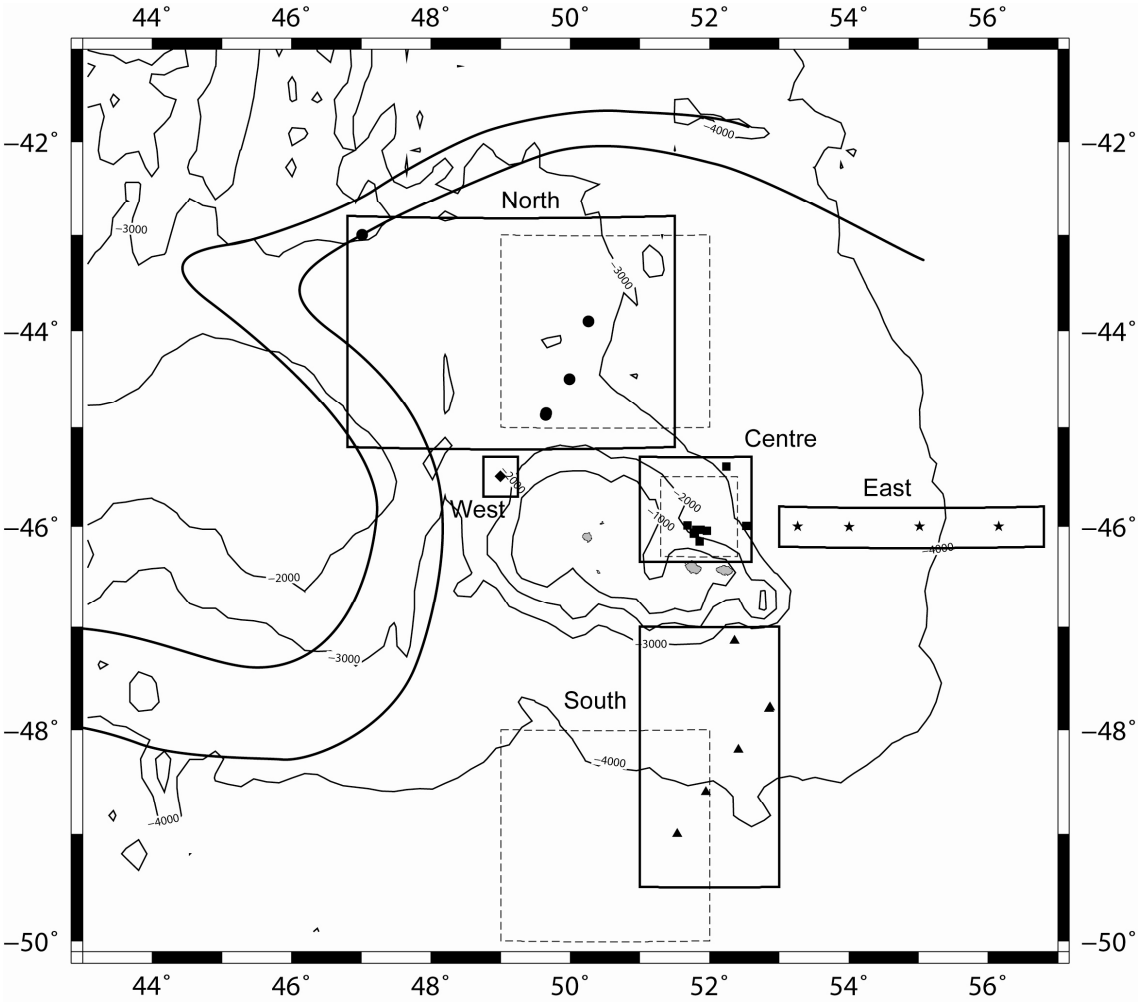

Figure 4.1 Map of station positions. Dashed boxes were determined by Venables *et al.* (2007) to regionalise the study area. These have been modified to encompass DON stations, solid boxes. 1000 m bathymetry contours and the circulation front of the ACC are included for reference (Pollard *et al.*, 2007b).

4.2 Method Verification and Quality Control

4.2.1 History and Principle of the DON Method

The measurement of DON in seawater still remains a controversial subject, and when compared to dissolved organic carbon (DOC), DON still lags behind in the number of studies tackling method development (Bronk, 2001). This is primarily the result of technical difficulties inherent in DON analysis which are not present during the analysis of DOC (Sharp, 2001). All the methods used for DON determinations require multiple analyses that include a determination of total dissolved nitrogen (TDN), and then determination of one or more of the inorganic components of the DIN pool. DON is then calculated by difference (Eq. 4.1).

$$DON = TDN - DIN \quad \text{Eq. 4.1}$$

$$DIN = NO_3^- + NO_2^- + NH_4^+ \quad \text{Eq. 4.2}$$

The DIN pool (Eq. 4.2) classically includes three fractions: nitrate (NO_3^-), nitrite (NO_2^-) and ammonium (NH_4^+) and would typically all be subtracted from TDN to give DON (Bronk, 2001; Sharp *et al.*, 2002). Unfortunately, NH_4^+ was not measured as part of the core suite of inorganic nutrients so can not be included as part of the DIN pool. However, it will now be argued that it was not necessary to measure NH_4^+. The reason for this is because NH_4^+ is a nutrient that contributes to regenerated production and is not contributing to NP, which is only fuelled by NO_3^- (Eppley and Peterson, 1979). If NH_4^+ was included in the DIN pool for the calculation of DON it would only have to be factored back out of the DON pool when assessing the DON pool in relation to ΔNO_3^- NP later on. Therefore to prevent this complication the DON pool will not be corrected for NH_4^+ thus allowing any variation in DON to be only attributable to ΔNO_3^- NP. NO_2^- can not be separated out of the DIN pool because it was not measured separately, however NO_2^- concentrations in surface waters of the Polar Front (PF) are typically in the range of 0.2 μmol l^{-1} (Whitehouse *et al.*, 2000), about 1% of total DIN stocks, so can therefore be considered to provide a minimal contribution towards any NP NO_2^- may fuel.

There are three families of methods for DON determination: UV-oxidation (UV) (Armstrong and Tibbitts, 1968; Armstrong *et al.*, 1966), persulphate oxidation (PO) (D'Elia *et al.*, 1977; Menzel and Vaccaro, 1964; Solórzano and Sharp, 1980; Valderrama, 1981) and high-temperature combustion (HTC) with varying success (Badr *et al.*, 2003; Hedges *et al.*, 1993; Sharp, 1973; Suzuki, 1993; Suzuki *et al.*, 1985; Suzuki *et al.*, 1992). Each have their own advantages and disadvantages with no one standing out from the rest as a clearly superior method (Bronk *et al.*, 2000; Sharp *et al.*, 2002). For this work the UV method was used for several reasons: the method was already established at NOC and well understood within the lab, it is consistent, cheap and has a relatively easy procedure. For a description of the method see Section 2.5. There are however, several drawbacks to the UV method and these will be explained next and

then some quality control checks will be shown in Section 4.2.2 so that the limitations of the method can be highlighted.

There is still uncertainty amongst the scientific community as to the best method for measuring DON. In the two most recent direct comparisons between the three families of methods, there still remains uncertainty (Bronk *et al.*, 2000; Sharp *et al.*, 2002). For example, the method comparison carried out by by Bronk *et al.* (2000) reported that the HTC and PO methods gave the best recoveries of TDN and gave consistent and comparable results. In contrast to this the standard UV method was described as unpredictable and found to have low recoveries of TDN unless the PO oxidant (potassium persulphate) was used in place of the standard UV oxidant (hydrogen peroxide). However, during a more extensive inter-lab method comparison, no one method proved to be better than the other, although, there was a suggestion that the UV method gave higher TDN values than the HTC method (Sharp *et al.*, 2002). This is contradictory to the results of Bronk *et al.* (2000) who suggested that incomplete conversion of DON to DIN was occurring with the UV method.

Given this lack of methodological agreement across the scientific community one must therefore proceed cautiously and consistently with whichever method is chosen, which in the case of this study, was the UV method. Therefore a series of tests and checks were carried out before and during the analysis of DON samples to ensure rigorous quality control. These included a one-off assessment of DIN recovery from a variety of standard compounds, followed by a routine assessment of DIN recovery from one compound during every batch of samples run. In addition to this an assessment of the blank was also made. Details of these quality controls are presented in Section 4.2.2.

4.2.2 Quality Control

To monitor the quality of DON analysis, several steps were put in place. These included an assessment of the blank, and the assessment of the oxidation efficiency of the UV-oxidisers.

Blank

The object of the blank is to assess the level of contamination a sample receives from when it is collected, until when it is analysed. In the case of DON analysis this

includes contamination from sample containers, storage conditions, labware and intermediate sample containment. Therefore a blank sample must undergo exactly the same treatment as a sample. However, because DON was measured with archive samples a blank solution was not prepared and used at the time of sampling in parallel with the samples. In addition to this, even with advanced planning the preparation of an appropriate blank solution for DON analysis is difficult in principle and will be discussed next.

Determining the sample blank for DON is not as simple as simply processing a sample of analyte-free seawater in the same way as many other analyses. The best example to illustrate this is that of DOC analysis, in which DOC-free seawater is generated by the oxidation of all the organic carbon (Armstrong *et al.*, 1966; Beattie *et al.*, 1961); the inorganic carbon can then be removed from the sample by acidification and purging with a carbon-free gas such as pure oxygen or nitrogen (Sharp, 1973). An analogous protocol is not possible for DON. This is because after the production of NO_3^-, through the oxidation of DON, the NO_3^- is not easily removable from the blank solution (Sharp, 2001). Therefore generating a suitable solution to act as the blank is not possible. One possible solution is to use artificial seawater (ASW) as the blank solution but this has problems because in doing so the results would only be representative of the DON contained within the ASW. Considering that ASW is made up from NaCl dissolved in Milli-Q water (Section 2.4.1), and is stored unfrozen in a carboy, it is not unreasonable to think that trace contaminants of nitrogen may be present within the NaCl and biological activity in the carboy may contribute to elevating the background levels of DON in the ASW. What an ASW blank of this nature does not offer is a true estimate of the contamination a CTD sample will incur. Nonetheless, an ASW blank does offer a limited opportunity to make a conservative (over) estimate of the blank from which an estimate of the limit of detection can be calculated. The ASW blanks for UV-oxidisers A and B respectively were 0.72 ± 0.49 μmol l^{-1} ($\bar{x} \pm 1\sigma$, n = 18) and 0.72 ± 0.52 μmol l^{-1} ($\bar{x} \pm 1\sigma$, n = 18). The limit of detection, calculated as 2σ, was 0.97 and 1.03 μmol l^{-1} for UV-oxidiser A and B respectively. In addition to this an ASW blank is also useful for blank correcting the DON standards as they are made up in a matrix of ASW.

An ASW blank does offer an upper limit of the DON blank but is not truly reflective of a real CTD sample. This creates a problem: how does one measure the contamination a real CTD seawater sample receives? The answer is: you can not, given

the experimental design. To partly tackle this problem it is possible to measure the NO_3^- contamination received by a CTD sample. This was done as follows: two aliquots were taken from each of five surplus DON samples. One aliquot was measured directly for NO_3^-, and the second aliquot was put in the UV-oxidiser, but the UV lamp was not switched on. These samples were then also measured for NO_3^-. This approach will give an estimate of the NO_3^- contamination a sample may receive during the UV-oxidation procedure, but not of the DON contamination. After carrying out this test on five samples and subtracting NO_3^- from the non-irradiated NO_3^- it was discovered that on average 0.3 μmol l^{-1} of NO_3^- was lost while the samples were in the UV-oxidiser (Table 4.1). Not a single sample showed evidence of NO_3^- contamination.

Table 4.1 Testing the impact of the UV-oxidation apparatus on sample NO_3^- concentration. All units are μmol l^{-1}.

Sample ID Station, bottle	NO_3^- in sample not passed through a UV-ox	NO_3^- in sample after passing through a UV-ox turned off	Difference
15538, 23	19.06	18.47	-0.59
15539, 23	11.58	11.37	-0.21
15539, 22	18.85	18.56	-0.29
15584, 19	13.19	13.04	-0.15
15589, 22	21.78	21.53	-0.25

On first inspection, this appears incorrect as one would find themselves adding a blank, rather than subtracting a blank, as would be usually expected. There is no clear reason in the literature why this may be happening. It may be possible that some NO_3^- is adhering to the surface of labware but this too can not be validated. The loss of NO_3^- is about 1.7% which is less than the overall 2.7% RSD calculated for the final DON data. This means that the losses are within the analytical error and can therefore be considered to be minimal.

To summarise, it has been suggested that using ASW as a blank solution is not a satisfactory medium to determine a blank relevant to a CTD sample. Also, it has been shown that there is a minimal, and quite possibly a negative blank of NO_3^- associated with the UV-oxidation procedure. Therefore, giving consideration to that the Sterilin® sample pots are made of polystyrene with a polyethylene lid, neither of which materials contain nitrogen (Howard and Statham, 1993), and are aseptically produced, and the

labware was thoroughly cleaned, then it would be reasonable to assume that minimal DON contamination had occurred. Given the uncertainties in either subtracting or adding a blank it was decided based on this evidence that no blank correction would be applied to the calculated DON values. It is quite possible that losses of NO_3^- observed during the UV-oxidation procedure are to some extent balanced by any contamination additive effect that may be present.

Oxidation efficiency

An important consideration of the DON method is that of quantifying the efficiency of the oxidation step. To test the efficiency of the UV-oxidation step that converts DON to NO_3^-, known concentrations of standard DON compounds were UV-irradiated, with the resultant release of NO_3^- allowing the calculation of oxidation efficiency. These tests showed that the oxidation efficiency of each of the substrates tested ranged from 68-86% (Table 4.2). These oxidation efficiencies compare well to Torres-Valdés *et al.* (2008) who reports oxidation efficiencies of 79% and 76% for urea and caffeine respectively. The reason for testing the oxidation efficiency is not to allow for a correction in the final DON numbers, but is more to check that the UV-oxidisers are working well. The DON pool is a complex mixture of many different nitrogen bearing compounds (Bronk, 2001) so applying an oxidation efficiency to seawater samples from a single DON standard is not applicable, thus an oxidation efficiency was not applied to the final DON numbers.

Table 4.2 Check of oxidation efficiencies of the UV-oxidisers by using standard DON compounds.

Compound	Lability	Expected NO_3^- recovery ($\mu mol\ l^{-1}$)	Oxidation efficiency (%) ($\bar{x} \pm \sigma$, of n samples)	
			UV-ox A	UV-ox B
Urea – low	High	5.0	86 ± 3 (n=3)	83 (n=2)
Urea – high	High	10.0	84 ± 4 (n=15)	86 ± 4 (n=16)
Guanosine	Medium	10.0	68 ± 10 (n=3)	67 (n=2)
Caffeine	Medium	10.0	68 (n=2)	74 (n=2)

Another important consideration of the experimental setup is whether the oxidation efficiency of the two identical UV-oxidisers was the same. This was tested by comparing the oxidation efficiency of the high urea standards placed in both oxidisers

during the course of running all the samples. By comparing the means of DON recovery for urea (high) between both oxidisers using a Student's *t*-test it can be seen that the oxidisers were giving equal recoveries (Table 4.2). The *t*-statistic is 1.37 and the critical value of *t* for p = 0.01 is 2.76 (df = 29), therefore showing that the mean recoveries from the two oxidisers was not significantly different at the 1% confidence level. This gives confidence that the results from the two oxidisers are comparable and can be used without bias to one oxidiser or the other. Statistics were taken from Miller and Miller (2000). The *t*-test was calculated using Eq. 4.3 and 4.4 where *s* is the pooled standard deviations of the two means. The assumption to check for equal variances of the standard deviations was tested using the *F*-test (Eq. 4.5).

$$t = \frac{\left(\bar{x}_1 - \bar{x}_2\right)}{s\sqrt{\frac{1}{n_1} + \frac{1}{n_2}}} \qquad \text{Eq. 4.3}$$

$$s = \sqrt{\frac{\left(n_1 - 1\right)s_1^2 + \left(n_2 - 1\right)s_2^2}{\left(n_1 + n_2 - 2\right)}} \qquad \text{Eq. 4.4}$$

$$F = \frac{s_1^2}{s_2^2} \qquad \text{Eq. 4.5}$$

4.2.3 Issues with Sample Analysis

While samples were being analysed it became evident that there was an issue with the quality of the samples. This was apparent in the DIN concentrations measured in parallel with the TDN samples. As the DON samples were taken at the same time as the nutrient samples that were analysed on the ship one would expect to be able to replicate the DIN concentration in the DON sample as that measured on the ship, so long as there are no issues with storing the DON samples. Therefore as a first quality control the DIN concentrations measured on the ship were compared with the DIN concentrations measured later in the lab. These samples will be referred to as DIN_S and DIN_L for shipboard and lab measurements of DIN respectively. When plotting DIN_L against DIN_S it is clear that there are a significant number of samples that do not agree therefore suggesting a problem with sample storage.

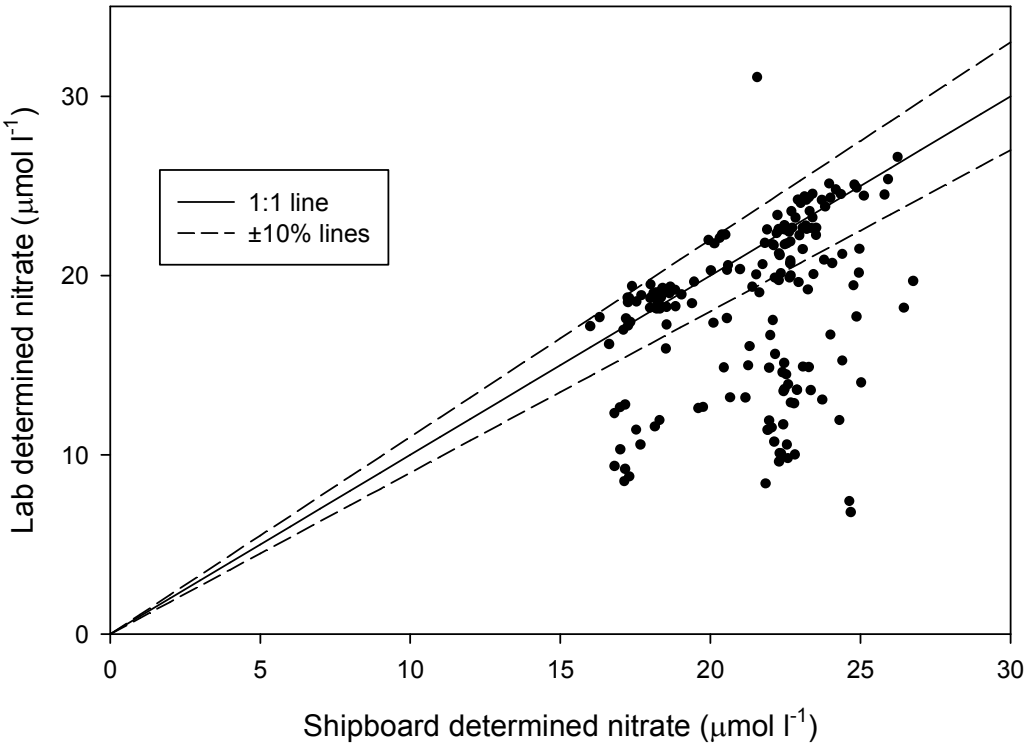

Figure 4.2 Comparison between shipboard determined NO_3^- and the archived samples collected from the same station, cast and Niskin measured in the lab during DON analysis.

Figure 4.2 shows that a large number of DIN_L samples measured in the lab do not agree with the DIN_S measured onboard the ship: ie all the samples that do not sit on the 1:1 line. Therefore, all the samples that do not sit on the 1:1 line are showing deviations in their concentrations between shipboard and lab analysis. This suggests an issue with either sample storage or a problem during DIN_L analysis in the lab. As all the necessary precautions were taken to ensure the correct operation and calibration of the nutrient analyser then it has to be assumed that there is an issue with the storage of samples. In general, the trend is for the DIN_L concentration to be lower than DIN_S, shown by the general trend of points sitting below the 1:1 line thus suggesting that DIN has been "lost" from the sample during storage. Possible reasons for loosing DIN during sample storage are not clear but may include losses to sample containers, incomplete freezing, biological degradation, sample leakage through the screw cap during freezing or chemical alteration during freezing. Pinpointing the reason and source of the loss was not possible which left the data-set in need of filtering to remove compromised samples. In an attempt to filter the data to remove the suspect samples a 10% inclusion bracket was applied to each data point. If a value for DIN_L was more

than ±10% different from the associated DIN_S sample it was discarded from any further data analysis.

4.3 Results

4.3.1 Profiles of DON

After the quality control measures in Section 4.2.2 and 4.2.3 were applied to the raw TDN data, the resultant data used for interpretation and discussion are plotted in Figure 4.3 with the profiles grouped by region according to Figure 4.1.

In general the profiles in the northern and southern regions do not show distinct vertical patterns and are relatively homogenous (Figure 4.3a and c). The only distinction between the regions is the range of DON concentrations measured: 2.8-5.0 and 2.0-4.4 μmol l^{-1} for the north and south respectively. Although these ranges are somewhat overlapping, the northern region had higher concentrations of DON than the southern region. The southern region gave the lowest DON concentrations measured throughout both legs of the cruise. The main body of profiles in the central region (Figure 4.3b) had a range of 2.4-4.9 μmol l^{-1} which matches well with the northern profiles (Figure 4.3a). However at three stations: M3.1, M3.5 and M3.7, there is a marked increase in concentration at ≈14 m. At these three stations, subsurface peaks ranging from 6.8-14.0 μmol l^{-1} can be clearly seen standing out from the rest of the profiles. These peaks are spiky in nature and only appear to be present at this one depth. These elevated concentrations were the highest DON values measured throughout both legs of the cruise.

Profiles in the east and west regions in Figure 4.1 were plotted together in Figure 4.3d. These stations included a transect to the east to M5 (M5, 15584, 15585, 15586), and one station to the west of the study site at M7 that sits on the western fringe of the Crozet Plateau Figure 4.1. Therefore the profiles should not be seen as representative of just one region. However, it is useful for comparing these two different areas. The eastern profiles gave lower DON concentrations, with a range of 2.4-4.3 μmol l^{-1}, than the western profile, which had a range of 4.1-6.0 μmol l^{-1}. The reason for the greater range shown in the western profile is result of a subsurface peak between 23 and 42 m. This peak is similar to the peaks seen in the central region (Figure 4.3b) but is less pronounced and spread over a greater depth range.

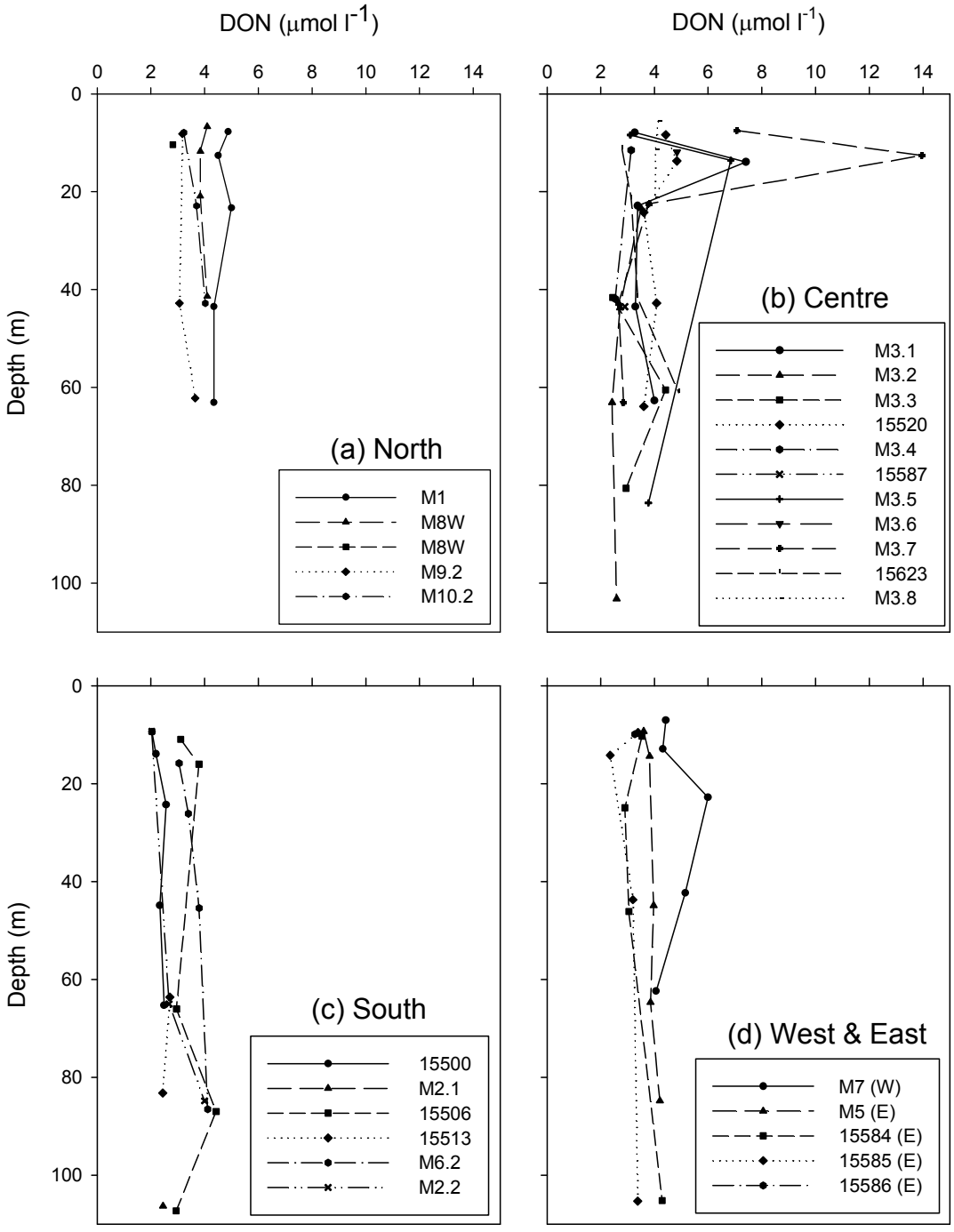

Figure 4.3 Profiles of DON grouped by region. Stations not sampled at an 'M' station are identified with their Discovery station number.

4.3.2 Integration of DON profiles

The profiles shown in Figure 4.3 were then integrated from 0-100 m to calculate the total inventory of DON (DON_t). The integration used was a trapezoidal type integration with an averaged DON concentration for each depth layer (Section 2.7). The form of the integration is shown in Eq. 4.6.

$$DON_t = \int_0^z dz * \overline{DON} \qquad \text{Eq. 4.6}$$

Where *dz* is the layer thickness and $\overline{DON}$ is the averaged DON concentration over this layer, expresses by Eq. 4.7

$$\overline{DON} = \frac{(DON_1 + DON_2)}{2} \qquad \text{Eq. 4.7}$$

As some of the profiles did not go as deep as 100 m the deepest data point available in the profile was directly extrapolated to 100 m. The same procedure was also applied to data points >100 m (max depth 107 m). It must be reiterated that the profiles used for integration and of course the integrated values have not taken into account the total DIN pool because the NH_4^+ fraction of the DIN has not been factored into the DON difference calculation expressed in Eqs. 4.1 and 4.2. Reasons for this were explained in 4.2.1. For the integrated DON_t see Table 4.3.

Table 4.3 Station number, position, region and 100 m integrated DON (mmol m^{-2}).

Station[a]	Date	Latitude	Longitude	Region	DON
M1	11/11/2004	43.90210	50.25695	N	451
M3.1	13/11/2004	46.06093	51.78600	C	394
M3.2	18/11/2004	46.03400	51.80540	C	287
15500	19/11/2004	47.13850	52.35400	S	239
M2.1	20/11/2004	47.78793	52.86709	S	245
15506	20/11/2004	48.19150	52.41310	S	345
15513	23/11/2004	48.59610	51.94780	S	263
M3.3	25/11/2004	46.06953	51.77467	C	298
15520	26/11/2004	45.39550	52.24040	C	389
M7	27/11/2004	45.49677	48.99530	W	462
M8W	02/12/2004	44.85659	49.65218	N	403
M8W	02/12/2004	44.87236	49.64711	N	281
M9.2	19/12/2004	42.99883	47.01016	N	337
M3.4	22/12/2004	46.07064	51.78076	C	270
M5	28/12/2004	45.99933	56.15163	E	393
15584	29/12/2004	45.99770	55.01050	E	344
15585	30/12/2004	46.00460	54.00370	E	313
15586	30/12/2004	45.99910	53.26650	E	327
15587	30/12/2004	45.99110	52.52280	C	290
M3.5	31/12/2004	46.05942	51.77793	C	485
M6.2	03/01/2005	49.00006	51.53536	S	369
M2.2	07/01/2005	47.80173	52.84923	S	277
M3.6	09/01/2005	46.14809	51.85655	C	484
M3.7	10/01/2005	46.03320	51.86850	C	421
15623	11/01/2005	45.99010	51.67870	C	399
M3.8	12/01/2005	46.04294	51.96072	C	404
15632	15/01/2005	44.50150	49.98560	N	385

[a]Locations not sampled at an 'M' station are identified with their Discovery station number.

Integrated DON concentrations as a whole ranged from 239-485 mmol m^{-2}. Split into their respective regions: north, central, south, east and west the average inventories are 378, 375, 290, 344 and 462 mmol m^{-2} respectively. Excluding the single western profile (462 mmol m^{-2}), the average inventories for the north and central regions are essentially the same, compared with lower concentrations in the south. The inventories for the eastern transect fall approximately midway between the values observed in the bloom and non-bloom regions.

4.4 Discussion

The aim of this chapter is to use the idea of DON buildup as a way of explaining the lack of latitudinal gradient in ^{234}Th-Cex. Therefore before any analysis is carried out on the DON data it must first be shown that it is possible to use nitrogen to draw

conclusions about carbon. This can be shown in two ways. The first is through plotting ^{234}Th-derived PON export (^{234}Th-Nex) against latitude, as was done for carbon in Figure 3.6c. This analogous plot is shown in Figure 4.4 and shows the same tends in ^{234}Th-Nex as that previously observed for ^{234}Th-Cex. During leg 1 there is a distinct north-south gradient in export with higher export in the northern region. This trend is not apparent during leg 2, and there is generally high export across the whole study region.

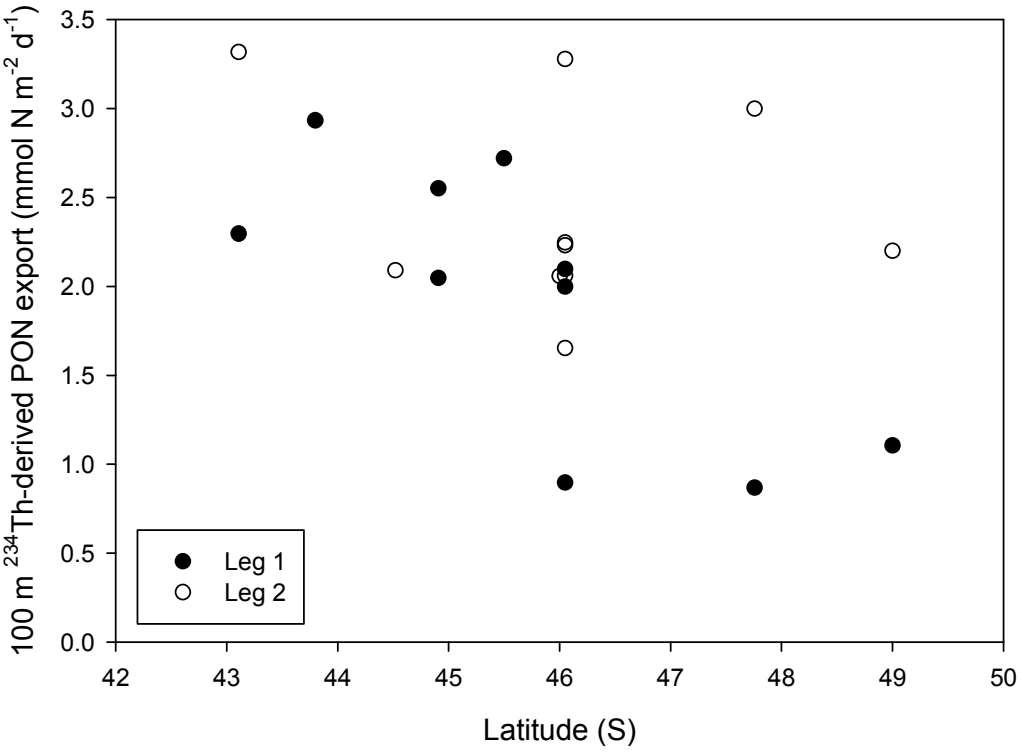

Figure 4.4 The latitudinal variation in 100 m integrated ^{234}Th-Nex integrated to 100 m.

The second method of demonstrating the relationship between carbon and nitrogen in exporting material is through directly comparing the observed ^{234}Th-Cex and ^{234}Th-Nex at each station. This is shown in Figure 4.5 by plotting data from Table 3.5 and reveals a good proportional relationship between the exports of these two elements. The Model II linear regression between the exporting material gives a C:N ratio of 6.99, which is in good agreement with the Redfield ratio of 6.6 (Fleming, 1940; Redfield, 1934a; b; 1958; Redfield *et al.*, 1963). The regression line was not forced through a zero-zero intercept and therefore has an intercept of -1.8 mmol C m^{-2} d^{-1}. This is interesting because it suggests that when zero POC is being exported about

0.2 mmol N m^{-2} d^{-1} is still being exported as PON. This may be a feasible scenario if carbon is being preferentially dissolved compared to nitrogen during the first steps of the remineralisation process. However it is not possible to test the variation in the C:N ratio with depth in the exporting particles because the elemental ratios were only collected from one depth at each station. It must be highlighted that the relationship between the ^{234}Th-Cex and ^{234}Th-Nex is the C:N ratio measured in the >53 μm particulate size fraction collected with the SAPS. For information on this see Section 3.3.

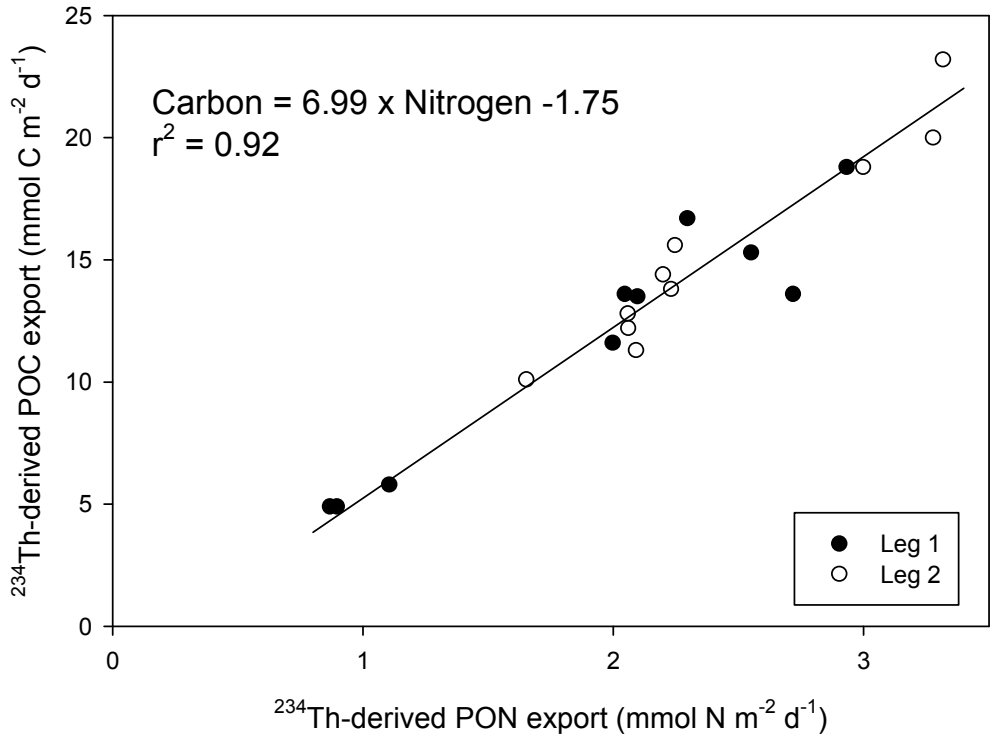

Figure 4.5 The relationship between 100 m integrated ^{234}Th-derived POC and PON export. The solid line is a Model II regression through all the data.

4.4.1 Comparison with DON in the Literature

The available literature on the global distribution of DON is increasing but still remains relatively small compared to literature on DOC. However, the general distributions globally are starting to become apparent (Bronk, 2001). The DON review by Bronk (2001) reports mean open ocean concentrations of 5.8 ± 2.0 μmol l^{-1} and 3.9 ± 1.8 μmol l^{-1} for the surface and deep ocean respectively. As expected the range of observed concentrations is greatest in the surface: 0.8-13 μmol l^{-1}, compared to deep

waters: 2-5 μmol l^{-1}. The surface DON concentrations measured in the CROXEZ data-set are therefore encompassed by the range of values reported in the literature, except for one sample collected at 13 m at M3.7 that had a concentration of 14.0 μmol l^{-1}. This station was sampled during an intense eddy bloom near the M3 station location towards the end of leg 2 (Allen *et al.*, 2006). This is the first indication of a possible connection of increasing DON concentrations with elevated chl-*a* levels, and will be investigated later in Section 4.4.3.

The literature cited within Bronk (2001) however, covers all oceanic regions and are too numerous to all be included here. Therefore only selected literature will be presented to cover the latitude ranges that encompass from the SubAntarctic Front (SAF) to the southern extent of the Antarctic Circumpolar Current (ACC). The values given in Table 4.4 have been selected from the respective papers to only include data collected in the top 100 m of the water column. Again it is clear that the CROZEX data-set of DON values are generally encompassed by the observed values reported in the literature. However it is clearer that the subsurface peaks measured in the central region (Figure 4.3b) at 13-14 m are at the top end, and indeed exceed, the highest values reported in the literature. This is an interesting observation because the central region of the bloom had the greatest surface chl-*a* during December and January (Venables *et al.*, 2007) (Figure 4.6).

Table 4.4 Literature values of DON concentrations (μmol l^{-1}) in the Southern Ocean in the top 100 m of the water column and between the SAF and the southern extent of the ACC.

Region	Date	DON	Reference
South Pcaific 103°W, 50-60°S	Feb 1994	3.0-5.5	Hansell and Waterhouse (1997)
South Atlantic 6°W, 50°S	Oct 1993	7.5-9.0	Kähler *et al.* (1997)
Drake Passage 56°W, 55-61°S	Dec 1997-Jan 1998	1.5-7.3	Sanders and Jickells (2000)
South Indian 143°E, 56-60°S	Jan 1995	4-9	Ogawa *et al.* (1999)
Drake Passage/ Weddell Sea	Dec 1991	3.9	Hubberten *et al.* (1995)
South Pacific 54°S, 176°W	Dec 1995-Jan 1996	4.0-4.3	Loh and Bauer (2000)

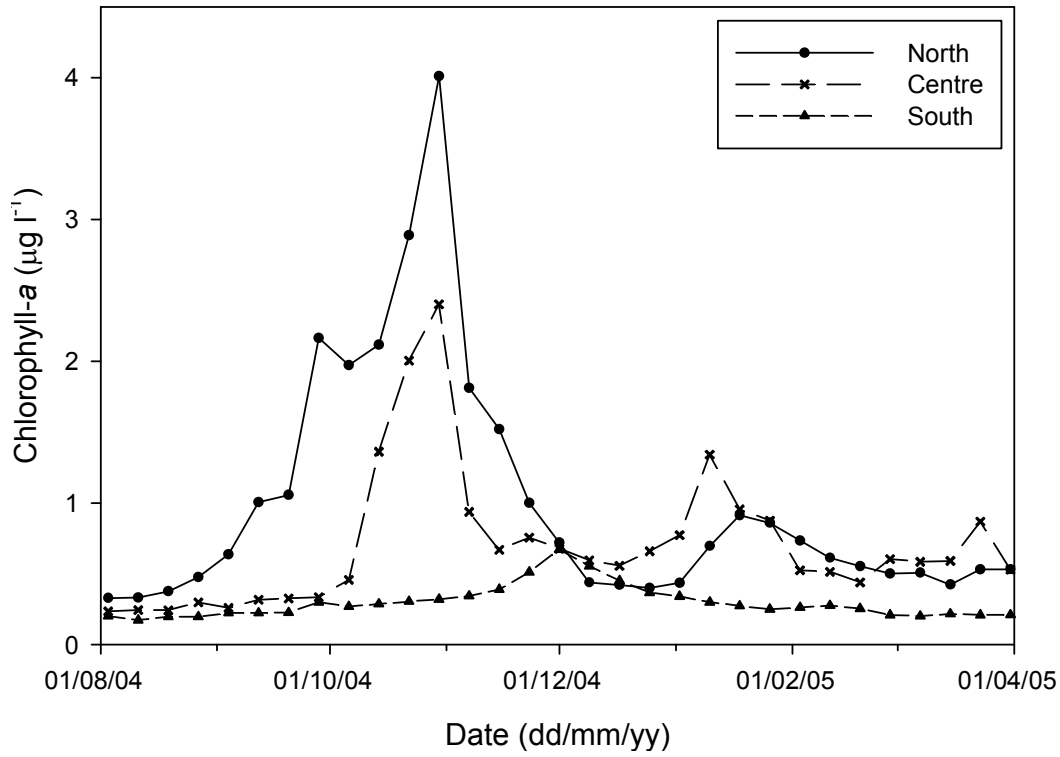

Figure 4.6 Remotely sensed temporal progression of chl-*a* in the north, centre and south. Data taken from Venables *et al.* (2007).

As a whole, the amount of literature on DON within this band of Southern Ocean is somewhat limited, and none of these have targeted a topographically associated bloom over an extended period of time: weeks to months. Thus this gives a novel opportunity to investigate the temporal evolution of the DON pool during the latter stages of a PF bloom.

4.4.2 Temporal and Spatial Variation of DON

On initial inspection of the DON integrations (Table 4.3) no clear patterns immediately stand out so have been plotted chronologically for each region in Figure 4.7. The integrations for the east and west regions are not included because there is only one western profile and the three eastern stations were all sampled within ≈2 days of each other therefore largely reducing the temporal variability to zero.

Figure 4.7 shows the temporal variation of DON inventories for the northern, central and southern regions through both legs of the cruise. It is possible to cluster groups of integrations that were taken in similar areas at similar times. This is shown on the graph by the ellipses grouping similar regional and temporal groups. Station

M3.2 is grouped with the southern stations because it was shown by Pollard *et al.* (2007b) that when M3.2 was sampled the water present here was water that had been laterally advected from south of the Crozet plateau (see Section 3.2.2 regarding more detailed discussion on M3.2). After calculating the mean of the clustered data points Figure 4.7 can be redrawn as Figure 4.8.

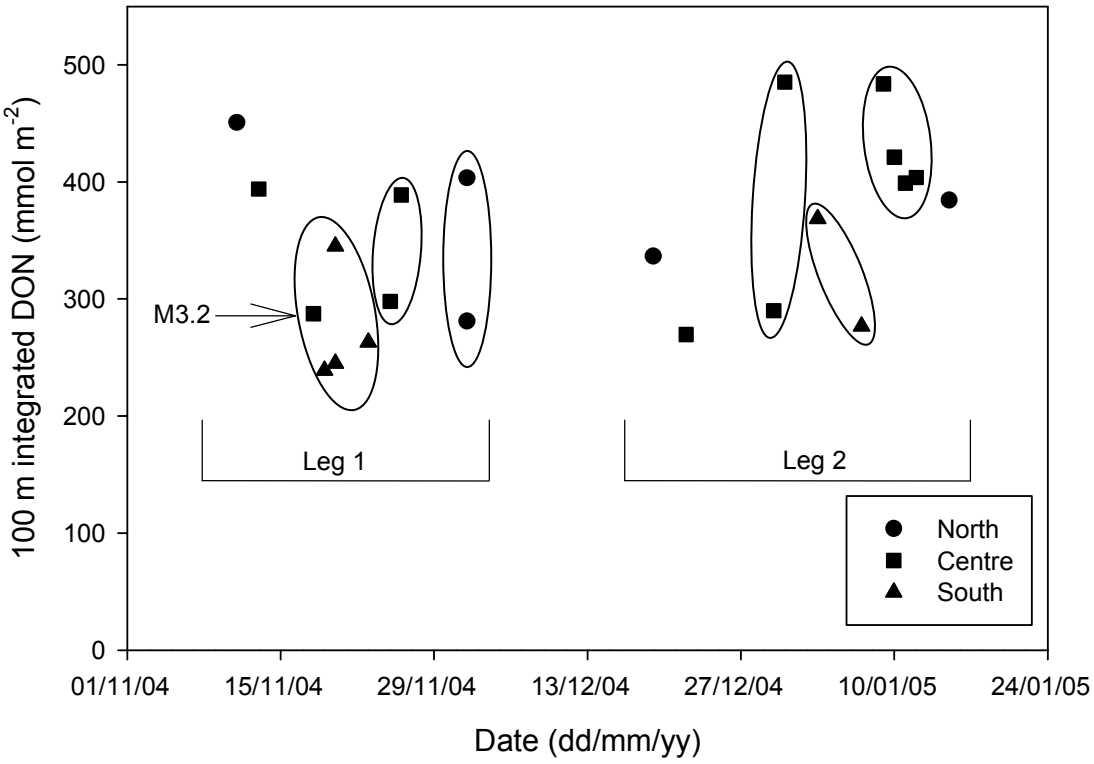

Figure 4.7 Temporal variation by region of 100 m integrated DON concentration. Ellipses group stations from the same region taken at similar times.

Figure 4.8 shows a much less cluttered view of how 100 m integrated DON varies temporally in the northern, central and southern regions. The southern region was only visited once during each leg therefore only giving two averaged data points. The southern stations show the least change in DON during the cruise with integrated DON slightly higher during leg 2. In the northern and central regions during leg 1 the integrated DON is fairly similar with declining levels of DON spanning the whole of leg 1 and the start of leg 2. After this the levels of DON increase sharply in the central region and slightly in the northern region.

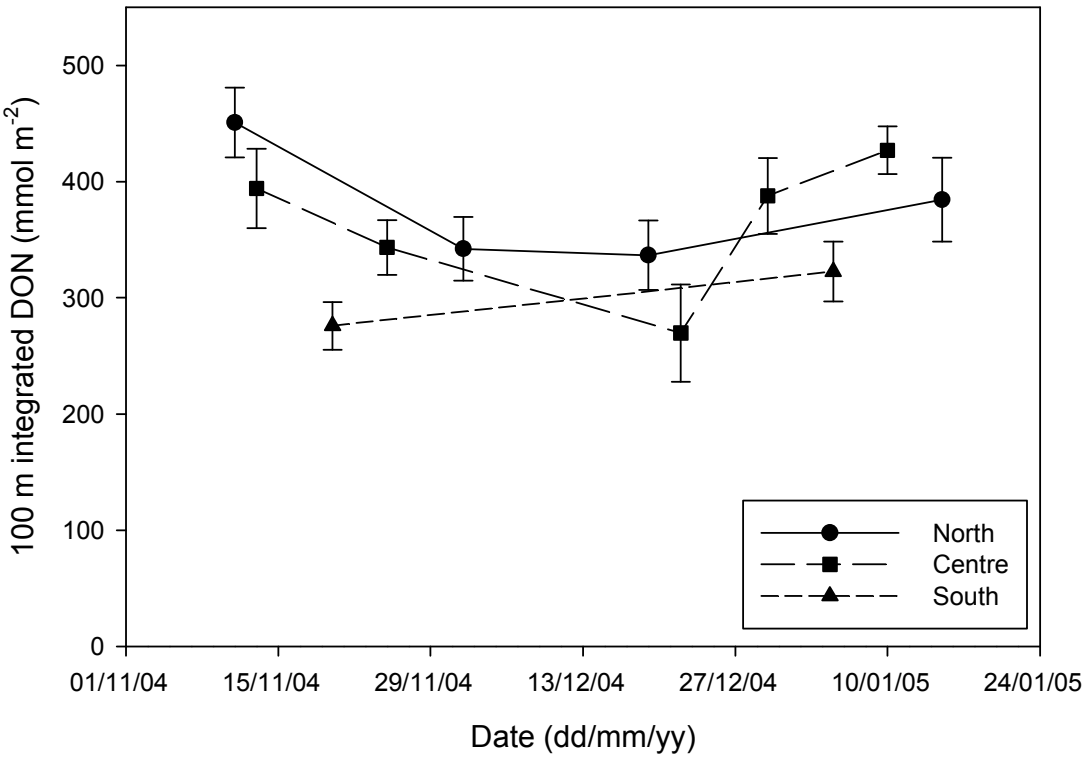

Figure 4.8 Re-plot of Figure 4.7 with the circled groups of data points averaged. Error bars are 1 σ.

The potential variations in spatial and temporal variability of DON noted in Figure 4.8 are an encouraging outcome of what initially appeared to be a weak DON data-set. Considering the trends in Figure 4.8 the overall spatial context of DON needs to be assessed. Figure 4.9 shows a weak, but distinct latitudinal gradient with generally higher DON concentrations in the northern bloom region, compared to lower DON concentrations in the southern non-bloom region. The regression line has a slope of 19 mmol N m^{-2} for each additional degree south; however the correlation has an r^2 of 0.13 and is only significant at the 7% level. The intercept in this case is meaningless. The latitudinal pattern in the DON field weakly supports the idea of increasing DON in higher chlorophyll regions thus adding evidence for the possibility of DON buildup in the high chlorophyll, productive region of the bloom.

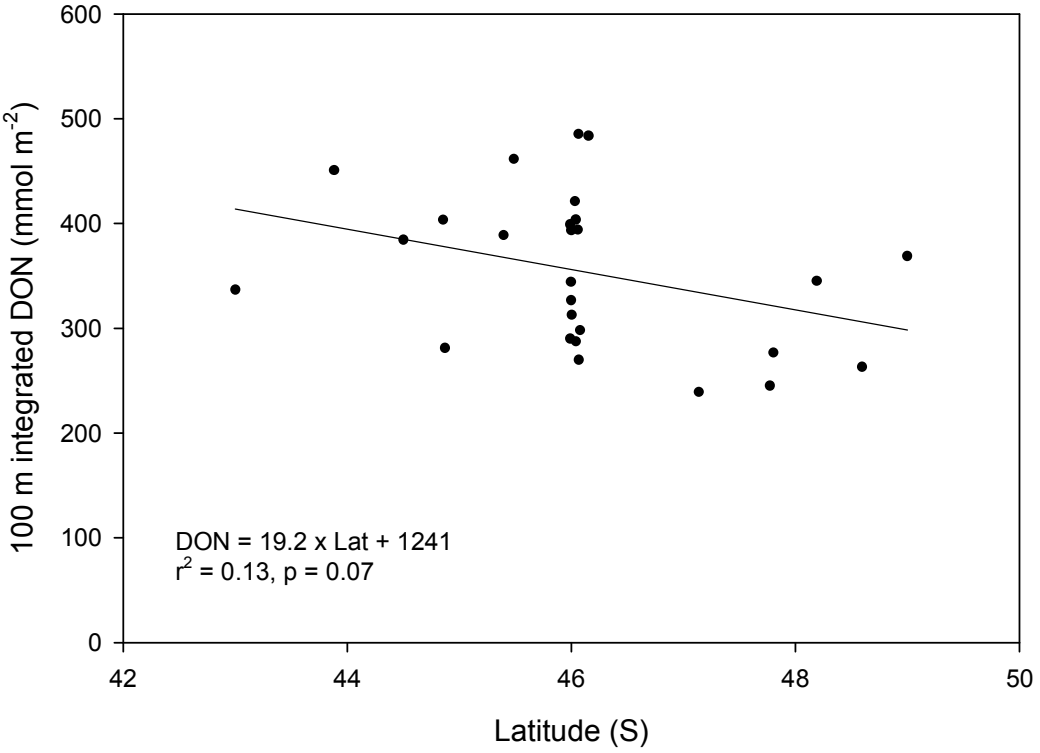

Figure 4.9 Latitudinal variation in 100 m integrated DON inventories. Solid line is a Model I regression to highlight the north-south trend.

4.4.3 Biological Control of DON

To put the DON data into context with the CROZEX bloom one must first be clear about the ideas to be tested. These were laid out at the start of the chapter in Section 4.1.1 and are primarily aimed at tackling the lack of latitudinal gradient in ^{234}Th-Cex export observed during leg 2. A hypothesis created to explain this lack of latitudinal gradient was that DON may be building up within the bloom region and thus reducing the amount of organic material available for export to mesopelagic depths.

So far it has been shown that there is variation in the DON field both spatially and temporally with the bulk of the variation occurring in the northern and central regions of the study area. This is an encouraging observation because these are the regions where the main bloom is present and thus suggests the need for investigating the relationship between DON and other biological parameters. Therefore the relationships between DON and chl-*a* and the rates of ^{14}C PP and Σ^{15}N uptake will now be investigated. This therefore introduces three new parameters into this chapter: chl-*a*, ^{14}C PP, and Σ^{15}N uptake. For each station with a DON integration, the 100 m integrated chl-*a* and 1% light depth integrated ^{14}C PP and Σ^{15}N uptake rates are summarised in Table 4.5. Each of these will now be presented.

Table 4.5 Station number, 100 m integrated chl-*a*, 1% light depth integrated ^{14}C PP and Σ^{15}N uptake for stations sampled for DON.

Station[a]	DON_t[b] (mmol N m^{-2} d^{-1})	Chl-*a* (mg m^{-2})	^{14}C PP[c] (mmol C m^{-2} d^{-1})	Σ^{15}N uptake[d] (mmol N m^{-2} d^{-1})
M1	451	167	90	7
M3.1	394	110	44	9
M3.2	287	51	31	
15500	239	45		
M2.1	245	47	36	8
15506	345	44		
15513	263	32		
M3.3	298	72	40	9
15520	389	107		
M7	462	142	64	14
M8W[e]	342	88	41	9
M9.2	337	40	10	7
M3.4	270	73	60	12
M5	393	30	34	4
15584	344	35		
15585	313	37		
15586	327	30		
15587	290	47		
M3.5	485	59	27	8
M6.2	369	38	25	7
M2.2	277	37	17	7
M3.6	484	171	250	38
M3.7	421	181	184	29
15623	399	110		
M3.8	404	81	138	23
15632	385	15		

[a]Locations not sampled at an 'M' station are identified with their Discovery station number.
[b]100 m integrated DON data has been carried forward from Table 4.3 for reference.
[c]Data taken from Seeyave *et al.* (2007).
[d]Data taken from Lucas *et al.* (2007).
[e]DON data for M8W have been averaged.

Figure 4.10 shows the plot of 100 m integrated DON and chl-*a*. The regression is DON = 1.50 × chl-*a* + 245 (r^2 = 0.40, p = <0.01, n = 26). What Figure 4.10 demonstrates is that the concentration of DON is linked to the chl-*a* concentration over a wider range of biomass conditions. The M3 eddy stations have been highlighted and are not separate from the bulk of data points so are not biasing the overall regression. This is the first piece of strong evidence that supports the hypothesis of DON buildup in waters of increasing chl-*a* concentration. Relationships of this sort are not common in the literature, but one relationship reported by Bode *et al.* (2001) from shelf waters off northern Spain agrees well once converted to comparable units: DON = 1.18 × chl-*a* + 421, (r^2 = 0.48). The higher intercept is not surprising because the Bode *et al.* (2001)

study was conducted in coastal waters where higher levels of background DON would be expected.

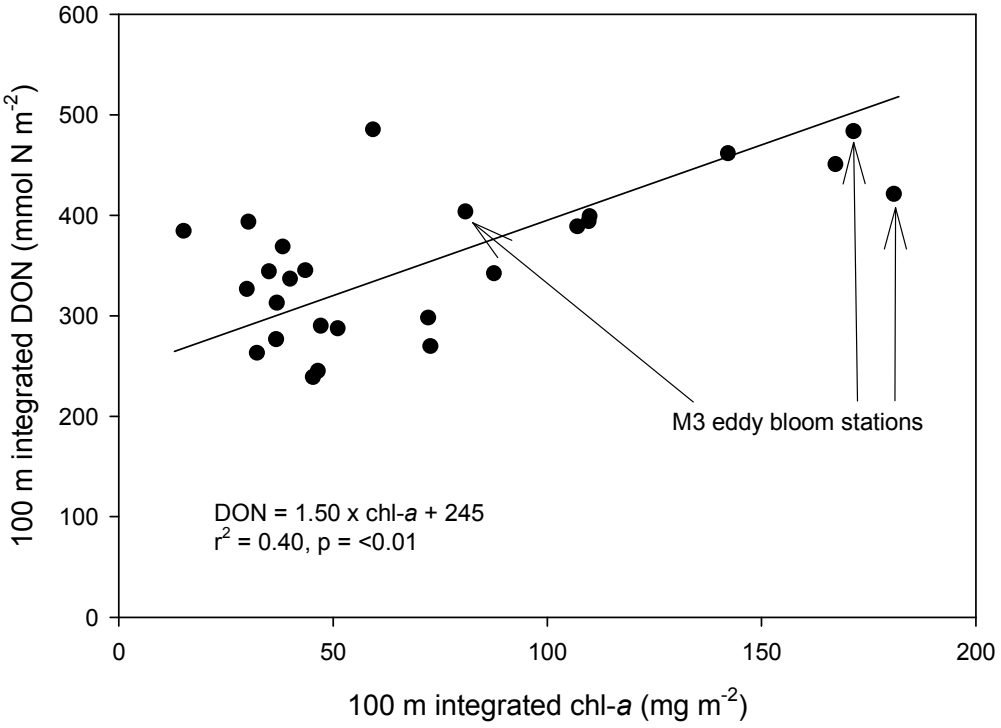

Figure 4.10 Relationship of 100 m integrated DON and chl-*a*. Solid line is a Model II regression.

Figure 4.11a and c show the relationship between 100 m integrated DON and ^{14}C PP and Σ^{15}N uptake. Only weak relationships exists between these parameters with r^2 (p value) for ^{14}C and ^{15}N being 0.27 (0.04) and 0.20 (0.09) respectively (Figure 4.11a & c). One possible explanation for these poor relationships could be because the ^{14}C PP and Σ^{15}N uptake rates are integrated to a depth of 1% light penetration which varies from station to station. This scenario has been investigated in Figure 4.11b & d with the ^{14}C PP and Σ^{15}N uptake data plotted against DON integrated down to the 1% light level. Again there are no clear relationships. The regressions for all four plots are given in Table 4.6. The M3 eddy bloom data points have been highlighted in Figure 4.11 because they are distinct from the bulk of the data and have a large influence on the regression statistics. Should the M3 eddy bloom stations be removed it is clear to see that the cluster of points to the left of plots a, b, c and d in Figure 4.11 would lack any trends, however they are included for completeness.

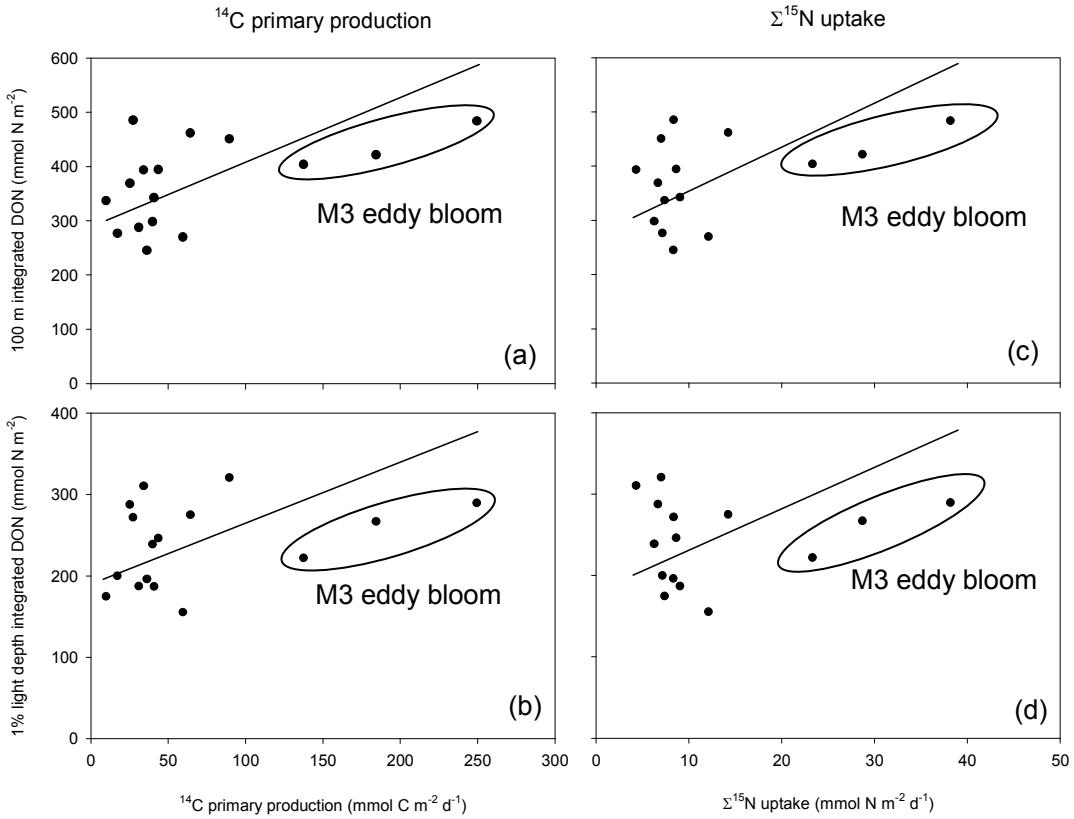

Figure 4.11 The relationships between integrated DON and ^{14}C PP and Σ^{15}N uptake. Figures a & c are 100 m integrations of DON and figures b & d are DON integrations to the 1% light level. Solid lines are Model II regressions.

Table 4.6 Tabulated Model II regressions for plots in Figure 4.11.

Figure	Gradient	Intercept	r^2	p	n
4.9a	1.19	289	0.27	0.04	16
4.9b	0.75	190	0.12	0.20	16
4.9c	8.10	273	0.20	0.09	15
4.9d	5.10	180	0.02	0.62	15

Showing the lack of any strong relationships between DON concentrations and ^{14}C PP and Σ^{15}N uptake is an interesting discovery in understanding the mechanisms involved in the fixation rates of carbon and nitrogen. However this should not be a total surprise because after the process of carbon and nitrogen fixation there are several possible routes that carbon and nitrogen can flow through and only one of these is a direct path into the dissolved organic matter (DOM). Should carbon and nitrogen flow through the organic particle phases contained within the food webs there are many steps of separation between initial fixation and its appearance in DOM, and in one case particles are directly exported and will never appear in DOM effectively removing it

from the surface ocean. Another possible explanation for the lack of any strong relationships between DON and ^{14}C PP and Σ ^{15}N is that these parameters were not measured on the same sample. DON was measured from samples collected from the stainless steel rosette and the rate measurements of ^{14}C PP and Σ ^{15}N were collected from the trace-metal clean rosette. However, a regression presented by Bode *et al.* (2001) for DON against ^{14}C PP is DON = 0.07 × PP + 5.46 (r^2 = 0.30, p = <0.01). Comparing this to the most significant of the four regressions (Figure 4.11a) after converting to comparable units as those used in Bode *et al.* (2001): (mmol N m^{-3} and mg C m^{-3} h^{-1}) the regression becomes DON = 0.06 × PP + 2.89 (r^2 = 0.27, p = 0.04). This shows that the rate of production of DON was very similar between the CROZEX bloom and the study of Bode *et al.* (2001). A study by Hansell and Waterhouse (1997) also reported a link between primary productivity and total organic nitrogen but did not report the strength of this relationship, and also concluded primary production was not controlling total organic carbon levels in the surface waters. Pan (2007) reported no relationships between primary production and DON and DOC in the Atlantic Ocean.

The lack of good evidence linking the DON pool to nitrogen and carbon fixation suggests that these parameters are not closely related. A possible explanation for this is that the DON pool and the processes of primary production process are separated by several stages. This means that nitrogen has to pass through several steps before it is released into the DON pool, which is only one of several pathways it may follow. The main mechanisms responsible for DON release are grazing (Bronk and Ward, 1999; Ward and Bronk, 2001) and particle dissolution (Skoog *et al.*, 2001). This implies that there is a need for inspecting DON in relation to a more fundamental parameter, with NO_3^- being the obvious choice.

4.4.4 The Flow of Nitrate into DON

The direct comparison of paired NO_3^- and DON data points from each archived DON sample is shown in Figure 4.12. Although there is a reasonable amount of scatter there is an observable trend of increasing DON with decreasing NO_3^-. One would not expect to observe a very tight correlation because the flow of nitrogen into the DON pool is only one of several paths that DON may follow once it is fixed from the NO_3^- pool. The regression of this relationship is DON = -0.25 × NO_3^- + 9.02, (r^2 = 0.18, p = <0.01) and although the r^2 value is not very high the regression is significant.

Therefore there is a meaningful relationship between the trend of increasing DON with decreasing NO_3^-.

The most compelling example of DON buildup resulting from NO_3^- decline is that of Butler *et al.* (1979) made at Station E1 in the English Channel. These data have been plotted on Figure 4.12 as a comparison to the CROZEX data and has a regression of DON = -0.62 × NO_3^- + 9.10, (r^2 = 0.72). The data from Station E1 does show a surprisingly efficient transfer of NO_3^- into DON when compared to the CROZEX data-set, however this may be accounted for by the shallow water depth (≈70 m) and potential for resuspension and recycling of exported particles in the water column, all of which is not as easy in the deep water column environment of the CROZEX bloom. That aside, it does support the idea of NO_3^- flowing into the DON pool which is then harder to export and may partly account for a reduction of export when compared to NP.

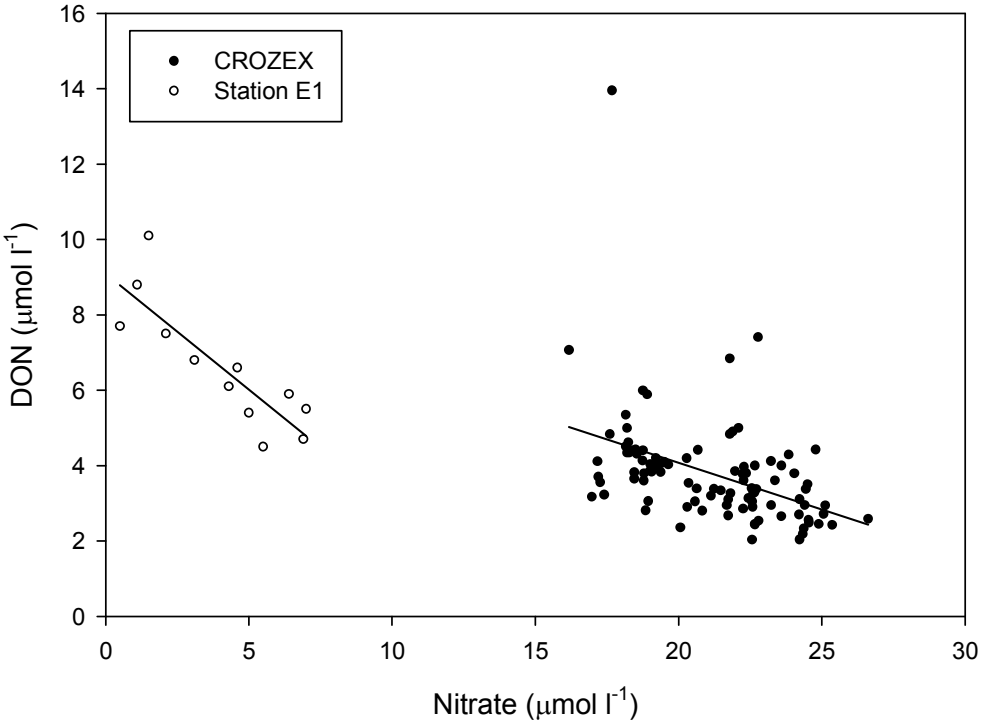

Figure 4.12 The relationship between NO_3^- and DON on a sample for sample basis. Data from Station E1 from the English Channel have been plotted for comparison (Butler *et al.*, 1979). Solid lines are Model I regressions.

Sanders *et al.* (2007) presented the latitudinal gradient in NP based on the seasonal draw-down of the nitrate pool (ΔNO_3^-) and showed a clear north-south gradient in estimates of NP (Figure 3.6b). Given the latitudinal trends observed in both ΔNO_3^- and integrated DON, the next link that must be established is that between ΔNO_3^- and integrated DON. Using the technique of Sanders *et al.*, (2007) seasonal ΔNO_3^- was calculated as the difference between the measured inventory of NO_3^- ($NO_{3\,s}^-$) and an inferred winter inventory of NO_3^- ($NO_{3\,w}^-$). $NO_{3\,w}^-$ was inferred by assuming that the 0-100 m concentration of NO_3^- was the same as the summer 100 m concentration. ΔNO_3^- was calculated with Eq 4.8. Preparation of data-sets prior to integrations is outlined in Section 2.7 to ensure consistency between data-set manipulations. The seasonal ΔNO_3^- up to the date of when each station was sampled is presented in Table 4.7, along with corresponding integrations of DON.

$$\Delta NO_3^- = NO_{3\,w}^- - NO_{3\,s}^- \qquad \text{Eq. 4.8}$$

Table 4.7 Station number, 100 m integrated DON and ΔNO_3^- measured up to the date of sampling.

Station[a]	DON[b] (mmol N m^{-2})	ΔNO_3^- (mmol N m^{-2})
M1	451	521
M3.1	394	7
M3.2	287	51
15500	239	12
M2.1	245	73
15506	345	42
15513	263	27
M3.3	298	65
15520	389	294
M7	462	498
M8W	342	375
M9.2	337	328
M3.4	270	131
M5	393	175
15584	344	285
15585	313	232
15586	327	80
15587	290	192
M3.5	485	216
M6.2	369	119
M2.2	277	142
M3.6	484	354
M3.7	421	426
15623	399	159
M3.8	404	467
15632	385	318

[a]Locations not sampled at an 'M' station are identified with their Discovery station number.
[b]100 m integrated DON data has been carried forward from Table 4.3 for reference.

When plotting the data in Table 4.7 a clear linear relationship is evident (Figure 4.13), which has a regression of DON = 0.46 × ΔNO_3^- + 256 (r^2 = 0.43, p = <0.01, n = 26). This presents clear evidence that ΔNO_3^- is directly related to DON concentrations and is linear over the range of conditions sampled. The gradient of 0.46 ± 0.07 suggests that 46 ± 7% of NO_3^- is entering the DON pool and is higher than other estimates reported in the literature. An extensive investigation of stocks and dynamics of DOM in the Ross Sea over multi-season sampling found that 10% and 11% of NP was released as DON and DOC respectively (Carlson *et al.*, 2000). In contrast, during a transect from the PF to the ice edge at 6°W during October and November, no evidence of DOM buildup was recorded (Kähler *et al.*, 1997). Bakker *et al.* (2006) calculated inferred DOC release after formulating a carbon budget of the SOIREE bloom and

estimated that DOC release constituted 8-37% of NP. In the Irminger Basin, North Atlantic, Sanders *et al.* (2005) estimated that 30% of ΔNO_3^- NP was accounted for in the DON pool. Hu and Smith (1998) also notes that between 8-19% of NO_3^- assimilated by Phaeocystis cultures and natural phytoplankton assemblages in the Ross Sea, Southern Ocean was released as DON. Mesocosm experiment in high latitude regions have also shown similar effects, with 6-22% of total nitrogen uptake (mostly NO_3^-) was recoverable as new DON (Conan *et al.*, 2007). Overall DOM release resulting from ΔNO_3^- NP seems to be a consistent feature.

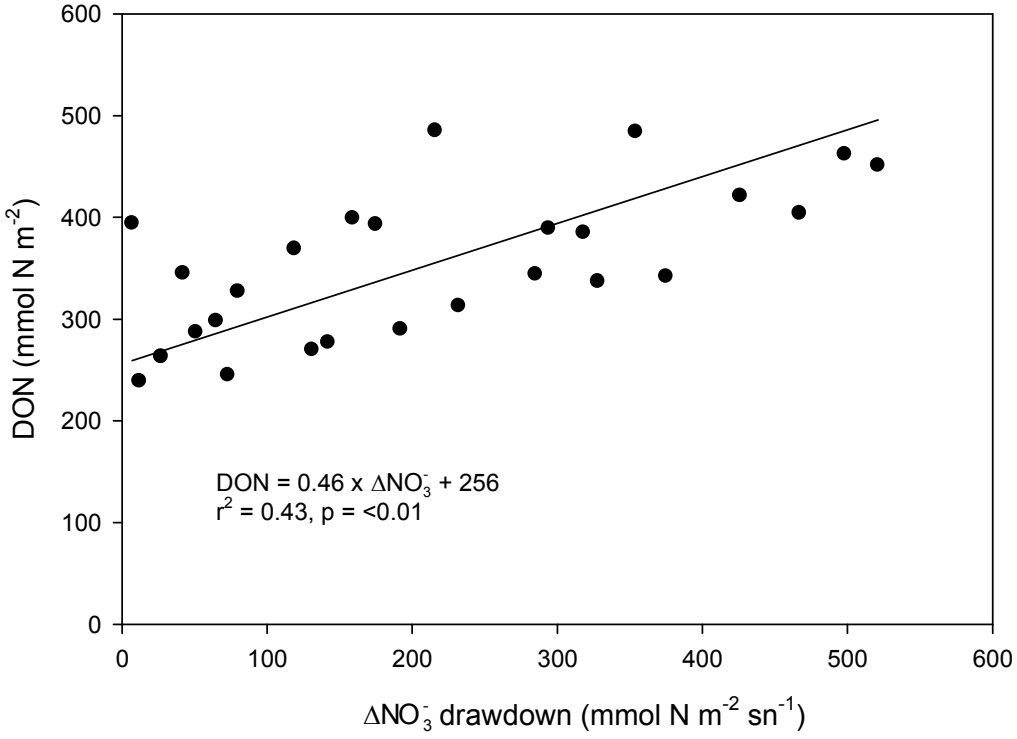

Figure 4.13 The relationship between 100 m integrated DON and ΔNO_3^- draw-down up to the date of sampling. Solid line is a Model II regression.

The connection of nitrogen uptake and subsequent release as DON is well documented in the literature (eg: Bronk *et al.*, 1994; Butler *et al.*, 1979; Townsend and Thomas, 2002; Varela *et al.*, 2005; Varela *et al.*, 2006). Nonetheless, making this quantitative link between the release of DON from ΔNO_3^- is an important step in understanding that DON may play a role in affecting export, as has been observed by others (Bronk *et al.*, 1994; Diaz and Raimbault, 2000; Roussenov *et al.*, 2006; Sanders *et al.*, 2005; Torres-Valdés *et al.*, 2008). If 46% of ΔNO_3^- NP in the CROZEX bloom is

entering the DON pool this has important implications for the overall flow of organic material flowing through the system and may go some way to bridging the gap observed between NP and export.

The discovery that the relationship between ΔNO_3^- NP and DON is linear does not promise that there is relatively more storage of DOM in the north compared to the south. The strength of the linear relationship in Figure 4.13 across the complete range of data implies that the partitioning of NO_3^- NP into the DOM pool is the same across the whole study area. The consequence of this means that although evidence of DOM storage is prominent in this data-set, it does not suggest that there is a relative difference in the amount of DOM stored in the north and south. This is an interesting conclusion because it agrees with the findings of Carlson *et al.* (2000) who reported relatively consistent DOC production of 11% despite significant spatial and temporal variation in the magnitude of DOC production. Based on these findings it strengthens the conclusion that DOM production is probably constant at 46% across the whole CROZEX study area and is not responsible for the lack of a latitudinal gradient in ^{234}Th-Cex observed on leg 2.

4.5 Conclusions

This chapter has highlighted several important areas of interest both methodologically and experimentally. The initial point to mention is the critical importance of handling samples at all stages of analysis, in particular sample storage. It was clear that the archived DON samples were the subject of alteration rendering a large number of samples unusable. Unfortunately the reason for this is not determinable but the use of Sterilin® pots has to be questioned. One possible solution would be to treat DON samples the same as DOC samples, which are generally acidified and stored in sealed combusted glass ampoules. This removes the possibility of not being sealed properly and also minimises organic contamination. However, glass is fragile and may break easily if not handled and transported carefully. Ultimately the sample container used has to fit the needs and limitations of the substrate to be measured. It was also noted that a suitable DON blank solution is also needed. Given the problem of not easily removing NO_3^- from solutions without additionally altering the solution itself is a tough problem and one that merits further investigation.

The spatial and temporal trends in the DON field were only evident once multiple occupation of various regions were averaged together. This revealed temporal trends of little variation in the low productivity southern region and decreasing concentrations of DON in the high productivity northern region. A latitudinal gradient of DON thus suggested a possible relationship with chl-*a*. Consequently a significant relationship between depth integrated chl-*a* and DON was discovered. In contrast to this no highly significant relationships between DON and ^{14}C PP and Σ^{15}N uptake were apparent and highlighted the many possible fates of fixed nitrogen, only one of which is directly into the DON pool.

The most important information to result from this chapter is the estimation of how much NO_3^- NP is accountable for as DON. The strong relationship between paired samples of DIN and DON lead onto an analysis of DON in relation to ΔNO_3^- NP. This revealed a significant relationship that estimated that 46% of NP was moving into the DON pool. This has the effect of reducing the amount of organic material available for export; but because the relative storage of DON is the same across the whole study area DON storage can not account for the lack of a latitudinal gradient in ^{234}Th-Cex observed on leg 2.

5 Particulate Organic Carbon and Nitrogen

5.1 Introduction

Previously in Chapter 4 the dissolved organic nitrogen (DON) field was investigated to evaluate the potential flow of nitrogen from the NO_3^- pool into the DON pool. It was concluded that about 46% of ΔNO_3^- new production (ΔNO_3^- NP) was accountable as DON, which then lacks the mechanism to be rapidly exported in the form of settling particles. This proportion of 46% was consistent across the whole study region and therefore lacks the ability of differential storage in different areas. Having drawn this conclusion a consistent analysis of particulate organic matter (POM) must also be made to assess the impact this may have on the potential export of organic particles.

The ^{234}Th-derived POC and PON export (^{234}Th-Cex and ^{234}Th-Nex respectively) estimated in Chapter 3 was based on the assumption that the larger particles (>53 μm) were the main contributors to downward flux (Section 3.3). However, a large fraction of POM resides in the <53 μm fraction (Simpson, 1982) that was consequently excluded from the ^{234}Th analysis. Smaller particles are also considered to have slower sinking rates (Asper, 1987) and must therefore be relatively suspended in relation to larger particles. Working on this assumption, the generation of a carbon budget for the CROZEX study area must therefore include an independent analysis of the stocks of POM.

This chapter will be modelled around Chapter 4 and will aim to construct inventories of particulate organic carbon (POC) and particulate organic nitrogen (PON) across the whole study area. In doing so, the POC and PON fields will then be assessed to formulate relationships between chl-*a* and finally ΔNO_3^- NP. Maintaining the same approach used in Chapter 4 will thus allow a consistent integration of data-sets. Samples for POC and PON were sampled routinely at all major "M" stations with usually two profiles of POC and PON made during each station occupation. Locations of all stations sampled are shown in Figure 5.1. The study area has been split up into the same regions as Chapter 4 (Figure 4.1): north, centre, south, east and west, and is based on the regions specified by Venables *et al.* (2007) (Section 4.1.2).

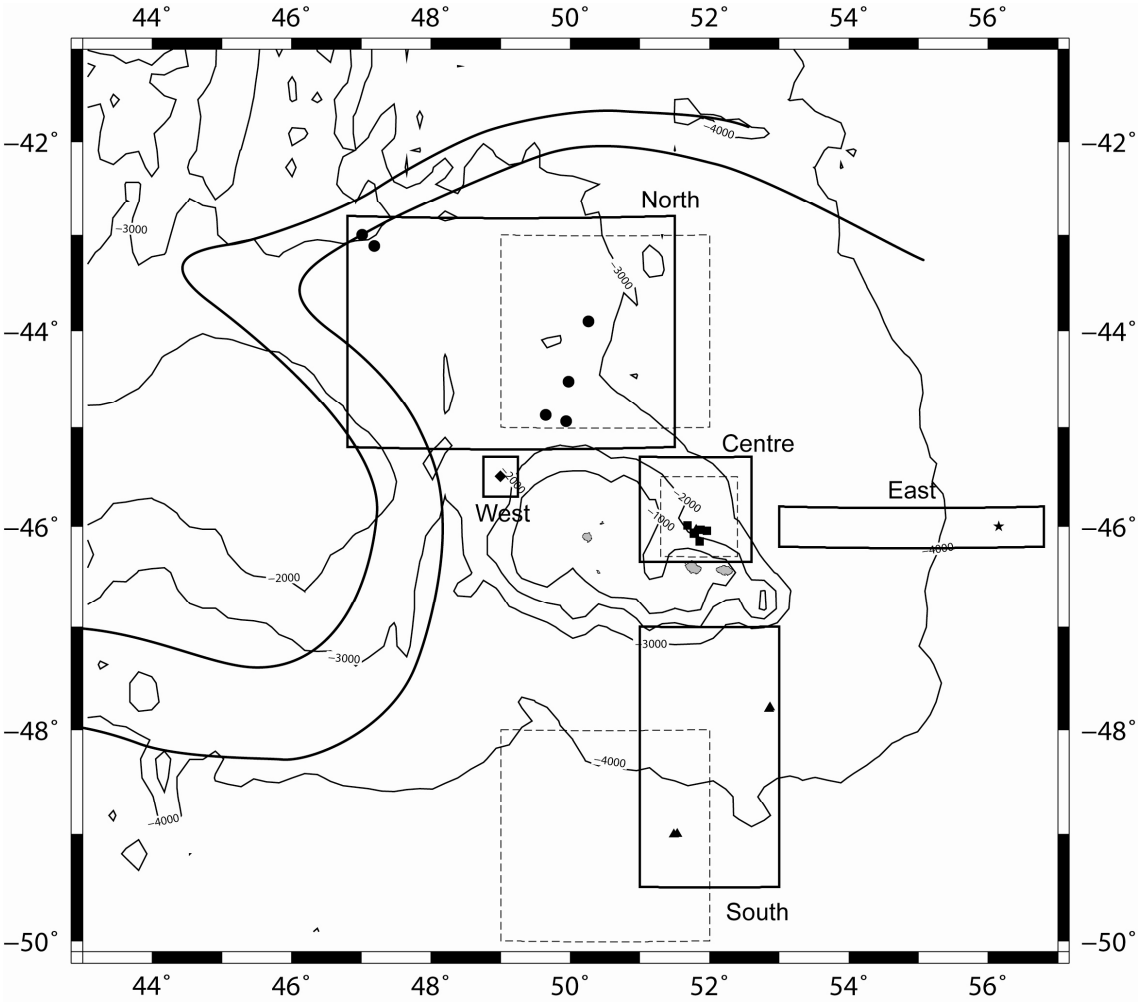

Figure 5.1 Map of station positions. Dashed boxes were determined by Venables *et al.* (2007) to regionalise the study area. These have been modified to encompass POC/N stations, solid boxes. 1000 m bathymetry contours and the circulation front of the ACC are included for reference (Pollard *et al.*, 2007b).

5.2 Results

5.2.1 Particulate Organic Carbon and Nitrogen

As POC and PON are measured at the same time on the same sample (Section 2.6.1), it is logical to present them in parallel. Figure 5.2 to Figure 5.5 present the profiles of POC and PON data, split into legs 1 and 2, further split into the differing regions described in Figure 5.1. Some of these plots contain large numbers of profiles thus not making individual profile identification easy. This however, is not important because the primary purpose of these vertical profiles is to demonstrate the general patterns and trends of the profiles and to allow easy cross comparison between the different regions.

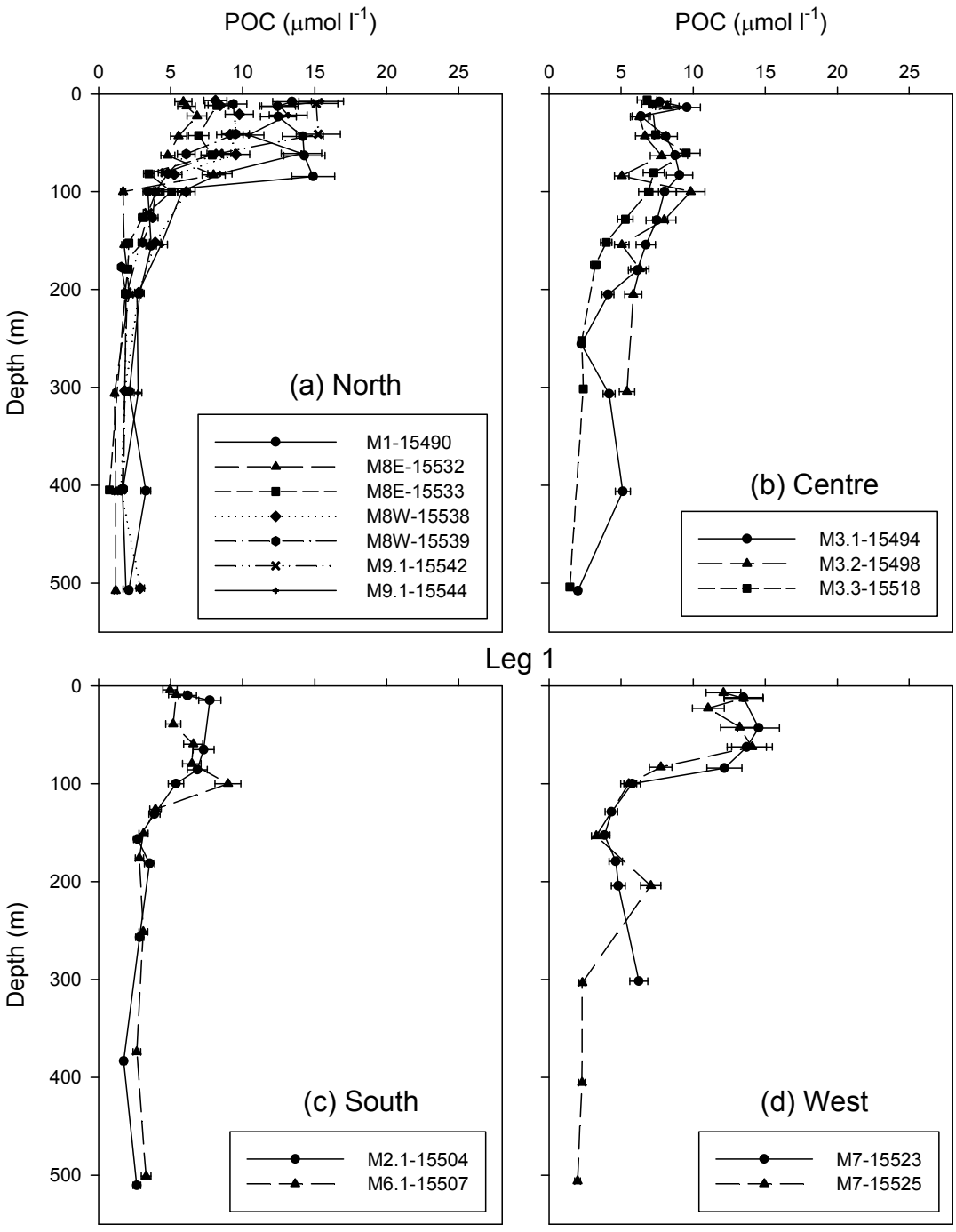

Figure 5.2 Leg 1 POC profiles grouped by region. Error bars are 1 σ.

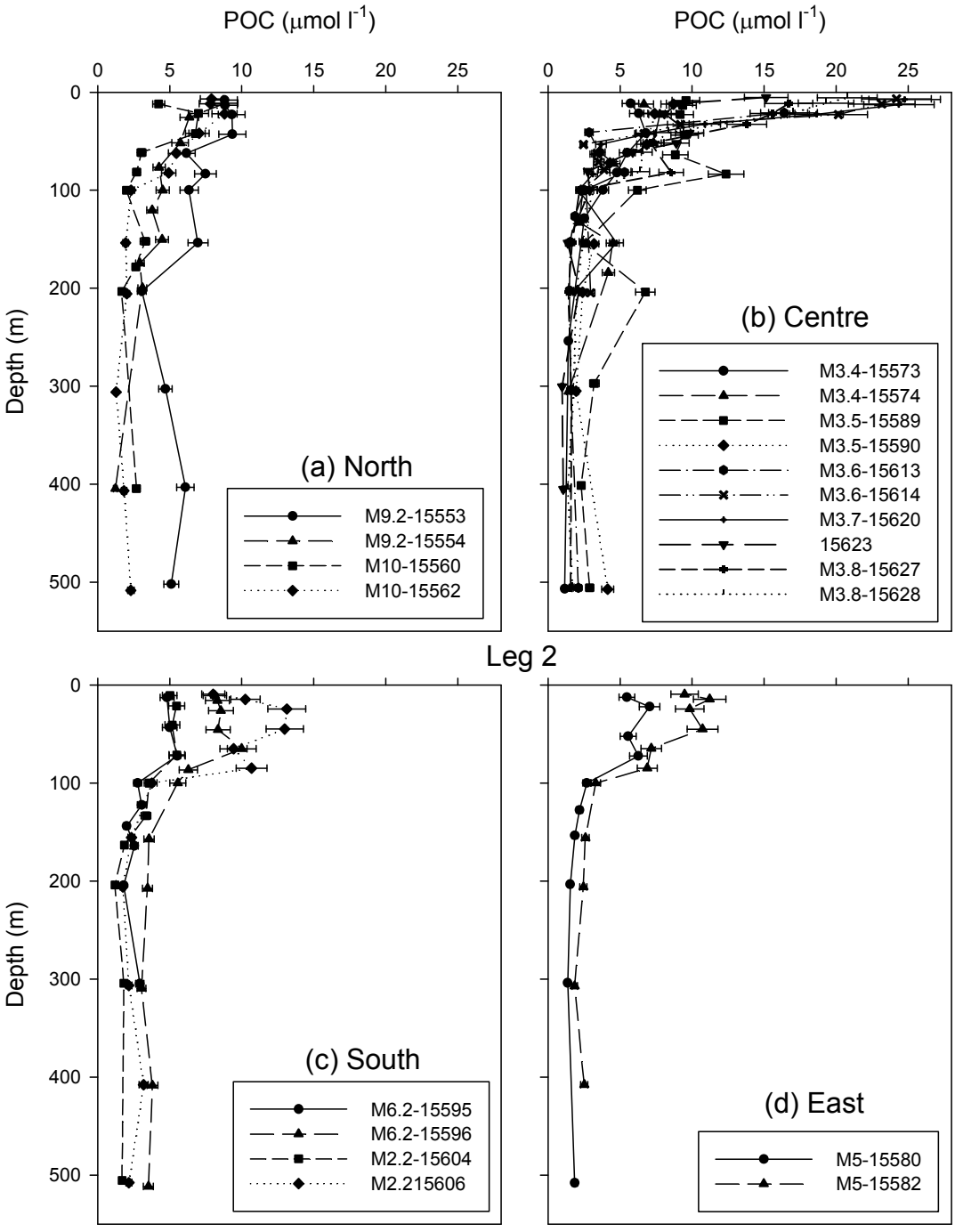

Figure 5.3 Leg 2 POC profiles grouped by region. Error bars are 1 σ.

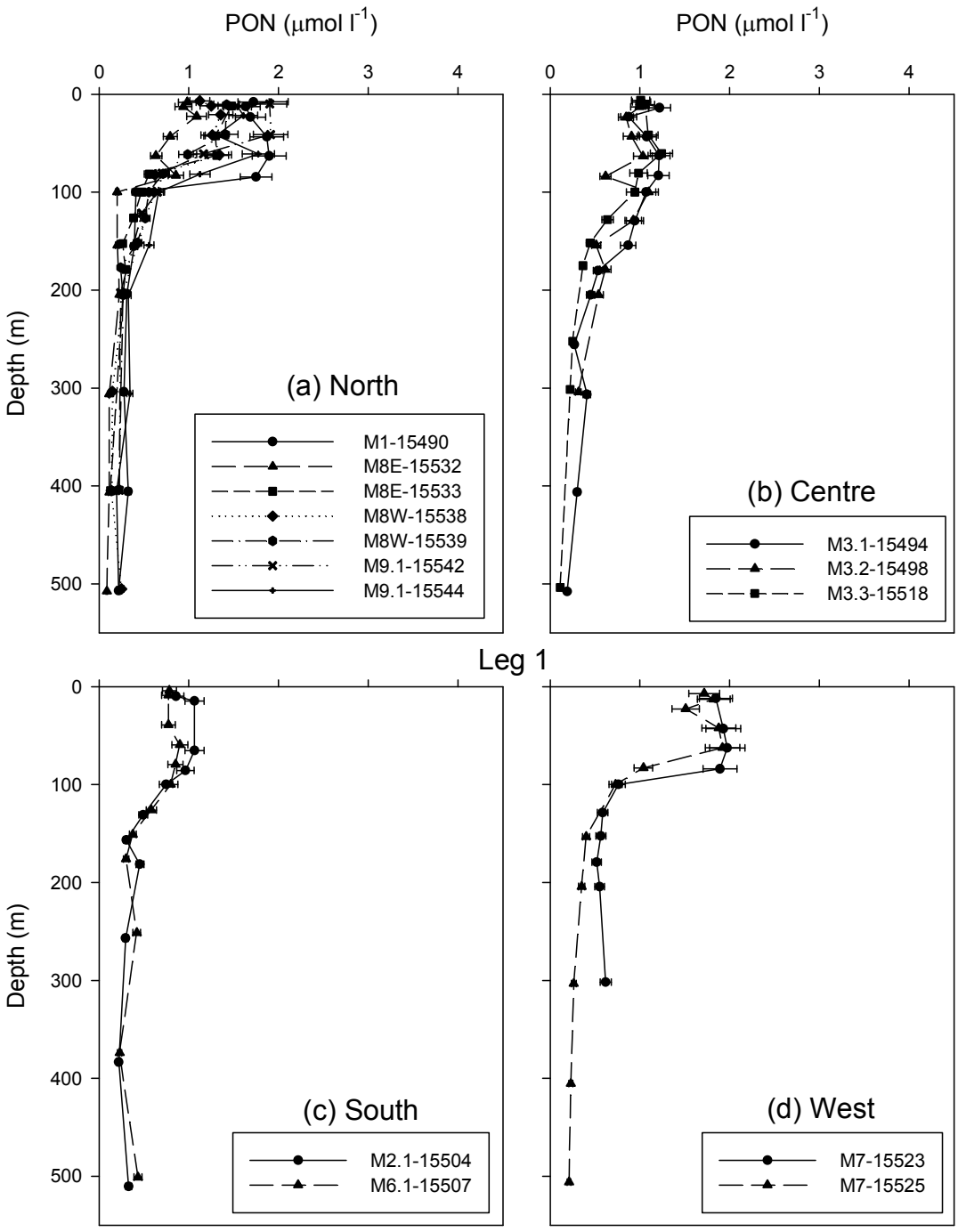

Figure 5.4 Leg 1 PON profiles grouped by region. Error bars are 1 σ.

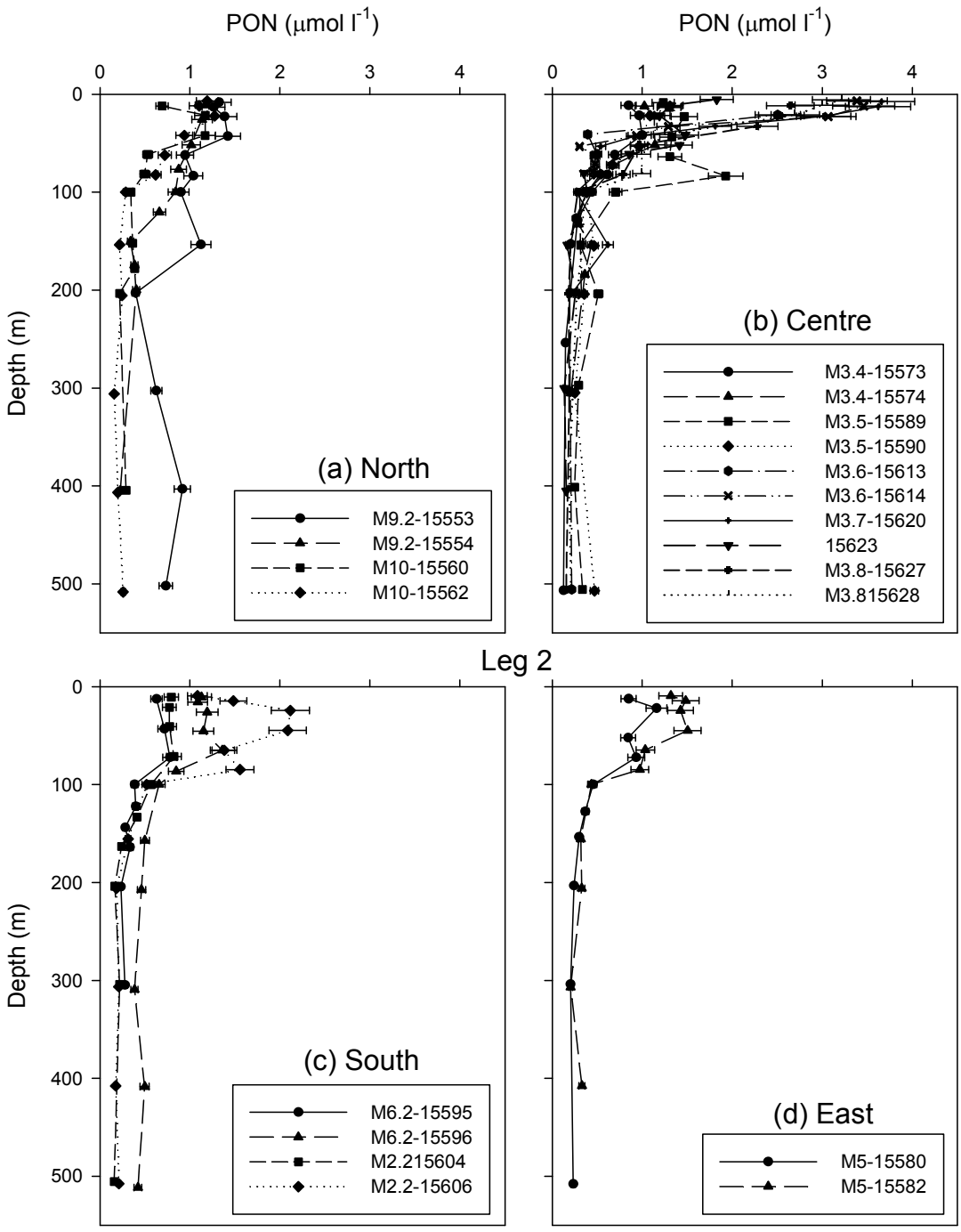

Figure 5.5 Leg 2 PON profiles grouped by region. Error bars are 1 σ.

5.2.2 Synopsis of POC and PON Data

The general trends of POC and PON profiles are the same. This is shown by the linear relationship between all the POC and PON samples plotted together in Figure 5.6 that gives a relationship of: POC = 6.68 × PON + 0.50 (r^2 = 0.96, n = 372). Therefore the patterns in distribution of both carbon and nitrogen will be representative of each other, thus only the patterns of carbon distribution will be described. The C:N ratio will be discussed in more detail in Section 5.3.1.

As would be expected, POC concentration decreases with depth and is consistent with the process of progressive remineralisation with increasing depth. This trend is clear when inspecting Figure 5.2-5.5, but is not as clear in Table 5.1 (POC) and Table 5.2 (PON) that summarise the profiles. Table 5.1 and Table 5.2 present the range of concentrations, subdivided by region, depth and leg. High variability in both surface and deep samples tends to prevent the identification of any trends between subdivisions of data.

Table 5.1 Concentration ranges of POC (μmol l^{-1}) measured on legs 1 and 2, separated by depth and study region.

Region	0-100 m		>100 m		Respective figures
	Leg 1	Leg 2	Leg 1	Leg 2	
North	1.7-15.3	2.0-9.4	0.8-3.9	1.2-7.0	Figure 5.2a and Figure 5.3a
Centre	5.0-9.8	2.13-24.8	1.4-8.0	1.0-6.8	Figure 5.2b and Figure 5.3b
South	5.0-9.0	2.8-13.1	1.8-4.0	1.2-3.6	Figure 5.2c and Figure 5.3c
West	5.5-14.5	-	2.0-7.1	-	Figure 5.2d
East	-	2.7-11.2	-	1.4-2.6	Figure 5.3d

Table 5.2 Concentration ranges of PON (μmol l^{-1}) measured on legs 1 and 2, separated by depth and study region.

Region	0-100 m		>100 m		Respective figures
	Leg 1	Leg 2	Leg 1	Leg 2	
North	0.2-1.9	0.8-1.4	0.1-.6	0.2-1.1	Figure 5.4a and Figure 5.5a
Centre	0.6-1.2	0.3-3.7	0.1-0.9	0.1-0.6	Figure 5.4b and Figure 5.5b
South	0.8-1.1	0.4-2.1	0.2-0.6	0.2-0.5	Figure 5.4c and Figure 5.5c
West	0.7-2.0	-	0.2-0.6	-	Figure 5.4d
East	-	0.5-1.5	-	0.2-0.3	Figure 5.5d

In an attempt to tease out trends in the POC data, Table 5.3 shows the region averaged POC concentrations at 10, 100 and 150 m to represent the surface, mixed layer and just below the mixed layer depth ranges. The eddy stations have been separated out for clarity. In the north there is a decrease at 10 m between legs 1 and 2, with more

consistent concentrations at 100 and 150 m. The central region has constant surface concentrations between legs 1 and 2, whereas at 100 and 150 m concentrations tend to decrease. In the south, 10 and 150 m concentrations are consistent between legs, whereas there is a marked decrease at 100 m. Overall the south appears to have lower concentrations with the north and centre seeming more comparable. The eddy stations have the highest concentration measured anywhere, but only in the surface because at deeper depths the concentrations were among the lowest measured. This highlights the structure of the eddy that had an intense bloom, and particle field, in the surface with very little material falling below the eddy structure. One feature of the southern stations that this analysis does not depict is the presence of a subsurface peak at M2.2 on leg 2 (Figure 5.3c), which occurs between 10 and 100 m.

Table 5.3 Average POC concentrations (μmol l^{-1}) in each region, at three depth horizons, for legs 1 and 2. The eddy stations in the central region have been separated out for clarity.

Depth	North		Centre		Eddy	South		West	East
(m)	Leg 1	Leg 2	Leg 1	Leg 2	Leg 2	Leg 1	Leg 2	Leg 1	Leg 2
10	10.8	7.5	7.7	7.7	19.4	5.8	6.5	12.8	7.5
100	4.3	3.8	8.3	3.7	2.6	7.2	3.9	5.7	3.0
150	3.2	4.2	5.2	3.2	2.4	2.9	2.8	3.6	2.2

5.3 Discussion

5.3.1 The C:N Ratio of Particulate Material

A fundamental parameter of POM is the elemental stoichiometry between phosphorus, nitrogen and carbon, which in average plankton is 1:16:106 respectively (Redfield, 1958). This is equivalent to a C:N ratio of 6.6:1. A composite plot of all the CTD bottle POC and PON data clearly shows a tight regression between POC and PON ($r^2 = 0.96$) and gives an average C:N ratio of 6.68 that is in very close agreement with the Redfield ratio (Figure 5.6). There is scatter around the regression with a C:N ratio range of 4.9-20.0 suggesting that differences in community structure, nutrient limitation and differential remineralisation rates are potentially present around the study region (Boyd and Trull, 2007 and references therein). However, the relative insensitivity of the C:N ratio to Fe limitation (Price, 2005) potentially rules this out as having a major impact on the C:N ratio variations observed. Likewise, Moore *et al.* (2007a) observed relatively little change in C:N stoichiometry in on-deck incubations under varying iron regimes. Species composition may be influencing the C:N ratio (Falkowski and Davis,

2004; Geider and La Roche, 2002; Ho *et al.*, 2003) because both diatoms and *Phaeocystis* blooms were encountered in the CROZEX study region (Poulton *et al.*, 2007). Only a direct comparison of C:N ratios with community structure would reveal any such relationships. Evidence for differential remineralisation between POC and PON is present in Figure 5.6 because the regression intercepts at 0.50 μmol l^{-1} C, suggesting that PON is remineralised preferentially.

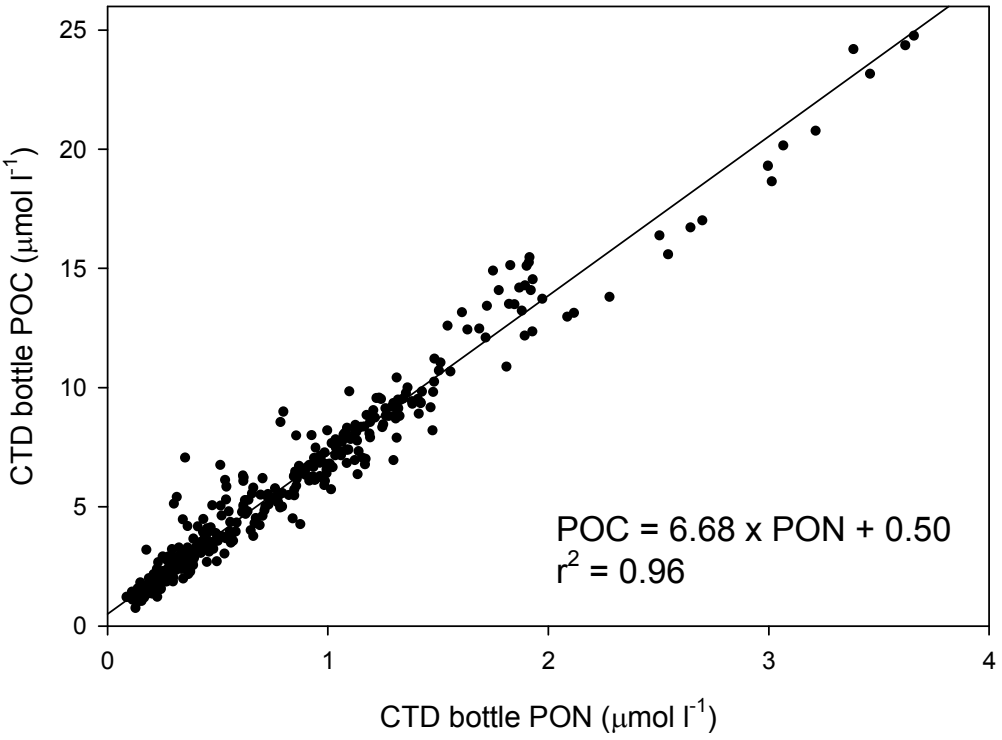

Figure 5.6 The relationship between POC and PON in all the CTD bottle samples. The solid line is a Model II regression.

When comparing the C:N ratio of all the samples against depth there is a general pattern of increasing C:N ratio with increasing depth. Additionally the scatter also increases with depth (Figure 5.7). The increasing C:N ratio means that nitrogen is being preferably remineralised, as noted in Figure 5.6, thus causing the organic matter to become relatively richer in carbon. The profile can be split into two regions (dotted horizontal line): less than 75 m (<75 m) and greater than 75 m (>75 m). In the top 75 m the C:N ratio appears to remain consistent and homogenous with a mean value of 6.95. The regression of the <75 m data has a very small gradient (-0.0001) and is not significant (p = >0.95), which suggests that the gradient is not significantly different from zero. Therefore the intercept of 6.95 can be considered as a representative mean

for the whole upper 75 m of the water column. Below 75 m a significant regression ($p = <0.01$) exists of increasing C:N with increasing depth. The gradient of this relationship is 0.005 mol:mol m^{-1}. These units are easier to understand if considered over a depth range of 100 m and equate to 0.5 molC:molN $100m^{-1}$. Therefore, 0.5 mole of carbon per 1 mole of nitrogen is being lost from the particulate material for every 100 m depth below 75 m.

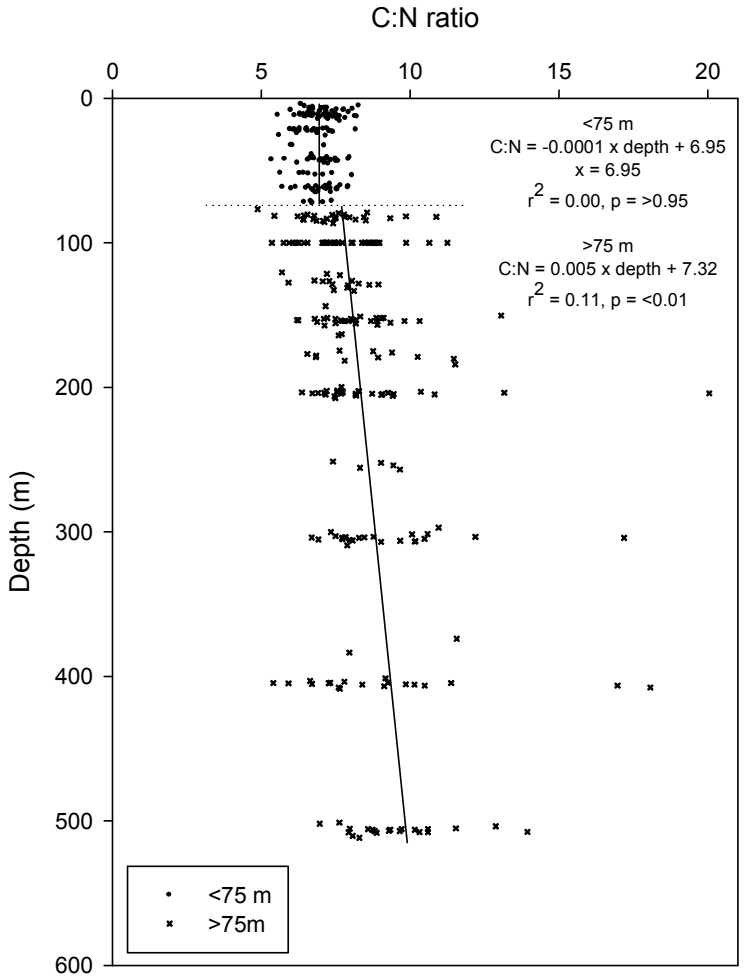

Figure 5.7 The C:N ratio plotted against depth for all the CTD bottle POC and PON observations. Solid lines are Model I regressions.

Therefore a conceptual model can be generated where the C:N ratio is consistent in the top 75 m of the water column, and below 75 m the C:N ratio gradually increases with depth. This split in the profile is probably caused by the mixed layer depth (MLD), which ranges between 40-100 m over the entire study area (Venables *et al.*, 2007). Below the MLD remineralisation processes, such as dissolution and respiration, are

dominant and serve to re-dissolve and oxidise particulate matter into the dissolved pool. The C:N ratio can be used to assess the process of remineralisation (Newton *et al.*, 1994). Thus the gradient of 0.005 mol:mol observed below 75 m suggests that these processes are acting more efficiently on the nitrogen fraction of the (POM). Other studies have also observed more rapid remineralisation of nitrogen over carbon (Boyd *et al.*, 1999; Christian *et al.*, 1997; Smith *et al.*, 1992). However, offsets in the Redfield ratio should be treated with caution and may only be the result of transient events, such as rapidly settling bloom material (Takahashi, 1986; Wong *et al.*, 1999). It is interesting to observe the general trend of increasing C:N ratio with increasing depth and warrants future investigation. For example, it would be interesting to calculate the inorganic C:N ratio for comparison with the POM C:N ratio. This would reveal more evidence for the idea of preferential remineralisation of organic nitrogen. For more information on C:N ratios see (Boyd *et al.*, 1999; Boyd and Trull, 2007). Discussion on spatial variation of C:N ratios will be discussed at the end of Section 5.3.2.

5.3.2 Spatial and Temporal Distribution of POC and PON

The inventories of POC and PON in the upper 100 m were calculated with a trapezoidal integration (Section 2.7) and are given in Table 5.4. Multiple inventories at the same station have been averaged. When plotting 100 m integrated POC and PON against latitude a clear relationship is not evident (Figure 5.8a and b). In the northern bloom region 100 m POC inventories have high variability ranging from about 540-1300 mmol C m^{-2}, when compared to lower variability in the southern non-bloom region of about 610-770 mmol C m^{-2}. The non-bloom stations fall well within the range of the bloom stations. PON follows the same trend (Figure 5.8b). For POC the average values north and south are 840 and 689 mmol C m^{-2} respectively suggesting that some latitudinal gradient does exist but is overshadowed by the large variability in the northern region. It must be reiterated that for consistency, M3.2 will also be considered as a southern station, which was the result of water advection from the south into the M3 location (Pollard *et al.*, 2007b).

Table 5.4 0-100 m integrated inventories of POC and PON. All errors are 1σ.

Station	Region	Date	Latitude	POC ($mmol/m^2$)	PON ($mmol/m^2$)	C:N
M1	N	11/11/2004	43.9021	1302±62	168±8	7.76
M3.1	C	13/11/2004	46.0609	821±39	110±5	7.45
M3.2[a]	S	18/11/2004	46.0340	708±33	90±4	7.84
M2.1	S	19/11/2004	47.7879	706±37	100±5	7.07
M6.1	S	22/11/2004	49.0081	614±29	82±4	7.51
M3.3	C	25/11/2004	46.0695	765±36	107±5	7.12
M7	W	27/11/2004	45.4968	1212±41	169±6	7.19
M8E	N	30/11/2004	44.9391	623±21	97±3	6.44
M8W	N	01/12/2004	44.8766	776±27	111±4	7.01
M9.1	N	03/12/2004	43.1170	1104±39	142±5	7.80
M9.2	N	18/12/2004	42.9988	696±24	110±4	6.34
M10.1	N	20/12/2004	44.5238	537±19	81±3	6.62
M3.4	C	22/12/2004	46.0706	579±19	84±3	6.87
M5	E	27/12/2004	45.9993	707±25	104±4	6.81
M3.5	C	31/12/2004	46.0594	779±27	114±4	6.82
M6.2	S	03/01/2005	49.0001	646±22	89±3	7.30
M2.2	S	06/01/2005	47.8017	772±28	117±4	6.61
M3.6	C	08/01/2005	46.1481	856±40	122±6	7.01
M3.7	C	10/01/2005	46.0332	959±69	145±10	6.60
15623[b]	C	11/01/2005	45.9901	724±42	103±6	7.02
M3.8	C	12/01/2005	46.0429	1042±41	154±6	6.75

[a]Station M3.2 has been grouped with the southern stations based on the discussion in Section 3.2.2.
[b]Station 15623 was located near the M3 eddy bloom.

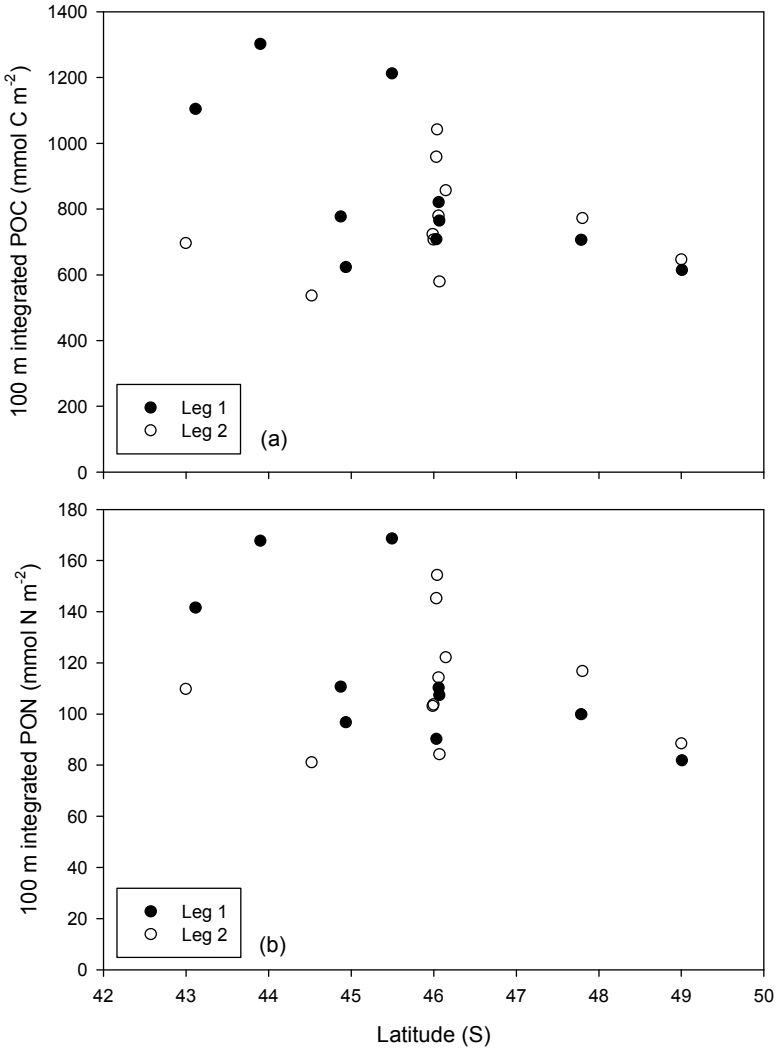

Figure 5.8 Latitudinal variation of POC (a) and PON (b). Legs 1 and 2 have been distinguished.

The large range of POC and PON in the north is probably because all the data from all time points in all conditions have been plotted on one graph. To separate out these variables the same approach as in Section 4.4.2 has been taken to try and diagnose the spatial and temporal variation. The results of this analysis are shown in Figure 5.9. The immediate features that stand out are the relatively constant inventories between the first and last visits to the southern sites. In the northern region there are sharply declining inventories of POC and PON to levels that are comparable to both the southern and central regions by the end of December. In contrast to this, the central region has a moderate increase in POC and PON at the end of leg 2 in January during the sampling of the eddy bloom and is reminiscent of Figure 4.8.

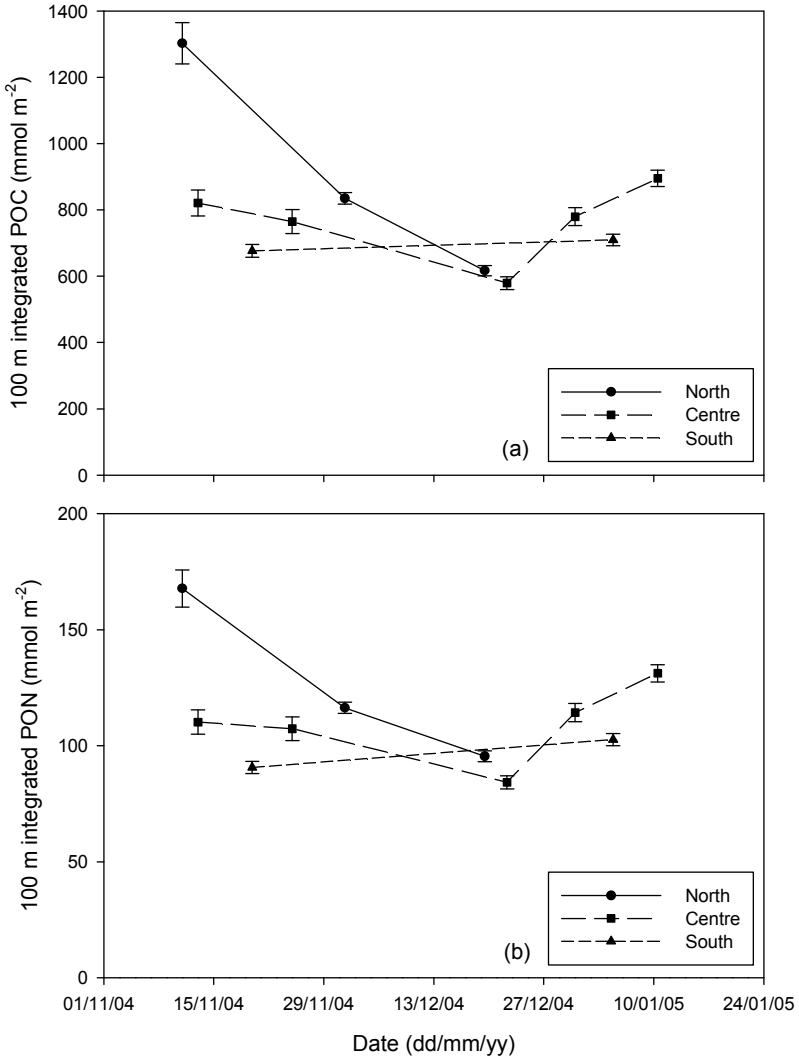

Figure 5.9 Temporal progression of 100 m integrated POC (a) and PON (b) in the northern, central and southern regions. Error bars are 1 σ.

Inspection of the C:N ratio in the different study regions gives mean values of 7.00, 6.96 and 7.27 in the northern, central and southern regions respectively (Table 5.4). None of these averages are significantly different (t-test) at the 95% confidence level and is consistent with investigation on elemental stoichiometry of phytoplankton (Moore *et al.*, 2007a).

5.3.3 Linking Nitrate to PON

The key step to making the analysis of the particulate field consistent to that of the DON field in Chapter 4 is to make the connection between PON and new production derived from nitrate draw-down (ΔNO_3^- NP). However before this is done, POC and PON will be cross compared to chl-*a*, the data of which is tabulated in Table 5.5.

Table 5.5 Station number, 100 m integrated chl-*a* and ΔNO_3^- NP measured up to the date of sampling.

Station	Region	POC[a] (mmol m^{-2})	PON[a] (mmol m^{-2})	Chl-*a* (mg m^{-2})	POC:chl-*a*[b] ratio	ΔNO_3 NP (mmol N m^{-2})
M1	N	1302	168	167	93	521
M3.1	C	821	110	110	90	7
M3.2[c]	S	708	90	51	166	51
M2.1	S	706	100	47	182	73
M6.1	S	614	82	34	216	33
M3.3	C	765	107	72	127	65
M7	W	1212	169	142	102	498
M8E	N	623	97	52	144	429
M8W	N	776	111	88	106	375
M9.1	N	1104	142	86	155	530
M9.2	N	696	110	40	209	328
M10.1	N	537	81	58	111	251
M3.4	C	579	84	73	96	131
M5	E	707	104	30	280	175
M3.5	C	779	114	59	158	216
M6.2	S	646	89	38	203	119
M2.2	S	772	117	37	253	142
M3.6	C	856	122	171	60	354
M3.7	C	959	145	181	64	426
15623	C	724	103	110	79	159
M3.8	C	1042	154	81	155	467

[a]POC and PON data has been carried forward from Table 5.4.
[b]The POC:Chl-a ratio was calculated after first converting the units of POC to mg m^{-2}.
[c]Station M3.2 has been grouped with the southern stations based on the discussion in Section 3.2.2.

The relationship between POC and PON with chl-*a* is shown in Figure 5.10 and is analogous to the similar relationship between DON and chl-*a* shown in Figure 4.10. Figure 5.10 reveals a relationship between the amount of POM and the amount of chl-*a*. Figure 5.10a allows the calculation of the POC to chl-*a* ratio (POC:chl *a*), which is an indicator of iron limitation, and tends to increase with increasing iron stress as phytoplankton become depleted in chl-*a* (Boyd *et al.*, 2000; Geider and La Roche, 1994; Greene *et al.*, 1991; Hoffmann *et al.*, 2006). The regression of Figure 5.10a, using the secondary axis, is: POC = 52.13 × chl-*a* + 5394, (r^2 = 0.46, p = <0.01). Taking the reciprocal of the gradient (1/52.13) reveals that chl-*a* constitutes about 2% of algal POC on a weight for weight basis. This estimate agrees well with estimates of chl-*a* biomass measured in on-deck iron perturbation experiments conducted by Moore *et al.* (2007b).

The mean POC:chl-*a* ratio in northern and southern regions is 136 and 204 respectively and a *t*-test shows that these means are statistically different (p = <0.02), thus providing evidence for enhanced chlorosis in the non-bloom region and supports

the conclusion of increased iron limitation in the southern region reported by others involved with direct biological measurements on CROZEX (Lucas *et al.*, 2007; Moore *et al.*, 2007a; Moore *et al.*, 2007b; Seeyave *et al.*, 2007; Zubkov *et al.*, 2007).

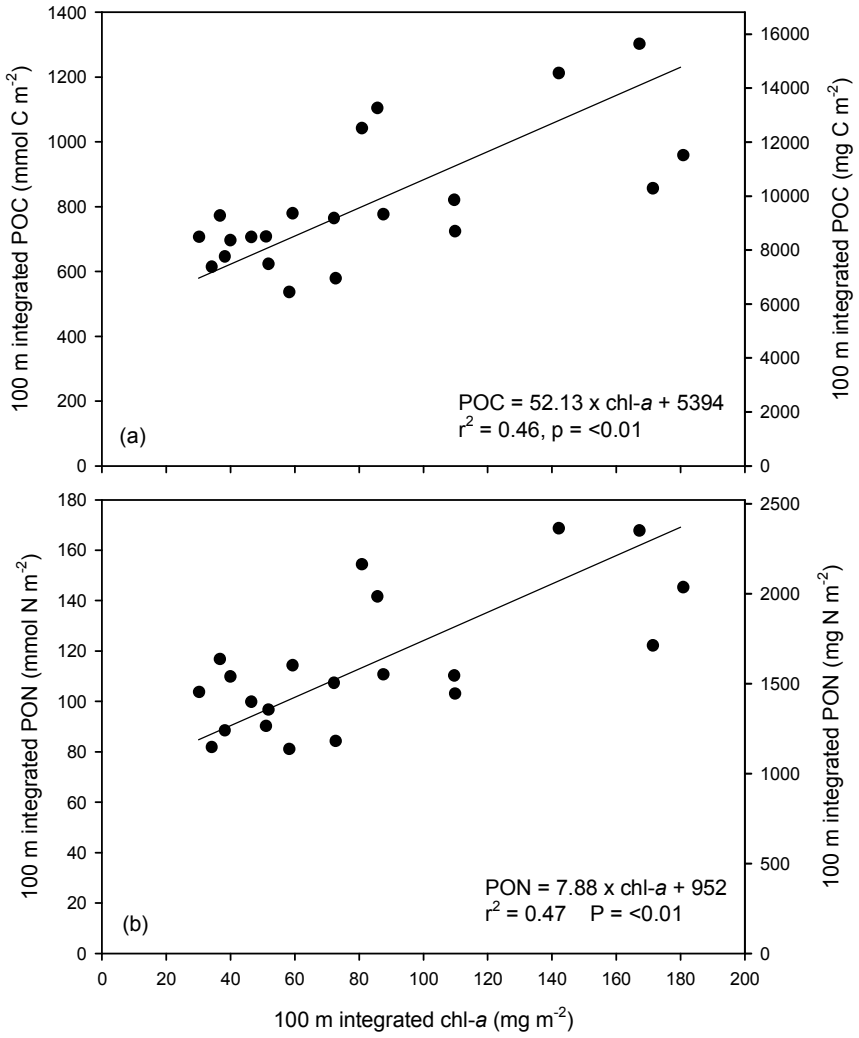

Figure 5.10 The relationships of 100 m integrations of POC (a) and PON (b) with chl-*a*. The right-hand secondary axis gives alternative units of POC and PON in mg m^{-2}. Solid lines are Model II regressions and the regression equations take units from the secondary axes.

The object of exploring the relationships in Figure 5.10 is to demonstrate the potential pathway that organic material may follow, rather than being directly exported. It is clear in Figure 5.10 that elevated levels in chl-*a* were accompanied with higher inventories in the particulate field, and confirms that particulate production is greater in the bloom region than the non-bloom region. However, measuring the POC and PON

inventories, and assuming these phases to be representative of a different stock than the exporting particulate matter, is an assumption that must be validated.

Particle size distribution is an area of concern and research for oceanographers interested in particle flux. The traditional belief is that it is the larger particles that are responsible for contributing towards the majority of particle flux as discussed in Section 2.3 and in Morris *et al.* (2007) (Bishop *et al.*, 1977; Fowler and Knauer, 1986). This is believed because larger particles tend to have faster sinking rates (Asper, 1987). However, the larger particles also tend to be less abundant (Simpson, 1982) thus resulting in biased sampling to the smaller sized particles when sampling smaller volumes of water (Buesseler *et al.*, 2006; Gardner *et al.*, 2003; Liu *et al.*, 2005; Moran *et al.*, 1999). During CROZEX POC and PON samples of 1-2 l were collected from the CTD and were filtered through GF/F filters, which have a nominal pore size of 0.7 μm and smaller (0.3 μm) once combusted to remove organic contamination prior to filtering (Nayar and Chou, 2003). Therefore it can be argued that POC and PON samples are made up mainly of small size particles that are not readily sinking. This allows the assumption that the POC and PON fields measured are probably different to the exporting particles and must therefore be investigated separately as has been done in this chapter. This therefore allows more confidence when making the comparison between ΔNO_3^- NP and PON in the same manner as was done for DON (Figure 4.13). Data for ΔNO_3^- NP is tabulated in Table 5.5.

The analysis of ΔNO_3^- NP and PON is shown in Figure 5.11 along with both linear and non-linear (quadratic) regression lines. The non-linear regression best describes the trend of the data-set ($r^2 = 0.67$) and thus suggests that PON and ΔNO_3^- NP are not proportional. The general shape of the non-linear curve fitted to the data is one of relatively consistent levels of PON with increasing ΔNO_3^- NP up to about 300 mmol N m^{-2} ΔNO_3^- NP. Above 300 mmol N m^{-2} there is a trend of increasing PON with increasing ΔNO_3^- NP. Using the non-linear equation the calculated 100 m inventory of PON at 300 mmol N m^{-2} ΔNO_3 NP is equal to a PON inventory of 108 mmol N m^{-2}. Using the regression of Figure 5.10b this is equivalent of a 100 m inventory of 63 mg m^{-2} of chl-*a*. Interestingly when the surface chl-*a* concentration is inferred using a relationship between surface chl-*a* (chl-a_s) and 100 m integrated chl-*a* (chl-a_i) of chl-a_s = 0.01 × chl-a_i + 0.01 ($r^2 = 0.84$, data not shown), this represents surface chl-*a* of 0.64 mg m^{-2}. This is almost exactly the same as the maximum surface

chl-*a* concentration remotely sensed in the southern region at the peak of the bloom of 0.67 mg m^{-2} (Venables *et al.*, 2007 and Figure 4.6). This suggests that estimates of ΔNO_3^- NP of <300 mmol N m^{-2} are probably representative of non-bloom HNLC conditions, and estimates of ΔNO_3^- NP of >300 mmol N m^{-2} are representative of bloom conditions. The non-linearity of Figure 5.11 can therefore be broken into two sections: an area of low productivity and low chlorophyll, and an area of high productivity and high chlorophyll. Each of these areas has a distinct response in the PON field that is probably ultimately driven by the biomass contained within the water column as suggested by Figure 5.10.

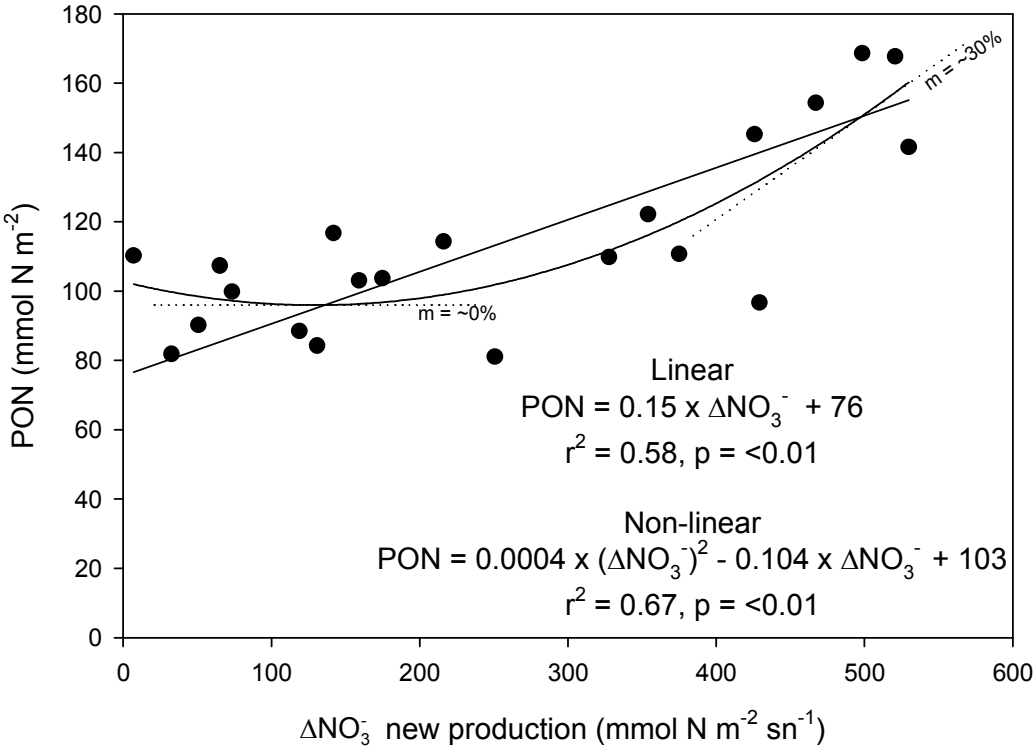

Figure 5.11 The relationship between 100 m integrated ΔNO_3^- NP and PON. The linear regression is a Model II fit and the non-linear regression is a quadratic fit. The dotted lines are estimates of the non-linear gradient at different points.

The accumulation of POM in the Southern Ocean during spring and summer is well documented (Bakker, 1998; Bakker *et al.*, 2006; Bakker *et al.*, 1997; El-Sayed *et al.*, 1983; Nelson and Smith, 1986; Smith and Gordon, 1997; Smith *et al.*, 1996; Sweeney *et al.*, 2000; Wilson *et al.*, 1986). Of these several studies have made estimates of the accumulation of POM from NP. Bakker *et al.* (1997) estimated 47% on

a transect during the austral spring at 6°W from the PF to near the ice edge. This estimate was later revised to 57% in Bakker (1998). Sweeney *et al.* (2000) estimated ≈74% in the Ross Sea during two cruises in late spring and summer; and results from SOIREE estimated 41% (Bakker *et al.*, 2006). Simply taking the linear regression in Figure 5.11 the gradient suggests that 15% of ΔNO_3^- NP is accounted for as PON, which is much lower than any of the values reported in the literature. However, because the non-linear regression returns a better r^2 value than the linear regression it would be unwise to not explore this further. Preliminary investigation suggests that the slopes at low and high ΔNO_3^- NP are about 0 and 30% respectively, see dotted lines plotted perpendicular to the curve at different levels of ΔNO_3^- NP (Figure 5.11). This is the first evidence for differential storage of organic material at differing levels of ΔNO_3^- NP and is a mechanism that may account for the lack of the latitudinal gradient seen in ^{234}Th-Cex on leg 2. In the north a total of 76% of ΔNO_3^- NP can be accounted for as DON + PON (46% + 30%), and in the south a total of 46% of ΔNO_3^- NP can be accounted for as DON + PON (46% + 0%). This opens the question: is there sufficient ^{234}Th-derived export to account for the remaining new production that has not been accounted for as dissolved and suspended particulate matter. This will be addressed in Chapter 6 and uses explanation 4, proposed at the end of Chapter 3, as a basis for an attempt to convert the daily rates of ^{234}Th-derived export to seasonal estimates of export to help answer this question.

5.4 Conclusions

The aim of this chapter was to explore the POC and PON field across the study region. This was done in a manner consistent with the DON field in Chapter 4 so that analogous conclusions could be drawn. Initial inspection of the profiles showed classical trends of decreasing POC and PON with depth. The northern and central bloom regions showed considerable variability in the top 100 m of the water column, which in part was driven by the wide range of conditions sampled such as the M3 eddy bloom on leg 2. The southern stations showed a marked increase in POC and PON on leg 2 at two stations. The overall C:N ratio of all the samples was in good agreement with the Redfield ratio of 6.6, however when the C:N ratio was normalised to depth a general trend of increasing C:N ratio with increasing depth was observed suggesting preferential remineralisation of carbon. Elemental stoichiometry of carbon and nitrogen

was found to not vary significantly between different regions when only considering the top 100 m of the water column.

Latitudinal variation of POC and PON did not show clear trends. However, when the data was sorted chronologically and by region some trends did emerge suggesting a link between chl-*a*, which was then confirmed when directly compared to chl-*a*. Overall, POC and PON are proportionally correlated with chl-*a*, however there was also a significant difference between the POC:chl-*a* ratios in the northern and southern regions suggesting the effects of iron limitation in the southern region.

The final assessment of the particulate field in relation to ΔNO_3^- NP revealed that a non-linear relationship existed between ΔNO_3^- NP and PON. On closer inspection this relationship could be split into two parts: low ΔNO_3^- NP and high ΔNO_3^- NP. In the low range of ΔNO_3^- NP the PON field showed little variation. In contrast, at higher ΔNO_3^- NP the PON field increased. Overall, high chl-*a* is associated with a high particulate field and high ΔNO_3^- NP, whereas low chl-*a* is associated with a constant level in the particulate field and low ΔNO_3^- NP.

6 Rationalisation of New Production and Export

6.1 Introduction

In the previous chapters an attempt was made to reconcile the observed patterns in carbon export using particulate and dissolved organic phases, in particular dissolved and particulate nitrogen. Through doing this it was possible to show that there is the potential for export to be dampened through the build-up of dissolved and particulate phases, with suspended particulate organic matter (sPOM) potentially being responsible for the lack of a strong north-south gradient in daily rates of ^{234}Th-derived carbon export (^{234}Th-Cex) observed on leg 2. To investigate if this is the case, the daily rates of ^{234}Th-Cex need to be scaled to seasonal estimates so they can be directly compared with the seasonal estimates of new production. Therefore, this chapter will start with a direct comparison of daily rate measurements of primary, new and export production, followed by an attempt to scale ^{234}Th-Cex to a seasonal estimate. Finally, a carbon budget for the northern and southern region will be constructed.

6.2 Estimates of New Production and Export

One of the major issues with trying to assess the biogeochemical patterns observed during CROZEX is that of time-scales. For example ^{14}C and ^{15}N productivity rates are measured using ≈24 h bottle incubations and are dependent on the conditions of the water sampled and the conditions under which the incubations were carried out, such as the light field (Section 3.4.2). Both of these may have been different in the days before and after the day of sampling therefore making the sampling day potentially unrepresentative of average conditions. In contrast the ^{234}Th technique is quasi-integrative over about one month (34.8 days Buesseler, 1998), a consequence of the mean life-time of ^{234}Th. This has the advantage of smoothing out daily variability but also has the drawback of 'remembering' a large ^{234}Th depletion event that may have happened several weeks earlier; which would not necessarily be distinguishable from a smaller, more recent, ^{234}Th depletion event.

6.2.1 Daily Rates of New Production and Export

Table 6.1 presents all the daily rate measurements that were directly measured through experimental means: ^{14}C primary production (^{14}C PP), total ^{15}N (Σ^{15}N) uptake,

^{15}N new production (^{15}N NP), ^{234}Th-derived carbon (^{234}Th-Cex) and nitrogen export (^{234}Th-Nex). From these data the *f*-ratio has been calculated (Eppley and Peterson, 1979), and an estimate of carbon new production (NP_C) made by applying the *f*-ratio to ^{14}C PP (Dugdale and Goering, 1967; Lucas *et al.*, 2007). The ^{234}Th export efficiency, *ThE* ratio, has been brought forward from Table 3.8 for carbon (ThE_C) and calculated for nitrogen (ThE_N). ThE_N ratios have been calculated using an analogous method as that used for carbon: ^{234}Th-Nex has been calculated as a percentage of total ^{15}N uptake (Σ^{15}N uptake) on a station by station basis. All the data in Table 6.1 are integrated down to 100 m.

An initial comparison of the 24 h bottle rate measurements, ^{14}C PP and Σ^{15}N uptake, was made by directly correlating ^{14}C PP and total Σ^{15}N uptake. This comparison is displayed in Figure 6.1 and shows a strong relationship with an r^2 of 0.90. The gradient of the slope is 7.23 moles of carbon per mole of nitrogen, which is in relatively good agreement with the Redfield ratio of 6.6. It must be pointed out that the strong relationship that exists between ^{14}C PP and Σ^{15}N uptake is not dictated by the three very high production rate measurements, all of which were from the M3 eddy bloom. If these stations are removed from the regression then the r^2 drops to 0.21 ($p = 0.07$) and the C:N uptake ratio remains similar at 7.34. This highlights the relative insensitivity of the C:N ratio in differing conditions as discussed in Section 5.3.1 (Boyd and Trull, 2007; Moore *et al.*, 2007a; Price, 2005). Based on this there is no good reason to exclude the very high M3 eddy stations from this analysis and leads to the conclusion that both ^{14}C PP and Σ^{15}N uptake are reasonably good predictors of each other over a large range of values.

Table 6.1 Summary of all the 100 m integrated daily rates of primary, new, export production and *f*-ratios, split into legs 1 and 2 and by region. The Eddy stations have also been separated out.

Station	Region	^{14}C PP[a]	Σ^{15}N uptake[b]	^{15}N NP[c]	*f*-ratio[d]	NP_C[e]	^{234}Th-Cex[f]	^{234}Th-Nex[g]	ThE_C[h] (%)	ThE_N[i] (%)
M1	N	89.6	7.0	3.9	0.56	50.2	18.3	2.9	20	41
M7	N	64.3	14.2	7.6	0.53	34.1	13.6	2.7	21	19
M8E	N	11.5	8.0	2.9	0.36	4.1	15.3	2.6	133	32
M8W	N	40.9	9.0	5.1	0.57	23.3	13.6	2.0	33	22
M9.1	N	57.4	15.9	6.4	0.40	22.9	16.7	2.3	29	14
	Mean	**52.7**	**10.8**	**5.2**	**0.48**	**27**	**15.5**	**2.5**	**47**	**26**
M3.1	C	43.6	8.6	3.3	0.39	17.0	13.5	2.1	31	24
M3.3	C	40.0	8.7	4.1	0.47	18.8	11.6	2.0	29	23
	Mean	**41.8**	**8.7**	**3.7**	**0.43**	**18**	**12.6**	**2.1**	**30**	**24**
M3.2[j]	C	31.1	n.d	n.d	n.d	n.d	4.9	0.9	16	n.d.
M2.1	S	36.3	8.3	3.8	0.45	16.3	4.9	0.9	13	11
M6.1	S	19.6	7.7	3.2	0.41	8.0	5.8	1.1	30	14
	Mean	**29.0**	**8.0**	**3.5**	**0.43**	**12**	**5.2**	**1.0**	**20**	**13**
M9.2	N	9.8	7.4	2.8	0.38	3.7	23.2	3.3	236	45
M10	N	35.6	9.0	3.2	0.36	12.8	11.3	2.1	32	23
M5	N	34.1	4.3	0.9	0.2	6.8	12.8	2.1	37	49
	Mean	**26.5**	**6.9**	**2.3**	**0.31**	**8**	**15.8**	**2.5**	**102**	**39**
M3.4	C	59.5	12.1	3.9	0.33	19.6	20.0	3.3	34	27
M3.5	C	27.3	8.4	2.9	0.34	9.3	15.6	2.2	57	26
	Mean	**43.4**	**10.3**	**3.4**	**0.34**	**14**	**17.8**	**2.8**	**46**	**27**
M6.2	S	25.2	6.7	2.1	0.31	7.8	14.4	2.2	57	33
M2.2	S	17.2	7.1	2.4	0.34	5.9	18.8	3.0	109	42
	Mean	**21.2**	**6.9**	**2.3**	**0.33**	**7**	**16.6**	**2.6**	**83**	**37**
M3.6	Eddy	249.5	38.2	25.0	0.65	162.2	13.8	2.2	6	6
M3.7	Eddy	184.3	28.7	21.8	0.76	140.1	10.1	1.7	5	6
M3.8	Eddy	137.6	23.3	14.2	0.61	83.9	12.2	2.1	9	9
	Mean	**190.5**	**30.1**	**20.3**	**0.67**	**129**	**12.0**	**2.0**	**7**	**7**

[a]PP_C (mmol C m^{-2} d^{-1}), carbon fixation measured using ^{14}C (Seeyave *et al.*, 2007).
[b]Σ^{15}N uptake (mmol N m^{-2} d^{-1}), measured using total ^{15}N uptake (Lucas *et al.*, 2007).
[c]^{15}N NP (mmol N m^{-2} d^{-1}), measured using $^{15}NO_3^-$ uptake (Lucas *et al.*, 2007).
[d]*f*-ratio is calculated as $^{15}NO_3^-/\Sigma^{15}$N (Lucas *et al.*, 2007).
[e]*f*-ratio NP_C (mmol C m^{-2} d^{-1}), calculated as *f*-ratio × ^{14}C PP (Lucas *et al.*, 2007).
[f]^{234}Th-Cex (mmol C m^{-2} d^{-1}), ^{234}Th-derived C export (Table 3.5) (Morris *et al.*, 2007).
[g]^{234}Th-Nex (mmol N m^{-2} d^{-1}), ^{234}Th-derived N export (Table 3.5) (Morris *et al.*, 2007).
[h]ThE_C is calculated as ^{234}Th-Cex/^{14}C PP (Table 3.8) (Morris *et al.*, 2007).
[i]ThE_N is calculated as ^{234}Th-Nex/Σ^{15}N uptake.
[j]Station M3.2 has been grouped with the southern stations based on the discussion in Section 3.2.2.
n.d. means not determined.

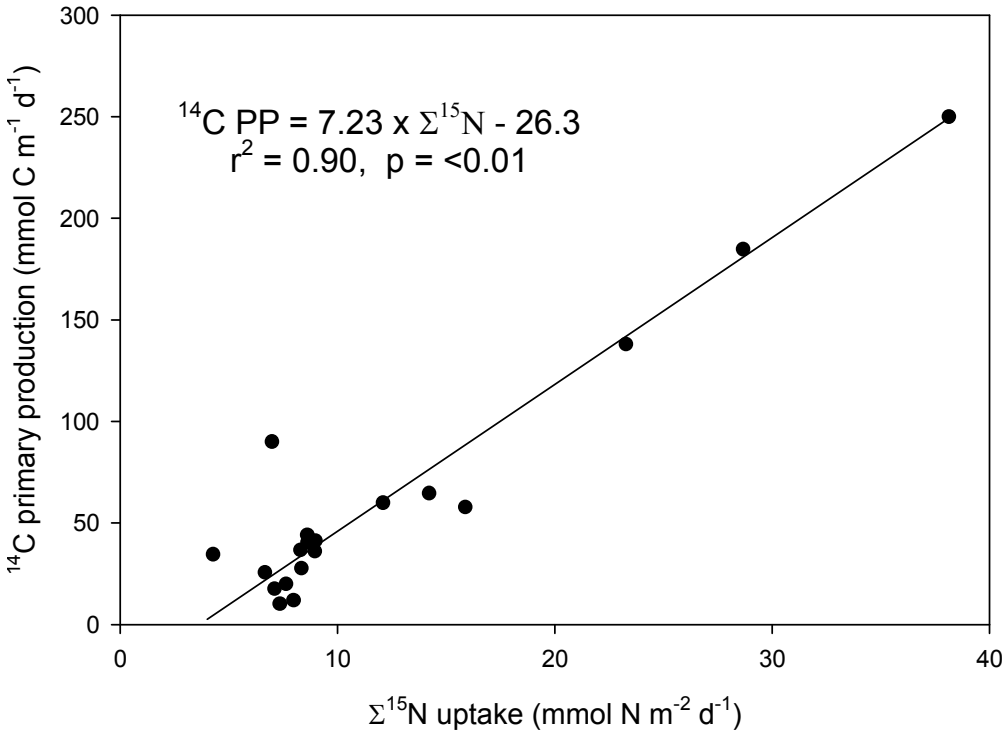

Figure 6.1 Relationship of integrated ^{14}C PP and Σ^{15}N uptake rates. Solid line is a Model II regression.

It has been argued, over appropriate spatial and temporal scales, that export production and new production should remain equivalent if the upward supply of new nutrients is to equal the downward flux of exporting material when in steady-state (Eppley and Peterson, 1979). With this concept in mind, if a cross comparison between the ^{234}Th-derived export estimates is to be made with 24 h bottle production measurements, then the ^{234}Th-derived export estimates of carbon and nitrogen must be compared to inferred NP_C and ^{15}N NP respectively. ^{15}N NP is, of course, determined directly through the uptake of $^{15}NO_3^-$ (Section 2.6.2 and Lucas *et al.*, 2007), however, NP_C estimates have to be inferred indirectly by multiplying ^{14}C PP by the *f*-ratio. The results of this are shown in Table 6.1 as NP_C but have to be treated with caution because C:N stoichiometry may be different between stations. However, given the generally Redfieldian stoichiometry noted multiple times (Figure 5.6 and Figure 6.1), and the continuing usefulness of the *f*-ratio as an estimate of export in high latitude regions (Yool *et al.*, 2007), the estimates of NP_C should be meaningful. Plots of ^{234}Th-Cex and ^{234}Th-Nex against NP_C and ^{15}N NP are shown in Figure 6.2.

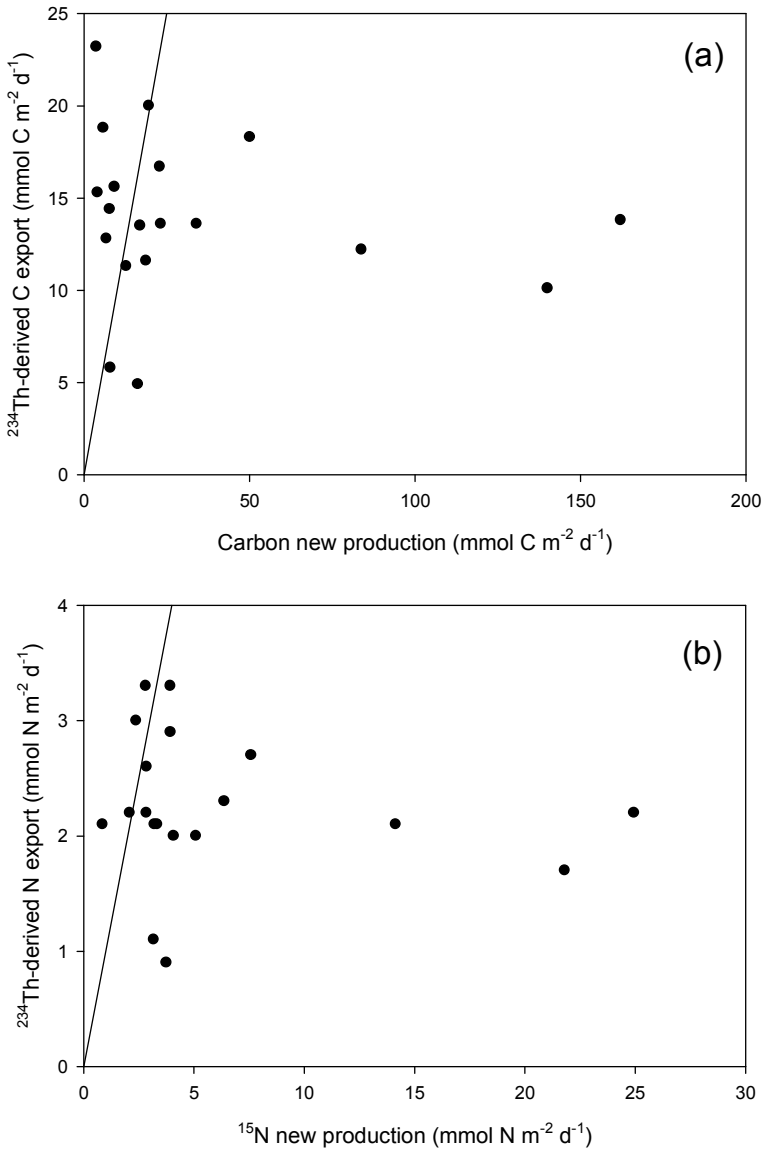

Figure 6.2 100 m integrated ^{234}Th-Cex and ^{234}Th-Nex export against carbon new production (NP_C) and ^{15}N new production (^{15}N NP) in plots a and b respecively. 1:1 lines have been plotted for reference.

The plots in Figure 6.2 reveal that no clear relationships exist between daily rates of NP and ^{234}Th-derived export. A 1:1 line has been plotted on both graphs for reference, if NP was equal to export then the data points would sit on this line. The majority of the data points in both cases sit to the right of the 1:1 line which suggests that generally NP is greater than export. Given the evidence in Chapters 4 and 5 that point towards a storage of dissolved and particulate matter in the surface waters it should come as no surprise to observe generally greater NP than export in Figure 6.2. This interpretation has to be made cautiously because the time-scales between the ^{234}Th-derived export and daily NP estimates are different for the reasons discussed in

Section 3.4.2. Briefly, NP estimates are based on 24 h bottle measurements and ^{234}Th-derived export is quasi-integrative over about 34 days. This issue of time-scales is almost certainly playing a role.

Although there are issues with temporal offsets when directly comparing the ^{234}Th-derived export with the 24 h NP rate measurements there is still some validity when combining the estimates of primary and export production to calculate export efficiencies for both ThE_C and ThE_N, which were then compared directly. ThE_C is calculated as the percentage of ^{234}Th-Cex to ^{14}C PP, values of which were calculated in Section 3.4.2 and carried forward to Table 6.1. ThE_N is calculated as the percentage of ^{234}Th-Nex to Σ^{15}N uptake, the values of which can be calculated from Table 6.1. Figure 6.3 shows the results of plotting ThE_C and ThE_N on a station by station basis and in general shows that with increasing ThE_C, ThE_N also increases. However this trend is not linear and the ThE_N starts to tail off at higher levels of ThE_C with a logarithmic function being the best fit for the data. It is worth noting that the three data points that are >100% ThE_C are not entirely driving this relationship because when these are excluded from the non-linear regression analysis the same trend is still present. For comparison the KEOPS ThE_C and ThE_N values from Savoye *et al.* (2008) are plotted on the same axis and these also show a similar relationship with a non-linear regression giving the best r^2 fit.

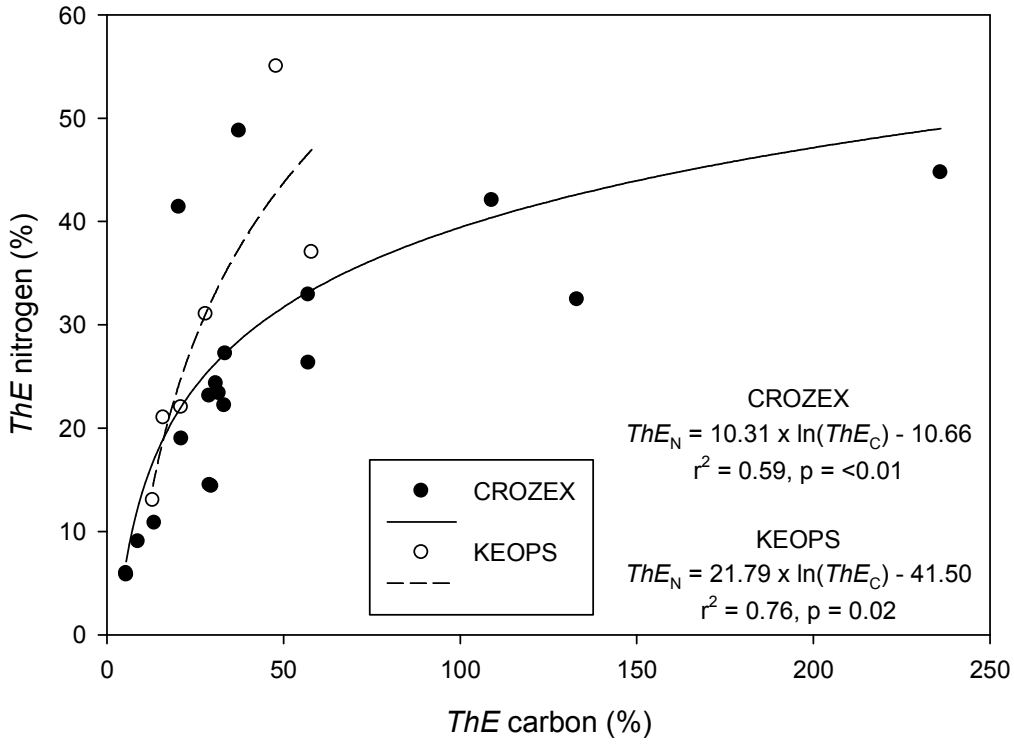

Figure 6.3 The export efficiency of carbon (ThE_C) against the export efficiency of nitrogen (ThE_N). The analgous data from KEOPS has been plotted for comparison (Savoye *et al.*, 2008). Solid lines are logarithmic fits to the data.

A graph of this shape suggests that nitrogen is preferentially stored in the mixed layer and is therefore being recycled more than carbon before it exits the mixed layer. This evidence for preferential recycling of nitrogen over carbon is also confirmed by comparing the *f*-ratio against the ThE_C (Figure 6.4). When these two parameters are plotted it is clear to see that as the ThE_C ratio increases there is a clear decrease in the *f*-ratio. Initially this is a linear relationship but at very high ThE_C ratios the *f*-ratio appears to level off at an *f*-ratio of about 0.35. A decreasing *f*-ratio means that a higher fraction of recycled nitrogen is being taken up. Therefore in simple terms as the export efficiency of carbon increases a higher fraction of nitrogen is recycled, thus implying that the export efficiency of nitrogen must be less.

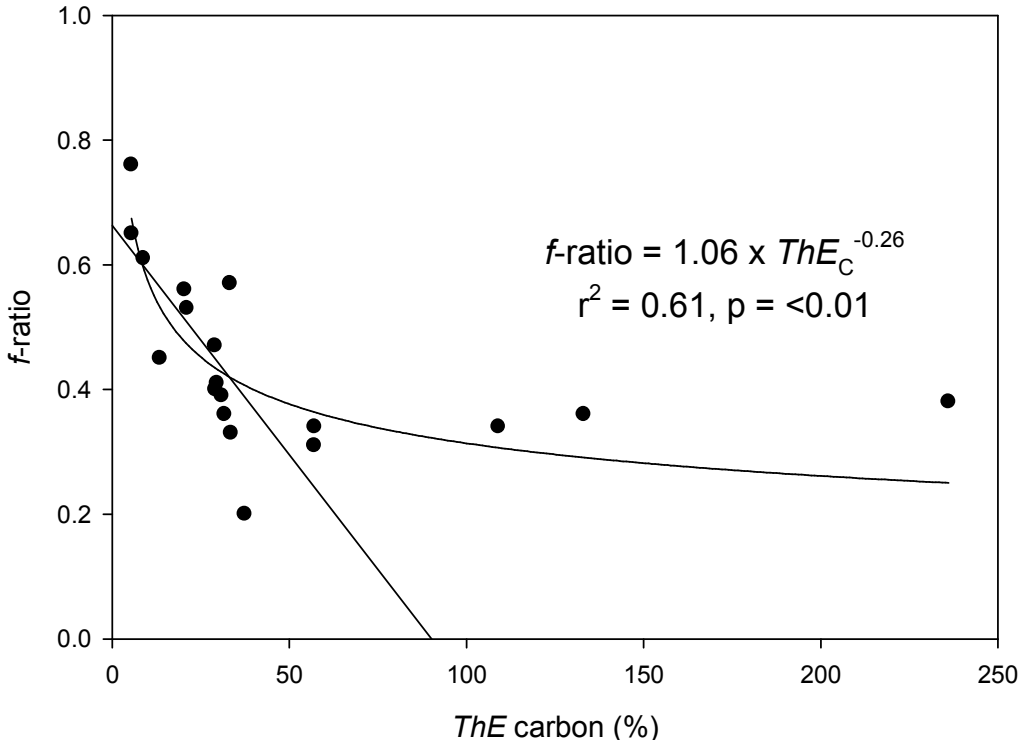

Figure 6.4 The *f*-ratio against the export efficiency of carbon (ThE_C).

6.2.2 Integrated Estimates of New Production and Export

The previous section investigated the relations between the daily rate measurements of primary, new and export production. This section aims to do the same but using an integrative approach to assess the export happening over a longer period of time, something approaching the seasonal total. For this compilation the sampling region has been split into the three distinct areas: north, centre and south, as described in Chapter 4. The mean latitude for the three regions has been calculated to allow easy graphical cross comparison between the various parameters. The information has been further categorised into legs 1 and 2, and overall. Results from stations in each of the three areas have been averaged to calculate the values presented in Table 6.2.

Integrated estimates of primary and new production (Int. PP and ΔNO_3^- NP respectively) were calculated by Sanders *et al.* (2007), and from these an integrated *f*-ratio (Int. *f*-ratio) was also calculated. In brief these parameters were calculated as follows. ΔNO_3^- NP is the estimated NO_3^- draw-down observed at each station, using the concentration at 100 m as the surface winter mixed layer concentration. ΔNO_3^- NP was then converted to carbon units using a Redfield ratio of 6.6. Int. PP was calculated using satellite-derived, temporally integrated chl-*a* data, converted to euphotic layer

depth integrated PP using the relationship of Seeyave *et al.* (2007). The Int. *f*-ratio presented here is different to the traditional *f*-ratio examined in Section 6.2.1 and presented by Lucas *et al.* (2007), but is instead the ratio of ΔNO_3^- NP to Int. PP. For full details of this data manipulation see the end of Section 4.4.4 and Sanders *et al.* (2007).

The results of DIC deficit and ^{15}N NP, along with their methods, are taken from Bakker *et al.* (2007) and Lucas *et al.* (2007) respectively; additionally see Section 2.6.2. The DIC deficit is the deficiency of DIC that is measured in the water column when compared to what would be expected when the mixed layer is in equilibrium with the atmosphere. DIC is fixed during photosynthesis thus allowing measured deficits to be equivalent to the new production in the water column.

Two methods of estimating integrated ^{234}Th-derived carbon export (^{234}Th-Cex) are also presented in Table 6.2. $^{234}Th\text{-}Cex_a$ is the daily export measurements scaled to 34.8 days (mean life-time of ^{234}Th), and $^{234}Th\text{-}Cex_b$ is the daily export measurement scaled to the length of the bloom. Each of these approaches to scaling the ^{234}Th-Cex to a seasonal estimate will now be explained.

Table 6.2 A summary of results from all the methods used to estimate primary, new, export production and *f*-ratio.

Parameter	Leg 1			Leg 2			Overall		
(mol C m^{-2})	North	Centre	South	North	Centre	South	North	Centre	South
Latitude (°S)	44.28	46.05	48.22	43.90	46.15	48.40	44.17	46.12	48.27
Int. PP	7.88	4.11	2.33	8.69	5.76	3.58	8.12	5.24	2.69
ΔNO_3^- NP	2.89	0.38	0.19	2.24	1.50	1.07	2.70	1.15	0.44
Int. *f*-ratio	0.37	0.09	0.08	0.26	0.26	0.30	0.34	0.21	0.14
DIC deficit	n.a.	n.a.	n.a.	n.a.	n.a.	n.a.	3.00[a]	n.a	1.30
^{15}N NP	n.a.	n.a.	n.a.	n.a.	n.a.	n.a.	2.69[b]	1.49	0.42[c]
$^{234}Th\text{-}Cex_a$[d]	0.56	0.44	0.18	0.60	0.50	0.58	0.57	0.48	0.34
$^{234}Th\text{-}Cex_b$[d]	1.38	0.61	0.10	1.89	1.34	1.07	1.55	1.13	0.49

[a]Includes stations 15565, 15556, M7 and N1 (Bakker *et al.*, 2007).
[b]Includes station M7 (Lucas *et al.*, 2007).
[c]Includes station M5 (Lucas *et al.*, 2007).
[d]$^{234}Th\text{-}Cex_a$ and $^{234}Th\text{-}Cex_b$ are integrated by 34.8 days and the bloom length respectively.
n.a. means not available.

Scaling the daily rate of ^{234}Th-Cex by 34.8 days is not an unreasonable method of data manipulation because, through the nature of the tracer, it is quasi-integrative over the mean life-time of ^{234}Th (Buesseler, 1998). By making the assumption that the thorium technique has the power of historical integration it is then possible to show that the peak of the bloom in the northern region is captured by a 34.8 day window

preceding leg 1 (Figure 6.5). These results are in Table 6.2 as ^{234}Th-Cex$_a$. In contrast, an approach to temporally integrate the daily rate of ^{234}Th-Cex to the length of the bloom was also made. The bloom length was calculated as the time between the start of the bloom to the date of sampling and was done separately for each station. The start of the bloom was estimated to be 01/09/04, 01/10/04 and 01/11/04 for the north, centre and south respectively (Figure 6.5). The measured daily rate of ^{234}Th-Cex was then scaled to the bloom length; for reference the daily rates of ^{234}Th-Cex and calculated bloom lengths are detailed in Tables 6.1 and 6.3 respectively. The results of this analysis are given as ^{234}Th-Cex$_b$ in Table 6.2.

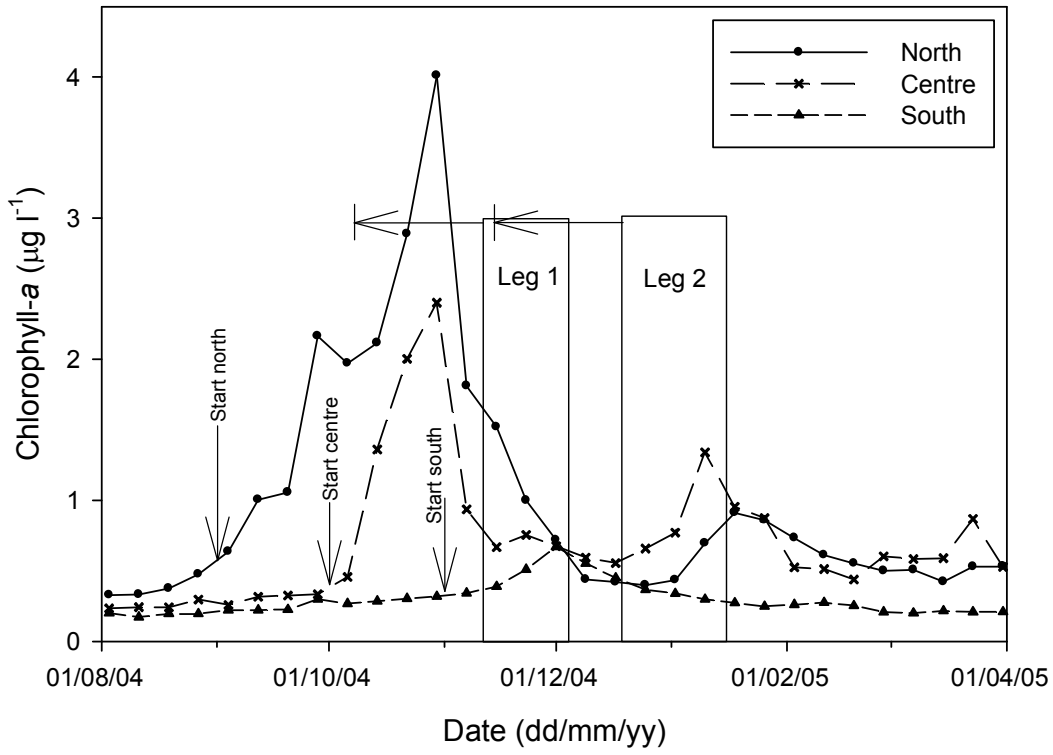

Figure 6.5 The timing of legs 1 and 2 in relation to the bloom progression. The 34.8 day envelope preceding each leg is marked with the horizontal arrows and the start of the bloom in the different regions are marked by the vertical arrows. Bloom progression taken from Venables *et al.* (2007).

When collating seasonal estimates of primary and new production, careful consideration must be given to how a season has been derived for the various estimates presented in Table 6.2. The seasonal estimates for ΔNO_3^- NP and DIC deficit are calculated up to the date of sampling so have an effective integrating period that spans from the start of the productive season until the time each station was sampled. Int. PP

was calculated by integrating surface chl-*a*, as represented in Figure 6.5, up to the date of sampling in the region specific to each station. Temporally integrated surface chl-*a* was then converted to Int. PP using the relationship published by Seeyave *et al.* (2007) of Int. PP = 461.8 × chl-*a* + 109.9. The Int. *f*-ratio was then calculated by a combination of Int. PP and ΔNO_3^- NP as described by Sanders *et al.* (2007). The seasonally integrated estimates of ^{15}N NP reported by Lucas *et al.* (2007) were integrated over the 31 week range covered by Figure 6.5 and were also derived through a relationship with surface chl-*a* (Lucas *et al.*, 2007). Although seasonally integrated ^{15}N NP is integrating over a longer time period than that for ΔNO_3^- NP, DIC deficit, Int. PP and Int. *f*-ratio, it will still be comparable. This is because seasonally integrated ^{15}N NP is related to surface chl-*a*, the bulk of which occurs prior to arrival in the study area (Figure 6.5). It is therefore recognised that there are differences in the temporal integrating period between the various methods of measuring primary and new production. However, because the sampling occurred after the main bloom event, this will tend to reduce integrating biases in parameters integrated over slightly different time periods.

Plotting the overall results of Table 6.2 graphically as Figure 6.6 the trends in the data become clear. Making the comparison of $^{234}Th\text{-}Cex_a$ with ΔNO_3^- NP, red and green lines respectively in Figure 6.6, $^{234}Th\text{-}Cex_a$ is consistently lower than ΔNO_3^- NP with this particularly prominent in the north where $^{234}Th\text{-}Cex_a$ is approximately a factor of five times lower. In comparison, when $^{234}Th\text{-}Cex_b$ is compared to ΔNO_3^- NP, blue and green lines respectively, $^{234}Th\text{-}Cex_b$ is more comparable with ΔNO_3^- NP for the central and southern regions but is approximately a factor of two lower in the north.

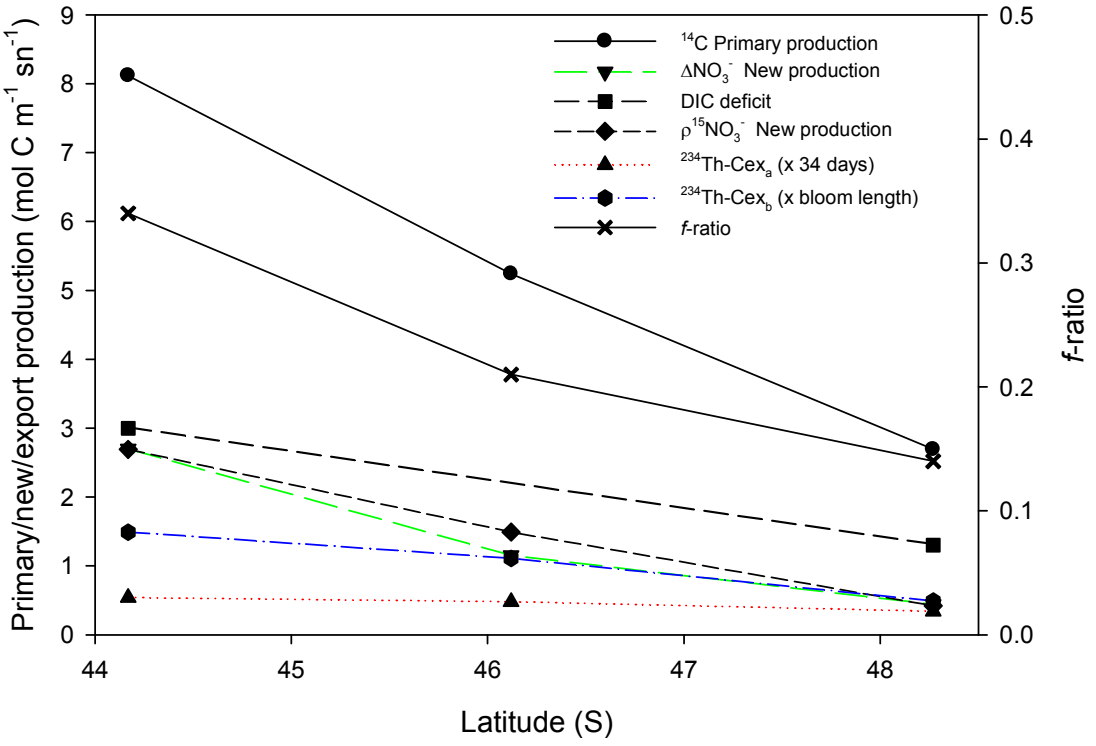

Figure 6.6 Graphical representation of the data in Table 6.2. Primary, new and export production as a function of latitude. The *f*-ratio has been plotted on a secondary axis.

Now that ^{234}Th-Cex has been scaled using two different methods the results of this must now be put into context with the results from Chapters 4 and 5 regarding the dissolved and suspended particulate matter. At the end of Chapter 5 it was concluded that in the north 76% of ΔNO_3^- NP was accountable for as DOM and POM, and in the south 46% of ΔNO_3^- NP was accountable for as DOM and POM. This means that export should account for the remainder of ΔNO_3^- NP, 24% in the north and 54% in the south. Using the two estimates of temporally integrated ^{234}Th-Cex, Figure 6.7 displays the proportion of ΔNO_3^- NP exported. For reference the 24% and 54% levels have been marked to show what export is required to balance ΔNO_3^- NP in the different regions. In the north the ^{234}Th-Cex$_a$ estimate falls close to the 24% whereas ^{234}Th-Cex$_b$ falls considerably above. In the south both estimates are significantly above the 54% required. Using the mean life-time of ^{234}Th to scale export seems to have worked reasonably well in the north but not in the south. Using the bloom length seems to have over estimated export in both regions. Neither of the methods can consistently scale daily rates of ^{234}Th-Cex to account for the remaining ΔNO_3^- NP. Additionally, this

approach also assumes that the inventories of DOM and POM are perfect, a situation that is almost certainly not true. Therefore an alternative approach should be explored.

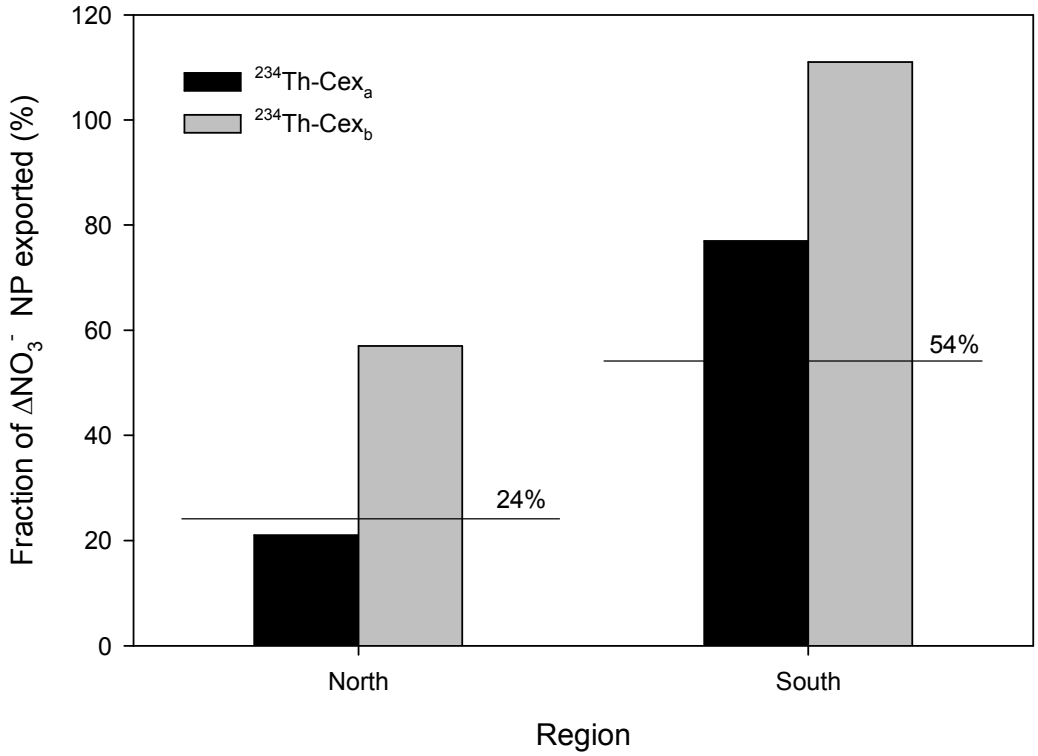

Figure 6.7 The proportion of ΔNO_3^- NP exported after scaling daily rates of ^{234}Th-Cex to the mean life-time of ^{234}Th (^{234}Th-Cex$_a$) and the bloom length (^{234}Th-Cex$_b$).

This still leaves the problem of attempting to formulate a consistent method of temporally integrating ^{234}Th-Cex. The mean life-time and bloom length methods used above are fairly crude approaches to temporally integrating ^{234}Th-Cex. ^{234}Th-Cex$_a$ made the assumption that the daily rates of ^{234}Th-Cex were only present for 34.8 days. Conversely, the ^{234}Th-Cex$_b$ made the assumption that the daily rates of ^{234}Th-Cex occurred for the whole of the bloom length. Both of these are simplistic assumptions that are unlikely to be appropriate for the different conditions in the north and south and thus resulted in the patterns in Figure 6.7. This leads to the realisation that a much more synergistic approach must be adopted that is more sympathetic to the varying conditions encountered across the CROZEX region. This approach needs to attempt to use complementary data to tie the daily rates of ^{234}Th-Cex to parameters that are naturally more integrative over the differing durations of the bloom in the different regions.

Therefore, the remainder of this chapter is dedicated to presenting a more sophisticated method of scaling the daily rates of ^{234}Th-Cex to a seasonal estimates of export of carbon using the simpler biogeochemical cycle of silicon. Through using a combination of the seasonal draw-down of silicate in the mixed layer and the ^{234}Th-derived biogenic silica export, the carbon export that would be expected over the course of the bloom season will be calculated. This will be done with the use of a recalibration model that will be explained in the following section.

6.3 Scaling Rates of ^{234}Th-Cex from Daily to Seasonal

One problem with balancing carbon or nitrogen budgets in the CROZEX region, or any other region, is that there are multiple phases that these elements pass through during their cycles as demonstrated in Chapters 3, 4 and 5. Starting with the inorganic phases, the material is fixed into organic material, this can then pass into particulate and dissolved phases before finally being exported and remineralised back into dissolved inorganic phases. In addition to these basic pathways, organic material will also possibly pass through several trophic levels within the food web further complicating the pathways that organic material can follow. With each of these pools containing uncertainties and errors associated with spatial and temporal sampling and with sample analysis, it is no wonder that budgeting is a difficult task.

Consequently, this therefore naturally leads on to the assessment of the simpler silicon cycle (Figure 6.8). Silicon has a much less tortuous pathway through its biogeochemical cycle thus instantly making it an easier budget to understand and close. Silicon is a highly important element for several plankton functional groups including diatoms (Tréguer *et al.*, 1995), silicoflagellates and radiolarians, with diatoms recorded as the dominant opaline functional group in the Southern Ocean (El-Sayed *et al.*, 1983). Diatoms use dissolved silicate to form opaline frustules (Lewin, 1962), which gives the diatom a structural siliceous exoskeleton, therefore making silicate an essential nutrient for their growth (Brzezinski, 1992; Brzezinski *et al.*, 1990; Lewin, 1962). Diatoms either then export directly out of the euphotic layer or are grazed by copepods. However, the silicon contained in grazed diatoms remains as opal because it is inert in the guts of copepods (Dagg *et al.*, 2003; Tande, 1985) and is not assimilated into higher trophic levels or moved into dissolved phases, as happens with carbon and nitrogen (Brzezinski and Nelson, 1989; Dugdale *et al.*, 1995). Once diatoms have been grazed

the ingested biogenic silica is efficiently packaged as an excretory faecal pellet that will then readily sink at rates of 100s m d^{-1} (Small *et al.*, 1979) thus allowing efficient export to mesopelagic depths (Dagg *et al.*, 2003). Opal only returns silicon to the dissolved inorganic phase, silicate, through the process of remineralisation (Broecker and Peng, 1982). This is much simpler than the carbon and nitrogen cycles that have multiple remineralisation pathways. The Southern Ocean is also a major sedimentary sink of silicon, accounting for up to 75% global deposits (Calvert, 1983; DeMaster, 1981; Ledford-Hoffman *et al.*, 1986; Treguer and Jacques, 1986). The silicate pump, driven through the export of diatoms, is therefore a critical component of the silicon cycle (Dugdale *et al.*, 1995).

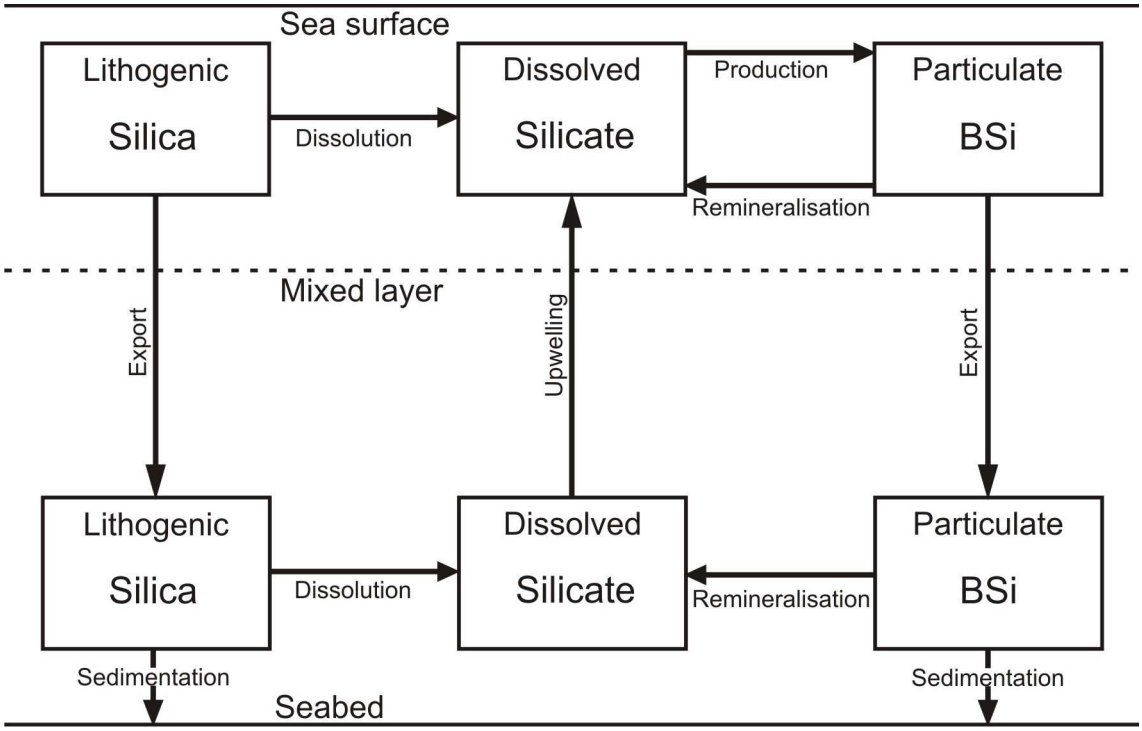

Figure 6.8 Schematic of the marine silicon cycle showing the major pools and fluxes between them.

Silicon related samples collected as part of the CROZEX data-set include profiles of dissolved silicate (dSi) and particulate biogenic silica (bSi). bSi was also measured in the large particles collected by the SAPS to measure the downward bSi flux using the ^{234}Th method described in Chapter 3. This information covers all the major pools of silicon and will allow a more complete assessment of the silicon cycle than was possible for the carbon and nitrogen cycles. In doing this, a re-evaluation of carbon

export from the mixed layer can be made based on the silicon cycle. Therefore this chapter will assess the silicon budget, firstly by calculating the various inventories of silicon: dSi and bSi and then calculate the ^{234}Th-derived bSi export (^{234}Th-bSiex). This will then allow a budget calculation of the amount of time that would be required to remove all the bSi from the system through export, which can then be used to scale up daily rates of ^{234}Th-Cex to a seasonal estimate.

To perform the recalibration it must be assumed that the lithogenic component will play little role in the overall silicon cycle. The particulate lithogenic pool in the surface ocean is sustained through riverine and aeolian inputs and is effectively minute fragments of lithogenic rock. Making the assumption that lithogenic silica is not making a significant contribution to the dissolved silicate pool is an important consideration. Had the study region been near to the outflow of a large river or close to a continental land mass then there would have been good reason to include the lithogenic component of the silicon cycle. However, the Crozet Islands are ≈2500 km from the nearest landmass, a considerable distance for terrestrially derived lithogenic material to travel. Therefore, considering the remoteness of the Crozet Islands from any major landmass these inputs are considered to be negligible. In addition to this only a small fraction of any lithogenic silica that may have found its way into the CROZEX region would have dissolved (Tréguer *et al.*, 1995). The alkaline digestion method used to measure bSi can also solubilise lithogenic silica, which can result in an overestimate of bSi (Ragueneau and Treguer, 1994). However, after testing of the method by Salter (2007) using calibration samples from the Conley (1998) bSi interlaboratory comparison study, it was decided that interferences from lithogenic silica are small enough so as not to introduce a significant bias. Therefore the lithogenic component was considered small enough to remove from the silicon cycle for the case of the recalibration. Should future investigations wish to test for interferences from lithogenic silica the method of Ragueneau *et al.* (2005), which uses Si:Al ratios to trace lithogenic material, can be used.

6.3.1 Model Description

This recalibration model works on the principle of calculating what the theoretical export of bSi should have been based on the draw-down of dSi (ΔdSi) to the date of sampling, corrected for any seasonal increases of bSi that have not yet been exported from the mixed layer. Therefore the length of the season for the recalibration

is defined as up to the date of sampling, akin to the new production estimates of ΔNO_3^- NP and DIC deficit as discussed in Section 6.2.2. Additionally, an upwelling component will be included to correct for additional dSi that has entered the mixed layer during the bloom season. This simple box model can be shown by extracting the relevant section of the silicon cycle from Figure 6.8 and is marked by the dotted box in Figure 6.9. The sedimentation and remineralisation fluxes of the deep bSi pool are unlikely to have any major impact on the surface water silicon cycle because deep bSi concentrations are relatively low, which will result in low fluxes from this pool. The only flux that has not been addressed is the upwelling of deep dSi into the mixed layer and will therefore be factored into the model.

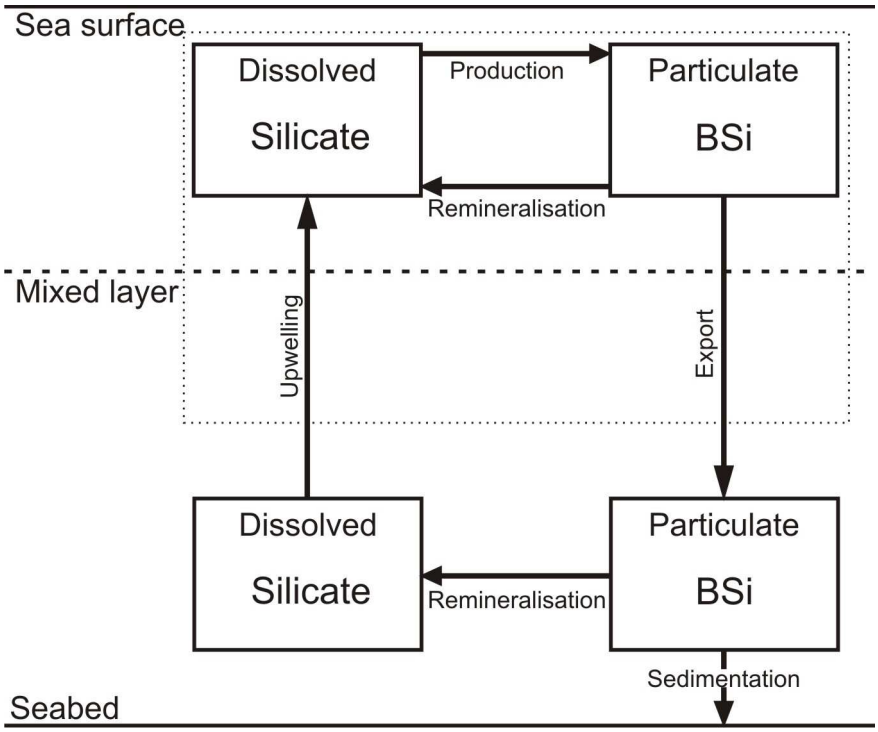

Figure 6.9 The part of the marine silicon cycle to be used to temporally integrate daily rates of ^{234}Th-Cex is contained within the dotted box.

The description of the model will, as far as possible, follow a logical order. The first two sections describe how the seasonal draw-down of dSi and seasonal accumulation bSi are calculated. This will be followed with the estimation of dSi upwelling based on vertical diffusion of dSi along concentration gradients of dSi. Then finally the calculation of theoretical bSi export will be explained and how this can be used to scale the daily rates of ^{234}Th-Cex to seasonal estimates of carbon export.

Seasonal draw-down of dissolved silicate

In calculating the seasonal ΔdSi an assumption had to be made on the winter concentration of silicate (dSi_w) found in the top 100 m of the water column. This was done in the same manner as that for NO_3^- in Section 4.4.4 and is the same technique presented in Sanders *et al.* (2007). In brief, it was assumed that the dSi_w concentration from 0-100 m was the same as the summer 100 m concentration (dSi_{100}). By extrapolating the 100 m concentration to the surface a pre-bloom 100 m inventory was inferred using Eq. 6.1 where z is the depth of integration.

$$dSi_w = \int_0^z dz \times dSi_{100} \qquad \text{Eq. 6.1}$$

The 100 m inventory of dSi when each station was sampled (dSi_s) was calculated using a trapezoidal integration (Section 2.7). The form of the integration is shown in Eq. 6.2.

$$dSi_s = \int_0^z dz \times \overline{dSi} \qquad \text{Eq. 6.2}$$

Where *dz* is the layer thickness and $\overline{dSi}$ is the averaged dSi concentration over each integral layer, expresses by Eq. 6.3.

$$\overline{dSi} = \frac{\left(dSi_1 + dSi_2\right)}{2} \qquad \text{Eq. 6.3}$$

The seasonal ΔdSi was then calculated with Eq. 6.4 by subtracting the inventory measured when the station was sampled, calculated by Eq. 6.2, from the inferred winter inventory, calculated by Eq. 6.1.

$$\Delta dSi = dSi_w - dSi_s \qquad \text{Eq. 6.4}$$

Seasonal accumulation of biogenic silica

Part of the model aims to assess the seasonal accumulation of bSi (ΔbSi) in the mixed layer, because any bSi present in the mixed layer had not yet been exported to mesopelagic depths. Therefore, inventories of bSi when a station was sampled (bSi_s) had to be corrected with an estimate of the winter standing stock of bSi (bSi_w). The estimate of bSi_w assumed that the 100 m inventories measured in the southern region on leg 1 were equivalent to the pre-bloom conditions across the whole study area. This was done because there had not been a significant bloom in the southern region when leg 1 sampled this area. bSi inventories were calculated with a trapezoidal integration (Section 2.7) using the same approach as Eqs. 6.2 and 6.3 and is summarised by Eq. 6.5 where $\overline{bSi}$ is the average bSi concentration over each integral layer akin to Eq. 6.3.

$$bSi = \int_0^z dz \times \overline{bSi} \qquad \text{Eq. 6.5}$$

ΔbSi was then calculated by Eq. 6.6 where bSi_w was equal to the average of bSi inventories of the four southern stations on leg 1 (131 mmol Si m^{-2}). For profiles of bSi split by region and into legs 1 and 2 see Appendix 2.

$$\Delta bSi = bSi_w - bSi_s \qquad \text{Eq. 6.6}$$

Upwelling of dSi

To assess the upwelling component (dSi_{up}) of the silicon cycle a similar approach was taken as that for assessing the upwelling of ^{234}Th in Section 3.2.1 (Morris *et al.*, 2007). Briefly, to summarise how this was done, the concentration gradient of dSi ($\partial dSi/\partial z$) across the 100 m depth horizon was calculated based on the dSi concentrations of samples taken adjacent to the 100 m depth horizon. A vertical turbulent diffusion coefficient (K_z) was then multiplied by the concentration gradient to calculate a daily rate of dSi upwelling (Eq. 6.7). A K_z of 0.38 cm^2 s^{-1}, measured using LADCP data was taken from Charette *et al.* (2007). The daily rate of dSi upwelling was then multiplied by the bloom length unique to each station, which is the length of time that the bloom had persisted at each station until the time that that station was sampled.

$$dSi_{up} = K_z \times \left(\frac{\partial dSi}{\partial z} \right) \quad \text{Eq. 6.7}$$

When this calculation was carried out it revealed that the amount of dSi upwelled was on average 8% of the seasonal draw-down and confirmed that upwelling is a small but significant contributor to mixed layer dSi inventories.

Theoretical bSi available for export and calculation of seasonal carbon export

By combining the results of Eqs. 6.4, 6.6 and 6.7 the theoretical total bSi available for export ($bSiex_t$) can be calculated by the sum of ΔdSi and dSi_{up} minus the storage of ΔbSi. This is represented by Eq. 6.8.

$$bSiex_t = \Delta dSi + dSi_{up} - \Delta bSi \quad \text{Eq. 6.8}$$

After calculating the theoretical $bSiex_t$ the mean was taken for each region. From these it was then possible to calculate how long the regional average daily rates of ^{234}Th-bSiex would have needed to persist in order to account for the theoretical $bSiex_t$. This is shown by Eq. 6.9 where *t* is the number of days required for the daily rates ^{234}Th-bSiex to remove $bSiex_t$ from the top 100 m of the water column.

$$t = \frac{bSiex_t}{^{234}Th\text{–}bSiex} \quad \text{Eq. 6.9}$$

Once values of *t* had been calculated for each region, north, centre and south, these were applied to the average ^{234}Th-Cex in each region to calculate seasonally integrated carbon export (Cex_t) (Eq. 6.10). Additionally, the regional values for *t* were also applied to the individual daily estimates of ^{234}Th-Cex (Eq. 6.10).

$$Cex_t = {}^{234}Th\text{–}Cex \times t \quad \text{Eq. 6.10}$$

6.3.2 Data Input and Model Results

The 100 m inventories of dSi_w, dSi_s, bSi_s, parameters used in the description of the model to re-calibrate ^{234}Th-Cex using the silicon cycle are presented in Table 6.3. Additionally, the daily dSi_{up} and bloom length are included. The $bSiex_t$ available for export at each station, output of results from Eq. 6.8, are in the last column of Table 6.3.

Table 6.3 100 m integrated inventories of dSi_w, dSi_s, bSi_s, dSi_{up}, bloom length and the theoretical $bSiex_t$ available for export during the season (sn). All errors are 1σ.

Station	dSi_w	dSi_s	bSi_s[a]	dSi_{up}[b]	Bloom	$bSiex_t$
	(mmol m^{-2})			(mmol m^{-2} d^{-1})	length (d)	(mmol m^{-2} sn^{-1})
North						
M1	1494±50	307±13	278±22	1.00	71	1111
M8E	1304±35	589±13	120±9	0.45	90	767
M8W	826±18	206±5	194±15	0.71	92	623
M9.1	1244±33	456±12	115±9	0.30	93	832
M9.2	663±18	194±5	59±5	0.58	109	604
M10.1	1142±30	462±11	239±20	0.62	110	641
					Mean	**763**
Centre						
M3.1	734±20	699±15	374±15	0.13	43	-202[c]
M3.3	1162±31	927±20	307±26	0.29	55	75
M3.4	1015±27	364±9	334±27	0.54	82	492
M3.5	1117±30	492±11	104±9	0.47	91	695
M3.6	1705±45	810±20	232±19	0.39	100	833
M3.7	1766±50	790±25	196±16	0.37	101	949
M3.8	2046±55	829±22	218±18	0.40	103	1171
					Mean	**702**
South						
M3.2[d]	1936±55	1540±41	219±18	0.23	17	312
M2.1	1832±49	1674±36	97±10	0.39	19	199
M6.1	1979±53	1836±41	140±12	0.15	21	137
M6.2	1136±30	319±8	311±25	0.81	63	688
M2.2	1183±32	378±10	292±24	0.69	66	690
					Mean	**405**

[a]bSi has to be corrected by the winter stock (131 mmol Si m^{-2}). See Section 6.3.2 for details.
[b]Upwelling has to be factored by the bloom length.
[c]M3.1 was excluded from this point onwards because it generated a negative number.
[d]Station M3.2 has been grouped with the southern stations based on the discussion in Section 3.2.2.

The regional means of $bSiex_t$, bold numbers in Table 6.3, now have to be combined with the ^{234}Th-bSiex to allow the calculation of the day multiplier (*t*) for each region using Eq. 6.9. ^{234}Th-bSiex was calculated using the ^{234}Th technique with the same approach as described in Chapters 2 and 3, but used a bSi:Th ratio instead to calculate bSi export. bSi was also measured as a quantitative split in the SAPS samples thus allowing the calculation of a bSi:Th ratio (Table 6.4). Using the ^{234}Th fluxes from

Table 3.3 the ^{234}Th-bSi export was calculated using Eq. 3.6. For clarity the 100 m ^{234}Th flux data from Table 3.3 have been repeated here in Table 6.4 to illustrate the calculation of ^{234}Th-bSiex.

Table 6.4 100 m ^{234}Th fluxes, bSi:Th ratios in the >53 μm SAPS samples and calculated ^{234}Th-bSiex. ^{234}Th-Cex rates have been carried forward from Table 3.5

Station	^{234}Th flux at 100 m (dpm m^{-2} d^{-1})	bSi:Th ratio (μmol dpm^{-1})	^{234}Th-bSiex (mmol m^{-2} d^{-1})	^{234}Th-Cex (mmol m^{-2} d^{-1})
North				
M1	2247 ± 342	2.8 ± 0.3	6.3 ± 1.2	18.8 ± 3.5
M8E	1621 ± 347	4.9 ± 0.6	7.9 ± 1.9	15.3 ± 3.8
M8W	2216 ± 324	6.1 ± 0.7	13.5 ± 2.5	13.6 ± 2.5
M9.1	2107 ± 327	4.2 ± 0.5	8.8 ± 1.7	16.7 ± 3.2
M9.2	2187 ± 330	6.5 ± 0.7	14.3 ± 2.7	23.2 ± 4.3
M10	1603 ± 351	1.0 ± 0.1	1.7 ± 0.4	11.3 ± 2.8
		Mean	**8.8**	**16.5**
Centre				
M3.3	1641 ± 338	9.0 ± 1.0	14.8 ± 3.5	11.6 ± 2.7
M3.4	1957 ± 319	7.1 ± 0.7	13.9 ± 2.7	20.0 ± 3.9
M3.5	1606 ± 346	9.7 ± 1.1	15.5 ± 3.8	15.6 ± 3.8
M3.6	1340 ± 325	9.5 ± 1.0	12.7 ± 3.4	13.8 ± 3.7
M3.7	1448 ± 335	6.8 ± 0.8	9.8 ± 2.5	10.1 ± 2.6
M3.8	1665 ± 340	5.5 ± 0.6	9.2 ± 2.1	12.2 ± 2.8
		Mean	**12.6**	**13.8**
South				
M3.2[a]	821 ± 376	7.8 ± 0.9	6.4 ± 3.0	4.9 ± 2.3
M2.1	677 ± 361	6.1 ± 0.7	4.1 ± 2.2	4.9 ± 2.7
M6.1	576 ± 383	7.0 ± 0.8	4.0 ± 2.7	5.8 ± 3.9
M6.2	1798 ± 326	17.4 ± 1.9	31.4 ± 6.6	14.4 ± 3.0
M2.2	2170 ± 310	12.2 ± 1.3	26.4 ± 4.7	18.8 ± 3.4
		Mean	**14.5**	**9.8**

[a]Station M3.2 has been grouped with the southern stations based on the discussion in Section 3.2.2.

The ^{234}Th-bSiex does not follow the same trend as ^{234}Th-Cex and ^{234}Th-Nex. During leg 1 the ^{234}Th-bSiex across the whole study region ranges from 4.0-14.8 mmol Si m^{-2} d^{-1}. During leg 2, unlike ^{234}Th-Cex, ^{234}Th-bSiex does show some spatial trend. In the northern region export is in the range of 1.7-15.5 mmol Si m^{-2} d^{-1} compared with consistently higher vales in the south with export of about ≈30 mmol Si m^{-2} d^{-1}. The most notable feature in ^{234}Th-bSiex is the upward shift in export between legs 1 and 2 in the southern region. Here there is a clear increase in export between occupations of these sites (Figure 6.10).

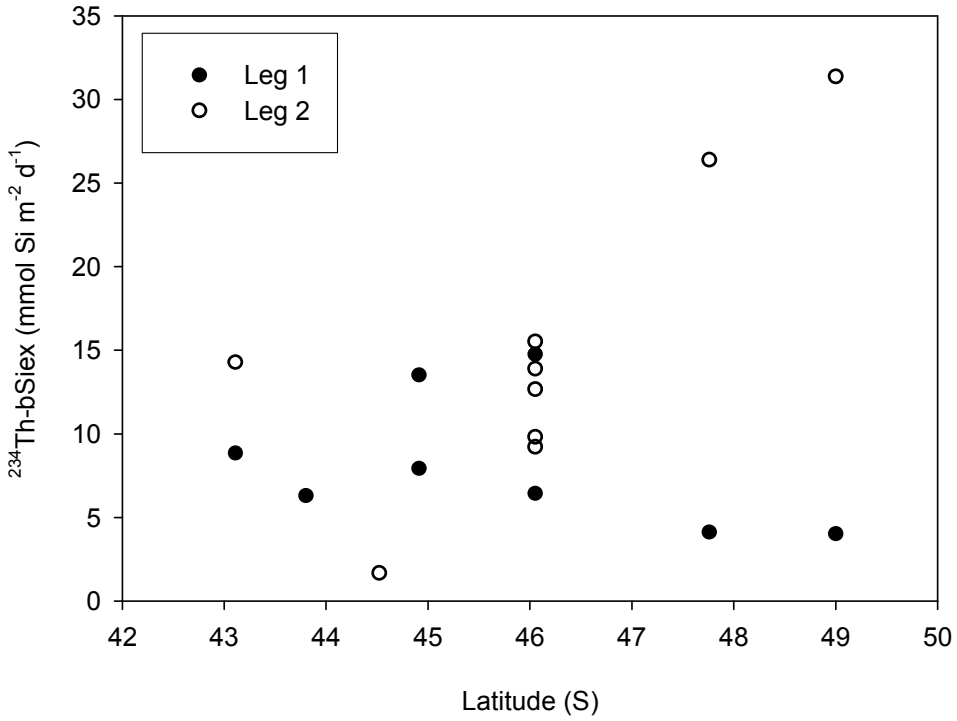

Figure 6.10 The latitudinal variation of 100 m ^{234}Th-bSiex for legs 1 and 2.

The daily export of ^{234}Th-bSiex can now be combined with the theoretical $bSiex_t$ predicted using the silicon budget from Table 6.3, to derive *t* (Eq. 6.9), which can be applied to the region averaged daily rates of ^{234}Th-Cex. This results in a new estimate of Cex_t, final column in Table 6.5.

Table 6.5 Regional ^{234}Th-bSiex and model predicted $bSiex_t$, used to calculate a scaling factor to re-calibrate the ^{234}Th-Cex to give Cex_t. sn^{-1} means per season.

Region	^{234}Th-bSiex (mmol m^{-2} d^{-1})	$bSiex_t$ (mmol m^{-2} sn^{-1})	Day multiplier	^{234}Th-Cex (mmol m^{-2} d^{-1})	Cex_t (mmol m^{-2} sn^{-1})
North	8.8	763	87	16.5	1436
Centre	12.6	702	56	13.8	768
South	14.5	405	28	9.8	273

When the new estimates of seasonal Cex_t are plotted again onto Figure 6.6 to compare them with the other estimates of primary, new and export production (Figure 6.11), it is clear that seasonal Cex_t (orange line) predominantly lies between ^{234}Th-Cex_a (red line) and ^{234}Th-Cex_b (blue line). However, Cex_t now shows a smooth decrease from north to south, mirroring the trend of PP and ΔNO_3^- NP (green line), but is at all stages persistently lower than ΔNO_3^- NP.

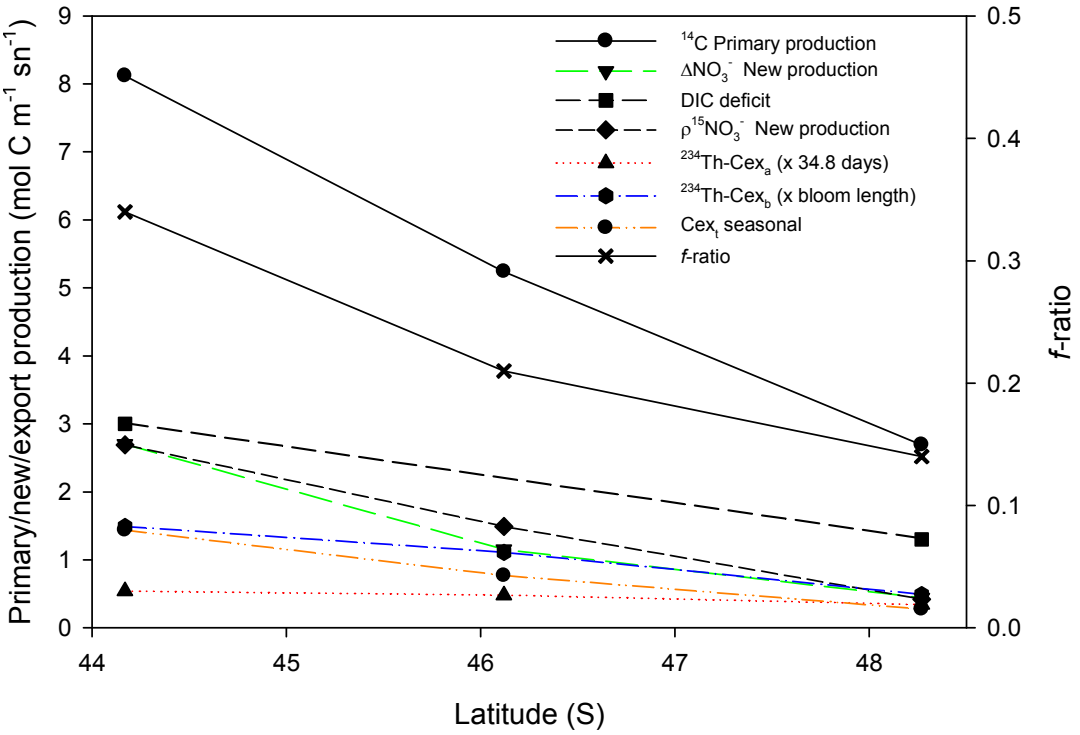

Figure 6.11 Update of Figure 6.6 with the Re-calibrated Cex plotted.

If the day multipliers of 87, 56 and 28 days for the north, centre and south regions are applied to each station individually in the respective regions then the re-calibrated estimates of carbon export are shown in Figure 6.12. This results in a clear north-south trend in carbon export with an approximately 4.8 times more carbon export in the northern region when compared to the southern region. This difference in north-south carbon export is much more in line with north-south gradients in integrated primary and new production estimates which show about 4-5 times more productivity in the north relative to the south (Figure 3.6). This is an encouraging result because it now helps to explain the lack of a north-south gradient in leg 2 ^{234}Th-Cex reported in Chapter 3 and Morris *et al.* (2007).

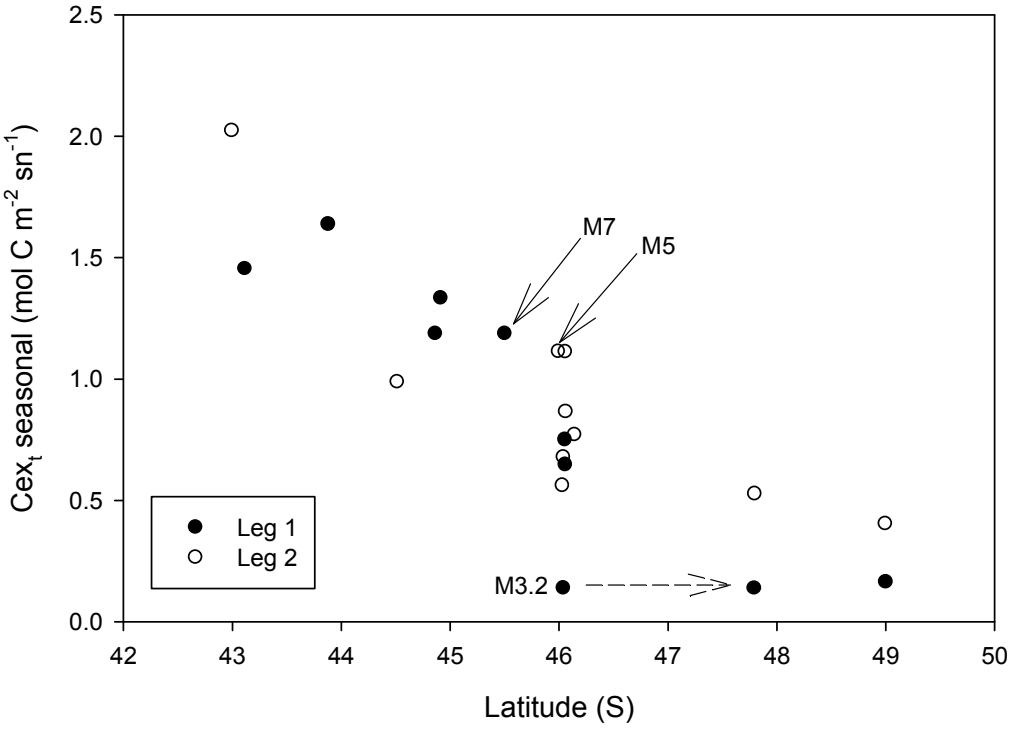

Figure 6.12 Re-calibration of carbon export when applying region averaged day multipliers. M3.2 which was under the influence of southern waters has been highlighted. M5 and M7 were re-scaled using the northern day multiplier.

6.4 Discussion

6.4.1 Carbon to Iron Ratios

This thorough investigation of the data now provides strong evidence for the existence of greater seasonal export in the northern bloom region, compared to the non-bloom control sites to the south. This naturally leads onto a discussion of the influence that iron has on the export of carbon. There are two issues of interest here:

(1) Does iron increase total seasonal carbon export?

(2) Does iron increase the efficiency of carbon export?

The first question has already been answered in as much as that there is a greater seasonal export of carbon in the northern bloom region when compared to the southern non-bloom region, when coupled with the evidence that there are higher concentrations of iron in the bloom region at the start of the bloom season (Planquette, 2008; Planquette *et al.*, 2007). However Planquette *et al.* (2007) and Planquette (2008) did

not directly compare seasonal estimates of carbon export with the pre-bloom stocks of dissolved iron on a station for station basis; primarily because the seasonal estimates of ^{234}Th-Cex were not available at the time. Despite this, Charette *et al.* (2007), Planquette *et al.* (2007) and Planquette (2008) did calculate the end of winter pre-bloom standing stocks of dissolved iron in the northern and southern regions to be 0.55 nmol l^{-1} and 0.16 nmol l^{-1} respectively. Planquette *et al.* (2007) and Planquette (2008) therefore argue that the pre-bloom stock of dFe in the northern region is enough to fertilise the bloom observed here based on the physiological iron requirements of phytoplankton to sustain the measured levels of NP calculated by Lucas *et al.* (2007). Given this evidence no further investigation into this will be made.

This now leads onto the second question of the efficiency of carbon export in relation to iron fertilisation. The efficiency of iron to sequester carbon is usually measured on a mole to mole basis, ie the number of moles of carbon sequestered for each mole of iron added, and is referred to as the carbon-to-iron ratio (C:Fe). C:Fe ratios were presented by Buesseler and Boyd (2003) to express the amount of carbon sequestered for each mole of iron added for the first wave of iron fertilisation experiments. This allows a convenient method of cross comparison between all iron fertilisation experiments. A word of caution here: ratios between iron and carbon have been presented in the literature as both C:Fe ratios (de Baar *et al.*, 2005) and Fe:C ratios (Boyd *et al.*, 2007), the former usually a very large number in the order of thousands to hundreds of thousands and the latter usually being a very small number as the reciprocal of the former. Nonetheless, once these ratios are in the same format they can be directly compared. Here, the C:Fe ratio will be used because it is an easier form of the ratio to understand and the ratio generated simply means the number of moles of carbon sequested per mole of iron added to the system.

Typically, C:Fe ratios are determined by calculating the excess of carbon and iron in the high productivity, high export region over the low productivity, low export region. In the case of CROZEX the seasonal excess of carbon export below 100 m is 1163 mmol C m^{-2} sn^{-1} (Table 6.5, 1436 – 273 = 1163). The determination of excess iron is calculated by taking into account a steady-state input of iron from the surrounding plateau. Atmospheric and upwelling inputs are considered to be the same in both the bloom and non-bloom regions that therefore only leaves the horizontal export from the plateau as the term generating the excess of iron in the bloom region (Charette *et al.*, 2007; Planquette, 2008; Planquette *et al.*, 2007). The horizontal flux of

iron from the plateau was estimated to be 390 nmol m^{-2} d^{-1}, over 100 days of winter mixing and a mixed layer of 100 m this equates to 0.039 mmol m^{-2}. This results in a C:Fe ratio of about 29800. However this is likely to be an upper estimate because the input of iron does not consider the continuation of iron input during the time of the bloom itself. If the input of iron is considered to continue at the same rate from the start of the bloom around the start of September, until the peak of the bloom at the end of October, an additional 58 days, then an additional 0.023 mmol m^{-2} will be added to the iron replete bloom area thus totalling the iron excess to 0.062 mmol m^{-2}. Therefore a lower estimate for the C:Fe ratio of about 18900 is thus calculated.

This C:Fe ratio range of 18900-29800 is substantially lower than C:Fe ratios estimated for the KEOPS project that estimated the seasonal sequestration efficiency of 668000, clearly much higher than that estimated for CROZEX (Blain *et al.*, 2007). When comparing the sequestration efficiency with other artificial iron fertilisation experiments in the Southern Ocean the average C:Fe ratio is about 4300 (range 1066-35680 (de Baar *et al.*, 2005)), the CROZEX C:Fe ratio is higher than the average, but within the ranges measured. Given that both the natural Fe experiments (CROZEX and KEOPS) give generally higher C:Fe ratios, there is evidence to suggest that natural systems are more efficient at exporting carbon than artificially fertilised systems.

6.4.2 The Difference Between New Production and Export

At the end of Chapter 3 it was shown that during leg 1 there was a clear north-south gradient in daily rates of carbon export, whereas during leg 2 this north-south gradient was not evident (Figure 3.6). This trend was different to the trends observed in temporally integrated primary and new production (Morris *et al.*, 2007 and Chapter 3). This suggested a potential disagreement between export when compared with temporally integrated primary and new production. Various ideas were explored during Chapters 4 and 5 to assess the dissolved and particulate fields in relation to the flow of organic material as the bloom progressed in the various regions. The analysis of the dissolved and particulate fields highlighted some strong relationships between DON and PON with chl-*a* and, more importantly with ΔNO_3^- NP, thus suggesting some important pathways that organic matter will follow once it has been fixed through PP.

Section 6.2 and 6.3 reconciled all the daily and seasonal rates of primary, new and export production and has attempted to determine the seasonal carbon export based

on evidence from a silicon budget. In doing so, two major findings have emerged. Firstly, the temporally and spatially averaged Cex_t now shows a consistent gradient of high export in the north, to low export in the south (Figure 6.11). Secondly, the lack of a north-south gradient on leg 2 now shows a similar pattern as leg 1 (Figure 6.12) and therefore now displays the same trend as temporally integrated primary and new production. This is an encouraging result of the silicon cycle recalibration, but it does however highlight the difference between new production and export production, with export production giving persistently lower values than new production across the whole study area. Consequently, this must therefore be explored in relation to the dissolved and particulate fields introduced in Chapters 4 and 5 in an attempt to reconcile the difference between new and export production. The left side of Table 6.6 gives a summary of primary, new and export production. The right side of Table 6.6 gives the fraction of PP exported (*e*-ratio) and the fraction of NP exported, which will be referred to as the *en*-ratio from hereon (Eq. 6.11). The *e*-ratio (Eq. 6.12) was derived by Murray *et al.* (1989) on the assumption that it is equal to the *f*-ratio (Eppley and Peterson, 1979). The *f*-ratio has been included for comparison purposes.

$$en\text{-}ratio = \left(\frac{POC\ export}{new\ production} \right) \times 100 \qquad \text{Eq. 6.11}$$

$$e = \frac{POC\ export}{primary\ production} = \frac{new\ production}{total\ production} = f \qquad \text{Eq. 6.12}$$

The *e*-ratio in the north is 18%, compared with 10% in the south. In comparison the *f*-ratio is 33% in the north and 16% in the south. The *e*- and *f*-ratios are conceivably the same in the south, but in the north the *e*-ratio is significantly smaller than the *f*-ratio, therefore in the north the assumption of Murray *et al.* (1989) does not hold true. The reasons for this are evident in the accumulation of DOM and suspended POM (sPOM) reported in Chapters 4 and 5. The assumption of the *e*-ratio requires that all NP is exported as POM, however over short time-scales this need not be true and accumulation of DOM and sPOM will prevent the *e*-ratio equalling the *f*-ratio. Over large enough temporal and spatial scales the removal of organic material from the mixed layer must be equal to the injection of inorganic material, otherwise there would

be a net accumulation or decline of organic material in the surface ocean. Consequently the removal term of the *e*-ratio (POC export) needs to include the removal of DOM and sPOM if it is to equal the *f*-ratio. This is indeed what occurs through the dispersion of DOM and sPOM through processes such as advection, diffusion, slow sinking and winter overturning. These processes act to balance the differences between the *e*-ratio and the *f*-ratio. In the CROZEX system it is therefore reasonable to arrive at different values of *e* and *f* given a scenario of organic matter build-up. The greater difference between *e* and *f* in the north is therefore supported by the idea that more sPOM is also stored in the north, as concluded in Chapter 5.

Table 6.6 Summary of Int. PP, ΔNO_3^- NP, and Cex_t. The seasonal percentage of primary and new production exported as measured by Cex_t.

Parameter	Overall (mol C m^{-2})			Fraction exported (%)			
	North	Centre	South	North	Centre	South	
Int. PP	8.12	5.24	2.69	**18**	15	**10**	*e*-ratio
ΔNO_3^- NP	2.70	1.15	0.43	**54**	67	**64**	*en*-ratio
Cex_t	1.44	0.77	0.27	-	-	-	
				33	22	**16**	*f*-ratio

Given the shorter than annual time-scales over which many studies investigate phytoplankton blooms, caution should be exercised when using the *e*-ratio to estimate the efficiency of POM export when used in the context of the *f*-ratio. Instead, the use of the *en*-ratio will provide a measure of export efficiency in relation to NP, because the *en*-ratio also takes into account the accumulation of organic material that is not readily exportable over shorter time-scales. With this information, and the results from Chapters 4 and 5, a carbon budget of the CROZEX area will now be presented.

6.4.3 CROZEX Carbon Budget

In Chapter 4 a robust relationship was found between 100 m integrated ΔNO_3^- NP and DON (Figure 4.13). This figure has now been carried forward as Figure 6.13a so that it may be explored in more detail in relation to where data points from different regions fall within the overall regression. The stations in the north and south have been circled and labelled accordingly. The regressions on the separate north and south clusters in Figure 6.13b are DON = 0.56 × ΔNO_3^- + 162 (r^2 = 0.68, p = >0.1) and

DON = 1.04 × ΔNO_3^- + 220 (r^2 = 0.14, p = >0.1) respectively. Neither of these regressions are statistically significant when compared to the overall regression of all the data points in Figure 6.13a. This suggests that the overall regression should be used when explaining the relationship between DON and ΔNO_3^- NP. The overall regression has a gradient of 0.46 and means that DON accounts for 46% of ΔNO_3^- NP (Figure 6.13a). A summary of these regressions are tabulated in Table 6.7.

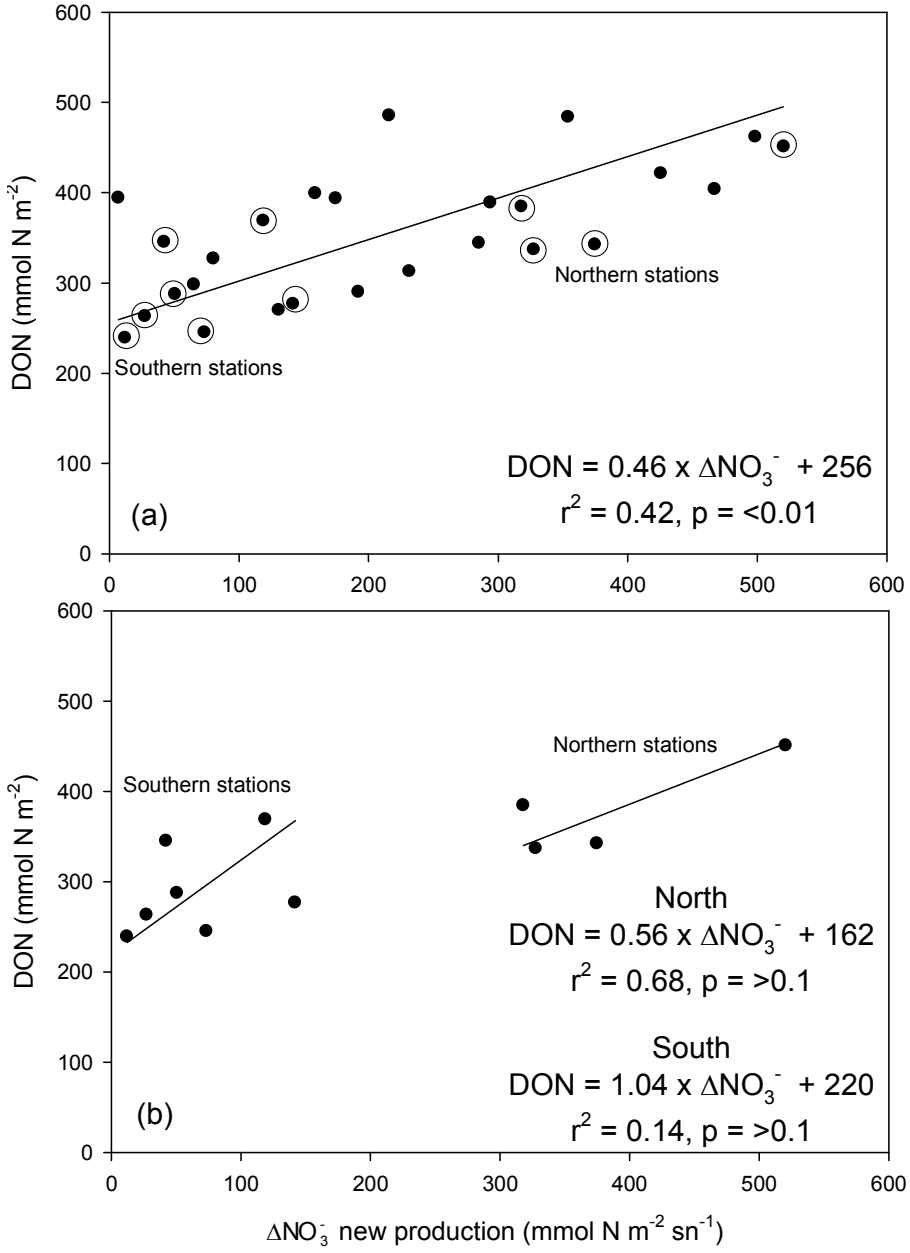

Figure 6.13 Overall Relationship between 100 m integrated ΔNO_3^- NP and DON (a), and separated by region (b). Solid lines are Model II regressions.

In a similar fashion to the relationship found between DON and ΔNO_3^- NP in Chapter 4; an analogous relationship was found between PON and ΔNO_3^- NP in Chapter 5 as Figure 5.11. This figure has been carried forward as Figure 6.14a. The linear regression in Figure 6.14 is shown against a non-linear quadratic fit to the data, which results in a higher r^2 value. This means that a non-linear function best describes the data with a shallower gradient at lower ΔNO_3^- NP and a steeper gradient at higher ΔNO_3^- NP. This suggests that there are possibly two different relationships between ΔNO_3^- NP and PON in the north and south. In Figure 6.14a the stations north and south have also been circled and labelled accordingly to explore the northern and southern clusters separately.

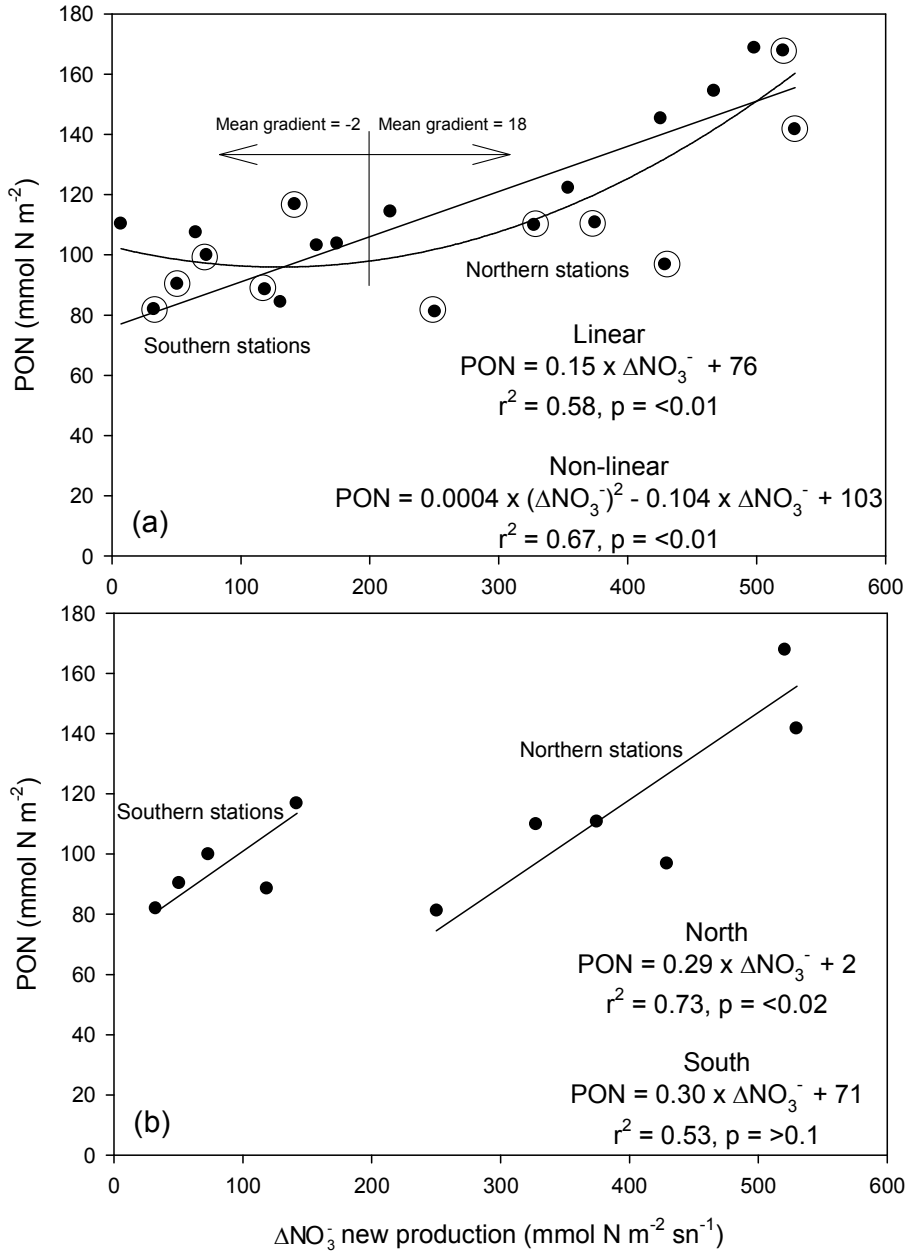

Figure 6.14 Overall relationships between 100 m integrated ΔNO_3^- with PON (a), and separated by region (b). Solid linear lines are Model II regressions and non-linear line is a quadratic regression.

When the north and south groups are separately tested by linear regression, the north has a statistically significantly relationship whereas the south does not (Figure 6.14b). However, neither of the linear regressions in Figure 6.14b are more significant than the linear or non-linear regressions in Figure 6.14a. As the non-linear regression has a higher r^2 value and follows the trend of all the data points, this will be used to describe the change of PON with increasing ΔNO_3^- NP. All the regressions in Figure 6.14 have been summarised in Table 6.7. By using a moving window of 5 units of

ΔNO_3^- NP, the average gradient of the non-linear curve was calculated for areas of high and low ΔNO_3^- NP, which represent the northern and southern stations respectively. This analysis gave average gradients of 0.18 and -0.02 and means that PON accounts for 18% and ≈0% of ΔNO_3^- NP in the north and south respectively Figure 6.14a.

Table 6.7 Summary of regression analysis from Figure 6.13 and Figure 6.14.

Plot	Gradient	Intercept	r^2	n	t-stat	p-value
DON						
Overall	**0.46 ± 0.07**	256 ± 19	0.42	26	4.21	<0.01
North	0.56 ± 0.16	162 ± 64	0.68	4	2.05	0.18
South	1.04 ± 0.36	220 ± 32	0.14	7	0.90	0.41
PON						
Overall	0.15 ± 0.02	76 ± 7	0.58	21	5.07	<0.01
Non-linear	**0.0004±0.0001x^2-0.104±0.07**	103 ± 7	0.67	21	3.09, -1.50	<0.01, 0.15
North	0.29 ± 0.06	2 ± 26	0.73	6	3.25	0.03
South	0.30 ± 0.09	71 ± 8	0.53	7	1.85	0.16

Now that the various pools of dissolved and particulate matter that flow from new production have been assessed in the north and south, it is now possible to incorporate these into a conceptual model of carbon flow in Figure 6.15 to generate a carbon budget. Figure 6.15 takes summarised Int. PP, ΔNO_3^- NP and Cex_t data from Table 6.6, which allows for the calculation of the *f*-ratio, e-ratio and *en*-ratio. The flux of organic material into the dissolved and suspended particulate pools can be calculated using the highlighted information taken from Table 6.7.

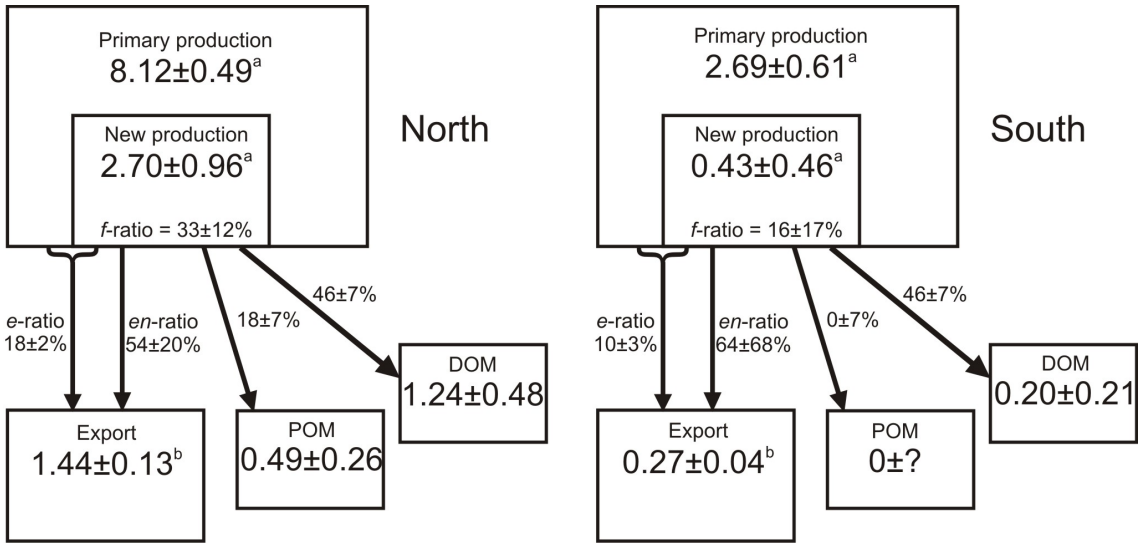

Figure 6.15 Schematic of the flow of organic carbon in the north and south regions. Quantities are in mols C m^{-2} sn^{-1} and the percentages are the relative fractions moving between the pools. [a]Errors are standard deviations of regional averages from Sanders *et al.* (2007). [b]Errors assume zero error in day multiplier.

Being able to make estimates of carbon pools and the fluxes between them is an important task as it allows an understanding of the efficiency with which various components operate. The most striking result from building this budget is the differences in the efficiency of the *en*-ratio. In the north 54% of NP can be directly accounted for through particle export, whereas in the south the *en*-ratio is estimated to be 63%, suggesting more efficient export of newly produced organic material in the south. Before the formation of the budget it would have been intuitive to hypothesise that the efficiency of export is higher in the north where the bloom is fertilised with iron. This is, in part, supported by a higher *e*-ratio in the north compared to the south (N>S). In contrast the *en*-ratio is lower in the north compared to the south (N<S). The reason for this is because the *en*-ratio includes the impact of the dissolved and suspended particulate pools that are not actively exporting, as discussed in Section 6.4.2. However, this leaves an interesting question of "why is sPOM storage different in the north and south?"

It was proposed by Francois *et al.* (2002) that areas of high *f*-ratio are more prone to lower transfer efficiencies of organic material to bathypelagic depths, whereas areas of low *f*-ratio are characteristic of higher transfer efficiencies. Typically high *f*-ratios are found in high latitude opal-dominated areas and low *f*-ratios are found in low latitude carbonate-dominated areas. Francois *et al.* (2002) suggested that areas with low *f*-ratios are subject to efficient recycling of organic material that ultimately results in

efficiently packaged material that is efficiently transferred to the deep-sea. Whereas, areas with high *f*-ratios generate loosely packaged aggregates that will not rapidly sink. Although the CROZEX area is at a high latitude, the *f*-ratio in the north was twice as high as the *f*-ratio in the south (Figure 6.15). Thus the mechanisms behind the findings of Francois *et al.* (2002) may be used to explain the differences in the *en*-ratio found in the CROZEX area. This suggests that the fraction of NP that is exported is probably being driven by differences in upper ocean communities, an idea that is highly feasible when considering works such as Francois *et al.* (2002) and Klaas and Archer (2002).

Testing the link between new and export production in relation to community structure would be a worthwhile task for future projects to consider in detail. However, during the CROZEX campaign an assessment of both the phytoplankton and mesozooplankton communities were made by Poulton *et al.* (2007) and Fielding *et al.* (2007) respectively. The main findings of Poulton *et al.* (2007) was the easy distinction of different phytoplankton groups both spatially and temporally. The northern region was dominated by the colonial prymnesiophyte *Phaeocystis antarctica*, and the southern region had a diverse community including large diatoms such as *Corethron pennatum* and *Dactyliosolen antarctica*. The southern stations on leg 2 also showed an abundance of the smaller diatom *Fragilariopsis kerguelensis*, whereas the small diatom *Thalassionema nitzschioides* was mainly found at the M3 central region. *Eucampia antarctica*, a large heavily silicified diatom, was only found in surface samples at M3, whereas Salter *et al.* (2007) reported widespread and large numbers of *E. antarctica* in samples collected in PELAGRA. This suggests that the start of the main northern bloom, a time which was not sampled, was dominated with large diatoms, which then gave way to a *P. antarctica* during the declining phase of the bloom.

The occurrence of mesozooplankton faecal pellets and calcite bearing coccolithophores was also observed in PELAGRA sediment trap samples, which highlights the diversity of actively exporting material (Salter *et al.*, 2007). Fielding *et al.* (2007) measured copepod grazing rates by estimating the chl-*a* content in the guts of copepods, and concluded that grazing pressure on the bloom is inversely related to ambient chl-*a* concentrations. This means that the grazing pressure in the southern region was much higher with up to 90% of daily PP grazed by copepods. As was discussed in Section 6.3 the impact of copepod grazing will be to generate efficiently exportable faecal pellets. This may explain the potentially lower fraction of sPOM formed in the southern region and thus suggest the reason why a higher *en*-ratio was

observed in the south (Figure 6.15). PP can be seen to produce two types of particulate material: an exportable fraction and a suspended fraction, and each plays a different role in the fate of organic material. The exportable fraction will rapidly exit the surface ocean and the suspended fraction will not. Therefore it is conceivable that organic material in the southern region is more efficiently grazed and packaged that will then be exported, thus reducing the magnitude of the sPOM pool.

It is clear that the mechanisms underpinning the export of organic material are complex and interrelated, and the link between the planktonic community and the ensuing POM export are closely coupled. This chapter does not contain all the information necessary to examine these links in detail but does highlight its importance and the direction that future investigations and research should follow. The importance of diatoms in Polar Frontal regions is well known, as discussed in Section 6.3. However it has also become clear that *P. antarctica* also plays an important but less well understood role in blooms such as CROZEX and may be responsible for significant export (DiTullio *et al.*, 2000; Smith *et al.*, 1991). Making the link between the mechanisms that drive the biological carbon pump and the resultant carbon export will be a key step to fully understanding the export of carbon to mesopelagic depths.

6.5 Conclusions

The aim of this chapter was to rationalise and integrate all the estimates of primary, new and export production and put them into context with the work from Chapters 3, 4 and 5. To begin this process the daily rates of ^{14}C PP and Σ^{15}N uptake were compared and proved to be good predictors of each other over a wide range of productivity. Both these measurements integrate over a 24 h period that will almost certainly contribute to the observed agreement. Next, a direct comparison was made between NP_C and ^{15}N NP with ^{234}Th-Cex and ^{234}Th-Nex respectively. If NP was equal to export these parameters should agree with a 1:1 relationship, however, this was found not to be the case. The majority of the NP estimates were higher than export estimates taken at the same station. Discussion suggested that this pattern was the result of organic matter storage within the surface waters and also highlighted the temporal differences between 24 h rate measurements and the longer integrating interval of ^{234}Th. A direct comparison of ThE_C and ThE_N revealed evidence of a higher export efficiency of carbon when compared to nitrogen and suggested that nitrogen was being

preferentially stored within surface waters. This was confirmed by comparing the *f*-ratio with ThE_C and showed that as the export efficiency of *ThE* increased the *f*-ratio decreased, thus implying a higher fraction of regenerated nitrogen was being used by phytoplankton.

The first attempt of scaling daily rates of ^{234}Th-Cex to seasonal estimates was calculated in two ways, by factoring by the mean life-time of the ^{234}Th (34.8 days), and by factoring by the length of the bloom up to the date of sampling. Neither of these methods generated consistent results when compared to ΔNO_3^- NP and inventories of DOM and POM and suggested the need for a more synergistic approach to scaling daily rates ^{234}Th-Cex to seasonal estimates. This lead to an approach that used a silicon budget to calculate the hypothetical duration of export in the different regions. This approach confirmed that seasonal estimates of carbon export were persistently lower than estimates of ΔNO_3^- NP with this difference greater in the north when compared to the south. By highlighting the difference between the *e*- and *f*-ratios over the time-scale of the CROZEX study, the observations of DOM and POM storage, noted in Chapters 4 and 5, then became relevant. The difference between the *e*- and *f*-ratios was greater in the north and was probably the result of greater POM storage in this region. It was then suggested that because the *e*- and *f*-ratios have the potential to operate over different time-scales that a new ratio should be used to expresses the export efficiency. The *en*-ratio, defined as the ratio between export and new production, takes into account the storage of organic material that is not readily exported.

A direct comparison of the *f*-ratio showed that it was about twice as big in the north compared to the south; a low *f*-ratio represents efficient recycling of nutrients. This means that the southern region was the site of efficient recycling whereas the north was not. Efficient recycling of nutrients results in efficiently packaged material that then has the capacity to be efficiently transferred to the deep-sea. This mirrors what was observed with the en-ratio which was also bigger in the south and represented a larger fraction of easily exportable POM.

By combining the seasonally integrated estimates of carbon export with estimates of iron input it was possible to calculate an iron sequestration efficiency. This is the ratio between carbon exported and iron input (C:Fe). In comparison to artificial iron fertilisation experiments the C:Fe ratio was favourably high suggesting that natural systems are more efficient at exporting carbon after iron fertilisation. However, in

comparison to KEOPS the CROZEX system had a sequestration efficiency that was an order of magnitude lower, thus suggesting the need for more research in this field of natural iron fertilisation.

7 Conclusions and Future Work

7.1 Introduction

This PhD was part of the multi-disciplinary CROZEX project that aimed to survey and assess the effect of an island archipelago in an HNLC region of the Southern Ocean on the biogeochemistry of the region. As part of the CROZEX project, the first objective of this thesis was to investigate the surface ocean particle flux from the CROZEX bloom with particular emphasis placed on the export of POC. This was achieved with the particle tracer ^{234}Th and was published as part of the CROZEX special issue in Deep-Sea Research II (Morris *et al.*, 2007) and provided the basis for Chapter 3. The results from the ^{234}Th study revealed different latitudinal trends when compared to seasonally integrated estimates of primary and new production. This raised questions about why this should be and lead to two testable ideas to explain the noted differences. The first of these was to test the idea of dissolved and particulate matter buildup in the productive north that would have the affect of reducing the relative amount of POC available for export. The second idea was that the duration of the export event in the north was longer than in the south thus resulting in greater total seasonal export. In summary, this thesis addressed five major questions:

(1) Were the daily rates of ^{234}Th-Cex greater in the high productivity bloom region when compared to a low productivity control region?

(2) How did the daily rates of ^{234}Th-Cex compare to integrated rates of primary and new production?

(3) What were the inventories and budgets of dissolved and particulate organic material in the surface of the water column and did these have an impact on the relative rates of POC export?

(4) Were the daily and integrated rate measurements of primary, new and export production comparable?

(5) Can the ^{234}Th-Cex estimates be re-evaluated to account for a longer export event in the high productivity region, when compared to the low productivity region?

7.2 Conclusions and Major findings

Chapter 3

The CROZEX cruises were split into two legs. The first leg arrived in the northern region about two weeks after the peak in chl-*a*, and arrived in the southern region about 10 days before the peak of a relatively small but significant bloom in this area. This resulted in about three times more ^{234}Th-Cex in the north. However, the second leg arrived in the northern region after the main bloom event had decayed away, and arrived in the southern region about four weeks after the peak of the small bloom. This resulted in broadly equal ^{234}Th-Cex across the whole study region that was comparable to ^{234}Th-Cex in the north on leg 1. Therefore, the latitudinal gradient of ^{234}Th-Cex observed on leg 1, was no longer apparent on leg 2. In contrast to this, estimates of seasonally integrated primary and new production calculated by Sanders *et al.* (2007) showed a strong north-south latitudinal gradient with about four times more primary and new production in the north. This suggested that rates of POC export relative to production were higher in the south and were probably because of enhanced organic matter storage in the north.

Chapter 4

As a first attempt to reconcile the lack of differences in ^{234}Th-Cex on leg 2 the inventories of DON were investigated. Preliminary manipulations of DON data suggested that temporal and spatial trends did exist with higher DON inventories in the north. This was confirmed by directly correlating inventories of DON and chl-*a*, which gave a good positive correlation. This was an encouraging result, but the key step was to examine the link between DON and the NO_3^- pool. This was first done by correlating DON and NO_3^- and showed a significant but weak relationship. Using a more sophisticated approach, DON inventories were correlated with estimates of ΔNO_3^- NP. This data analysis revealed a good linear relationship at the complete range of ΔNO_3^- NP values and showed that 46% of new production could be accounted for in the DON pool.

Chapter 5

Akin to the DON investigation, the inventories of POC/N were also investigated. Initial inspection of C:N ratios revealed homogeneity within the mixed layer and then

gently increasing ratios below the mixed layer with increasing depth; this was probably the result of preferential remineralisation of organic carbon during sinking. Temporal and spatial trends also existed for POC/N again reinforced by good correlations with integrated chl-*a*; similar to those found for DON. Using the same approach as for DON, PON was correlated with ΔNO_3^- NP to investigate the magnitude of nitrogen flow from the NO_3^- pool into the PON pool. This analysis revealed a non-linear relationship that was best described with a quadratic fit through the data. This provided strong evidence for differential rates of nitrogen flowing from the NO_3^- pool into the PON pool across the study region. Areas of higher ΔNO_3^- NP in the north were categorised with proportionally higher inventories of PON when compared to areas of lower ΔNO_3^- NP. This provided the first piece of evidence that the lack of a latitudinal gradient in ^{234}Th-Cex export on leg 2 might be the result of proportionally greater storage of NO_3^- as PON in the north when compared to the south.

Chapter 6

Coming to the conclusion that increases in dissolved and particulate organic matter might account for the difference in spatial patterns between new and export production required that seasonally integrated carbon export be calculated. To start this process all the estimates of primary, new and export production were collated and compared. This comparison showed that Σ^{15}N uptake rates and ^{14}C PP correlated well over a wide range of productivity. However, when ^{234}Th-Cex and ^{234}Th-Nex was compared to NP_C and ^{15}N NP no relationships were found. This is almost certainly because of time-scale differences between the different rate measurements and one that could only be addressed if the gap in time-scales could be closed.

The re-calibration of the daily rates of ^{234}Th-Cex was based on the simpler silicon cycle, for which a more complete and independent budget could be constructed. The result of the re-calibration generated about 4.8 times more carbon export in the north compared with the south. This new latitudinal gradient of seasonally integrated carbon export now mirrored seasonally integrated latitudinal estimates of primary and new production of Sanders *et al.* (2007). However, the seasonally integrated carbon export did not account for all the seasonally integrated new production. This result forces a conclusion that DOM and sPOM phases must be playing an important role in storing organic material that results from NP. Drawing this conclusion allowed the

inclusion of information about the DOM and sPOM phases to construct a carbon budget describing the northern and southern regions.

Through constructing the carbon budgets it became apparent that the *e*-ratio, which was higher in the north, did not agree with the *en*-ratio, which was higher in the south. Therefore one conclusion that can be made is that although the *e*-ratio is higher in the north, which implies that the efficiency of export is higher, a more appropriate estimate of export efficiency is represented by the *en*-ratio, which implies that the efficiency of export of NP is higher in the south. This is of importance because it is the actively exporting particles, which results from NP, that will remove carbon to a greater depth for sequestration. Therefore, it is the export efficiency of NP, not PP, that should be the focus of export studies concerned with particle flux.

7.3 Future Work

This study was the first of its kind to assess the carbon export from a naturally iron-fertilised bloom in an HNLC ocean region. Previous investigations of carbon export from artificial iron fertilisation experiments had yielded variable results that were probably the consequence of limited temporal sampling during the declining phase of the bloom. The CROZEX study aimed to tackle this by sampling a naturally iron-fertilised bloom during the declining phase. Much was learnt from this, as described in the previous section, but it also now poses new questions for future directions of work. In addition to this there are also technical aspects of the data-sets presented within the thesis that would benefit from detailed investigation.

The ^{234}Th technique

The ^{234}Th data-set contains a variety of opportunities for future investigation. On several occasions vertical profiles had subsurface peaks below the initial area of disequilibrium. Although these peaks were factored into the calculation of integrated ^{234}Th disequilibrium, they were not investigated in relation to any other parameters to assess why they were found at some stations and not others. For example, were they linked to remineralisation or were they just the result of settling particles accumulating on a density boundary. Unfortunately, none of the CROZEX data-sets contain any information on bacterial respiration rates; however if bacterial enumeration was carried out, this is one possible line of investigation. Information on water column density

structure does exist thus opening another line of investigation and would allow an initial assessment as the causing factor of these subsurface peaks.

The ^{234}Th technique relies heavily on the measurement of elemental ratios between ^{234}Th and the element of interest, for example: carbon, nitrogen, silicon, calcite or iron. During CROZEX this ratio was only measured at one depth on one size fraction. It is now the recommendation that this elemental ratio be measured at multiple depths on at least two size fractions: >53 μm and 1-53 μm (Buesseler *et al.*, 2006). Future work would benefit greatly from this and would result in greater certainty and understanding on how elemental ratios vary.

Sampling for total ^{234}Th on CROZEX used the 10 l technique and thus required about 12 l of seawater per sample when including seawater to rinse apparatus. This high demand for water dictated that ^{234}Th required a dedicated CTD cast to allow other parameters to sample enough water. This has several drawbacks. The ^{234}Th profile was always separated from the other state variables in both time and space. Additionally, the ^{234}Th 10 l technique is also very time consuming and is only sustainable on a two day cycle when only one person is making the measurement. The development of the small volume technique in 2001 opened the doorway to ^{234}Th measurements on 2-5 l of seawater per sample (Benitez-Nelson *et al.*, 2001; Buesseler *et al.*, 2001b). Coupled with the inclusion of a ^{229}Th yield monitor (Pike *et al.*, 2005) total ^{234}Th analysis is now a fully integratable parameter that can be measured side-by-side with other core parameters on the same CTD cast. This not only reduces the need for an additional CTD cast, but it also removes temporal and spatial separation between measurements for cross comparison purposes. The smaller volume of seawater needed reduces filtering time and opens the option of either higher sampling resolution or freeing up time to focus on collecting and processing samples to measure elemental ratios. Finally, the small volume technique removes the time consuming and fiddly need to fold filters, again freeing up valuable time at sea. Therefore, future work should aim to adopt the small volume technique for ^{234}Th analysis.

Particulate and dissolved studies

An interesting pattern of increasing C:N ratios with increasing depth was observed in the POC/N data-set. This trend was surmised to be the result of preferential remineralisation of organic nitrogen over organic carbon. If this was the case then this

should be evident in the C:N ratio in the inorganic pool. The C:N ratio of the inorganic pool is calculated through the ratio of DIN and DIC, both of which are part of the CROZEX data-set. Additionally, if future studies collected information on both DON and DOC, it would be possible to calculate the C:N ratio within the DOM. The C:N ratio of POM has been used as an index of solubilisation/remineralisation (Newton *et al.*, 1994) ratios. If this information is combined with the C:N ratios in DOM and the dissolved inorganic phases this will improve our understanding of remineralisation processes.

The final outcome of this thesis was the construction of a carbon budget for the high productivity northern region and the low productivity southern region. This was formed through several major parameters but would have benefited from several other complementary measurements that should be considered for future work. All the information of the DOM pool came from DON samples, which as discussed, is an inherently difficult parameter to measure because it is measured by difference thus resulting in greater uncertainties. DOC on the other hand, is measured directly by high temperature combustion after the acidification and sparging of inorganic carbon. One drawback is that DOC suffers from a higher risk of contamination and thus requires greater care at all steps of sampling and analysis. This however, is worth the extra effort because the preferred sample storage container, heat sealed glass ampoules, are almost certainly better for storing samples than Steriline pots. Additionally, during the analysis of DOC, DON can be analysed in parallel (Pan *et al.*, 2005). Another parameter of great use would have been bSi production rates as measured by the ^{32}Si uptake method (Brzezinski and Phillips, 1997). Future work including this rate measurement will allow validation of bSi formation rates that was only possible through inferred silicate draw-down estimates during CROZEX. Providing an independent estimate of bSi production will provide greater certainty in this part of the silicon cycle.

Ecosystem function

One of the major challenges of oceanography concerned with particle export is that of establishing a link between surface ocean biology and the flux of particles to mesopelagic depths. There is no doubt that surface productivity is needed in order for the biological pump to exist. However, correlating surface productivity and the deep flux of POM over inter-annual time-scales has proved difficult and determining the factors that affect the efficiency of the biological pump is still an open question (Boyd

and Newton, 1995). One idea, the ballast hypothesis, argues that POM can be ballasted with biominerals, such as calcite and silica, thus promoting efficient POM export (Armstrong *et al.*, 2001; Klaas and Archer, 2002). However, this cause-and-effect relationship is argued to be vice versa (Passow, 2004; Passow and De la Rocha, 2006). Clearly, ensuring that future work adequately samples biomineral flux, in particular calcite and opal, should be a high priority. Additionally, coupling biomineral flux with planktonic community structure would allow a better understanding of the relationship between surface productivity and POM export.

The CROZEX project was successful at surveying the latter stages of the bloom and provided this thesis with twenty estimates of POC export during this time frame. However, the cruise was not in the survey region before the bloom or during the growth phase thus preventing any sampling during this time. The idea of a longer export event in the bloom region was a major assumption of the re-calibration of ^{234}Th-Cex in Chapter 6. This assumption could be tested in future work by ensuring that the timing of a cruise coincided with the growth, peak and decline of a bloom. Although this may result in a very long cruise, this could be overcome by splitting a cruise into two legs that could collaborate with passage legs in an appropriate ocean region. Additionally, sampling a bloom area before the bloom has occurred would also be preferable to using a different site as the control comparison. Another approach to assessing the particle export from a bloom over a longer time-scale is to use a different proxy tracer that has a longer integrating time. This can be achieved with the ^{210}Pb/^{210}Po isotope pair that has the ability to integrate over several months and has been shown to yield export results comparable with the ^{234}Th method (Buesseler *et al.*, 2008b; Shimmield *et al.*, 1995). Therefore future studies may benefit from the study of a wider range of isotope pairs.

The time-scales of rate measurements has been a frequent topic of discussion throughout this thesis and will be the final idea suggested for future investigation. ^{234}Th particle flux studies are quasi-integrative over the mean life-time of the tracer (34.8 days), whereas productivity rate measurements typically span 12-24 hours. Bridging this gap would improve estimates of export efficiency but doing so is a huge challenge. One approach is to use satellite observations to estimate upper ocean productivity over a time-scale appropriate to ^{234}Th but to make the best use of satellite observations *in situ* calibration is needed. Additionally, in situ calibrations would be made using bottle incubations thus carrying all the methodological caveats associated with bottle incubations into the satellite calibration. A different approach to measuring oceanic

productivity may be one solution and the oxygen triple-isotope technique may be suitable for tackling the problem of time-scales. This technique has the ability to integrate oceanic productivity over a period of weeks (Luz and Barkan, 2000) thus instantly bridging the different time-scales between the ^{234}Th method and the estimate of productivity. Therefore this has to be worthy of future investigation.

7.4 Closing Statement

The investigation of particle flux from the surface ocean into the deep ocean has progressed on many fronts over recent years, whether through the development of neutrally buoyant sediment traps, or through the use of proxy particle tracers like ^{234}Th. These techniques have opened new avenues of investigation and broadened our understanding of biogeochemical processes. However, there still remains a wealth of unanswered questions that can help to refine our current understanding of how these processes function as part of the compete ocean system. The major difficulty of progressing this subject is knowing the specifics of the right questions to ask.

Appendix 1

Total ^{234}Th and ^{238}U activities and ^{234}Th:^{238}U activity ratios with 1σ errors for all stations.

Station name and number	Date (dd/mm/yy)	Depth (m)	Total ^{234}Th (dpm l^{-1})	^{238}U (dpm l^{-1})	^{234}Th:^{238}U
15492 - M1	11/11/04	12	1.40 ± 0.07	2.38 ± 0.08	0.59 ± 0.04
		17	1.51 ± 0.10	2.38 ± 0.08	0.64 ± 0.05
		26	1.43 ± 0.07	2.38 ± 0.08	0.60 ± 0.04
		46	1.36 ± 0.07	2.38 ± 0.08	0.57 ± 0.04
		66	1.59 ± 0.08	2.38 ± 0.08	0.67 ± 0.04
		87	1.97 ± 0.10	2.38 ± 0.08	0.83 ± 0.05
		117	2.67 ± 0.16	2.39 ± 0.08	1.12 ± 0.08
		158	2.39 ± 0.17	2.39 ± 0.08	1.00 ± 0.08
		209	2.41 ± 0.13	2.40 ± 0.08	1.00 ± 0.06
		1014	2.66 ± 0.14	2.45 ± 0.08	1.08 ± 0.07
15495 - M3.1	13/11/04	6	1.68 ± 0.08	2.38 ± 0.08	0.70 ± 0.04
		41	1.90 ± 0.10	2.38 ± 0.08	0.80 ± 0.05
		77	1.80 ± 0.09	2.39 ± 0.08	0.75 ± 0.05
		126	2.05 ± 0.10	2.39 ± 0.08	0.86 ± 0.05
		153	2.63 ± 0.13	2.39 ± 0.08	1.10 ± 0.07
		203	2.19 ± 0.13	2.39 ± 0.08	0.91 ± 0.06
		228	2.18 ± 0.11	2.39 ± 0.08	0.91 ± 0.05
		254	2.56 ± 0.13	2.40 ± 0.08	1.07 ± 0.06
		304	2.48 ± 0.12	2.40 ± 0.08	1.03 ± 0.06
		1010	2.72 ± 0.13	2.45 ± 0.08	1.11 ± 0.07
15498 - M3.2	18/11/04	13	2.01 ± 0.14	2.39 ± 0.08	0.84 ± 0.07
		44	2.06 ± 0.10	2.39 ± 0.08	0.86 ± 0.05
		63	2.07 ± 0.10	2.39 ± 0.08	0.87 ± 0.05
		83	2.20 ± 0.11	2.39 ± 0.08	0.92 ± 0.05
		103	2.48 ± 0.16	2.39 ± 0.08	1.04 ± 0.08
		128	2.23 ± 0.11	2.39 ± 0.08	0.93 ± 0.06
		154	2.32 ± 0.11	2.40 ± 0.08	0.97 ± 0.06
		179	2.27 ± 0.13	2.40 ± 0.08	0.95 ± 0.06
		206	2.37 ± 0.13	2.40 ± 0.08	0.99 ± 0.06
		304	2.70 ± 0.15	2.41 ± 0.08	1.12 ± 0.07
15503 - M2.1	20/11/04	12	2.05 ± 0.10	2.38 ± 0.08	0.86 ± 0.05
		42	2.25 ± 0.13	2.38 ± 0.08	0.94 ± 0.06
		63	2.18 ± 0.11	2.38 ± 0.08	0.91 ± 0.05
		83	2.11 ± 0.10	2.38 ± 0.08	0.88 ± 0.05
		128	2.40 ± 0.12	2.39 ± 0.08	1.00 ± 0.06
		153	2.36 ± 0.14	2.39 ± 0.08	0.99 ± 0.07
		178	2.50 ± 0.13	2.39 ± 0.08	1.04 ± 0.06
		254	2.43 ± 0.12	2.40 ± 0.08	1.01 ± 0.06
		381	2.48 ± 0.12	2.42 ± 0.08	1.03 ± 0.06
		506	2.53 ± 0.13	2.43 ± 0.08	1.04 ± 0.06
15512 - M6.1	23/11/04	12	2.05 ± 0.10	2.38 ± 0.08	0.86 ± 0.05
		42	2.21 ± 0.18	2.38 ± 0.08	0.93 ± 0.08
		62	2.25 ± 0.11	2.38 ± 0.08	0.94 ± 0.06
		83	2.18 ± 0.12	2.38 ± 0.08	0.91 ± 0.06
		104	2.42 ± 0.12	2.38 ± 0.08	1.01 ± 0.06

Station name and number	Date (dd/mm/yy)	Depth (m)	Total ^{234}Th (dpm l^{-1})	^{238}U (dpm l^{-1})	^{234}Th:^{238}U
		126	2.20 ± 0.13	2.39 ± 0.08	0.92 ± 0.06
		154	2.33 ± 0.11	2.39 ± 0.08	0.98 ± 0.06
		177	2.25 ± 0.12	2.39 ± 0.08	0.94 ± 0.06
		204	2.42 ± 0.12	2.39 ± 0.08	1.01 ± 0.06
		507	2.66 ± 0.13	2.43 ± 0.08	1.10 ± 0.07
15517 - M3.3	25/11/04	14	1.77 ± 0.09	2.39 ± 0.08	0.74 ± 0.04
		44	1.83 ± 0.15	2.39 ± 0.08	0.76 ± 0.07
		65	1.78 ± 0.09	2.39 ± 0.08	0.74 ± 0.04
		85	1.82 ± 0.09	2.39 ± 0.08	0.76 ± 0.05
		105	2.16 ± 0.11	2.39 ± 0.08	0.90 ± 0.05
		130	2.14 ± 0.11	2.39 ± 0.08	0.90 ± 0.05
		156	2.33 ± 0.12	2.39 ± 0.08	0.97 ± 0.06
		179	2.42 ± 0.13	2.39 ± 0.08	1.01 ± 0.06
		205	2.37 ± 0.12	2.40 ± 0.08	0.99 ± 0.06
		307	2.54 ± 0.13	2.41 ± 0.08	1.05 ± 0.07
15523 - M7	27/11/04	12	1.35 ± 0.07	2.38 ± 0.08	0.56 ± 0.03
		43	1.47 ± 0.13	2.38 ± 0.08	0.62 ± 0.06
		63	1.47 ± 0.08	2.38 ± 0.08	0.62 ± 0.04
		84	1.69 ± 0.09	2.39 ± 0.08	0.71 ± 0.04
		103	2.17 ± 0.11	2.39 ± 0.08	0.91 ± 0.05
		129	2.43 ± 0.13	2.39 ± 0.08	1.01 ± 0.06
		153	2.66 ± 0.13	2.39 ± 0.08	1.11 ± 0.07
		179	2.39 ± 0.12	2.40 ± 0.08	1.00 ± 0.06
		204	2.36 ± 0.14	2.40 ± 0.08	0.98 ± 0.07
		302	2.64 ± 0.13	2.41 ± 0.08	1.09 ± 0.06
15533 - M8E	30/11/04	12	1.56 ± 0.10	2.38 ± 0.08	0.66 ± 0.05
		43	1.75 ± 0.13	2.38 ± 0.08	0.74 ± 0.06
		63	1.84 ± 0.10	2.38 ± 0.08	0.77 ± 0.05
		82	1.95 ± 0.11	2.38 ± 0.08	0.82 ± 0.05
		101	2.47 ± 0.13	2.39 ± 0.08	1.04 ± 0.06
		126	2.43 ± 0.14	2.39 ± 0.08	1.02 ± 0.07
		153	2.45 ± 0.13	2.39 ± 0.08	1.03 ± 0.06
		179	2.46 ± 0.13	2.40 ± 0.08	1.03 ± 0.06
		204	2.44 ± 0.14	2.40 ± 0.08	1.02 ± 0.07
		405	2.55 ± 0.13	2.42 ± 0.08	1.06 ± 0.06
15539 - M8W	02/12/04	10	1.36 ± 0.07	2.39 ± 0.08	0.57 ± 0.04
		41	1.50 ± 0.08	2.39 ± 0.08	0.63 ± 0.04
		62	1.66 ± 0.11	2.39 ± 0.08	0.69 ± 0.05
		81	1.80 ± 0.09	2.39 ± 0.08	0.75 ± 0.04
		103	2.24 ± 0.12	2.39 ± 0.08	0.93 ± 0.06
		127	2.23 ± 0.14	2.39 ± 0.08	0.93 ± 0.06
		152	2.47 ± 0.13	2.39 ± 0.08	1.03 ± 0.06
		177	2.35 ± 0.12	2.40 ± 0.08	0.98 ± 0.06
		205	2.33 ± 0.12	2.40 ± 0.08	0.97 ± 0.06
		404	2.54 ± 0.21	2.41 ± 0.08	1.05 ± 0.09
15542 - M9.1	03/12/04	10	0.94 ± 0.05	2.38 ± 0.08	0.39 ± 0.03
		41	1.31 ± 0.08	2.38 ± 0.08	0.55 ± 0.04
		61	1.93 ± 0.09	2.39 ± 0.08	0.81 ± 0.05
		81	2.31 ± 0.14	2.39 ± 0.08	0.97 ± 0.07

Station name and number	Date (dd/mm/yy)	Depth (m)	Total ^{234}Th (dpm l^{-1})	^{238}U (dpm l^{-1})	^{234}Th:^{238}U
		101	2.55 ± 0.14	2.39 ± 0.08	1.06 ± 0.07
		121	2.36 ± 0.12	2.40 ± 0.08	0.99 ± 0.06
		122	2.38 ± 0.13	2.40 ± 0.08	0.99 ± 0.06
		122	2.31 ± 0.13	2.40 ± 0.08	0.96 ± 0.06
		203	2.44 ± 0.23	2.40 ± 0.08	1.02 ± 0.10
		404	2.63 ± 0.18	2.41 ± 0.08	1.09 ± 0.08
15548	05/12/04	1004	2.46 ± 0.14	2.44 ± 0.08	1.01 ± 0.07
		1003	2.51 ± 0.19	2.44 ± 0.08	1.03 ± 0.09
		1003	2.47 ± 0.16	2.44 ± 0.08	1.01 ± 0.07
		1004	2.39 ± 0.12	2.44 ± 0.08	0.98 ± 0.06
		1002	2.59 ± 0.14	2.44 ± 0.08	1.06 ± 0.07
		1005	2.22 ± 0.11	2.44 ± 0.08	0.91 ± 0.05
		1005	2.27 ± 0.11	2.44 ± 0.08	0.93 ± 0.06
		1003	2.54 ± 0.15	2.44 ± 0.08	1.04 ± 0.07
		1004	2.42 ± 0.16	2.44 ± 0.08	0.99 ± 0.07
		1005	2.54 ± 0.18	2.44 ± 0.08	1.04 ± 0.08
15554 - M9.2	19/12/04	11	1.43 ± 0.13	2.38 ± 0.08	0.60 ± 0.06
		26	1.58 ± 0.15	2.38 ± 0.08	0.66 ± 0.07
		52	1.54 ± 0.09	2.39 ± 0.08	0.65 ± 0.04
		77	1.71 ± 0.06	2.39 ± 0.08	0.72 ± 0.03
		102	2.09 ± 0.08	2.39 ± 0.08	0.87 ± 0.04
		120	1.89 ± 0.07	2.40 ± 0.08	0.79 ± 0.04
		150	2.17 ± 0.08	2.40 ± 0.08	0.91 ± 0.04
		175	2.3 ± 0.18	2.40 ± 0.08	0.96 ± 0.08
		200	2.16 ± 0.08	2.40 ± 0.08	0.90 ± 0.04
		405	2.41 ± 0.08	2.41 ± 0.08	1.00 ± 0.05
15560 - M10	20/12/04	12	1.62 ± 0.09	2.38 ± 0.08	0.68 ± 0.04
		22	1.72 ± 0.06	2.38 ± 0.08	0.72 ± 0.03
		42	1.71 ± 0.07	2.38 ± 0.08	0.72 ± 0.04
		62	1.81 ± 0.08	2.38 ± 0.08	0.76 ± 0.04
		81	2.08 ± 0.17	2.38 ± 0.08	0.87 ± 0.08
		112	2.20 ± 0.10	2.39 ± 0.08	0.92 ± 0.05
		152	2.44 ± 0.18	2.39 ± 0.08	1.02 ± 0.08
		178	2.39 ± 0.09	2.39 ± 0.08	1.00 ± 0.05
		203	2.31 ± 0.08	2.40 ± 0.08	0.96 ± 0.05
		404	2.61 ± 0.18	2.42 ± 0.08	1.08 ± 0.08
15574 - M3.4	23/12/04	12	1.63 ± 0.06	2.38 ± 0.08	0.68 ± 0.03
		23	1.77 ± 0.14	2.38 ± 0.08	0.74 ± 0.06
		52	1.61 ± 0.07	2.38 ± 0.08	0.67 ± 0.04
		73	1.66 ± 0.07	2.39 ± 0.08	0.7 ± 0.04
		103	2.03 ± 0.09	2.39 ± 0.08	0.85 ± 0.05
		133	2.11 ± 0.09	2.39 ± 0.08	0.88 ± 0.05
		154	2.23 ± 0.09	2.39 ± 0.08	0.93 ± 0.05
		184	2.23 ± 0.10	2.40 ± 0.08	0.93 ± 0.05
		305	2.33 ± 0.11	2.41 ± 0.08	0.97 ± 0.06
		409	2.45 ± 0.10	2.42 ± 0.08	1.02 ± 0.05
15580 - M5	27/12/04	13	1.63 ± 0.16	2.38 ± 0.08	0.69 ± 0.07
		22	1.60 ± 0.05	2.38 ± 0.08	0.67 ± 0.03
		52	1.69 ± 0.15	2.38 ± 0.08	0.71 ± 0.07

Station name and number	Date (dd/mm/yy)	Depth (m)	Total ^{234}Th (dpm l^{-1})	^{238}U (dpm l^{-1})	^{234}Th:^{238}U
		72	1.67 ± 0.08	2.38 ± 0.08	0.70 ± 0.04
		103	1.85 ± 0.06	2.38 ± 0.08	0.78 ± 0.04
		128	1.95 ± 0.06	2.38 ± 0.08	0.82 ± 0.04
		154	2.17 ± 0.10	2.39 ± 0.08	0.91 ± 0.05
		203	2.33 ± 0.14	2.39 ± 0.08	0.98 ± 0.07
		304	2.28 ± 0.12	2.41 ± 0.08	0.95 ± 0.06
		508	2.64 ± 0.10	2.43 ± 0.08	1.09 ± 0.05
15590 - M3.5	31/12/04	12	1.71 ± 0.11	2.39 ± 0.08	0.72 ± 0.05
		22	1.75 ± 0.07	2.39 ± 0.08	0.73 ± 0.04
		53	1.81 ± 0.16	2.39 ± 0.08	0.76 ± 0.07
		72	1.87 ± 0.06	2.39 ± 0.08	0.78 ± 0.04
		104	2.13 ± 0.09	2.39 ± 0.08	0.89 ± 0.05
		129	2.08 ± 0.07	2.40 ± 0.08	0.87 ± 0.04
		155	2.13 ± 0.08	2.40 ± 0.08	0.89 ± 0.04
		204	2.32 ± 0.22	2.40 ± 0.08	0.97 ± 0.10
		305	2.37 ± 0.20	2.41 ± 0.08	0.98 ± 0.09
		507	2.40 ± 0.11	2.42 ± 0.08	0.99 ± 0.06
15595 - M6.2	03/01/05	13	1.65 ± 0.07	2.38 ± 0.08	0.69 ± 0.04
		43	1.86 ± 0.17	2.38 ± 0.08	0.78 ± 0.08
		72	1.78 ± 0.07	2.38 ± 0.08	0.75 ± 0.04
		104	1.73 ± 0.06	2.39 ± 0.08	0.73 ± 0.03
		122	1.99 ± 0.08	2.39 ± 0.08	0.83 ± 0.04
		144	2.31 ± 0.08	2.39 ± 0.08	0.97 ± 0.05
		164	2.31 ± 0.11	2.39 ± 0.08	0.97 ± 0.05
		204	2.21 ± 0.11	2.39 ± 0.08	0.93 ± 0.06
		305	2.31 ± 0.08	2.41 ± 0.08	0.96 ± 0.05
		507	2.28 ± 0.12	2.43 ± 0.08	0.94 ± 0.06
15604 - M2.2	06/01/05	11	1.46 ± 0.05	2.38 ± 0.08	0.62 ± 0.03
		21	1.58 ± 0.06	2.38 ± 0.08	0.66 ± 0.03
		41	1.58 ± 0.05	2.38 ± 0.08	0.67 ± 0.03
		71	1.63 ± 0.07	2.38 ± 0.08	0.69 ± 0.04
		103	1.99 ± 0.06	2.38 ± 0.08	0.83 ± 0.04
		133	2.16 ± 0.08	2.39 ± 0.08	0.90 ± 0.05
		163	2.42 ± 0.08	2.39 ± 0.08	1.01 ± 0.05
		204	2.33 ± 0.08	2.39 ± 0.08	0.97 ± 0.04
		304	2.35 ± 0.11	2.41 ± 0.08	0.98 ± 0.06
		506	2.66 ± 0.09	2.43 ± 0.08	1.10 ± 0.05
15613 - M3.6	09/01/05	21	1.71 ± 0.06	2.38 ± 0.08	0.72 ± 0.04
		41	1.93 ± 0.07	2.39 ± 0.08	0.81 ± 0.04
		61	2.08 ± 0.13	2.39 ± 0.08	0.87 ± 0.06
		82	2.00 ± 0.07	2.39 ± 0.08	0.84 ± 0.04
		102	2.18 ± 0.07	2.40 ± 0.08	0.91 ± 0.04
		127	2.02 ± 0.07	2.40 ± 0.08	0.84 ± 0.04
		153	2.22 ± 0.09	2.40 ± 0.08	0.93 ± 0.05
		202	2.27 ± 0.10	2.40 ± 0.08	0.95 ± 0.05
		304	2.25 ± 0.16	2.41 ± 0.08	0.94 ± 0.07
		506	2.44 ± 0.09	2.42 ± 0.08	1.00 ± 0.05
15620 - M3.7	10/01/05	13	1.55 ± 0.05	2.38 ± 0.08	0.65 ± 0.03
		23	1.77 ± 0.06	2.38 ± 0.08	0.74 ± 0.04

Station name and number	Date (dd/mm/yy)	Depth (m)	Total ^{234}Th (dpm l^{-1})	^{238}U (dpm l^{-1})	^{234}Th:^{238}U
		42	1.90 ± 0.06	2.39 ± 0.08	0.80 ± 0.04
		63	1.92 ± 0.06	2.39 ± 0.08	0.80 ± 0.04
		83	2.17 ± 0.10	2.39 ± 0.08	0.91 ± 0.05
		103	2.04 ± 0.10	2.40 ± 0.08	0.85 ± 0.05
		128	1.95 ± 0.10	2.40 ± 0.08	0.81 ± 0.05
		154	2.31 ± 0.07	2.40 ± 0.08	0.96 ± 0.04
		255	2.35 ± 0.11	2.41 ± 0.08	0.98 ± 0.06
		507	2.52 ± 0.09	2.42 ± 0.08	1.04 ± 0.05
15627 - M3.8	12/01/05	12	1.48 ± 0.06	2.38 ± 0.08	0.62 ± 0.03
		22	1.72 ± 0.16	2.38 ± 0.08	0.72 ± 0.07
		33	1.77 ± 0.14	2.38 ± 0.08	0.74 ± 0.07
		52	1.67 ± 0.05	2.39 ± 0.08	0.70 ± 0.03
		82	2.15 ± 0.07	2.39 ± 0.08	0.90 ± 0.04
		104	2.04 ± 0.08	2.39 ± 0.08	0.85 ± 0.04
		153	2.25 ± 0.12	2.40 ± 0.08	0.94 ± 0.06
		204	2.23 ± 0.15	2.40 ± 0.08	0.93 ± 0.07
		304	2.32 ± 0.12	2.41 ± 0.08	0.96 ± 0.06
		506	2.42 ± 0.10	2.42 ± 0.08	1.00 ± 0.05
15632	15/01/05	1012	2.45 ± 0.12	2.45 ± 0.08	1.00 ± 0.06
		1011	2.40 ± 0.09	2.45 ± 0.08	0.98 ± 0.05
		1011	2.38 ± 0.08	2.45 ± 0.08	0.97 ± 0.05
		1012	2.61 ± 0.18	2.45 ± 0.08	1.07 ± 0.08
		1012	2.44 ± 0.11	2.45 ± 0.08	1.00 ± 0.06
		1012	2.42 ± 0.08	2.45 ± 0.08	0.99 ± 0.05
		1012	2.46 ± 0.20	2.45 ± 0.08	1.00 ± 0.09
		1012	2.39 ± 0.08	2.45 ± 0.08	0.97 ± 0.04
		1012	2.55 ± 0.09	2.45 ± 0.08	1.04 ± 0.05

Appendix 2

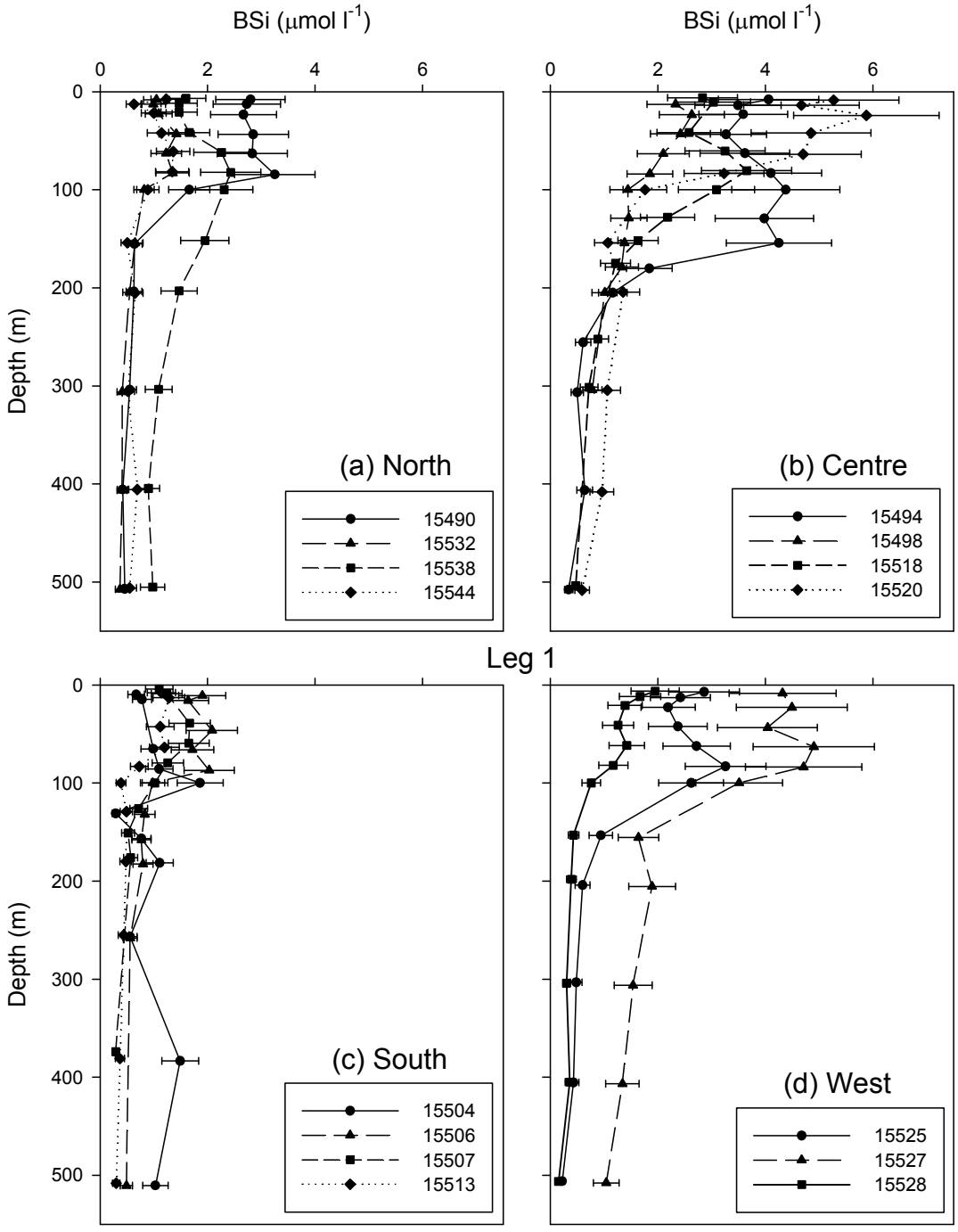

Figure A2.1 Profiles of bSi for leg 1 split into study region. Error bars are 1 σ.

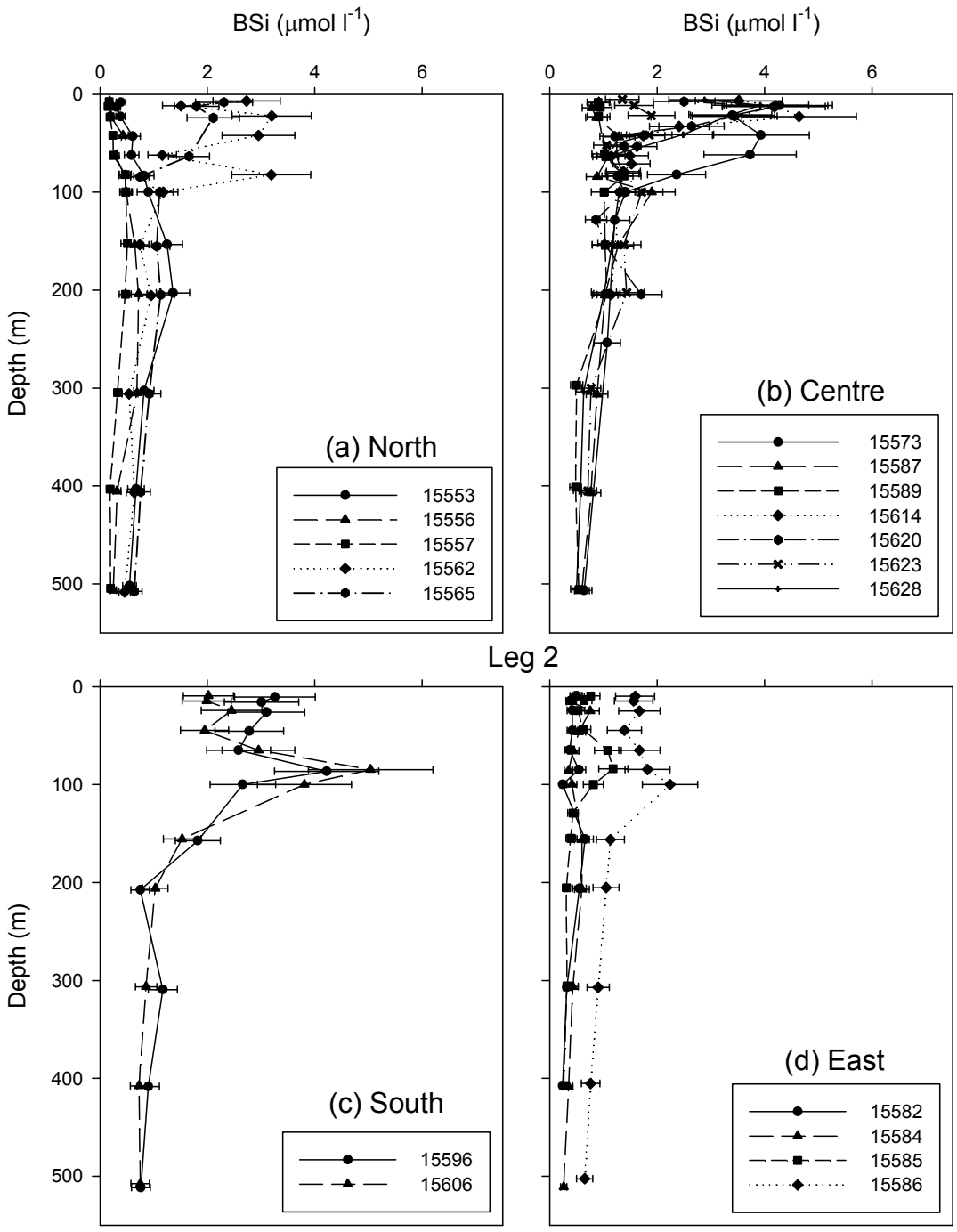

Figure A2.2 Profiles of bSi for leg 2 split into region. Error bars are 1 σ.

References

Allen, J., Bakker, D., Read, J., Pollard, R., Charette, M., Venables, H., Planquette, H., Morris, P., Sanders, R., Moore, C.M., Seeyave, S., (2006) An 'eddy-centric' bloom north of the Crozet Islands; sub-mesoscale entrainment of island nutrients or vertical diffusion? Challenger Conference for Marine Science, Oban, Scotland.

Armstrong, F.A.J., Tibbitts, S., (1968) Photochemical combustion of organic matter in sea water, for nitrogen, phosphorus and carbon determination. *Journal of the Marine Biological Association*, 48, 143-152.

Armstrong, F.A.J., Williams, P.M., Strickland, J.D.H., (1966) Photo-oxydation of organic matter in sea water by ultra-violet radiation, analytical and other applications. *Nature*, 211(5048), 481-483.

Armstrong, R.A., Lee, C., Hedges, J.I., Honjo, S., Wakeham, S.G., (2001) A new, mechanistic model for organic carbon fluxes in the ocean based on the quantitative association of POC with ballast minerals. *Deep-Sea Research II*, 49(1-3), 219-236.

Asper, V.L., (1987) Measuring the flux and sinking speed of marine snow aggregates. *Deep-Sea Research Part A*, 34(1), 1-17.

Bacon, M.P., Anderson, R.F., (1982) Distribution of thorium isotopes between dissolved and particulate forms in the deep sea. *Journal of Geophysical Research-Oceans and Atmospheres*, 87(C3), 2045-2056.

Bacon, M.P., Cochran, J.K., Hirschberg, D., Hammar, T.R., Fleer, A.P., (1996) Export flux of carbon at the equator during the EqPac time-series cruises estimated from ^{234}Th measurements. *Deep-Sea Research II*, 43(4-6), 1133-1153.

Bacon, M.P., Rutgers van der Loeff, M.M., (1989) Removal of thorium-234 by scavenging in the bottom nepheloid layer of the ocean. *Earth and Planetary Science Letters*, 92(2), 157-164.

Badr, E.S.A., Achterberg, E.P., Tappin, A.D., Hill, S.J., Braungardt, C.B., (2003) Determination of dissolved organic nitrogen in natural waters using high-temperature catalytic oxidation. *Trends in Analytical Chemistry*, 22(11), 819-827.

Bakker, D.C.E., (1998) Process studies of the air-sea exhange of carbon dioxide in the Atlantic Ocean. PhD Thesis, University of Groningen, Groningen.

Bakker, D.C.E., Boyd, P.W., Abraham, E.R., Charette, M.A., Gall, M.P., Hall, J.A., Law, C.S., Nodder, S.D., Safi, K., Singleton, D.J., Tanneberger, K., Trull, T.W., Waite, A.M., Watson, A.J., Zeldis, J., (2006) Matching carbon pools and fluxes for the Southern Ocean Iron Release Experiment (SOIREE). *Deep-Sea Research I*, 53(12), 1941-1960.

Bakker, D.C.E., DeBaar, H.J.W., Bathmann, U.V., (1997) Changes of carbon dioxide in surface waters during spring in the Southern Ocean. *Deep-Sea Research II*, 44(1-2), 91-127.

Bakker, D.C.E., Nielsdottir, M.C., Morris, P.J., Venables, J., Watson, A.J., (2007) The island mass effect and biological carbon uptake for the subantarctic Crozet Archipelago. *Deep-Sea Research II*, 54(18-20), 2174-2190.

Bakker, D.C.E., Watson, A.J., Law, C.S., (2001) Southern Ocean iron enrichment promotes inorganic carbon drawdown. *Deep-Sea Research II*, 48(11-12), 2483-2507.

Bateman, H., (1910) Solution of a system of differential equations occuring in the therory of radioactive transformations. *Proceedings of the Cambridge Philosophical Society*, 15, 423-427.

Beattie, J., Bricker, C., Garvin, D., (1961) Photolytic determination of trace amounts of organic material in water. *Analytical Chemistry*, 33(13), 1890-1892.

Behrenfeld, M.J., Falkowski, P.G., (1997) A consumer's guide to phytoplankton primary productivity models. *Limnology and Oceanography*, 42(7), 1479-1491.

Belkin, I.M., Gordon, A.L., (1996) Southern Ocean fronts from the Greenwich meridian to Tasmania. *Journal of Geophysical Research-Oceans*, 101(C2), 3675-3696.

Benitez-Nelson, C.R., Buesseler, K.O., van der Loeff, M.R., Andrews, J., Ball, L., Crossin, G., Charette, M.A., (2001) Testing a new small-volume technique for determining ^{234}Th in seawater. *Journal of Radioanalytical and Nuclear Chemistry*, 248(3), 795-799.

Bennett, S.A., Achterberg, E.P., Connelly, D.P., Statharn, P.J., Fones, G.R., Gernian, C.R., (2008) The distribution and stabilisation of dissolved Fe in deep-sea hydrothermal plumes. *Earth and Planetary Science Letters*, 270(3-4), 157-167.

Bertrand, E.M., Saito, M.A., Rose, J.M., Riesselman, C.R., Lohan, M.C., Noble, A.E., Lee, P.A., DiTullio, G.R., (2007) Vitamin B_{12} and iron colimitation of phytoplankton growth in the Ross Sea. *Limnology and Oceanography*, 52(3), 1079-1093.

Bhat, S.G., Krishnaswamy, S., Lal, D., Rama, Moore, W.S., (1969) ^{234}Th/^{238}U ratios in the ocean. *Earth and Planetary Science Letters*, 5, 483-491.

Bishop, J.K.B., Edmond, J.M., Ketten, D.R., Bacon, M.P., Silker, W.B., (1977) The chemistry, biology, and vertical flux of particulate matter from the upper 400 m of the equatorial Atlantic Ocean. *Deep-Sea Research*, 24(6), 511-548.

Bishop, J.K.B., Wood, T.J., Davis, R.E., Sherman, J.T., (2004) Robotic observations of enhanced carbon biomass and export at 55°S during SOFeX. *Science*, 304(5669), 417-420.

Blain, S., Queguiner, B., Armand, L., Belviso, S., Bombled, B., Bopp, L., Bowie, A., Brunet, C., Brussaard, C., Carlotti, F., Christaki, U., Corbiere, A., Durand, I., Ebersbach, F., Fuda, J.L., Garcia, N., Gerringa, L., Griffiths, B., Guigue, C., Guillerm, C., Jacquet, S., Jeandel, C., Laan, P., Lefevre, D., Lo Monaco, C., Malits, A., Mosseri, J., Obernosterer, I., Park, Y.H., Picheral, M., Pondaven, P., Remenyi, T., Sandroni, V., Sarthou, G., Savoye, N., Scouarnec, L., Souhaut, M., Thuiller, D., Timmermans, K., Trull, T., Uitz, J., van Beek, P., Veldhuis, M., Vincent, D., Viollier, E., Vong, L., Wagener, T., (2007) Effect of natural iron fertilization on carbon sequestration in the Southern Ocean. *Nature*, 446(7139), 1070-1074.

Blain, S., Treguer, P., Belviso, S., Bucciarelli, E., Denis, M., Desabre, S., Fiala, M., Jezequel, V.M., Le Fevre, J., Mayzaud, P., Marty, J.C., Razouls, S., (2001) A biogeochemical study of the island mass effect in the context of the iron hypothesis: Kerguelen Islands, Southern Ocean. *Deep-Sea Research I*, 48(1), 163-187.

Bode, A., Varela, M., Canle, M., Gonzalez, N., (2001) Dissolved and particulate organic nitrogen in shelf waters of northern Spain during spring. *Marine Ecology Progress Series*, 214, 43-54.

Bourdon, B., Turner, S., Henderson, G.M., Lundstrom, C.C., (2003) Introduction to U-series geochemistry. *Reviews in Mineralogy & Geochemistry*, 52, 1-21.

Boyd, P., Newton, P., (1995) Evidence of the Potential Influence of Planktonic Community Structure on the Interannual Variability of Particulate Organic-Carbon Flux. *Deep-Sea Research I*, 42(5), 619-639.

Boyd, P.W., Jickells, T., Law, C.S., Blain, S., Boyle, E.A., Buesseler, K.O., Coale, K.H., Cullen, J.J., de Baar, H.J.W., Follows, M., Harvey, M., Lancelot, C., Levasseur, M., Owens, N.P.J., Pollard, R., Rivkin, R.B., Sarmiento, J., Schoemann, V., Smetacek, V., Takeda, S., Tsuda, A., Turner, S., Watson, A.J., (2007) Mesoscale iron enrichment experiments 1993-2005: Synthesis and future directions. *Science*, 315(5812), 612-617.

Boyd, P.W., Law, C.S., Wong, C.S., Nojiri, Y., Tsuda, A., Levasseur, M., Takeda, S., Rivkin, R., Harrison, P.J., Strzepek, R., Gower, J., McKay, R.M., Abraham, E., Arychuk, M., Barwell-Clarke, J., Crawford, W., Crawford, D., Hale, M., Harada, K., Johnson, K., Kiyosawa, H., Kudo, I., Marchetti, A., Miller, W., Needoba, J., Nishioka, J., Ogawa, H., Page, J., Robert, M., Saito, H., Sastri, A., Sherry, N., Soutar, T., Sutherland, N., Taira, Y., Whitney, F., Wong, S.K.E., Yoshimura, T., (2004) The decline and fate of an iron-induced subarctic phytoplankton bloom. *Nature*, 428(6982), 549-553.

Boyd, P.W., Sherry, N.D., Berges, J.A., Bishop, J.K.B., Calvert, S.E., Charette, M.A., Giovannoni, S.J., Goldblatt, R., Harrison, P.J., Moran, S.B., Roy, S., Soon, M., Strom, S., (1999) Transformations of biogenic particulates from the pelagic to the deep ocean realm. *Deep-Sea Research II*, 46(11-12), 2761-2792.

Boyd, P.W., Trull, T.W., (2007) Understanding the export of biogenic particles in oceanic waters: Is there consensus? *Progress in Oceanography*, 72(4), 276-312.

Boyd, P.W., Watson, A.J., Law, C.S., Abraham, E.R., Trull, T., Murdoch, R., Bakker, D.C.E., Bowie, A.R., Buesseler, K.O., Chang, H., Charette, M., Croot, P., Downing, K., Frew, R., Gall, M., Hadfield, M., Hall, J., Harvey, M., Jameson, G., LaRoche, J., Liddicoat, M., Ling, R., Maldonado, M.T., McKay, R.M., Nodder, S., Pickmere, S., Pridmore, R., Rintoul, S., Safi, K., Sutton, P., Strzepek, R., Tanneberger, K., Turner, S., Waite, A., Zeldis, J., (2000) A mesoscale phytoplankton bloom in the polar Southern Ocean stimulated by iron fertilization. *Nature*, 407(6805), 695-702.

Braarud, T., (1935) The phytoplankton and its conditions of growth. *Hvalrådets Skrifter, Scientific results of marine biological research*, 10, 1-173.

Braarud, T., Klem, A., (1931) Hydrographical and chemical investigations in the sea off Møre and in the Romsdalsfjord. *Hvalrådets Skrifter, Scientific results of marine biological research*, 1, 1-88.

Broecker, W.S., (1974) Chemical Oceanography. Harcourt Brace Jovanovich Inc, New York.

Broecker, W.S., (1987) The biggest chill. *Natural History Magazine*, 97, 74-82.

Broecker, W.S., (1991) The great ocean conveyer. *Oceanography*, 4(2), 79-89.

Broecker, W.S., Peng, T.-H., (1982) Tracers in the Sea. Eldigio, New York.

Bronk, D.A., (2001) Dynamics of DON. In: D.A. Hansell, C.A. Carlson (Eds.), Biogeochemistry of marine dissolved organic matter. Academic Press, San Diego, pp. chapter 5.

Bronk, D.A., Glibert, P.M., Ward, B.B., (1994) Nitrogen Uptake, Dissolved Organic Nitrogen Release, and New Production. *Science*, 265(5180), 1843-1846.

Bronk, D.A., Lomas, M.W., Glibert, P.M., Schukert, K.J., Sanderson, M.P., (2000) Total dissolved nitrogen analysis: comparisons between the persulfate, UV and high temperature oxidation methods. *Marine Chemistry*, 69(1-2), 163-178.

Bronk, D.A., Ward, B.B., (1999) Gross and net nitrogen uptake and DON release in the euphotic zone of Monterey Bay, California. *Limnology and Oceanography*, 44(3), 573-585.

Brzezinski, M.A., (1992) Cell-cycle effects on the kinetics of silicic acid uptake and resource competition among diatoms. *Journal of Plankton Research*, 14(11), 1511-1539.

Brzezinski, M.A., Nelson, D.M., (1989) Seasonal changes in the silicon cycle within a Gulf Stream warm-core ring. *Deep-Sea Research Part A*, 36(7), 1009-1030.

Brzezinski, M.A., Olson, R.J., Chisholm, S.W., (1990) Silicon Availability and Cell-Cycle Progression in Marine Diatoms. *Marine Ecology Progress Series*, 67(1), 83-96.

Brzezinski, M.A., Phillips, D.R., (1997) Evaluation of ^{32}Si as a tracer for measuring silica production rates in marine waters. *Limnology and Oceanography*, 42(5), 856-865.

Bucciarelli, E., Blain, S., Treguer, P., (2001) Iron and manganese in the wake of the Kerguelen Islands (Southern Ocean). *Marine Chemistry*, 73(1), 21-36.

Buesseler, K.O., (1998) The decoupling of production and particulate export in the surface ocean. *Global Biogeochemical Cycles*, 12(2), 297-310.

Buesseler, K.O., Andrews, J.A., Hartman, M.C., Belastock, R., Chai, F., (1995) Regional estimates of the export flux of particulate organic carbon derived from thorium-234 during the JGOFS EqPac program. *Deep-Sea Research II*, 42(2-3), 777-804.

Buesseler, K.O., Andrews, J.E., Pike, S.M., Charette, M.A., (2004) The effects of iron fertilization on carbon sequestration in the southern ocean. *Science*, 304(5669), 414-417.

Buesseler, K.O., Andrews, J.E., Pike, S.M., Charette, M.A., Goldson, L.E., Brzezinski, M.A., Lance, V.P., (2005) Particle export during the southern ocean iron experiment (SOFeX). *Limnology and Oceanography*, 50(1), 311-327.

Buesseler, K.O., Bacon, M.P., Cochran, J.K., Livingston, H.D., (1992) Carbon and nitrogen export during the JGOFS North Atlantic Bloom Experiment estimated from ^{234}Th:^{238}U disequilibria. *Deep-Sea Research I*, 39(7-8), 1115-1137.

Buesseler, K.O., Ball, L., Andrews, J., Benitez-Nelson, C., Belastock, R., Chai, F., Chao, Y., (1998) Upper ocean export of particulate organic carbon in the Arabian Sea derived from thorium-234. *Deep-Sea Research II*, 45, 2461-2487.

Buesseler, K.O., Ball, L., Andrews, J., Cochran, J.K., Hirschberg, D.J., Bacon, M.P., Fleer, A., Brzezinski, M., (2001a) Upper ocean export of particulate organic carbon and biogenic silica in the Southern Ocean along 170°W. *Deep-Sea Research II*, 48(19-20), 4275-4297.

Buesseler, K.O., Barber, R.T., Dickson, M.L., Hiscock, M.R., Moore, J.K., Sambrotto, R., (2003) The effect of marginal ice-edge dynamics on production and export in the Southern Ocean along 170°W. *Deep-Sea Research II*, 50(3-4), 579-603.

Buesseler, K.O., Benitez-Nelson, C.R., Moran, S.B., Burd, A., Charette, M., Cochran, J.K., Coppola, L., Fisher, N.S., Fowler, S.W., Gardner, W., Guo, L.D., Gustafsson, O., Lamborg, C., Masque, P., Miquel, J.C., Passow, U., Santschi, P.H., Savoye, N., Stewart, G., Trull, T., (2006) An assessment of particulate organic carbon to thorium-234 ratios in the ocean and their impact on the application of ^{234}Th as a POC flux proxy. *Marine Chemistry*, 100(3-4), 213-233.

Buesseler, K.O., Benitez-Nelson, C.R., Rutgers van der Loeff, M., Andrews, J., Ball, L., Crossin, G., Charette, M.A., (2001b) An intercomparison of small- and large-volume techniques for thorium-234 in seawater. *Marine Chemistry*, 74(1), 15-28.

Buesseler, K.O., Boyd, P.W., (2003) Will ocean fertilization work? *Science*, 300(5616), 67-68.

Buesseler, K.O., Doney, S.C., Karl, D.M., Boyd, P.W., Caldeira, K., Chai, F., Coale, K.H., de Baar, H.J.W., Falkowski, P.G., Johnson, K.S., Lampitt, R.S., Michaels, A.F., Naqvi, S.W.A., Smetacek, V., Takeda, S., Watson, A.J., (2008a) Environment - Ocean iron fertilization - Moving forward in a sea of uncertainty. *Science*, 319(5860), 162-162.

Buesseler, K.O., Lamborg, C., Cai, P., Escoube, R., Johnson, R., Pike, S., Masque, P., McGillicuddy, D., Verdeny, E., (2008b) Particle fluxes associated with mesoscale eddies in the Sargasso Sea. *Deep-Sea Research II*, 55(10-13), 1426-1444.

Buesseler, K.O., Lamborg, C.H., Boyd, P.W., Lam, P.J., Trull, T.W., Bidigare, R.R., Bishop, J.K.B., Casciotti, K.L., Dehairs, F., Elskens, M., Honda, M., Karl, D.M., Siegel, D.A., Silver, M.W., Steinberg, D.K., Valdes, J., Van Mooy, B., Wilson, S., (2007) Revisiting carbon flux through the ocean's twilight zone. *Science*, 316(5824), 567-570.

Buma, A.G.J., Debaar, H.J.W., Nolting, R.F., Vanbennekom, A.J., (1991) Metal enrichment experiments in the Weddell-Scotia Seas - Effects of iron and manganese on various plankton communities. *Limnology and Oceanography*, 36(8), 1865-1878.

Butler, E.I., Knox, S., Liddicoat, M.I., (1979) Relationship between inorganic and organic nutrients in sea water. *Journal of the Marine Biological Association*, 59(1), 239-250.

Calvert, S.E., (1983) Sedimentary geochemistry of silicon. In: S.R. Aston (Ed.), Silicon Geochemistry and Biogeochemistry. Academic Press, London.

Carlson, C.A., Hansell, D.A., Peltzer, E.T., Smith, W.O., (2000) Stocks and dynamics of dissolved and particulate organic matter in the southern Ross Sea, Antarctica. *Deep-Sea Research II*, 47(15-16), 3201-3225.

Carpenter, E.J., Romans, K., (1991) Major role of the cyanobacterium *Trichodesmium* in nutrient cycling in the North Atlantic Ocean. *Science*, 254(5036), 1356-1358.

Charette, M.A., Buesseler, K.O., (2000) Does iron fertilization lead to rapid carbon export in the Southern Ocean? *Geochemistry, Geophysics, Geosystems*, 1, 2000GC000069.

Charette, M.A., Gonneea, M.E., Morris, P.J., Statham, P., Fones, G., Planquette, H., Salter, I., Garabato, A.N., (2007) Radium isotopes as tracers of iron sources fueling a Southern Ocean phytoplankton bloom. *Deep-Sea Research II*, 54(18-20), 1989-1998.

Charette, M.A., Moran, S.B., (1999) Rates of particle scavenging and particulate organic carbon export estimated using ^{234}Th as a tracer in the subtropical and equatorial Atlantic Ocean. *Deep-Sea Research II*, 46(5), 885-906.

Chen, J.H., Edwards, R.L., Wasserburg, G.J., (1986) ^{238}U, ^{234}U and ^{232}Th in seawater. *Earth and Planetary Science Letters*, 80(3-4), 241-251.

Chisholm, S.W., Falkowski, P.G., Cullen, J.J., (2001) Dis-crediting ocean fertilization. *Science*, 294(5541), 309-310.

Christian, J.R., Lewis, M.R., Karl, D.M., (1997) Vertical fluxes of carbon, nitrogen, and phosphorus in the North Pacific Subtropical Gyre near Hawaii. *Journal of Geophysical Research-Oceans*, 102(C7), 15,667-15,677.

Coale, K.H., Bruland, K.W., (1985) ^{234}Th:^{238}U disequilibria within the California Current. *Limnology and Oceanography*, 30(1), 22-33.

Coale, K.H., Bruland, K.W., (1987) Oceanic stratified euphotic zone as elucidated by ^{234}Th:^{238}U disequilibria. *Limnology and Oceanography*, 32(1), 189-200.

Coale, K.H., Johnson, K.S., Chavez, F.P., Buesseler, K.O., Barber, R.T., Brzezinski, M.A., Cochlan, W.P., Millero, F.J., Falkowski, P.G., Bauer, J.E., Wanninkhof, R.H., Kudela, R.M., Altabet, M.A., Hales, B.E., Takahashi, T., Landry, M.R., Bidigare, R.R., Wang, X.J., Chase, Z., Strutton, P.G., Friederich, G.E., Gorbunov, M.Y., Lance, V.P., Hilting, A.K., Hiscock, M.R., Demarest, M., Hiscock, W.T., Sullivan, K.F., Tanner, S.J., Gordon, R.M., Hunter, C.N., Elrod, V.A., Fitzwater, S.E., Jones, J.L., Tozzi, S., Koblizek, M., Roberts, A.E., Herndon, J., Brewster, J., Ladizinsky, N., Smith, G., Cooper, D., Timothy, D., Brown, S.L., Selph, K.E., Sheridan, C.C., Twining, B.S., Johnson, Z.I., (2004) Southern ocean iron enrichment experiment: Carbon cycling in high- and low-Si waters. *Science*, 304(5669), 408-414.

Coale, K.H., Johnson, K.S., Fitzwater, S.E., Gordon, R.M., Tanner, S., Chavez, F.P., Ferioli, L., Sakamoto, C., Rogers, P., Millero, F., Steinberg, P., Nightingale, P., Cooper, D., Cochlan, W.P., Landry, M.R., Constantinou, J., Rollwagen, G., Trasvina, A., Kudela, R., (1996) A massive phytoplankton bloom induced by an ecosystem-scale iron fertilization experiment in the equatorial Pacific Ocean. *Nature*, 383(6600), 495-501.

Cochran, J.K., Barnes, C., Achman, D., Hirschberg, D.J., (1995) Thorium-234/Uranium-238 disequilibrium as an indicator of scavenging rates and particulate organic carbon fluxes in the Northeast Water Polynya, Greenland. *Journal of Geophysical Research-Oceans*, 100(C3), 4399-4410.

Cochran, J.K., Buesseler, K.O., Bacon, M.P., Wang, H.W., Hirschberg, D.J., Ball, L., Andrews, J., Crossin, G., Fleer, A., (2000) Short-lived thorium isotopes (^{234}Th, ^{228}Th) as indicators of POC export and particle cycling in the Ross Sea, Southern Ocean. *Deep-Sea Research II*, 47(15-16), 3451-3490.

Cochran, J.K., Masqué, P., (2003) Short-lived U/Th series radionuclides in the ocean: Tracers for scavenging rates, export fluxes and particle dynamics. *Reviews in Mineralogy & Geochemistry*, 52, 461-492.

Cochran, J.K., Roberts, K.A., Barnes, C., Achman, D., (1997) Radionuclides as indicators of particle and carbon dynamics on East Greenland Shelf. In: P. Germain, J.C. Guarry, P. Guegueniat, H. Metivier (Eds.), Radioprotection - Colloques. Proceedings of RADOC 96-97 Radionuclides in the Ocean. Les Éditions de Physique, Cherbourg, pp. 129-136.

Conan, P., Søndergaard, M., Kragh, T., Thingstad, F., Pujo-Pay, M., Williams, P., Markager, S., Cauwet, G., Borch, N.H., Evans, D., Riemann, B., (2007) Partitioning of organic production in marine plankton communities: The effects of inorganic nutrient ratios and community composition on new dissolved organic matter. *Limnology and Oceanography*, 52(2), 753-765.

Conley, D.J., (1998) An interlaboratory comparison for the measurement of biogenic silica in sediments. *Marine Chemistry*, 63(1-2), 39-48.

Cooper, L.H.N., (1935) Iron in the sea and in marine plankton. *Proceedings of the Royal Society of London, Series B*, 118(810), 419-438.

Coppola, L., Roy-Barman, M., Mulsow, S., Povinec, P., Jeandel, C., (2005) Low particulate organic carbon export in the frontal zone of the Southern Ocean (Indian sector) revealed by ^{234}Th. *Deep-Sea Research I*, 52(1), 51-68.

D'Elia, C.F., Steudler, P.A., Corwin, N., (1977) Determination of total nitrogen in aqueous samples using persulfate digestion. *Limnology and Oceanography*, 22(4), 760-764.

Dagg, M.J., Urban-Rich, J., Peterson, J.O., (2003) The potential contribution of fecal pellets from large copepods to the flux of biogenic silica and particulate organic carbon in the Antarctic Polar Front region near 170°W. *Deep-Sea Research II*, 50(3-4), 675-691.

de Baar, H.J.W., Boyd, P.W., Coale, K.H., Landry, M.R., Tsuda, A., Assmy, P., Bakker, D.C.E., Bozec, Y., Barber, R.T., Brzezinski, M.A., Buesseler, K.O., Boye, M., Croot, P.L., Gervais, F., Gorbunov, M.Y., Harrison, P.J., Hiscock, W.T., Laan, P., Lancelot, C., Law, C.S., Levasseur, M., Marchetti, A., Millero, F.J., Nishioka, J., Nojiri, Y., van Oijen, T., Riebesell, U., Rijkenberg, M.J.A., Saito, H., Takeda, S., Timmermans, K.R., Veldhuis, M.J.W., Waite, A.M., Wong, C.S., (2005) Synthesis of iron fertilization experiments: From the Iron Age in the Age of Enlightenment. *Journal of Geophysical Research-Oceans*, 110(C9), C09S16.

de Baar, H.J.W., Buma, A.G.J., Nolting, R.F., Cadee, G.C., Jacques, G., Treguer, P.J., (1990) On iron limitation of the Southern Ocean - experimental observations in the Weddell and Scotia Seas. *Marine Ecology Progress Series*, 65(2), 105-122.

Deacon, G., (1984) The Antarctic circumpolar ocean. Cambridge University Press, Cambridge.

Delanghe, D., Bard, E., Hamelin, B., (2002) New TIMS constraints on the uranium-238 and uranium-234 in seawaters from the main ocean basins and the Mediterranean Sea. *Marine Chemistry*, 80(1), 79-93.

DeMaster, D.J., (1981) The supply and accumulation of silica in the marine environment. *Geochimica Et Cosmochimica Acta*, 45(10), 1715-1732.

Denman, K.L., Brasseur, G., Chidthaisong, A., Ciais, P., Cox, P.M., Dickinson, R.E., Hauglustaine, D., Heinze, C., Holland, E., Jacob, D., U. Lohmann, Ramachandran, S., Dias, P.L.d.S., Wofsy, S.C., X. Zhang, (2007) Couplings Between Changes in the Climate System and Biogeochemistry. In: S. Solomon, M.M. D. Qin, Z. Chen, M. Marquis, K.B. Averyt, M.Tignor, H.L. Miller (Eds.), Climate Change 2007: The Physical Science Basis. Contribution of Working Group I to the Fourth Assessment Report of the Intergovernmental Panel on Climate Change. Cambridge University Press, Cambridge, United Kingdom.

Diaz, F., Raimbault, P., (2000) Nitrogen regeneration and dissolved organic nitrogen release during spring in a NW Mediterranean coastal zone (Gulf of Lions): implications for the estimation of new production. *Marine Ecology Progress Series*, 197, 51-65.

Dickson, A.G., Sabine, C.L., Christian, J.R., (Eds.), (2007) PICES Special Publication 3: Guide to best practices for ocean CO_2 measurements.

Discovery-Reports, (1929) Discovery investigations station list 1925-1927, University Press of Cambridge.

DiTullio, G.R., Grebmeier, J.M., Arrigo, K.R., Lizotte, M.P., Robinson, D.H., Leventer, A., Barry, J.B., VanWoert, M.L., Dunbar, R.B., (2000) Rapid and early export of *Phaeocystis antarctica* blooms in the Ross Sea, Antarctica. *Nature*, 404(6778), 595-598.

Donaghay, P.L., Liss, P.S., Duce, R.A., Kester, D.R., Hanson, A.K., Villareal, T., Tindale, N.W., Gifford, D.J., (1991) The role of episodic atmospheric nutrient inputs in the chemical and biological dynamics of ocean ecosystems. *Oceanography*, 4(2), 62-70.

Dore, J.E., Karl, D.M., (1996) Nitrification in the euphotic zone as a source for nitrite, nitrate, and nitrous oxide at Station ALOHA. *Limnology and Oceanography*, 41(8), 1619-1628.

Dore, J.E., Lukas, R., Sadler, D.W., Karl, D.M., (2003) Climate-driven changes to the atmospheric CO_2 sink in the subtropical North Pacific Ocean. *Nature*, 424(6950), 754-757.

Dore, J.E., Popp, B.N., Karl, D.M., Sansone, F.J., (1998) A large source of atmospheric nitrous oxide from subtropical North Pacific surface waters. *Nature*, 396(6706), 63-66.

Duce, R.A., Tindale, N.W., (1991) Atmospheric Transport of Iron and Its Deposition in the Ocean. *Limnology and Oceanography*, 36(8), 1715-1726.

Dugdale, R.C., Goering, J.J., (1967) Uptake of new and regenerated forms of nitrogen in primary productivity. *Limnology and Oceanography*, 12(2), 196-206.

Dugdale, R.C., Menzel, D.W., Ryther, J.H., (1961) Nitrogen fixation in the Sargasso Sea. *Deep-Sea Research*, 7(4), 297-300.

Dugdale, R.C., Wilkerson, F.P., Minas, H.J., (1995) The role of a silicate pump in driving new production. *Deep-Sea Research I*, 42(5), 697-719.

Dunne, J.P., Murray, J.W., (1999) Sensitivity of ^{234}Th export to physical processes in the central equatorial Pacific. *Deep-Sea Research I*, 46(5), 831-854.

Ehrhardt, M., Koeve, W., (1999) Determination of particulate organic carbon and nitrogen. In: K. Grasshoff, K. Kremling, M. Ehrhardt (Eds.), Methods of Seawater Analysis. Wiley-VCH, Wienheim, pp. chapter 17.

El-Sayed, S.Z., Biggs, D.C., Holm-Hansen, O., (1983) Phytoplankton standing crop, primary productivity, and near-surface nitrogenous nutrient fields in the Ross Sea, Antarctica. *Deep Sea Research Part A. Oceanographic Research Papers*, 30(8), 871-886.

Eppley, R.W., Peterson, B.J., (1979) Particulate organic matter flux and planktonic new production in the deep ocean. *Nature*, 282(5740), 677-680.

Falkowski, P.G., Barber, R.T., Smetacek, V., (1998) Biogeochemical controls and feedbacks on ocean primary production. *Science*, 281(5374), 200-206.

Falkowski, P.G., Davis, C.S., (2004) Natural proportions. *Nature*, 431(7005), 131.

Falkowski, P.G., Laws, E.A., Barber, R.T., Murray, J.W., (2003) Phytoplankton and their role in primary, new, and export production. In: M.J.R. Fasham (Ed.), Ocean Biogeochemisrty. Springer-Verlag, Berlin.

Faure, G., (1986) Principles of Isotope Geology. John Wiley & Sons, New York.

Fielding, S., Ward, P., Pollard, R.T., Seeyave, S., Read, J.F., Hughes, J.A., Smith, T., Castellani, C., (2007) Community structure and grazing impact of mesozooplankton during late spring/early summer 2004/2005 in the vicinity of the Crozet Islands (Southern Ocean). *Deep-Sea Research II*, 54(18-20), 2106-2125.

Fleming, R.H., (1940) The compostion of plankton and units for reporting populations and production, Proceedings of the Sixth Pacific Science Congress of the Pacific Science Association, pp. 535-540.

Fowler, S.W., Knauer, G.A., (1986) Role of large particles in the transport of elements and organic compounds through the oceanic water column. *Progress in Oceanography*, 16(3), 147-194.

Franck, V.M., Brzezinski, M.A., Coale, K.H., Nelson, D.M., (2000) Iron and silicic acid concentrations regulate Si uptake north and south of the Polar Frontal Zone in the Pacific Sector of the Southern Ocean. *Deep-Sea Research II*, 47(15-16), 3315-3338.

Francois, R., Honjo, S., Krishfield, R., Manganini, S., (2002) Factors controlling the flux of organic carbon to the bathypelagic zone of the ocean. *Global Biogeochemical Cycles*, 16(4), 1087.

Garabato, A.C.N., Polzin, K.L., King, B.A., Heywood, K.J., Visbeck, M., (2004) Widespread intense turbulent mixing in the southern ocean. *Science*, 303(5655), 210-213.

Gardner, W.D., Richardson, M.J., Carlson, C.A., Hansell, D., Mishonov, A.V., (2003) Determining true particulate organic carbon: bottles, pumps and methodologies. *Deep-Sea Research II*, 50(3-4), 655-674.

Geider, R.J., La Roche, J., (1994) The role of iron in phytoplankton photosynthesis, and the potential for iron-limitation of primary productivity in the sea. *Photosynthesis Research*, 39(3), 275-301.

Geider, R.J., La Roche, J., (2002) Redfield revisited: variability of C:N:P in marine microalgae and its biochemical basis. *European Journal of Phycology*, 37(1), 1-17.

Gervais, F., Riebesell, U., Gorbunov, M.Y., (2002) Changes in primary productivity and chlorophyll *a* in response to iron fertilization in the Southern Polar Frontal Zone. *Limnology and Oceanography*, 47(5), 1324-1335.

Glibert, P.M., Lipschultz, F., McCarthy, J.J., Altabet, M.A., (1982) Isotope dilution models of uptake and remineralization of ammonium by marine plankton. *Limnology and Oceanography*, 27(4), 639-650.

Gran, H.H., (1931) On the conditions for the production of plankton in the sea. *Rapports et Procès-Verbaux des Réunions*, 75, 37-46.

Greene, R.M., Geider, R.J., Falkowski, P.G., (1991) Effect of iron limitation on photosynthesis in a marine diatom. *Limnology and Oceanography*, 36(8), 1772-1782.

Gross, M.G., Gross, E., (1996) Oceanography: A View of the Earth. Prentice-Hall Inc, New Jersey.

Gustafsson, O., Buesseler, K.O., Geyer, W.R., Moran, S.B., Gschwend, P.M., (1998) An assessment of the relative importance of horizontal and vertical transport of particle-reactive chemicals in the coastal ocean. *Continental Shelf Research*, 18(7), 805-829.

Haidar, A.T., Thierstein, H.R., Deuser, W.G., (2000) Calcareous phytoplankton standing stocks, fluxes and accumulation in Holocene sediments off Bermuda (N. Atlantic). *Deep-Sea Research II*, 47(9-11), 1907-1938.

Hansell, D.A., Waterhouse, T.Y., (1997) Controls on the distributions of organic carbon and nitrogen in the eastern Pacific Ocean. *Deep-Sea Research I*, 44(5), 843-857.

Hansen, H.P., Koroleff, F., (1999) Determination of nutrients. In: K. Grasshoff, K. Kremling, M. Ehrhardt (Eds.), Methods of Seawater Analysis. Wiley-VCH, Weinheim, pp. chapter 10.

Hart, T.J., (1934) The phytoplankton of the South-West Atlantic and the Bellingshausen Sea. *Discovery Reports*, 8, 1-268.

Hart, T.J., (1942) Phytoplankton periodicity in Antarctic surface waters. *Discovery Reports*, 21, 261-356.

Harvey, H.W., (1933) On the rate of diatom growth. *Journal of the Marine Biological Association*, 19(1), 253-276.

Harvey, H.W., (1937) The supply of iron to diatoms. *Journal of the Marine Biological Association*, 22(1), 205-219.

Hedges, J., Lee, C., Wangersky, P., (1993) On the measurement of DOC and DON in seawater - Comment. *Marine Chemistry*, 41(1-3), 289-290.

Hilton, J., Lishman, J.P., Mackness, S., Heaney, S.I., (1986) An automated method for the analysis of 'particulate' carbon and nitrogen in natural waters. *Hydrobiologia*, 141(3), 269-271.

Ho, T.Y., Quigg, A., Finkel, Z.V., Milligan, A.J., Wyman, K., Falkowski, P.G., Morel, F.M.M., (2003) The elemental composition of some marine phytoplankton. *Journal of Phycology*, 39(6), 1145-1159.

Hoffmann, L.J., Peeken, I., Lochte, K., Assmy, P., Veldhuis, M., (2006) Different reactions of Southern Ocean phytoplankton size classes to iron fertilization. *Limnology and Oceanography*, 51(3), 1217-1229.

Holeton, C.L., Nedelec, F., Sanders, R., Brown, L., Moore, C.M., Stevens, D.P., Heywood, K.J., Statham, P.J., Lucas, C.H., (2005) Physiological state of phytoplankton communities in the Southwest Atlantic sector of the Southern Ocean, as measured by fast repetition rate fluorometry. *Polar Biology*, 29(1), 44-52.

Honjo, S., Doherty, K.W., (1988) Large aperture time-series sediment traps; design objectives, construction and application. *Deep-Sea Research Part A*, 35(1), 133-149.

Hood, R.R., Coles, V.J., Capone, D.G., (2004) Modeling the distribution of *Trichodesmium* and nitrogen fixation in the Atlantic Ocean. *Journal of Geophysical Research-Oceans*, 109(C6), C06006.

Howard, A.G., Statham, P.J., (1993) Inorganic Trace Analysis: Phylosophy and Practice. John Wiley & Sons Ltd, Chichester.

Hu, S., Smith, W.O., (1998) The effects of irradiance on nitrate uptake and dissolved organic nitrogen release by phytoplankton in the Ross Sea. *Continental Shelf Research*, 18(9), 971-990.

Hubberten, U., Lara, R.J., Kattner, G., (1995) Refractory organic compounds in polar waters: Relationship between humic substances and amino acids in the Arctic and Antarctic. *Journal of Marine Research*, 53(1), 137-149.

Iglesias-Rodriguez, M.D., Halloran, P.R., Rickaby, R.E.M., Hall, I.R., Colmenero-Hidalgo, E., Gittins, J.R., Green, D.R.H., Tyrrell, T., Gibbs, S.J., von Dassow, P., Rehm, E., Armbrust, E.V., Boessenkool, K.P., (2008) Phytoplankton calcification in a high-CO_2 world. *Science*, 320(5874), 336-340.

Jacobson, M.Z., (2005) Studying ocean acidification with conservative, stable numerical schemes for nonequilibrium air-ocean exchange and ocean equilibrium chemistry. *Journal of Geophysical Research-Atmospheres*, 110(D7), D07302.

Jenkins, W.J., Naveira, A., Schlosser, P., Lott, D.E., Newton, R., (2007) Oceanic volcanic ^{3}He: where is it going?, EOS, Transactions, American Geophysical Union, Fall Meet, Suppl., pp. Abstract OS32A-02.

Jennings, J.C., Gordon, L.I., Nelson, D.M., (1984) Nutrient depletion indicates high primary productivity in the Weddell Sea. *Nature*, 309(5963), 51-54.

Johnson, K.M., Sieburth, J.M., Williams, P.J.L., Brandstrom, L., (1987) Coulometric total carbon dioxide analysis for marine studies: Automation and calibration. *Marine Chemistry*, 21(2), 117-133.

Johnson, K.S., Gordon, R.M., Coale, K.H., (1997) What controls dissolved iron concentrations in the world ocean? *Marine Chemistry*, 57(3-4), 137-161.

Johnson, K.S., Karl, D.M., (2002) Is ocean fertilization credible and creditable? *Science*, 296(5567), 467-467.

Joos, F., Sarmiento, J.L., Siegenthaler, U., (1991a) Estimates of the effect of Southern Ocean iron fertilization on atmospheric CO_2 concentrations. *Nature*, 349(6312), 772-775.

Joos, F., Siegenthaler, U., Sarmiento, J.L., (1991b) Possible effects of iron fertilization in the Southern Ocean on atmospheric CO_2 concentration. *Global Biogeochemical Cycles*, 5(2), 135-150.

Kähler, P., Bjornsen, P.K., Lochte, K., Antia, A., (1997) Dissolved organic matter and its utilization by bacteria during spring in the Southern Ocean. *Deep-Sea Research II*, 44(1-2), 341-353.

Kaufman, A., Li, Y.-H., Turekian, K.K., (1981) The removal rates of ^{234}Th and ^{228}Th from waters of the New York Bight. *Earth and Planetary Science Letters*, 54(3), 385-392.

Keeling, C.D., Whorf, T.P., Wahlen, M., Vanderplicht, J., (1995) Interannual Extremes in the Rate of Rise of Atmospheric Carbon-Dioxide since 1980. *Nature*, 375(6533), 666-670.

Kirkwood, D., (1996) Nutrients: Practical notes on their determination in sea water. *ICES Techniques in Marine Environmental Sciences*, 17, 1-25.

Klaas, C., Archer, D.E., (2002) Association of sinking organic matter with various types of mineral ballast in the deep sea: Implications for the rain ratio. *Global Biogeochemical Cycles*, 16(4), 1116.

Knauer, G.A., Martin, J.H., Bruland, K.W., (1979) Fluxes of particulate carbon, nitrogen, and phosphorus in the upper water column of the northeast Pacific. *Deep-Sea Research*, 26(1), 97-108.

Korb, R.E., Whitehouse, M., (2004) Contrasting primary production regimes around South Georgia, Southern Ocean: large blooms versus high nutrient, low chlorophyll waters. *Deep-Sea Research I*, 51(5), 721-738.

Krishnaswami, S., (2001) Uranium-Thorium series isotopes in ocean profiles. In: J.H. Steele, K.K. Turekian, S.A. Thorpe (Eds.), Encyclopedia of Ocean Sciences. Academic Press, pp. 3146-3156.

Ku, T.L., Knauss, K.G., Mathieu, G.G., (1977) Uranium in open ocean: concentration and isotopic composition. *Deep-Sea Research*, 24(11), 1005-1017.

Lam, P.J., Bishop, J.K.B., (2007) High biomass, low export regimes in the Southern Ocean. *Deep-Sea Research II*, 54(5-7), 601-638.

Law, C.S., Abraham, E.R., Watson, A.J., Liddicoat, M.I., (2003) Vertical eddy diffusion and nutrient supply to the surface mixed layer of the Antarctic Circumpolar Current. *Journal of Geophysical Research-Oceans*, 108(C8), 3272.

Ledford-Hoffman, P.A., Demaster, D.J., Nittrouer, C.A., (1986) Biogenic silica accumulation in the Ross Sea and the importance of Antarctic continental shelf deposits in the marine silica budget. *Geochimica et Cosmochimica Acta*, 50(9), 2099-2110.

Lewin, J.C., (1962) Silicification. In: R.A. Lewin (Ed.), Physiology and Biochemistry of Algae. Academic Press, New York, pp. 929.

Libes, S.M., (1992) An Introduction to Marine Biogeochemistry. John Wiley & Sons, Inc, New York.

Liebig, J., (1847) Chemistry in its Application to Agriculture and Physiology. Taylor and Walton, London.

Liu, Z.F., Stewart, G., Cochran, J.K., Lee, C., Armstrong, R.A., Hirschberg, D.J., Gasser, B., Miquel, J.C., (2005) Why do POC concentrations measured using Niskin bottle collections sometimes differ from those using in-situ pumps? *Deep-Sea Research I*, 52(7), 1324-1344.

Loh, A.N., Bauer, J.E., (2000) Distribution, partitioning and fluxes of dissolved and particulate organic C, N and P in the eastern North Pacific and Southern Oceans. *Deep-Sea Research I*, 47(12), 2287-2316.

Lucas, M., Seeyave, S., Sanders, R., Moore, C.M., Williamson, R., Stinchcombe, M., (2007) Nitrogen uptake responses to a naturally Fe-fertilised phytoplankton bloom during the 2004/2005 CROZEX study. *Deep-Sea Research II*, 54(18-20), 2138-2173.

Luz, B., Barkan, E., (2000) Assessment of oceanic productivity with the triple-isotope composition of dissolved oxygen. *Science*, 288(5473), 2028-2031.

Martin, J.H., (1990) Glacial-Interglacial CO_2 Change: The Iron Hypothesis. *Paleoceanography*, 5(1), 1-13.

Martin, J.H., (1991) Iron, Liebig's Law and The Greenhouse. *Oceanography*, 4(2), 52-55.

Martin, J.H., Coale, K.H., Johnson, K.S., Fitzwater, S.E., Gordon, R.M., Tanner, S.J., Hunter, C.N., Elrod, V.A., Nowicki, J.L., Coley, T.L., Barber, R.T., Lindley, S., Watson, A.J., Vanscoy, K., Law, C.S., Liddicoat, M.I., Ling, R., Stanton, T., Stockel, J., Collins, C., Anderson, A., Bidigare, R., Ondrusek, M., Latasa, M., Millero, F.J., Lee, K., Yao, W., Zhang, J.Z., Friederich, G., Sakamoto, C., Chavez, F., Buck, K., Kolber, Z., Greene, R., Falkowski, P., Chisholm, S.W., Hoge, F., Swift, R., Yungel, J., Turner, S., Nightingale, P., Hatton, A., Liss, P., Tindale, N.W., (1994) Testing the iron hypothesis in ecosystems of the Equatorial Pacific Ocean. *Nature*, 371(6493), 123-129.

Martin, J.H., Fitzwater, S.E., Gordon, R.M., (1990a) Iron deficiency limits phytoplankton growth in Antarctic waters. *Global Biogeochemical Cycles*, 5(1), 5-12.

Martin, J.H., Gordon, R.M., Fitzwater, S.E., (1990b) Iron in Antarctic Waters. *Nature*, 345(6271), 156-158.

Menzel, D.W., Vaccaro, R.F., (1964) The measurement of dissolved organic and particulate carbon in seawater. *Limnology and Oceanography*, 9(1), 138-142.

Metzl, N., Tilbrook, B., Poisson, A., (1999) The annual fCO_2 cycle and the air-sea CO_2 flux in the sub-Antarctic Ocean. *Tellus*, 51B(4), 849-861.

Miller, J.N., Miller, J.C., (2000) Statistics and Chemometrics for Analytical Chemistry. Pearson, Harlow.

Moore, C.M., Hickman, A.E., Poulton, A.J., Seeyave, S., Lucas, M.I., (2007a) Iron-light interactions during the CROZet natural iron bloom and EXport experiment (CROZEX): II - Taxonomic responses and elemental stoichiometry. *Deep-Sea Research II*, 54(18-20), 2066-2084.

Moore, C.M., Seeyave, S., Hickman, A.E., Allen, J.T., Lucas, M.I., Planquette, H., Pollard, R.T., Poulton, A.J., (2007b) Iron-light interactions during the CROZet natural iron bloom and EXport experiment (CROZEX) I: Phytoplankton growth and photophysiology. *Deep-Sea Research II*, 54(18-20), 2045-2065.

Moore, W.S., (2000) Determining coastal mixing rates using radium isotopes. *Continental Shelf Research*, 20(15), 1993-2007.

Moran, S.B., Buesseler, K.O., (1993) Size-fractionated ^{234}Th in continental shelf waters off New England: Implications for the role of colloids in oceanic trace metal scavenging. *Journal of Marine Research*, 51(4), 893-922.

Moran, S.B., Charette, M.A., Pike, S.M., Wicklaund, C.A., (1999) Differences in seawater particulate organic carbon concentration in samples collected using small- and large- volume methods: the importance of DOC adsorption to the filter blank. *Marine Chemistry*, 67(1-2), 33-42.

Morris, P.J., Sanders, R., Turnewitsch, R., Thomalla, S., (2007) ^{234}Th-derived particulate organic carbon export from an island-induced phytoplankton bloom in the Southern Ocean. *Deep-Sea Research II*, 54(18-20), 2208-2232.

Mortlock, R.A., Froelich, P.N., (1989) A simple method for the rapid determination of biogenic opal in pelagic marine sediments. *Deep-Sea Research Part A*, 36(9), 1415-1426.

Murray, J.W., Downs, J.N., Strom, S., Wei, C.L., Jannasch, H.W., (1989) Nutrient assimilation, export production and ^{234}Th scavenging in the eastern equatorial Pacific. *Deep-Sea Research Part A*, 36(10), 1471-1489.

Nayar, S., Chou, L.M., (2003) Relative efficiencies of different filters in retaining phytoplankton for pigment and productivity studies. *Estuarine Coastal and Shelf Science*, 58(2), 241-248.

Neftel, A., Moor, E., Oeschger, H., Stauffer, B., (1985) Evidence from polar ice cores for the increase in atmospheric CO_2 in the past 2 centuries. *Nature*, 315(6014), 45-47.

Nelson, D.M., Smith, W.O., (1986) Phytoplankton bloom dynamics of the western Ross Sea ice edge–II. Mesoscale cycling of nitrogen and silicon. *Deep-Sea Research Part A*, 33(10), 1389-1412.

Nevison, C., Butler, J.H., Elkins, J.W., (2003) Global distribution of N_2O and the ΔN_2O-AOU yield in the subsurface ocean. *Global Biogeochemical Cycles*, 17(4), 1119.

Newton, P.P., Lampitt, R.S., Jickells, T.D., King, P., Boutle, C., (1994) Temporal and spatial variability of biogenic particle fluxes during the JGOFS northeast Atlantic process studies at 47°N, 20°W. *Deep-Sea Research I*, 41(11-12), 1617-1642.

Nodder, S.D., Charette, M.A., Waite, A.M., Trull, T.W., Boyd, P.W., Zeldis, J., Buesseler, K.O., (2001) Particle transformations and export flux during an in situ iron-stimulated algal bloom in the Southern Ocean. *Geophysical Research Letters*, 28(12), 2409-2412.

Northcote, L.C., Neil, H.L., (2005) Seasonal variations in foraminiferal flux in the Southern Ocean, Campbell Plateau, New Zealand. *Marine Micropaleontology*, 56(3-4), 122-137.

Nowlin, W.D., Klinck, J.M., (1986) The physics of the Antarctic Circumpolar Current. *Reviews of Geophysics*, 24(3), 469-491.

Ogawa, H., Fukuda, R., Koike, I., (1999) Vertical distributions of dissolved organic carbon and nitrogen in the Southern Ocean. *Deep-Sea Research I*, 46(10), 1809-1826.

Orr, J.C., Fabry, V.J., Aumont, O., Bopp, L., Doney, S.C., Feely, R.A., Gnanadesikan, A., Gruber, N., Ishida, A., Joos, F., Key, R.M., Lindsay, K., Maier-Reimer, E., Matear, R., Monfray, P., Mouchet, A., Najjar, R.G., Plattner, G.K., Rodgers, K.B., Sabine, C.L., Sarmiento, J.L., Schlitzer, R., Slater, R.D., Totterdell, I.J., Weirig, M.F., Yamanaka, Y., Yool, A., (2005) Anthropogenic ocean acidification over the twenty-first century and its impact on calcifying organisms. *Nature*, 437(7059), 681-686.

Orsi, A.H., Whitworth, T., Nowlin, W.D., (1995) On the meridional extent and fronts of the Antarctic Circumpolar Current. *Deep-Sea Research I*, 42(5), 641-673.

Pan, X., (2007) The marine biogeochemistry of dissolved organic carbon and dissolved organic nutrients in the Atlantic Ocean. PhD Thesis, University of Southampton, Southampton.

Pan, X., Sanders, R., Tappin, A.D., Worsfold, P.J., Achterberg, E.P., (2005) Simultaneous determination of dissolved organic carbon and total dissolved nitrogen on a coupled high-temperature combustion total organic carbon-nitrogen chemiluminescence detection (HTC TOC-NCD) system. *Journal of Automated Methods & Management in Chemistry*(4), 240-246.

Passow, U., (2004) Switching perspectives: Do mineral fluxes determine particulate organic carbon fluxes or vice versa? *Geochemistry Geophysics Geosystems*, 5(4), Q04002.

Passow, U., De la Rocha, C.L., (2006) Accumulation of mineral ballast on organic aggregates. *Global Biogeochemical Cycles*, 20(1), GB1013.

Peng, T.H., Broecker, W.S., (1991a) Dynamic limitations on the Antarctic iron fertilization strategy. *Nature*, 349(6306), 227-229.

Peng, T.H., Broecker, W.S., (1991b) Factors limiting the reduction of atmospheric CO_2 by iron fertilization. *Limnology and Oceanography*, 36(8), 1919-1927.

Peterson, M.L., Wakeham, S.G., Lee, C., Askea, M.A., Miquel, J.C., (2005) Novel techniques for collection of sinking particles in the ocean and determining their settling rates. *Limnology and Oceanography: Methods*, 3, 520-532.

Pike, S.M., Buesseler, K.O., Andrews, J., Savoye, N., (2005) Quantification of ^{234}Th recovery in small volume sea water samples by inductively coupled plasma mass spectrometry. *Journal of Radioanalytical and Nuclear Chemistry*, 263(2), 355-360.

Planquette, H., (2008) Iron biogeochemistry in the waters surrounding the Crozet Islands, Southern Ocean. PhD Thesis, University of Southampton, Southampton.

Planquette, H., Statham, P.J., Fones, G.R., Charette, M.A., Moore, C.M., Salter, I., Nedelec, F.H., Taylor, S.L., French, M., Baker, A.R., Mahowald, N., Jickells, T.D., (2007) Dissolved iron in the vicinity of the Crozet Islands, Southern Ocean. *Deep-Sea Research II*, 54(18-20), 1999-2019.

Pollard, R., Sanders, R., Lucas, M., Statham, P., (2007a) The crozet natural iron bloom and EXport experiment (CROZEX). *Deep-Sea Research II*, 54(18-20), 1905-1914.

Pollard, R.T., Lucas, M.I., Read, J.F., (2002) Physical controls on biogeochemical zonation in the Southern Ocean. *Deep-Sea Research II*, 49(16), 3289-3305.

Pollard, R.T., Read, J.F., (2001) Circulation pathways and transports of the Southern Ocean in the vicinity of the Southwest Indian Ridge. *Journal of Geophysical Research-Oceans*, 106(C2), 2881-2898.

Pollard, R.T., Sanders, R., (2006) RRS *Discovery* cruises 285/286, 3 Nov - 10 Dec 2004, 13 Dec 2004 - 21 Jan 2005: CROZet circulation, iron fertilization and EXport production experiment (CROZEX). Cruise report No. 60, Southampton Oceanography Centre, Southampton.

Pollard, R.T., Venables, H.J., Read, J.F., Allen, J.T., (2007b) Large-scale circulation around the Crozet Plateau controls an annual phytoplankton bloom in the Crozet Basin. *Deep-Sea Research II*, 54(18-20), 1915-1929.

Poulton, A.J., Moore, C.M., Seeyave, S., Lucas, M.I., Fielding, S., Ward, P., (2007) Phytoplankton community composition around the Crozet Plateau, with emphasis on diatoms and Phaeocystis. *Deep-Sea Research II*, 54(18-20), 2085-2105.

Prentice, I.C., Farquhar, G.D., Fasham, M.J.R., Goulden, M.L., Heimann, M., Jaramillo, V.J., Kheshgi, H.S., Le Quéré, C., Scholes, R.J., Wallace, D.W.R., (2001) The carbon cycle and atmospheric carbon dioxide. In: J.T. Houghton, Y. Ding, D.J. Griggs, M. Noguer, P.J. van der Linden, X. Dai, K. Maskell, C.A. Johnson (Eds.), Climate Change 2001: The Scientific Basis. Contributions of Working Group I to the Third Assessment Report of the International Panel on Climate Change. Cambridge University Press, Cambridge, pp. chapter 3.

Price, N.M., (2005) The elemental stoichiometry and composition of an iron-limited diatom. *Limnology and Oceanography*, 50(4), 1159-1171.

Primeau, F., (2005) Characterizing transport between the surface mixed layer and the ocean interior with a forward and adjoint global ocean transport model. *Journal of Physical Oceanography*, 35(4), 545-564.

Ragueneau, O., Savoye, N., Del Amo, Y., Cotten, J., Tardiveau, B., Leynaert, A., (2005) A new method for the measurement of biogenic silica in suspended matter of coastal waters: using Si:Al ratios to correct for the mineral interference. *Continental Shelf Research*, 25(5-6), 697-710.

Ragueneau, O., Treguer, P., (1994) Determination of biogenic silica in coastal waters: applicability and limits of the alkaline digestion method. *Marine Chemistry*, 45(1-2), 43-51.

Raven, J.A., Falkowski, P.G., (1999) Oceanic sinks for atmospheric CO_2. *Plant Cell and Environment*, 22(6), 741-755.

Read, J.F., Pollard, R.T., Allen, J.T., (2007) Sub-mesoscale structure and the development of an eddy in the Subantarctic Front north of the Crozet Islands. *Deep-Sea Research II*, 54(18-20), 1930-1948.

Redfield, A.C., (1934a) James Johnstone Memorial Volume. Lancashire Sea-Fisheries Laborotory. *Nature*, 134(3394), 753-754.

Redfield, A.C., (1934b) On the proportions of organic derivatives in sea water and their relation to the composition of plankton. In: R.J. Daniel (Ed.), James Johnstone Memorial Volume. University Press of Liverpool, Liverpool, pp. 176-192.

Redfield, A.C., (1958) The biological control of chemical factors in the environment. *American Scientist*, 46(3), 205-221.

Redfield, A.C., Ketchum, B.H., Richards, F.A., (1963) The influence of organisms on the composition of sea-water. In: M.N. Hill, E.D. Goldberg, C.O.D. Iselin (Eds.), Composition of Sea-water: Comparitive and Descriptive Oceanography. Interscience, New York, pp. 26-77.

Rengarajan, R., Sarin, M.M., Krishnaswami, S., (2003) Uranium in the Arabian Sea: role of denitrification in controlling its distribution. *Oceanologica Acta*, 26(5-6), 687-693.

Riebesell, U., Zondervan, I., Rost, B., Tortell, P.D., Zeebe, R.E., Morel, F.M.M., (2000) Reduced calcification of marine plankton in response to increased atmospheric CO_2. *Nature*, 407(6802), 364-367.

Roussenov, V., Williams, R.G., Mahaffey, C., Wolff, G.A., (2006) Does the transport of dissolved organic nutrients affect export production in the Atlantic Ocean? *Global Biogeochemical Cycles*, 20(3), GB3002.

Rutgers van der Loeff, M., Sarin, M.M., Baskaran, M., Benitez-Nelson, C., Buesseler, K.O., Charette, M., Dai, M., Gustafsson, O., Masque, P., Morris, P.J., Orlandini, K., Baena, A.R.Y., Savoye, N., Schmidt, S., Turnewitsch, R., Voge, I., Waples, J.T., (2006) A review of present techniques and methodological advances in analyzing ^{234}Th in aquatic systems. *Marine Chemistry*, 100(3-4), 190-212.

Rutgers van der Loeff, M., Vöge, I., (2001) Does Fe fertilisation enhance the export production as measured through the ^{234}Th/^{238}U disequilibrium in surface water? *Reports on Polar and Marine Research*, 400, 222-225.

Rutgers van der Loeff, M.M., (2001) Uranium-Thorium decay series in the oceans overview. In: J.H. Steele, K.K. Turekian, S.A. Thorpe (Eds.), Encyclopedia of Ocean Sciences. Academic Press, pp. 3135-3145.

Rutgers van der Loeff, M.M., Buesseler, K., Bathmann, U., Hense, I., Andrews, J., (2002) Comparison of carbon and opal export rates between summer and spring bloom periods in the region of the Antarctic Polar Front, SE Atlantic. *Deep-Sea Research II*, 49(18), 3849-3869.

Rutgers van der Loeff, M.M., Friedrich, J., Bathmann, U.V., (1997) Carbon export during the Spring Bloom at the Antarctic Polar Front, determined with the natural tracer ^{234}Th. *Deep-Sea Research II*, 44(1-2), 457-478.

Rutgers van der Loeff, M.M., Moore, W.S., (1999) Determination of natural radioactive tracers. In: K. Grasshoff, K. Kremling, M. Ehrhardt (Eds.), Methods of Seawater Analysis. Wiley-VCH, Weinheim, pp. chapter 13.

Ruud, J.T., (1930) Nitrates and phosphates in the Southern Sea. *ICES Journal of Marine Science. Journal du Conseil*, 5(3), 347-360.

Salter, I., (2007) Particle fluxes in the north-east Atlantic and the Southern Ocean. PhD Thesis, University of Southampton, Southampton.

Salter, I., Lampitt, R.S., Sanders, R., Poulton, A., Kemp, A.E.S., Boorman, B., Saw, K., Pearce, R., (2007) Estimating carbon, silica and diatom export from a naturally fertilised phytoplankton bloom in the Southern Ocean using PELAGRA: A novel drifting sediment trap. *Deep-Sea Research II*, 54(18-20), 2233-2259.

Sanders, R., Brown, L., Henson, S., Lucas, M., (2005) New production in the Irminger Basin during 2002. *Journal of Marine Systems*, 55(3-4), 291-310.

Sanders, R., Jickells, T., (2000) Total organic nutrients in Drake Passage. *Deep-Sea Research I*, 47(6), 997-1014.

Sanders, R., Lampitt, R., Boorman, B., Brown, L., Guyard, P., Leaute, F., Popova, E., Saw, K., Turnewitsch, R., Zubkov, M., (2003) Particle export in the North Atlantic: an integrated attack using production rates, tracers and a novel drifting sediment trap. Ocean Sciences Meeting, Portland, Oregon. Eos, Transactions, AGU, 84(52), Abstract OS32L-02.

Sanders, R., Morris, P.J., Stinchcombe, M., Seeyave, S., Venables, H., Lucas, M., (2007) New production and the *f* ratio around the Crozet Plateau in austral summer 2004-2005 diagnosed from seasonal changes in inorganic nutrient levels. *Deep-Sea Research II*, 54(18-20), 2191-2207.

Santschi, P.H., Li, Y.-H., Bell, J., (1979) Natural radionuclides in the water of Narragansett Bay. *Earth and Planetary Science Letters*, 45(1), 201-213.

Sarmiento, J.L., (1991a) Oceanic uptake of anthropogenic CO_2: The major uncertainties. *Global Biogeochemical Cycles*, 5(4), 309-313.

Sarmiento, J.L., (1991b) Slowing the buildup of fossil CO_2 in the atmosphere by iron fertilization: A comment. *Global Biogeochemical Cycles*, 5(1), 1-2.

Sarmiento, J.L., Orr, J.C., (1991) Three-dimensional simulations of the impact of Southern Ocean nutrient depletion on atmospheric CO_2 and ocean chemistry. *Limnology and Oceanography*, 36(8), 1928-1950.

Sarthou, G., Timmermans, K.R., Blain, S., Treguer, P., (2005) Growth physiology and fate of diatoms in the ocean: a review. *Journal of Sea Research*, 53(1-2), 25-42.

Savoye, N., Benitez-Nelson, C., Burd, A.B., Cochran, J.K., Charette, M., Buesseler, K.O., Jackson, G.A., Roy-Barman, M., Schmidt, S., Elskens, M., (2006) ^{234}Th sorption and export models in the water column: A review. *Marine Chemistry*, 100(3-4), 234-249.

Savoye, N., Trull, T.W., Jacquet, S.H.M., Navez, J., Dehairs, F., (2008) ^{234}Th-based export fluxes during a natural iron fertilization experiment in the Southern Ocean (KEOPS). *Deep-Sea Research II*, 55(5-7), 841-855.

Schmidt, S., Reyss, J.L., (1991) Uranium concentrations of Mediterranean seawaters with high salinities. *Comptes Rendus de l'Academie des Sciences Serie II*, 312(5), 479-484.

Schuster, U., Watson, A.J., (2007) A variable and decreasing sink for atmospheric CO_2 in the North Atlantic. *Journal of Geophysical Research-Oceans*, 112(C11), C11006.

Sedwick, P.N., Blain, S., Queguiner, B., Griffiths, F.B., Fiala, M., Bucciarelli, E., Denis, M., (2002) Resource limitation of phytoplankton growth in the Crozet Basin, Subantarctic Southern Ocean. *Deep-Sea Research II*, 49(16), 3327-3349.

Seeyave, S., Lucas, M.I., Moore, C.M., Poulton, A.J., (2007) Phytoplankton productivity and community structure in the vicinity of the Crozet Plateau during austral summer 2004/2005. *Deep-Sea Research II*, 54(18-20), 2020-2044.

Sharp, J.H., (1973) Total organic carbon in seawater - comparison of measurements using persulfate oxidation and high temperature combustion. *Marine Chemistry*, 1(3), 211-229.

Sharp, J.H., (2001) Analytical Methods for Total DOM Pools. In: D.A. Hansell, C.A. Carlson (Eds.), Biogeochemistry of marine dissolved organic matter. Academic Press, San Diego, pp. chapter 2.

Sharp, J.H., Rinker, K.R., Savidge, K.B., Abell, J., Benaim, J.Y., Bronk, D., Burdige, D.J., Cauwet, G., Chen, W.H., Doval, M.D., Hansell, D., Hopkinson, C., Kattner, G., Kaumeyer, N., McGlathery, K.J., Merriam, J., Morley, N., Nagel, K., Ogawa, H., Pollard, C., Pujo-Pay, M., Raimbault, P., Sambrotto, R., Seitzinger, S., Spyres, G., Tirendi, F., Walsh, T.W., Wong, C.S., (2002) A preliminary methods comparison for measurement of dissolved organic nitrogen in seawater. *Marine Chemistry*, 78(4), 171-184.

Shimmield, G.B., Ritchie, G.D., Fileman, T.W., (1995) The impact of marginal ice zone processes on the distribution of ^{210}Pb, ^{210}Po and ^{234}Th and implications for new production in the Bellingshausen Sea, Antarctica. *Deep-Sea Research II*, 42(4-5), 1313-1335.

Simpson, H.J., (1966). Global Chemical Cycles and their Alteration. Dahlam Konferenzen, Berlin.

Simpson, W.R., (1982) Particulate matter in the oceans - Sampling methods, concentration, size distribution and particle dynamics. *Oceanography and Marine Biology*, 20, 119-172.

Skoog, A., Lara, R., Kattner, G., (2001) Spring-summer cycling of DOC, DON and inorganic N in a highly seasonal system encompassing the Northeast Water Polynya, 1993. *Deep-Sea Research I*, 48(12), 2613-2629.

Small, L.F., Fowler, S.W., Unlu, M.Y., (1979) Sinking rates of natural copepod fecal pellets. *Marine Biology*, 51(3), 233-241.

Smith, D.C., Simon, M., Alldredge, A.L., Azam, F., (1992) Intense hydrolytic enzyme activity on marine aggregates and implications for rapid particle dissolution. *Nature*, 359(6391), 139-142.

Smith, W.O., Codispoti, L.A., Nelson, D.M., Manley, T., Buskey, E.J., Niebauer, H.J., Cota, G.F., (1991) Importance of *Phaeocystis* blooms in the high-latitude ocean carbon cycle. *Nature*, 352(6335), 514-516.

Smith, W.O., Gordon, L.I., (1997) Hyperproductivity of the Ross Sea (Antarctica) polynya during austral spring. *Geophysical Research Letters*, 24(3), 233-236.

Smith, W.O., Nelson, D.M., DiTullio, G.R., Leventer, A.R., (1996) Temporal and spatial patterns in the Ross Sea: Phytoplankton biomass, elemental composition, productivity and growth rates. *Journal of Geophysical Research-Oceans*, 101(C8), 18455-18465.

Solórzano, L., Sharp, J.H., (1980) Determination of total dissolved nitrogen in natural waters. *Limnology and Oceanography*, 25(4), 751-754.

Speicher, E.A., Moran, S.B., Burd, A.B., Delfanti, R., Kaberi, H., Kelly, R.P., Papucci, C., Smith, J.N., Stavrakakis, S., Torricelli, L., Zervakis, V., (2006) Particulate organic carbon export fluxes and size-fractionated POC/^{234}Th ratios in the Ligurian, Tyrrhenian and Aegean Seas. *Deep-Sea Research I*, 53(11), 1810-1830.

Stanley, R.H.R., Buesseler, K.O., Manganini, S.J., Steinberg, D.K., Valdes, J.R., (2004) A comparison of major and minor elemental fluxes collected in neutrally buoyant and surface-tethered sediment traps. *Deep-Sea Research I*, 51(10), 1387-1395.

Steemann Nielsen, E., (1952) The use of radio-active carbon (C^{14}) for measuring organic production in the sea. *Journal du Conseil*, 18(2), 117-140.

Sunda, W.G., Huntsman, S.A., (1997) Interrelated influence of iron, light and cell size on marine phytoplankton growth. *Nature*, 390(6658), 389-392.

Suzuki, Y., (1993) On the measurement of DOC and DON in seawater. *Marine Chemistry*, 41(1-3), 287-288.

Suzuki, Y., Sugimura, Y., Itoh, T., (1985) A catalytic oxidation method for the determination of total nitrogen dissolved in seawater. *Marine Chemistry*, 16(1), 83-97.

Suzuki, Y., Tanoue, E., Ito, H., (1992) A high-temperature catalytic oxidation method for the determination of dissolved organic carbon in seawater: analysis and improvement. *Deep-Sea Research*, 39(2), 185-198.

Sweeney, C., Smith, W.O., Hales, B., Bidigare, R.R., Carlson, C.A., Codispoti, L.A., Gordon, L.I., Hansell, D.A., Millero, F.J., Park, M.O., Takahashi, T., (2000) Nutrient and carbon removal ratios and fluxes in the Ross Sea, Antarctica. *Deep-Sea Research II*, 47(15-16), 3395-3421.

Takahashi, K., (1986) Seasonal Fluxes of Pelagic Diatoms in the Sub-Arctic Pacific, 1982-1983. *Deep-Sea Research Part A*, 33(9), 1225-1251.

Tanaka, N., Takeda, Y., Tsunogai, S., (1983) Biological effect on removal of Th-234, Po-210 and Pb-210 from surface water in Funka Bay, Japan. *Geochimica et Cosmochimica Acta*, 47(10), 1783-1790.

Tande, K.S., (1985) Assimilation efficiency in herbivorous aquatic organisms - The potential of the ratio method using ^{14}C and biogenic silica as markers. *Limnology and Oceanography*, 30(5), 1093-1099.

Taylor, S.R., (1964) Abundance of chemical elements in the continental crust: a new table. *Geochimica et Cosmochimica Acta*, 28(8), 1273-1285.

Thomalla, S., Turnewitsch, R., Lucas, M., Poulton, A., (2006) Particulate organic carbon export from the North and South Atlantic gyres: The $^{234}Th/^{238}U$ disequilibrium approach. *Deep-Sea Research II*, 53(14-16), 1629-1648.

Timmermans, K.R., Davey, M.S., van der Wagt, B., Snoek, J., Geider, R.J., Veldhuis, M.J.W., Gerringa, L.J.A., de Baar, H.J.W., (2001) Co-limitation by iron and light of *Chaetoceros brevis*, *C. dichaeta* and *C. calcitrans* (Bacillariophyceae). *Marine Ecology Progress Series*, 217, 287-297.

Torres-Valdés, S., Sanders, R., Williams, R.G., Roussenov, V., McDonagh, E., McLeod, P., Landol, A.M., R., Chamberlain, K., (2008) Distribution of dissolved organic nutrients and their role in sustaining export production over the subtropical Atlantic Ocean. *Global Biogeochemical Cycles*, submitted.

Townsend, D.W., Thomas, M., (2002) Springtime nutrient and phytoplankton dynamics on Georges Bank. *Marine Ecology Progress Series*, 228, 57-74.

Treguer, P., Jacques, G., (1986) The Antarctic Ocean. *Recherche*, 17(178), 746-755.

Treguer, P., Legendre, L., Rivkin, R.T., Ragueneau, O., Dittert, N., (2003) Water column biogeochemistry below the euphotic zone. In: M.J.R. Fasham (Ed.), Ocean Biogeochemistry. Springer-Verlag, Berlin.

Tréguer, P., Nelson, D.M., Vanbennekom, A.J., Demaster, D.J., Leynaert, A., Quéguiner, B., (1995) The silica balance in the world ocean: A reestimate. *Science*, 268(5209), 375-379.

Tsuda, A., Takeda, S., Saito, H., Nishioka, J., Nojiri, Y., Kudo, I., Kiyosawa, H., Shiomoto, A., Imai, K., Ono, T., Shimamoto, A., Tsumune, D., Yoshimura, T., Aono, T., Hinuma, A., Kinugasa, M., Suzuki, K., Sohrin, Y., Noiri, Y., Tani, H., Deguchi, Y., Tsurushima, N., Ogawa, H., Fukami, K., Kuma, K., Saino, T., (2003) A mesoscale iron enrichment in the western Subarctic Pacific induces a large centric diatom bloom. *Science*, 300(5621), 958-961.

Tsunogai, S., Minagawa, M., (1976) Vertical flux of organic materials estimated from Th-234 in the ocean. Joint Oceanographic Assembly, Edinburgh, 156.

Tsunogai, S., Taguchi, K., Harada, K., (1986) Seasonal variation in the difference between observed and calculated particulate fluxes of Th-234 in Funka Bay, Japan. *Journal of the Oceanographical Society of Japan*, 42(2), 91-98.

Turnewitsch, R., Springer, B.M., (2001) Do bottom mixed layers influence Th-234 dynamics in the abyssal near-bottom water column? *Deep-Sea Research Part I-Oceanographic Research Papers*, 48(5), 1279-1307.

Ussher, S.J., Achterberg, E.P., Worsfold, P.J., (2004) Marine biogeochemistry of Iron. *Environmental Chemistry*, 1(2), 67-80.

Valderrama, J.C., (1981) The simultaneous analysis of total nitrogen and total phosphorus in natural waters. *Marine Chemistry*, 10(2), 109-122.

Valdes, J.R., Price, J.F., (2000) A neutrally buoyant, upper ocean sediment trap. *Journal of Atmospheric and Oceanic Technology*, 17(1), 62-68.

Varela, M.M., Bode, A., Fernandez, E., Gonzalez, N., Kitidis, V., Varela, M., Woodward, E.M.S., (2005) Nitrogen uptake and dissolved organic nitrogen release in planktonic communities characterised by phytoplankton size-structure in the Central Atlantic Ocean. *Deep-Sea Research I*, 52(9), 1637-1661.

Varela, M.M., Bode, A., Moran, X.A.G., Valencia, J., (2006) Dissolved organic nitrogen release and bacterial activity in the upper layers of the Atlantic Ocean. *Microbial Ecology*, 51(4), 487-500.

Venables, H.J., Pollard, R.T., Popova, E.E., (2007) Physical conditions controlling the development of a regular phytoplankton bloom north of the Crozet Plateau, Southern Ocean. *Deep-Sea Research II*, 54(18-20), 1949-1965.

Verardo, D.J., Froelich, P.N., McIntyre, A., (1990) Determination of organic carbon and nitrogen in marine sediments using the Carlo Erba NA-1500 Analyzer. *Deep-Sea Research Part A*, 37(1), 157-165.

Vöge, I., Savoye, N., Berg, G.M., Bertoïa, C., Klaas, C., Bathmann, U., Strass, V., Friedrich, J., Dehairs, F., (2006) ^{234}Th-based export production during the European Iron Fertilization Experiment (EIFEX). Ocean Sciences Meeting, Honolulu, Hawaii, USA, Abstract OS35M-17.

Waples, J.T., Benitez-Nelson, C., Savoye, N., Rutgers van der Loeff, M., Baskaran, M., Gustafsson, O., (2006) An introduction to the application and future use of ^{234}Th in aquatic systems. *Marine Chemistry*, 100(3-4), 166-189.

Ward, B.B., Bronk, D.A., (2001) Net nitrogen uptake and DON release in surface waters: importance of trophic interactions implied from size fractionation experiments. *Marine Ecology Progress Series*, 219, 11-24.

Watson, A.J., (2001) Iron limitation in the oceans. In: D.R. Turner, K.A. Hunter (Eds.), The Biogeochemistry of Iron in Seawater. John Wiley & Sons, Ltd, Chichester.

Watson, A.J., Robinson, C., Robinson, J.E., Williams, P.J.L., Fasham, M.J.R., (1991) Spatial Variability in the Sink for Atmospheric Carbon-Dioxide in the North-Atlantic. *Nature*, 350(6313), 50-53.

Wei, C.L., Murray, J.W., (1991) Th-234/U-238 Disequilibria in the Black-Sea. *Deep-Sea Research Part A*, 38, S855-S873.

Welschmeyer, N.A., (1994) Fluorometric analysis of chlorophyll *a* in the presence of chlorophyll *b* and pheopigments. *Limnology and Oceanography*, 39(8), 1985-1992.

Whitehouse, M.J., Priddle, J., Brandon, M.A., (2000) Chlorophyll/nutrient characteristics in the water masses to the north of South Georgia, Southern Ocean. *Polar Biology*, 23(6), 373-382.

Whitworth, T., Nowlin, W.D., (1987) Water masses and currents of the Southern Ocean at the Greenwich Meridian. *Journal of Geophysical Research-Oceans*, 92(C6), 6462-6476.

Wilson, D.L., Smith, W.O., Nelson, D.M., (1986) Phytoplankton bloom dynamics of the western Ross Sea ice edge–I. Primary productivity and species specific production. *Deep-Sea Research Part A*, 33(10), 1375-1387.

Winckler, G., Newton, R., Schlosser, P., (2007) Evidence for a Hydrothermal Plume in the Pacific Sector of the Southern Ocean. EGU General Assembly, Vienna, Abstract EGU2007-A-05690.

Windholz, M., Budavari, S., Stroumtsos, L.Y., Fertig, M.N., (1976) The Merck Index. Merck & Co, Rahway.

Wong, C.S., Whitney, F.A., Crawford, D.W., Iseki, K., Matear, R.J., Johnson, W.K., Page, J.S., (1999) Seasonal and interannual variability in particle fluxes of carbon, nitrogen and silicon from time series of sediment traps at Ocean Station P, 1982-1993: relationship to changes in subarctic primary productivity. *Deep-Sea Research II*, 46(11-12), 2735-2760.

Yool, A., Martin, A.P., Fernandez, C., Clark, D.R., (2007) The significance of nitrification for oceanic new production. *Nature*, 447(7147), 999-1002.

Zeebe, R.E., Archer, D., (2005) Feasibility of ocean fertilization and its impact on future atmospheric CO_2 levels. *Geophysical Research Letters*, 32(9), L09703.

Zeebe, R.E., Archer, D., (2006) Is large scale iron fertilization a feasible strategy to sequester anthropogenic CO_2. Ocean Sciences Meeting, Honolulu, Hawaii. Eos, Transactions, AGU, 87(36), Abstract OS34F.

Zubkov, M.V., Holland, R.J., Burkill, P.H., Croudace, I.W., Warwick, P.E., (2007) Microbial abundance, activity and iron uptake in vicinity of the Crozet Isles in November 2004-January 2005. *Deep-Sea Research II*, 54(18-20), 2126-2137.